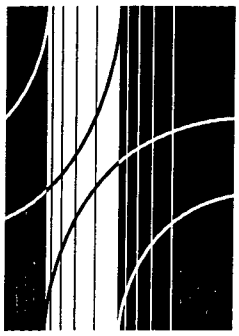

Joint
Transportation
Research
Program

JTRP

PB99-115230

FHWA/IN/JTRP-97/4

Final Report

STRENGTH AND DURABILITY OF CONCRETE: EFFECTS OF CEMENT PASTE-AGGREGATE INTERFACES

PART II

SIGNIFICANCE OF TRANSITION ZONES ON PHYSICAL AND MECHANICAL PROPERTIES OF PORTLAND CEMENT MORTAR

Turng-Fang F. Lee
Menashi D. Cohen

August 1998

Indiana
Department
of Transportation

Purdue
University

FINAL REPORT

FHWA/IN/JHRP-97/4

STRENGTH AND DURABILITY OF CONCRETE: EFFECTS OF CEMENT PASTE-AGGREGATE INTERFACES

PART II:
SIGNIFICANCE OF TRANSITION ZONES ON PHYSICAL AND MECHANICAL PROPERTIES OF PORTLAND CEMENT MORTAR

by

Turng-Fang F. Lee
Research Assistant
and
Menashi D. Cohen
Research Engineer

Purdue University
School of Civil Engineering

Joint Transportation Research Program

Project No.: C-36-37EE
File No.: 5-8-31

Prepared in Cooperation with the
Indiana Department of Transportation and
the U.S. Department of Transportation
Federal Highway Administration

Purdue University
West Lafayette, IN 47907

August 1998

TECHNICAL REPORT STANDARD TITLE PAGE

1. Report No.	2. Government Accession No.	3. Recipient's Catalog No.
FHWA/IN/JTRP-97/4		

4. Title and Subtitle

Strength and Durability of Concrete: Effects of Cement Paste-Aggregate Interfaces

Part I: Theoretical Study on Influence of Interfacial Transition Zone on Properties of Concrete Materials

Part II: Significance of Transition Zones on Phyiscal and Mechanical Properties of Portland Cement Mortar.

5. Report Date
August, 1998

6. Performing Organization Code

7. Author(s)
Part I: Yiguo Zhang and Wai-Fah Chen
Part II: Turng-Fan F. Lee and Menashi D. Cohen

8. Performing Organization Report No.
FHWA/IN/JTRP-97/4

9. Performing Organization Name and Address
Joint Transportation Research Program
1284 Civil Engineering Building
Purdue University
West Lafayette, Indiana 47907-1284

10. Work Unit No.
PB99-115230

11. Contract or Grant No.
HPR-2071

12. Sponsoring Agency Name and Address
Indiana Department of Transportation
State Office Building
100 North Senate Avenue
Indianapolis, IN 46204

13. Type of Report and Period Covered
Final Report

14. Sponsoring Agency Code

15. Supplementary Notes

Prepared in cooperation with the Indiana Department of Transportation and Federal Highway Administration.

16. Abstract

This research was based on a two-part basic research investigation studying the effects of cement paste-aggregate interfaces (or interfacial transition zones-ITZ) on strength and durability of concrete. Part I dealt with the theoretical study and Part II dealt with the experimental.

Part I, the theoretical part, illustrates the effect of ITZ on the concrete properties by assuming its elastic moduli to be varied continuously in the region. A four-phase composite model is employed and three functions are chosen to model the moduli variation in the ITZ. A theoretical solution for an n-layered spherical inclusion model is used to estimate the overall effective moduli of the modified four-phase model. The influence of material and geometric characteristics of the ITZ, as well as that of the aggregate on the overall effective moduli is investigated. The effects of three different moduli variations in ITZ on the overall moduli are compared. Their potential application is discussed. Finally, by comparing the prediction of the proposed models to a set of data on mortar, it is found that the elastic modulus at the interface is about 20-70% lower than that in the bulk paste for portland cement mortar, and 10-40% lower for silica fume mortar.

Part II, the experimental part, illustrates the relationship between the ITZ microstructure and the mechanical properties of the concrete. The mechanical properties studied included the dynamic modulus of elasticity, dynamic shear modulus, logarithmic decrement of damping, flexural tensile strength, and compressive strength. In addition, the effects of changing the water-to-cementitious material ratio by mass, aggregate type, volume fraction of aggregate, and silica fume substitution, on these properties were investigated. A criterion based on water quantity and the specific surface area of aggregate by mass in a mixture was developed to eliminate biased date from the analysis process. This criterion was used to detect mixing and compaction problems that may have resulted in erroneous values of mechanical properties of specimen. In order to realize the compaction condition of the fresh mixture, an index of compaction (called gross porosity) was introduced. The three-phase model of Hashin-Shtrikman bounds was employed, tested, and validated with the experimental data from this research. A modification of this model linked the theory of Hashin-Shtrikman bounds to the results of this research on dynamic moduli of the transition zone. A form of optimal water content is recommended. This optimal water content may be used for a mixture to gain its possibly highest moduli, strengths and density. Thus, the rule of the optimal water content may potentially be applied to optimize the mixture design for conventional and high-strength concrete with consideration of ITZ.

17. Key Words	18. Distribution Statement
Interface transition zone (ITZ), four-phase composite model, elasticity, effective moduli, elastic moduli, dynamic modulus, shear modulus, logarithmic decrement, damping, flexural tensile strength, compressive strength, porosity, microstructure, Hashin-Shtrikman model.	No restrictions. This document is available to the public through the National Technical Information Service, Springfield, VA 22161

19. Security Classif. (of this report)	20. Security Classif. (of this page)	21. No. of Pages	22. Price
Unclassified	Unclassified	Part I - 43 Part II - 261	

Form DOT F 1700.7 (8-69)

TABLE OF CONTENTS

LIST OF TABLES

LIST OF FIGURES

LIST OF ABBREVIATIONS

Ed : dynamic modulus of elasticity (GPa)

Gd: dynamic shear modulus (Gpa)

K: bulk modulus

δ: logarithmic decrement of damping

Va: Volume fraction of aggregate

W/C: Water-to-Cementitious ingredient ratio by mass

C/S: CaO-to-SiO_2 molar ratio

SA: specific Surface Area of aggregate by mass (cm^2/g)

SSD: Saturated Surface Dry

LOI: Loss-on-Ignition

MIP: Mercury Intrusion Porosimetry

SEM: Scanning Electron Microscopy

BEI: Backscatter Electron Image

EDS: Energy Dispersive X-ray Spectrometry

MOR: Modulus of Rupture

HS bounds: Hashin-Shtrikman bounds (upper bound and lower bound)

PC mortar: plain Portland Cement mortar

xy% SF mortar: Silica Fume mortar, having xy% of cement weight substituted by silica fume.

mixture proportion pq_rs_xy: volume fraction of aggregate 0.pq, W/C 0.rs, and xy% of cement weight are substituted by silica fume.

CHAPTER 1
INTRODUCTION, OBJECTIVE, SCOPE, AND APPROACH

1.1 Introduction

Concrete is a porous and highly heterogeneous, multiphase, composite material with aggregate, bulk cement paste, and a transition zone of cement paste-aggregate as its important constituents. Its physical behavior is complex, not only dependent on the mechanical properties of its components, but also determined by the structure of the composite matrix. It is therefore difficult to develop a complete model of the concrete structure from which the mechanical behavior of concrete can be reliably predicted. However, a knowledge of the structure and properties of individual components of concrete and the relationship between these components can be used to control properties of concrete. This approach is often used in development of high-performance concrete.

Improved engineering properties of concrete, such as high stiffness, high rigidity, high strength, high toughness, high workability, high resistance to wear, low permeability, low shrinkage, low creep, and good durability, are of major interest in evolving high-performance concrete. Two research approaches are typically used in studying the engineering properties of high-performance concrete: the chemical approach and the physical approach (mainly the mechanical property studies). Although all of the mechanical properties can be related to the chemical properties of the components of concrete, a study of the mechanical properties is also necessary. This is because mechanical properties such as stiffness, rigidity, strength, toughness, and damping can directly supply information for establishing the complete constitutive laws and the creep-relaxation model of concrete. From a mechanical point of view, a new constitutive law that is a combination of the three constitutive laws of the three major ingredients of

concrete (aggregate, bulk paste, and the transition zone) will potentially be a powerful tool in the development of high-performance concrete. The influence of any change in the ingredients on the concrete matrix can be evaluated using this kind of constitutive law.

Before establishing the constitutive law or the creep or relaxation models for the concrete based on the properties of individual ingredients, a thorough study must be done on the mechanical properties of the three major constituents of concrete: aggregate, bulk paste, and transition zone. The properties of aggregate and bulk paste have been studied extensively. However, due to experimental difficulty, information about the transition zone is so far rather rare.

In addition, many efforts have recently been devoted to the development of high-strength concrete. In making a high-strength concrete, one important strategy is to focus on how to increase the stiffness and strength of the cement paste-aggregate transition zone to a level comparable to that of bulk paste and aggregate. This may be achieved by adding mineral admixtures such as silica fume, fly ash, or ground granulated furnace slag to the concrete mixture. The next question is how much the moduli and strength of transition zones can be increased by adding these admixtures. The answers to these questions need to be provided by experiments. Some researchers have measured the hardness of transition zones. For example, Tamimi [1994] measured changes in the Vickers micro-hardness as the function of the distance from the aggregate surface. However, it is hard to find the relationship between micro-hardness and moduli or strength. In another work, Lindholm [1990] showed the micro-strain fields at the crack tip by using Scanning Electronic Microscopy (SEM) with automated image analysis capability. This method may potentially be applied for the experimental study of transition zones in the future. Nevertheless, in practice it is hard to find an instrument to measure with accuracy the mechanical properties of the transition zone due to its small size (reported thickness 10 to 50 μm). Since it is impossible to study the mechanical properties of the transition zone directly, an indirect way must be developed. This work presents the development of such an indirect method and reports the research results.

The layout of this report is as follows. Chapter 1 presents the research objective and scope. Chapter 2 discusses the literature review regarding transition zone. Chapter 3 describes materials used for experiments. Chapter 4 defines the experimental methods applied in this research. The experimental results are reported in the next three chapters as follows. Chapter 5 sets up a criterion to identify mixing and compaction problems and is used to eliminate the biased experimental data resulting from mixing and compaction problems. Chapter 6 establishes a theoretical basis for interpretation of experimental data, and Chapter 7 presents an interpretation of the experimental data regarding dynamic moduli of transition zones. This is performed by applying the theory developed in Chapter 6 and by using the criterion established in Chapter 5 as the boundary condition for this theory. In addition, the significance of transition zones on physical and mechanical properties of mortar is also discussed in Chapter 7. Chapter 8 provides a summary and conclusion to this research, and Chapter 9 describes some recommendations for future research.

1.2 Project Objective and Scope

The objective of this project is to study the significance of transition zones on physical and mechanical properties of mortar. The scope of this research is separated into two studies: experimental and theoretical. The experimental study involves determination of dynamic modulus of elasticity, dynamic shear modulus, flexural tensile strength, compressive strength, and damping. The theoretical study involves modification of the model of three-phase Hashin-Shtrikman bounds. The purpose of this theoretical study is to offer a mathematical way to interpret the experimental data of dynamic moduli. The overall objective and scope of this research are summarized in Figure 1.1.

1.3 Approach to the Objective

The issue of the average thickness of the transition zone is somewhat controversial and was a subject of several studies. Based on SEM observation, Khokhrin

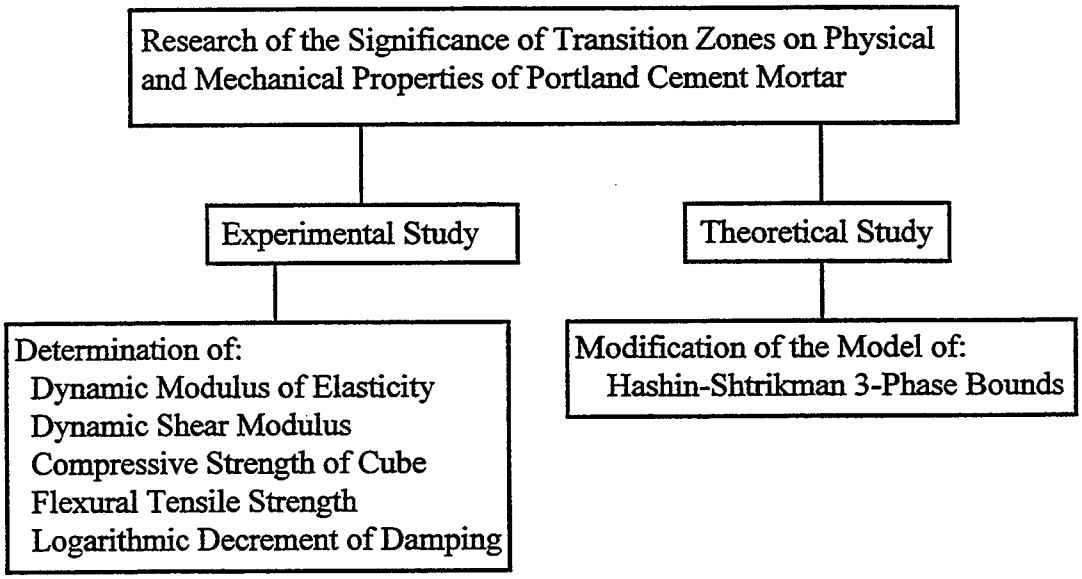

Figure 1.1 Flow Chart of the Objective and Scope of This Research

[1973] reported a 60-μm thickness of transition zones between lightweight aggregate and paste. In another study, Bentur and Cohen [1987] suggested the thickness of transition zones to be about 20 to 50 μm. Winslow et al. [1994] proposed a value in the range of 15 to 20 μm as measured by Mercury Intrusion Porosimetry (MIP). Mehta and Monteiro [1993] suggested a range of 10 to 50 μm for the thickness of transition zones. Based on the investigation of roughness number, Zanpini et al. [1995] proposed a range of 96 to 128 μm. Monteiro et al. [1985] used SEM and X-ray diffraction to confirm the diffusion mechanism of ions, which forms calcium hydroxide and ettringite in transition zones, and proposed that the thickness of transition zones depends on the size and shape of sand particles. However, regardless of the actual value of this, it is difficult to measure directly the mechanical properties of transition zones. Due to the lack of specific techniques to measure directly the mechanical properties of transition zones, an indirect way needs to be developed.

In general, there are two ways to design experiment for studying the physical and mechanical properties of a transition zone indirectly. One is to increase the volume fraction of aggregate (Va), but keep size and gradation of aggregate the same. This will cause the increase of the volume fraction of transition zone. By studying the relationships between the physical and mechanical properties of the matrix and the variation of Va, the influence of physical and mechanical properties of the transition zone on these properties of matrix can be evaluated. However, this method has certain drawbacks. Cohen et al. [1995] have tried to estimate the average stiffness and rigidity of transition zones by using the logarithmic mixture rule. In another study, Lutz and Monteiro [1995] tried to determine the bulk and shear moduli of transition zones by introducing a power law. The results of both studies show that the stiffness, rigidity, and bulk modulus of the transition zone may be less than that of the bulk paste. Ordinarily, among the three constituents of concrete or mortar, aggregate has the highest stiffness, rigidity, and bulk modulus. If Va increases, the volume fraction of transition zones will also increase. The increasing volume of transition zones will lower the stiffness of concrete matrix. However, the increasing volume of aggregate will also raise the stiffness of concrete, thus making the

interpretation of test data difficult. The other way is to keep Va constant, but crush the aggregate to finer size. Assuming that the average thickness of transition zones is approximately equal for large and small aggregates, reducing the aggregate size will increase the volume of transition zones and will also decrease the volume of bulk paste by the same amount. In this case, the volume fraction of transition zones is related to the specific surface area of aggregate (SA). By studying the relationships between the physical and mechanical properties of the matrix and SA, the physical and mechanical properties of transition zones may be estimated. Actually, these relationships reflect the relative properties of transition zones and bulk paste. The physical and mechanical properties of bulk paste can be determined by studying the sample of pure paste, and can be regarded as the reference values in this method. The latter method has been introduced by Cohen et al. [1994] and is adopted in this research.

The mechanical variables studied include dynamic modulus of elasticity (Ed), dynamic shear modulus (Gd), logarithmic decrement damping (δ), compressive strength (of cube), and flexural strength. The necessity to study these mechanical variables is explained below.

First, since they are dynamic properties, the dynamic moduli can be used directly as the parameters of constitutive law. Even for a static problem, dynamic moduli can be used utilizing the pre-established dynamic-static moduli relationship. The use of this procurator is advantageous as it can be easily determined using non-destruction methods.

Secondly, some researchers may study the rheology of concrete such as creep and relaxation by adopting viscoelasticity models for all three major constituents of concrete. The stiffness modulus and damping property are two fundamental elements in viscoelasticity models. Thus, logarithmic decrement damping of the transition zone is one of the material properties to be studied in this research. In practice, however, the logarithmic decrement damping must be transformed into a damping coefficient before it can be used for viscoelasticity models.

Finally, in the conventional compression test of concrete, ASTM C-39, "Compressive Strength of Cylindrical Concrete Specimens", a uniaxial load is generally

applied to a cylindrical specimen. The microcracks initiate in the transition zones, then extend to the bulk paste. At this stage, some transgranular cracks (cleavages) may occur and propagate through aggregates. At the later stage of loading, the coalescence of cracks finally leads to the collapse of the concrete member when the ultimate strength, the highest point in the stress-strain curve, is reached. In this test, the shape and surface texture of aggregates play important roles in determining the strength of concrete. Both factors provide friction and interlocking effects inside the concrete specimens. Moreover, the strength of aggregate can contribute in part to the strength of concrete, if transgranular cracking takes place. In this research, the compressive strength tests were performed on one-inch cubes. In fact, although the concrete is under a uniaxial compressive loading, the cracks inside the specimen may be induced by a tensile strain. This was studied theoretically by Yamaguchi and Chen [1990, 1991]. They have concluded that the crack caused by tensile strain is a dominant factor for crack propagation in mortar and eventually influences concrete strength. Therefore, the investigation of tensile crack should be one of the focuses in studying concrete strength. Consequently, the tensile strength was selected as one of the important mechanical variables to be studied.

Unlike the uniaxial compression test, which is affected by the aggregate strength, a tensile strength test such as the ASTM C-78, "Flexural Strength of Concrete (Using Simple Beam with Third-point Loading Test)", can alleviate the effect of aggregate and may provide a reasonable way to study the tensile strength of transition zones. In addition, the flexural strength test, or Modulus of Rupture (MOR) test, may be a valid representation of concrete property that is of interest because the concrete members tend to be loaded in flexure rather than in direct tension or compression. The effect of aggregate can be greatly diminished, if the dominant crack, which is the crack caused by the collapse of matrix, is formed mainly by the coalescence of tensile cracks in the transition zones and bulk paste. As a result, if the transition zone is weaker than bulk paste, the specimen with more transition zones in the crack path or with a dominant crack passing through percolated transition zones will show an apparent decrease of tensile strength.

In brief, properties such as dynamic modulus of elasticity (Ed), dynamic shear modulus (Gd), logarithmic decrement of damping (δ), compressive strength, and flexural tensile strength (MOR) of the cementitious matrix with the variation of SA were evaluated in this research program. The purpose was to see how these mechanical variables change with the variation of SA, which effectively means with the change of the volume of the transition zone. Because the transition zone is more abundant in mortar than in concrete, mortar rather than concrete was chosen as the material for test specimens.

The relationship between the above mentioned mechanical variables and the quantity of transition zones can be affected by several factors. These include aggregate type, aggregate content, water-to-cement ratio, and admixtures added. Because the mechanical properties of concrete are highly affected by these factors, they may also have a similar effect on the mechanical properties of the transition zone.

An early work of Langton and Roy [1980] explored the difference in morphology of the transition zone present near reactive and non-reactive aggregates. They proposed that two layered zones developed in the transition zone between non-reactive aggregates and portland cement paste, and that four layers were characteristically present in the transition zone of reactive aggregates. They also concluded that the roughness of the aggregate resulted in no major effect on the basic structure of transition zones. A later work of Monteiro and Mehta [1986, (1)] suggested that a hydrated calcium carbonate - calcium hydroxide compound precipitated in the transition zones between carbonate aggregate and cement paste. They concluded that this was due to the calcite, etching from carbonate rock, and reacting with the cement paste in the transition zone to form a smaller crystal compound. They suggested that this process might strengthen the transition zone. Their investigation also led to the development of a grain refinement technique [Monteiro and Mehta, 1986, (2)]. A later research by Mehta and Monteiro [1988] compared the characteristics of transition zones around quartz and limestone aggregates. They concluded that the transition zone around limestone aggregate is strengthened while the transition zone around quartz aggregate does not show signs of strength increase.

In this research, dolomite aggregate was used for the study, and the data was compared with that of quartzite. In addition, one type of light-weight aggregate, perlite, was chosen for the study as well. The purpose was to see how much the mechanical properties of transition zones around lightweight aggregate can vary. In a sense, they can be quite different because this kind of aggregate is capable of absorbing a large quantity of water, thus potentially changing the structure of transition zones. In addition, it is quite interesting to investigate whether or not aggregate content influences the transition zone properties. As it is known, if aggregate content is too high, the compaction problem may occur. Hence, aggregate type and content were two factors that were also studied.

It is a well-established fact that the water-to-cementitious material ratio by mass (W/C) plays a major role in determining the mechanical properties of concrete. The W/C may also affect the mechanical properties of transition zones. Therefore, the effect of W/C was studied as well.

In addition, some researchers have investigated the effect of silica fume admixture on the mechanical properties of concrete. These include the work by Alexander and Milne [1995], Babu and Prakash [1995], Lydon and Iacovou [1995], and Katz and Bentur [1994]. Others have focused their studies on the effect of silica fume on the transition zone: Bentur et al. [1988] and Cohen et al. [1994]. The experimental results of these researchers showed that silica fume may influence the physical and mechanical properties of concrete, mortar, and the transition zone. Thus, the effect of silica fume was also studied in this research.

In order to eliminate, or minimize, the effect of entrapped air in the mixtures, a vacuum mixing with a vacuum of 27 mmHg applied for three minutes was performed. Results were compared with those of non-vacuumed specimens.

In summary, the goal of this research was to investigate the role of the transition zone in mortar and its influence on the mechanical properties. This was done by varying SA and measuring mechanical variables on the mortars. These mechanical variables included Ed, Gd, δ, compressive strength, and flexural tensile strength. The effects of

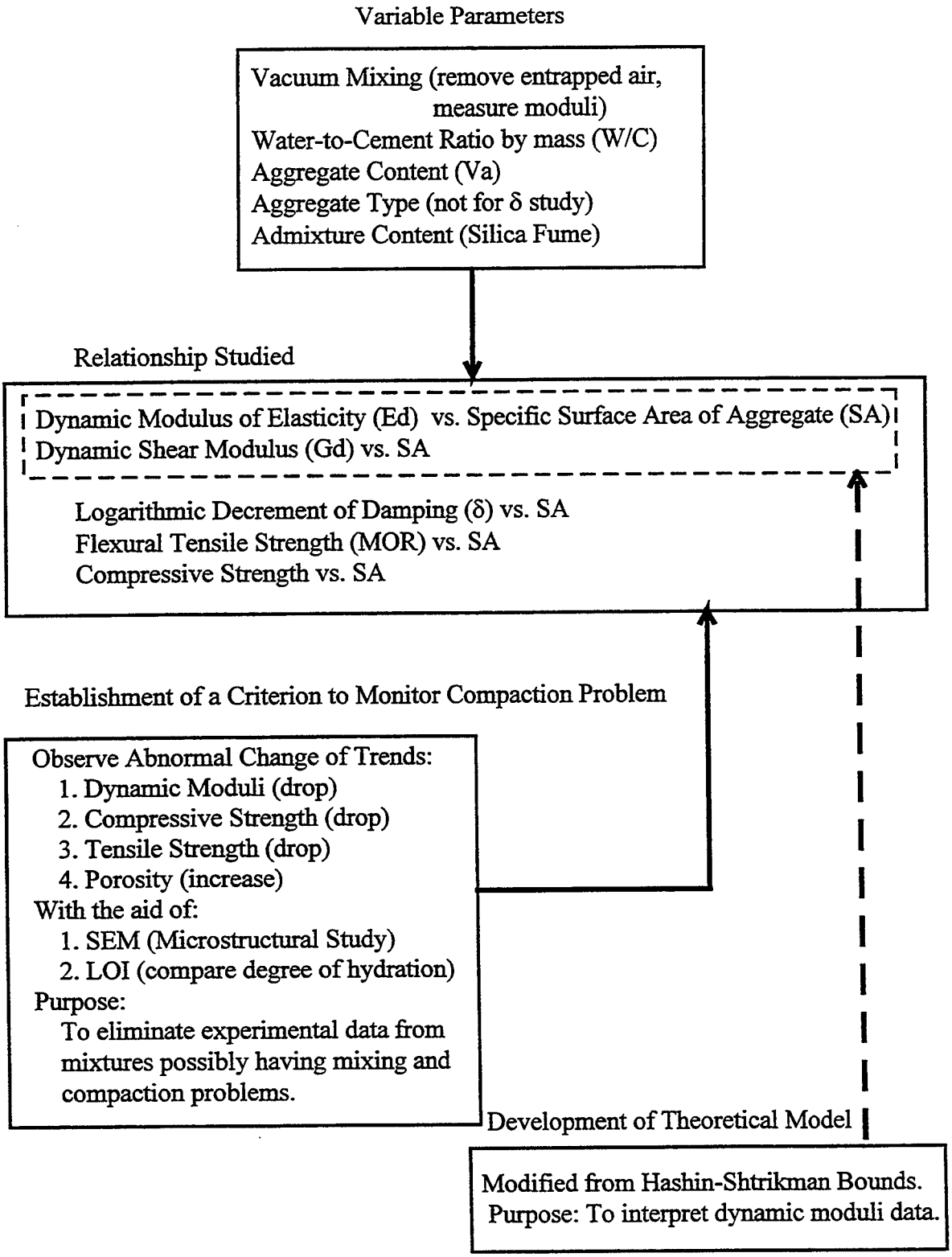

Figure 1.2 Flow Chart of the Research Program

varying the aggregate type and content, W/C, silica fume addition, and vacuum mixing were studied as well. Figure 1.2 provides a summary of the research program.

In order to assist with the analysis of experimental data, a criterion based on the volume of water and SA in the mixture was developed to eliminate the abnormal data. Practically, this criterion was used to detect mixing and compaction problems that may lower the moduli and strength of specimens. In addition, a three-phase model of Hashin-Shtrikman bounds is employed and verified with the experimental data. A modification of this model links the theory of Hashin-Shtrikman bounds to the study presented in this research on dynamic moduli of the transition zone.

Ishai noticed the influence of pores or cracks on the elastic modulus and studied the relationship between them [Ishai 1961, Cohen and Ishai 1967]. Several models have also been proposed to describe the influence of volume of pores or cracks on the elastic modulus of specimen. These include the differential scheme, the self-consistent scheme, and the Mori-Tanaka method [Mori and Tanaka, 1973]. Scrivener and Gartner [1988] measured the porosity of transition zones by SEM and concluded that there is a dramatic increase of porosity in the cement paste in the vicinity of an aggregate surface. Thus, porosity may be an important factor to be studied. With the aid of MIP, porosity was measured in this research. In addition, the increasing proportion of porosity contributed by transition zones was able to be determined.

In order to study the degree of compaction of specimens, a gross porosity was calculated from the difference between theoretical maximum bulk density and the experimental bulk density of a one-day-old specimen. Actually, this gross porosity represents the porosity of a fresh mixture and is an indicator of the degree of compaction, rather than porosity itself. This is because the hydration reaction of paste at later age will change the porosity and properties of the specimen.

The microscopic features and crack patterns of specimens were investigated by SEM. The images of porous features and crack patterns were correlated with the mechanical properties. In addition, in order to determine the chemical compositions of

aggregate, bulk paste, and transition zones, a technique of Energy Dispersive X-ray Spectrometry (EDS) was also employed in this study.

The degree of hydration of the specimens was studied by the Loss-on-Ignition (LOI) method. Its purpose was to observe whether or not W/C of both bulk paste and transition zones varies with changing SA. It is known that when aggregate content is increased to a certain amount, compaction problem may occur in the specimen. This compaction problem is closely related to the water available for hydration, and aggregate content may locally alter the water accessibility for the cement grains.

CHAPTER 2

LITERATURE REVIEW

2.1 Characteristics of Aggregate-Paste Interfacial Transition Zones

At the macroscopic level visible to unaided human eyes, concrete may be considered to be a two-phase material, consisting of aggregate particles dispersed in a matrix of cement paste. However, at the microscopic level, the complexity of concrete micro structure begins to show up. The structure of hydrated cement paste in the vicinity of aggregate particles is usually different from the structure of bulk paste in the system. In fact, many aspects of concrete behavior under stress can be explained when the transition zone of cement paste-aggregate is treated as a third phase.

2.1.1 Formation of the Transition Zone

A comprehensive report of researches on the transition zone has been presented by Ollivier et al. [1995]. Based on the description given by Maso [1980], the structural characteristics of transition zones are understood. In freshly compacted concrete, the water film around the aggregates, especially beneath the particles, accounts for a locally high W/C. Owing to this high W/C, relatively large crystals of ettringite and calcium hydroxide produced due to the hydration of cement are formed in the vicinity of aggregate or in the transition zone. Therefore, the transition zone is usually more porous than the bulk paste. In addition, the so called "wall effect" [Neville, 1993] between aggregate surface and cement grains may also contribute to a greater porosity in the transition zone.

2.1.2 Microstructure of the Transition Zone

Because of the locally higher W/C and "wall effect," the rate and characteristics of hydration in the vicinity of aggregate grains differ from that of the bulk paste, and result in higher porosity in this area. This is proposed by Maso [1980] to be the major cause and consequence of the existence of the transition zone. However, even if the porosity in the vicinity of aggregate is the same as that of bulk paste, the difference in stiffness and rigidity between aggregate and paste can result in a region of transforming different radial or hoop stresses and the occurrence of stress concentration. This mechanical phenomenon was studied by Zhao and Chen [1994] and is shown in Figures 5 and 6 of their report. In addition, another report by Chen and Zhao [1995] also presented the relationship between stress concentration factor and the stiffness discrepancy among aggregate, transition zones, and bulk paste.

The porosity of transition zones is mainly studied using two techniques: SEM and MIP. Scrivener et al. [1988] are the pioneers in applying quantitative SEM analysis to measure the porosity of the transition zone. Their results show that the degree of porosity is high near the surface of the aggregate and drops to a relatively constant level after about 30 μm from the aggregate surface. At the same time, the amount of anhydrous material is low near the surface of the aggregate and increases to a stable value at about 30 μm from the aggregate surface. However, some researchers attribute their results to artifact. Scrivener and Gartner [1988] also used the same SEM technique to measure variation in the amount of porosity, calcium hydroxide, and anhydrous material as a function of the distance from the aggregate surface. The specimens they used were portland cement pastes with and without silica fume. Each specimen had a single piece of granite, dolomite, or garnet aggregate cast within it. Similar results as above were found. The porosity increased in the paste close to the surface of the aggregate, while the content of anhydrous grains decreased. The amount of calcium hydroxide in the paste was found to be similar and independent of the distance to the aggregate surface. Recently, Scrivener and Nemati [1996] used equipment developed at U. C. Berkeley to study the porosity of concrete by intruding Wood's metal into a concrete sample with a

pressure of 1,500 psi. This allows Wood's metal to penetrate pores down to 0.08 μm. Their investigation on the images of SEM indicates that the pores in transition zones are interconnected and permeated preferentially, rather than the bulk paste.

Based on the MIP experiment, Winslow and Liu [1990] have reported that the pore structure in plain paste is less porous than that in the concrete paste, which includes transition zones. It is known that MIP measures the volume of pores of transition zones only if the transition zone porous system forms an interconnected cluster through the specimen. Winslow et al. [1994] studied the percolation of transition zones by MIP, and interpreted the results with an aid of a hard core/soft shell computer model. This microstructural model of cement paste, used to study percolation of capillary pores, was developed by Bentz and Garboczi [1991]. A similar work, based on combining MIP data and a simulated result of percolation of a three-dimensional mortar model, has been presented by Bourdette et al. [1995]. These researches on percolation suggested that percolation may increase the porosities of concrete and mortar.

2.1.3 Morphology of Hydration Products in the Transition Zone

A review on morphology and microstructure of the transition zone of cement paste and rock has been reported by Langton and Roy [1980]. Using SEM, Barnes et al. [1979] have studied the micro-morphological features of the transition zone. These features included formation of a duplex film on the surface of sand grain; development of large well-formed calcium hydroxide crystals at intervals near the surface of aggregate with their c-axes roughly parallel to it; development of stacked-platelet secondary calcium hydroxide in open spaces immediately adjacent to the duplex film; and hydration leading to the presence of hollow-shell hydration grain in the transition zone. In another work these researches [1978 (1) and (2)] described the hollow shell hydration phenomenon and reported in detail the morphology of the duplex film. It is a two-layer structure typically about 1 to 1.5 μm thick. The lower layer, which is in direct contact with the aggregate surface, was shown to be preferentially, but not perfectly, oriented calcium hydroxide by X-ray diffraction. The upper layer is rod-shaped calcium-silicate-

hydrate (C-S-H) gel. The rods project more or less normal to the aggregate surface. After three days of hydration, the C-S-H gel rods transformed to a reticulated network.

The use of X-ray diffraction to detect the preferential orientation of calcium hydroxide in transition zones was first proposed by Hadley [1972], and afterward modified and developed by Grandet and Ollivier [1980].

Yuan and Odler [1987] studied CaO-to-SiO_2 (C/S) molar ratio in the transition zones by microprobe analysis. In the vicinity of aggregate, C/S is about 6. At about 120 μm from the aggregate surface, the ratio decreases to 3. The C/S of C-S-H gel found in transition zones is in the range of 3.5 to 4, instead of 1.5 to 2 in the bulk paste.

The concentration profile of ettringite was studied by Monteiro and Mehta [1985]. They proposed that much larger quantities of ettringite were precipitated immediately next to the aggregate surface than farther away from it via the "through-solution" mechanism.

2.1.4 Influence of Mineral Admixtures on Microstructure of the Transition Zone

Silica fume influences the microstructure of transition zones by pozzolanic reaction and also by acting as microfiller. This has been studied by Bentur and Cohen [1987]. The contribution of densified transition zones by silica fume to the strength of concrete has been reported by Bentur et al. [1988].

Mehta and Monteiro [1988] have studied the effects of aggregate type, cement type, and mineral admixtures on the microstructure of transition zones. In their study, they compared the influence of quartz and limestone aggregates, Type I portland and type K expansive cements, and three kinds of mineral admixtures, such as condensed silica fume, granulated blast-furnace slag, and fly ash.

Another investigation on the influence of admixtures such as fly ash, silica fume, and slag, on the morphology of transition zones has been published by Charles-Gibergues et al. [1982]. They also described the characteristics of portland cement paste hydration in the transition zone.

2.1.5 The Transition Zone of Calcareous Aggregate

The microstructure of transition zones can be affected by a chemical reaction between aggregate and cement paste. The reactivity of calcareous aggregate with portland cement paste has been reported by Grandet and Ollivier [1980] to form a calcium carbo-aluminate C_3A-$CaCO_3$-$11H_2O$. However, an alternative explanation of this chemical reaction was made by Monteiro and Mehta [1986 (1)]. They reported that calcite reacts with calcium hydroxide, resulting in the formation of calcium carbonate with a varying composition of $CaCO_3$-$Ca(OH)_2$-H_2O.

Ping et al. [1991] used electrical conductivity to study structural characteristics of the transition zone. Their experimental results indicate that the transition zone between quartz particles and portland cement paste is always less dense than bulk paste regardless of the aggregate size; and the thickness of the transition zone decreases as the aggregate size is reduced. The same general features occur for the transition zone between larger limestone particles and portland cement paste. However, a transition zone denser than bulk paste for much smaller limestone particle was observed. According to the authors, the denser transition zones were possibly due to a chemical reaction occurring between the limestone particles and the portland cement paste.

A theoretical study on electrical conductivity influenced by transition zone was performed by Garboczi et al. [1995] by using a three-phase model: aggregate, bulk paste, and the transition zone. A computer model was developed to simulate the DC electrical conductivity of mortar.

2.1.6 Other Properties of the Transition Zone

The bond strength between aggregate and cement paste is a local property which involves the characteristics of transition zones, including the chemical reactivity of aggregate. This bond strength was studied by Zimbelmann [1985]. His experiments showed that the bond strength between portland cement paste and limestone is higher as compared to that between portland cement paste and granite. Consequently, he concluded

that this added adhesion is due to the chemical reaction between limestone and cement paste.

A review of the basic nature of the cement-aggregate bond and its effect on concrete performance was presented by Struble et al. [1980]. By applying Weibull's statistical theory, Monteiro and Andrade [1987] used the split tensile test to analyze the tensile bond strength between cement paste and basalt, amphibole-gneiss, granite, and limestone aggregates with smooth, sand-blasted, or rough surface condition.

Ping and Beaudoin [1992] studied the relationship of electrical conductivity of transition zones and aggregate-paste bond strength. They concluded that decreasing the thickness of the water-layer around the aggregate, and the W/C of mixture, can lead to increase in the bond strength.

The interaction between sintered fly ash lightweight aggregate and cement paste in the transition zone was studied by Wasserman and Bentur [1996]. They concluded that at early age due to the physical process of absorption of the aggregate, the transition zone is densified. In addition, they also suggested that a chemical process of pozzolanic activity at later age contributes to the strength of concrete.

The transport property such as water permeability was investigated by Wakeley and Roy [1982]. Their result showed that transition zone by itself does not appear to play a significant role with regard to water permeability.

In other studies, Tamimi [1994] measured hardness in the paste and detected a drop in the Vickers Micro-hardness in transition zones around aggregate. Vervuurt and Van Mier [1995] used optical microscopy to perform a digital image analysis on the process of bond-cracks in cementitious material, and determined the parameters in their numerical model of fracture law.

2.2 Influence of the Transition Zone on Mechanical Properties

The presence of easily cleavable and highly soluble calcium hydroxide crystals and the coarser porosity can affect the mechanical performance of the transition zone. The platelike calcium hydroxide crystals tend to form in oriented layers with the c-axis

perpendicular to the aggregate surface. Thus, the microcracks are formed easily in the direction perpendicular to the c-axis. Besides, the large calcium hydroxide crystals possess less adhesion capacity, not only because of the lower surface area and correspondingly weaker van der Waals forces of attraction, but also because they serve as preferred cleavage sites owing to their oriented structure. In addition to the oriented calcium hydroxide crystals, the larger volume of capillary voids and the presence of microcracks in the transition zone even before the concrete is subjected to external stresses are responsible for the lower stiffness and strength of the transition zone compared to the bulk paste in the concrete and mortar.

The transition zone is the weakest constituent in concrete, and therefore, it exercises a great influence on the mechanical behavior of concrete than can be expected based on its size. It is because of the presence of transition zones that concrete fails at a considerably lower stress level than the strength of either of the other two constituents. Since not much energy is needed to extend the cracks already existing in the transition zone, higher incremental strains are obtained at a load of 40 to 70 percent of the ultimate strength. At this stage, the aggregate and bulk paste remain elastic, whereas concrete itself shows inelastic behavior. This phenomenon confirms the conclusions of Karihaloo et al. [1993]. They proposed that the microcracks formed at paste-aggregate transition zones are the cause of pre-peak nonlinear behavior, and the transition from linear to nonlinear response of a cementitious material under loading is primarily governed by the extent of available microcracks of transition zones.

From a mechanical property point of view, the extent of microcracks in paste-aggregate transition zones is governed by the degree of strain mismatch between aggregate and bulk cement paste under the applied loading. For a stress equilibrium condition, the strain differences among aggregate, bulk cement paste, and transition zones can be related to the discrepancy of modulus of elasticity and shear modulus. This also introduces the stress concentration phenomenon between two constituents with different moduli. In fact, the transition zone serves as a bridge between aggregate particle and bulk cement paste. Even when the individual components are of high stiffness, the stiffness of

the concrete may be low because of the broken bridge's effect that does not permit stress transfer.

CHAPTER 3

MATERIALS

Three kinds of aggregates were used in this research.

1. Crushed dolomite sand (from Delphi, Indiana). This sand was sieved into five different ASTM size fractions: #4~#8, #8~#16, #16~#30, #30~#50, and #50~#100 by using a mechanical sieve shaker. The sieves are in accordance with the sieves specified in ASTM E-11, Standard Specification for Wire-Cloth Sieves for Testing Purpose. The specific gravity and absorption of the sand were both determined according to ASTM C-128, "Standard Test Method for Specific Gravity and Absorption of Fine Aggregate". The moisture content of sand was measured in accordance with ASTM C-566, "Standard Test Method for Total Moisture Content of Aggregate by Drying". The specific surface area of sand was determined by using the Kozeny-Carman equation [Loudon, 1952]. This empirical equation counts in a Kozeny's constant, porosity between sand particles, and water permeability through sand stockpile.

2. Natural quartzite sand (from Baraboo, Wisconsin).

3. Perlite, which is a lightweight aggregate. It is an amorphous silicate of volcanic origin containing a low percentage of crystalline silica.

The cement used was ASTM type I portland cement (from Lonestar) designated 332. Received and compacted silica fume was used as the mineral admixture in some of the mixtures. It was a high-quality, commercial grade with specific surface area of 24,300 m^2/kg and more than 90% amorphous silicon dioxide. The mixing water used was de-ionized water.

CHAPTER 4

EXPERIMENTAL PROGRAM

This chapter presents the experimental program. Section 4.1 deals with mixture design and preparation of specimens. Sections 4.2 discusses the methods for testing the physical and mechanical properties of specimens. Section 4.3 presents the microstructural study, including SEM and MIP. Section 4.4 presents the LOI technique that was used to compare the degree of hydration of paste within mortars.

4.1 Mixture Proportioning and Specimen Preparation

The mixture proportioning concept and mixing method are presented below. In addition, the curing procedure of the specimens is also discussed.

4.1.1 Mixture Proportioning

In all three types of mixture proportions used in this research, the mixture proportions shown in Table 4.1 were used for studying mixing and compaction problems. Plain portland cement mortars (PC mortars) were mixed with W/C 0.42 and several levels of volume fraction of aggregate (Va). The values of Va were 0.25 and varying from 0.40 to 0.70 at every 0.05 interval. Five different fractions of dolomite aggregate size were prepared. They were ASTM Sieve No. #4~#8, #8~#16, #16~#30, #30~#50, and #50~#100. These five sand fractions were used for the Va levels of 0.25, 0.40, 0.45, 0.50, and 0.55. Three sand fractions, #4~#8, #8~#16, and #16~#30, were used for Va = 0.60. Two sand fractions, #4~#8 and #8~#16, were used for Va = 0.65, and one sand fraction, #4~#8, was used for Va = 0.70. Only single fraction of sand was used in one specimen. Three specimens were cast for each mixture.

Table 4.1 Mixture Proportions for Studying Mixing and Compaction Problems.

W/C	Cement Weight (g)	SF (%)	Va	Aggregate Weight (g)	Aggregate Size (ASTM Sieve No.)	Specimen Quantity
0.42	800	0.0	0.25	520	#4~#8	3
					#8~#16	3
					#16~#30	3
					#30~#50	3
					#50~#100	3
0.42	600	0.0	0.40	780	#4~#8	3
					#8~#16	3
					#16~#30	3
					#30~#50	3
					#50~#100	3
0.42	570	0.0	0.45	912	#4~#8	3
					#8~#16	3
					#16~#30	3
					#30~#50	3
					#50~#100	3
0.42	570	0.0	0.50	1113	#4~#8	3
					#8~#16	3
					#16~#30	3
					#30~#50	3
					#50~#100	3
0.42	450	0.0	0.55	1075	#4~#8	3
					#8~#16	3
					#16~#30	3
					#30~#50	3
					#50~#100	3
0.42	375	0.0	0.60	1100	#4~#8	3
					#8~#16	3
					#16~#30	3
0.42	375	0.0	0.65	1359	#4~#8	3
					#8~#16	3
0.42	250	0.0	0.70	1142	#4~#8	3

Note: SF (%) is the percentage of cement weight substituted by silica fume.

The purpose in designing this mixture series was to determine which of the mixtures will experience mixing and compaction problems. It is assumed that the mixing and compaction problems are related to SA in the mortar, and that SA can be increased by increasing Va or using finer aggregate.

Second, the series of mixtures presented in Table 4.2 was designed to investigate how varying the SA in the mortars influences the properties (mainly mechanical) of mortars, such as Ed, Gd, δ, flexural tensile strength, compressive strength, porosity, and LOI. SA is actually expressed in terms of the calculated volume of transition zones in the mortar with an assumption that the thickness of transition zones around all the aggregates is constant. By keeping Va constant, using finer aggregate means increasing SA. Further, increasing SA means increasing the volume of transition zones. However, this will also reduce the volume of the bulk paste (at the same level). Therefore, the relationship between these properties of mortars and SA reflects the difference in the properties between the transition zone and bulk paste.

Three different W/C, 0.35, 0.42, and 0.50, were used to study how the relationship between the mechanical properties and SA is influenced by W/C. Besides, three different levels of Va, 0.25, 0.40, and 0.55, were also used. The purpose was to observe how Va content affects the relationship between the mechanical properties and SA.

In some mortars, 7% of cement weight was substituted by silica fume (7% SF mortars). The purpose was to study how silica fume affects the relationship between the mechanical properties and SA.

Finally, in order to study how aggregate type influences the relationship between the mechanical properties and SA, some mixtures were designed and are shown in Table 4.3 according to the mixture proportions used by Cohen et al.[1994]. In their experiments, quartzite sand was used for the mortar specimens. Va was kept at 0.37. W/C was kept at 0.52. Silica fume contents used were at 0% and 10% replacement of cement weight. The tests on the specimens with mixture proportions shown in Table 4.3 were mainly performed on dolomite and perlite mortars. The purpose of this testing was to

Table 4.2 Mixture Proportions for Comparing the Effect of W/C, Va, and Silica Fume on Ed, Gd, δ, Tensile Strength, and Compressive Strength.

W/C	Cement Weight (g)	SF (%)	Va	Aggregate Weight (g)	Aggregate Size (ASTM Sieve No.)	Specimen Quantity
0.42	520	0.0	0.25	800	#4~#8 #8~#16 #16~#30 #30~#50 #50~#100	3 3 3 3 3
0.42	528	7.0	0.25	744	#4~#8 #8~#16 #16~#30 #30~#50 #50~#100	3 3 3 3 3
0.35	766	0.0	0.40	650	#4~#8 #8~#16 #16~#30 #30~#50 #50~#100	3 3 3 3 3
0.35	778	7.0	0.40	604.5	#4~#8 #8~#16 #16~#30 #30~#50 #50~#100	3 3 3 3 3
0.42	780	0.0	0.40	600	#4~#8 #8~#16 #16~#30 #30~#50 #50~#100	3 3 3 3 3
0.42	790	7.0	0.40	558	#4~#8 #8~#16 #16~#30 #30~#50 #50~#100	3 3 3 3 3
0.50	866	0.0	0.40	600	#4~#8 #8~#16 #16~#30 #30~#50 #50~#100	3 3 3 3 3
0.50	876	7.0	0.40	558	#4~#8 #8~#16 #16~#30 #30~#50 #50~#100	3 3 3 3 3
0.42	1075	0.0	0.55	450	#4~#8 #8~#16 #16~#30 #30~#50 #50~#100	3 3 3 3 3
0.42	1090	7.0	0.55	418.5	#4~#8 #8~#16 #16~#30 #30~#50 #50~#100	3 3 3 3 3

Table 4.3 Mixture Proportions for Studying the Influence of Different Aggregate Types on the Transition Zone.

W/C	Cement Weight (g)	SF (%)	Va	Aggregate Weight (g)	Aggregate Size (ASTM sieve no.)	Specimen Quantity
0.52	570	0.0	0.37	744	#4~#8	3
					#8~#16	3
					#16~#30	3
					#30~#50	3
					#50~#100	3
0.52	513	10.0	0.37	756	#4~#8	3
					#8~#16	3
					#16~#30	3
					#30~#50	3
					#50~#100	3

compare the relationship between dynamic moduli and SA for quartzite, dolomite, and perlite mortars.

The preparation of samples was done using mixture proportions listed in Tables 4.1, 4.2, and 4.3. Five different size fractions of crushed dolomite sand (from Delphi, Indiana) were prepared and mixed with Type I portland cement (from Lonestar, designated 332) to make dolomite mortar specimens. Two kinds of sandstone, one ASTM standard quartz sand C-190 and C-109 (from Ottawa, Illinois), the other quartzite sand (from Baraboo, Wisconsin), were also prepared and mixed with Type I portland cement to make mortar specimens. The quartzite sand was sieved according to the five different size fractions mentioned above. These quartz and quartzite mortars were used for the studies of the dynamic moduli and SEM. The purpose of these tests was to compare the difference in mechanical moduli of transition zones between limestone-base mortars and sandstone-base mortars. Five different size fractions of Perlite aggregates were also mixed with the same cement in accordance with proportions shown in Tables 4.2 and 4.3 and were used to make perlite mortars. The purpose of this experiment was to study the mechanical properties of transition zones of lightweight aggregate.

4.1.2 Mixing, Casting, and Curing

Two mixing methods were used. One was a normal mixing procedure and utilized a Hobart mixer. This procedure followed ASTM C-305, "Standard Practice for Mechanical Mixing of Hydraulic Cement Pastes and Mortars of Plastic Consistency". The other was a vacuum mixing procedure. During this procedure, a vacuum of 27 mmHg was applied for three minutes only during mixing in order to minimize the loss of water.

After mixing, the mixture was cast into a steel mold that had an internal dimension of 12 in. × 1 in. × 1 in. and was placed on a vibrating table. The fresh specimens with molds were kept in a moisture room at 24°C for 24 hours and then demolded. After demolding, the specimens were cured in a saturated lime solution at ambient temperature and were tested for the dynamic moduli at 1, 3, 7, 28, and 56 days.

Afterward, the specimens were cut into 4 inches × 1 in. × 1 in prisms and 1 inch cubes, and the flexural tensile strength test and compressive strength test were performed under the Saturated Surface Dry (SSD) condition. MIP and SEM experiments were performed after an oven drying process on the 56 days old mature specimens.

4.2 Testing Procedures of Physical and Mechanical Properties

In this section, the gross porosity is defined, and its relation to the degree of compaction is discussed. The instruments and procedures applied to measure Ed, Gd, δ, flexural strength, and compressive strength are also described.

4.2.1 Gross Porosity and Compaction

Figure 4.1(a) shows a schematic composition of fresh mortar and is used for explaining the meaning of gross porosity. The gross porosity is defined as the voids volume between solid particles per unit bulk volume of mortar specimen. These solid particles include silica fume particles, cement grains, and fine aggregate particles. The voids are filled with water and entrapped air when the mortar is in a very fresh condition. Thus, the gross porosity can be regarded as an index of compaction of solid particles.

In order to determine the gross porosity, a smeared density of solid particles (D_S) needs to be introduced. It is calculated in accordance with the mass and volume fractions of all kinds of particles included in the mixture by

$$D_s = \frac{W_{SF} + W_{Cement} + W_{Sand}}{V_{SF} + V_{Cement} + V_{Sand}} \tag{4.1}$$

where W_{SF} and V_{SF} is the mass and volume of silica fume,
W_{Cement} and V_{Cement} is the mass and volume of cement, and
W_{Sand} and V_{Sand} is the mass and volume of Sand.

Then, the bulk volume of specimen (V_{bulk}) can be determined from the following formula:

$$V_{bulk} = (W_{SSD} - W_{merged}) / D_W \tag{4.2}$$

where W_{SSD} is the mass of SSD specimen in the air,

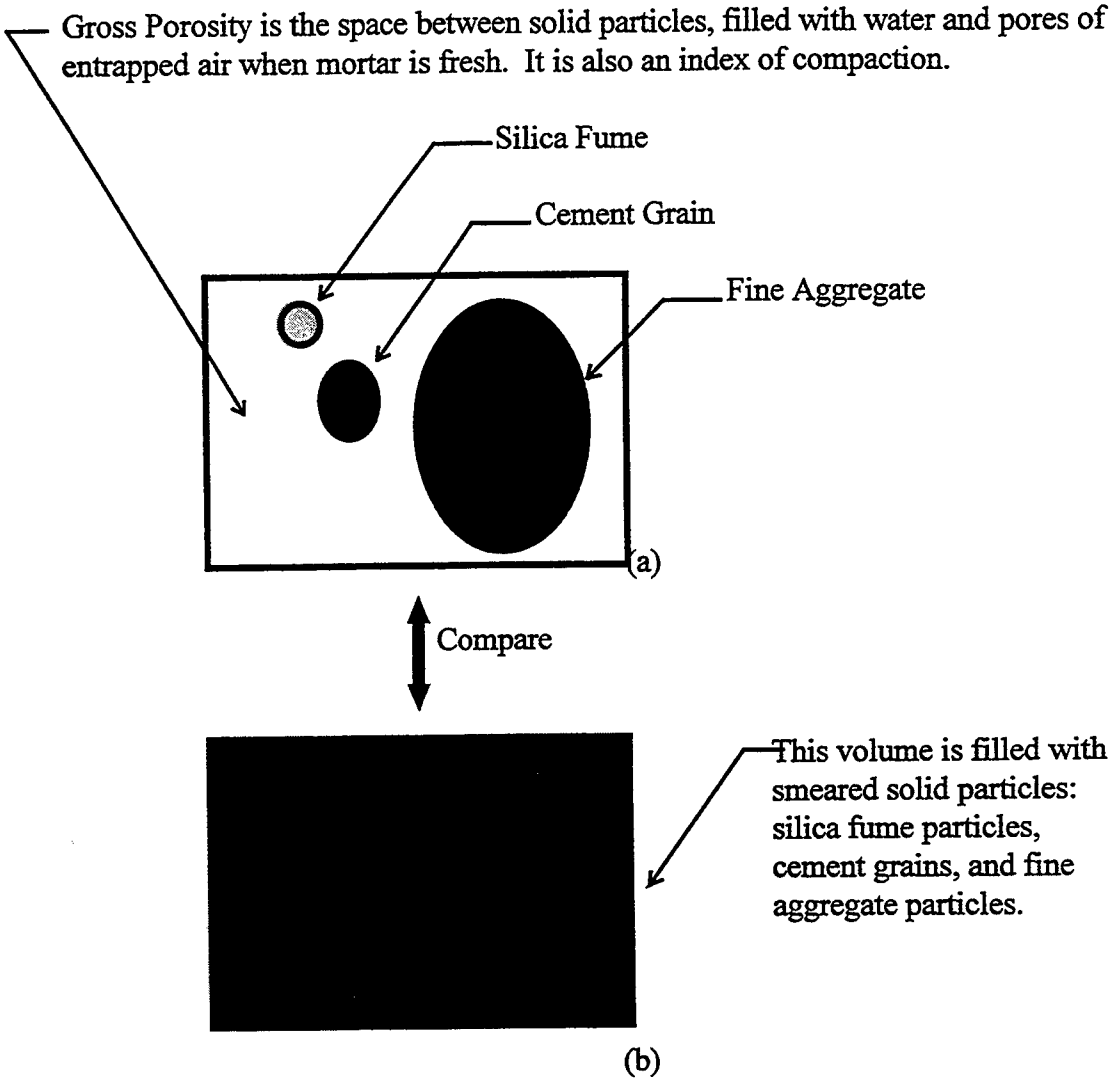

Figure 4.1 Gross Porosity acts as an Index of Compaction

W_{merged} is the net mass of specimen immerged in water, and
D_W is density of water.

Subtracting the mass expressed by Figure 4.1(a) (W_{SSD}) from that expressed by Figure 4.1(b) (W_S), it is the mass difference between the voids are filled with smeared solid particles and they are filled with water. Thus, the volume of voids in Figure 4.1(a) (V_{void}) can be determined as

$$V_{void} = \frac{W_S - W_{SSD}}{D_S - D_W} \tag{4.3}$$

where W_S is the mass of bulk volume of specimen, which is virtually filled with the smeared solid particles only. $W_S = D_S \times V_{bulk}$.

In this derivation, the minor effect of entrapped air is neglected. Eventually, the gross porosity is derived as

$$Gross \cdot Porosity = \frac{V_{void}}{V_{bulk}} = \frac{D_S \times V_{bulk} - W_{SSD}}{(D_S - D_W) \times V_{bulk}} \tag{4.4}$$

The gross porosity is good for representing the volume of voids filled with water inside a very fresh specimen. For a hydrated specimen, the porosity obtained this way may not reflect a real condition. This is because the voids are filled with hydration products due to the chemical reaction of cement grains and silica fume particles.

In fact, this gross porosity is closely related to the compaction condition of solid particles in a fresh specimen. If the gross porosity is large, the solid particles are relatively far apart from each other. On the other hand, if the gross porosity is small, the solid particles are closer to each other.

4.2.2 Dynamic Modulus of Elasticity and Dynamic Shear Modulus

Most of the dynamic moduli were measured by using Grindo-Sonic MK4 sonometer in accordance with a resonant frequency method. A description of the resonant frequency method was reported by Malhotra and Sivasundaram [1991]. In this

method, the mortar specimen is struck lightly with a small hammer. The impact causes the specimen to vibrate at its natural frequencies. The amplitude and frequency of the resonant vibrations are obtained by using a waveform spectrum analyzer that determines the component frequencies via the fast Fourier transform. The fundamental resonance frequency can be read directly from the instrument. This method is considered by ASTM as an alternate to ASTM C-215, "Test Method for Fundamental Transverse, Longitudinal, and Torsional Frequencies of Concrete Specimens". The advantages of this method over the forced resonance procedure in ASTM C-215 are the greater speed of testing and the capability of testing specimens having a wide range of dimension.

In this study, the dynamic modulus of elasticity was measured in flexural and longitudinal modes. The dynamic shear modulus was determined by measuring in torsional mode. The support of specimen for each kind of mode is in accordance with ASTM C-215. The moduli are calculated in accordance with the formula proposed by Spinner and Tefft [1961]. For the flexural mode, the dynamic modulus of elasticity is calculated by

$$E = 0.9464\frac{\rho l^4 f^2 T}{b^2} \tag{4.5}$$

$$T \cong 1 + 6.585(1 + 0.0752\nu + 0.8109\nu^2)\frac{b^2}{l^2} \tag{4.6}$$

where ρ is bulk density of the material,
l is length of the specimen,
f is fundamental resonance frequency,
b is cross section dimension in the direction of vibration,
ν is Poisson's ratio, and
T is correction factor.

For the longitudinal mode, the dynamic modulus of elasticity is calculated by

$$E = \frac{4\rho l^2 f^2}{K} \tag{4.7}$$

$$K \cong 1 - \frac{\pi^2 \nu^2 b^2}{6l^2} \tag{4.8}$$

For the torsional mode, the dynamic shear modulus is calculated by

$$G = 4\rho l^2 f^2 R \tag{4.9}$$

$$R \cong 1.1856(1 + 0.019\frac{b^3}{l^3}) \tag{4.10}$$

Another method used to measure the dynamic moduli is the ultrasonic pulse velocity method. This method was discussed by Naik and Malhotra [1991]. A portable and simple V-Meter manufactured by James Instrument was applied. The calculation of dynamic modulus of elasticity was proposed by Naik [1979] as

$$E = \frac{V_l^2 \rho}{[\frac{1}{3(1-2\nu)} + \frac{2}{3(1+\nu)}]} \tag{4.11}$$

where V_l $(= l/t)$ is the longitudinal velocity, and
t is the measured travel time of ultrasonic pulse.

4.2.3 Logarithmic Decrement of Damping

The logarithmic decrement of damping (δ) was measured by using the CE2622 Geotest Sonometer with Oscilloscope. A description of this method was reported by Malhotra and Sivasundaram [1991]. In reference to Figure 4.2, δ is defined as

$$\delta = \pi/Q$$

where Q = fo/(fb - fa) is defined as the damping factor,
fo is the resonant frequency, and
fa and fb are the frequencies on either side of resonance at which the amplitude is 0.707 times the amplitude at resonance.

The logarithmic decrement of damping was also measured in flexural, longitudinal, and torsional modes. The support of the specimen was also in accordance with ASTM C-215.

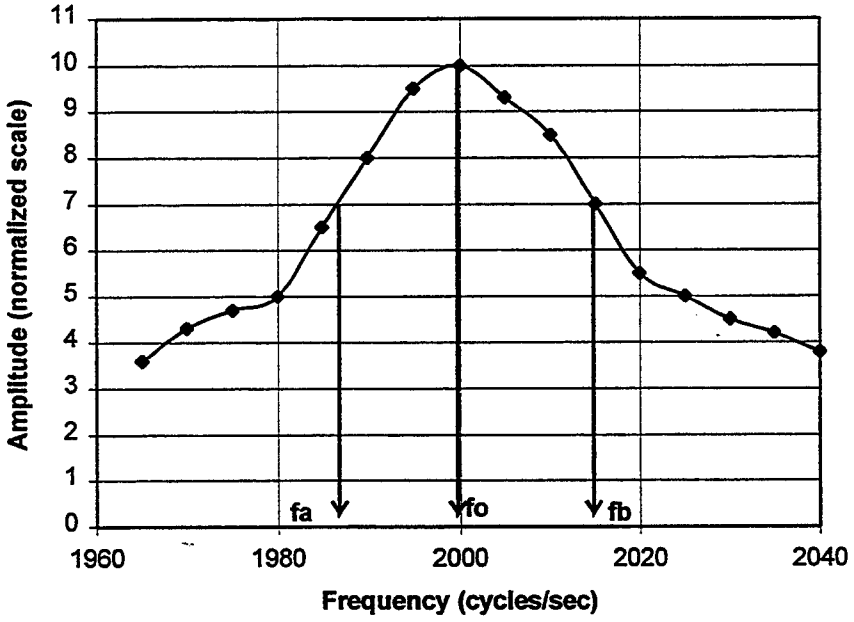

Figure 4.2 Logarithmic Decrement of Damping is calculated from Resonance Curve. fo is the resonant frequency. fa and fb are the frequencies on either side of resonance at which the amplitude is 0.707 times the amplitude at resonance.

4.2.4 Flexural Tensile Strength and Compressive Strength

The flexural tensile strength test and the compressive strength test were performed on SSD specimens at 56 days. The flexural tensile strength test was in accordance with ASTM C-78, "Standard Test Method for Flexural Strength of Concrete (Using Simple Beam with Third-Point Loading)," with a loading rate that constantly increases the extreme fiber stress to 125 psi/min. The specimen size was 4 in. × 1 in. × 1 in. A schematic view of support of specimen is shown in Figure 4.3. The compressive strength test was performed on one-inch cubes with a loading rate of 35 psi/sec. The purpose of controlling the loading rate was to make sure that the test was under a quasi-static loading condition.

4.3 Microstructural Study

The microstructural study applied the techniques of MIP and SEM. These experiments were performed on 56 days old mature specimens. The original prism specimens were cut by a diamond saw to avoid the artificial cracks. The sliced individuals were then immersed in acetone. The purpose was to stop hydration in the specimens and to reduce the vapor pressure in order to prevent the unnecessary cracks during the subsequent drying process. Then, the individual samples were oven-dried at 105°C, which is a necessary process in preparing the experimental specimens for the apparatus used. At this stage, the specimens for MIP experiment were ready.

However, some further manipulations are needed for preparing SEM specimens. The dry specimens were then inserted into a plastic mode and impregnated in ultra-low viscosity epoxy mixture, evacuated, and oven-cured at 80°C for 24 hours, then demolded. The hardened, impregnated specimens were again sliced and the surface to be examined was polished using successively finer grades of diamond grit from 45 μm down to 15 μm. Final polishing is delicately conducted by using 3 μm and 1 μm impregnated diamond cloth in order to properly reveal the information of the polished surface. Afterward, the polished surfaces of the specimens was coated with Palladium for two minutes in a chamber evacuated to 100 millitorr.

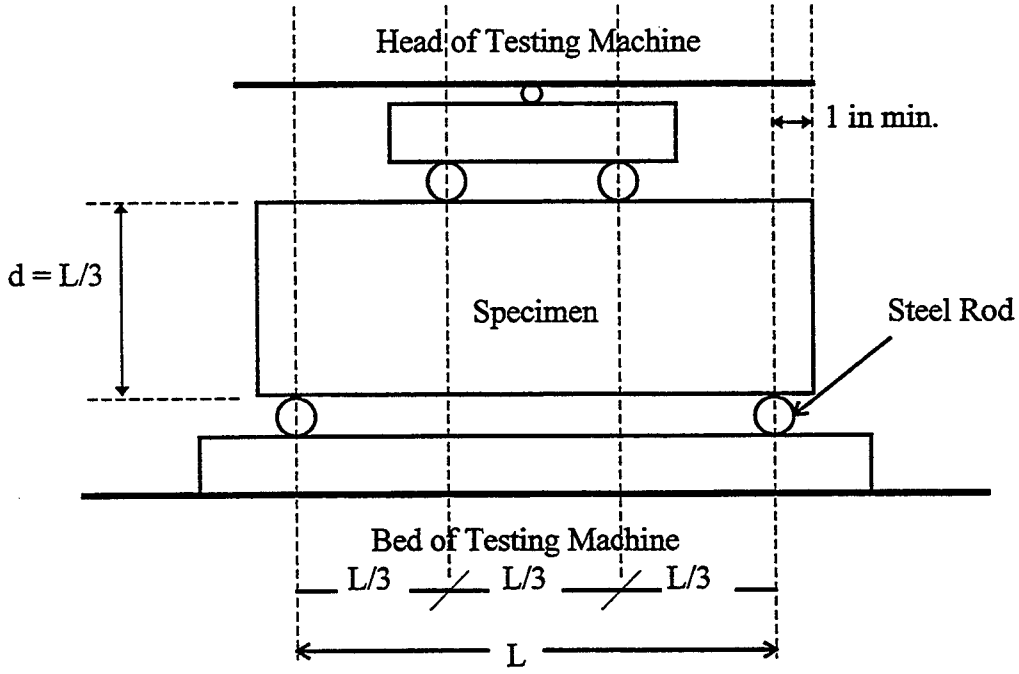

Figure 4.3 A Schematic View of Simple Beam with Third-Point Loading Method.

4.3.1 Mercury Intrusion Porosimetry (MIP)

MIP was performed by using the Micromeritics Autopore II 9220. This apparatus is capable of a minimum intruding pressure of 20 torr (mmHg), and a maximum of 414 MPa (60,000 psi). The contact angle of mercury on cement paste was assumed to be 130°. Thus, in accordance with the Washburn equation:

$$d = \frac{-4\gamma \cos\theta}{P} \tag{4.12}$$

where d is the diameter of pores,
γ is surface tension of mercury (480 dyne/cm),
θ is contact angle, and
P is pressure of intrusion,

the corresponding range of intruded pore diameters was between 0.04 cm and 25 Angstrom.

4.3.2 Scanning Electron Microscopy (SEM)

The microstructural features and cracks patterns were investigated through the Backscatter Electron Image (BEI) of SEM. The SEM study in this research was performed by using an Akashi Beam Technology 55A SEM, which was operated at 15 KeV and equipped with a GW Electronics 30-A backscatter detector and a Tracor Northern 5505 EDS system. In addition, this SEM apparatus was also coupled to both Princeton Gamma Tech. IMIX Version 7 image analysis system and Quartz PCI image manipulation software.

The BEI micrographs were used to study two objects. One was the pore image of the mortar specimen, and the other was the pattern of tensile cracks in the broken specimen. Special attention was given to the image characteristics of transition zones. The specimens were broken by applying the method as ASTM C-496, "Standard Test Method for Splitting Tensile Strength of Cylindrical Concrete Specimens". Thus, the cracks shown in the BEI micrograph are mainly the tensile cracks.

4.4 Comparison of Degree of Hydration Using Loss-on-Ignition (LOI) Data

One way to compare the degree of hydration within mortar specimens is to compare the mass of non-evaporable water in unit mass of 105 °C oven dry mortars. If the data shows a larger value, the non-evaporable water is more abundant in a unit mass of specimen. Thus, the degree of hydration is higher. On the other hand, if the data shows a smaller value, the degree of hydration is lower. The non-evaporable water content can be determined by measuring the mass loss of the mortar specimen from the end of a 105 °C oven dry treatment to the end of a 1050 °C ignition process. The ignition process was maintained for 40 minutes in this LOI experiment, and the mass of specimens used varied from 1.9 grams to 4.7 grams.

Because dolomite can be dedolomizated beneath 1050 °C, the mass of evaporated carbon dioxide is also counted in the LOI data for dolomite mortars. Consequently, if the LOI data of dolomite mortars are used for comparison, the Va must be kept the same as possible for each specimen. Thus, each LOI data includes the same mass of carbon dioxide. As a result, the difference between the LOI data represents the difference of mass of non-evaporable water in unit mass of specimens.

CHAPTER 5

RESULTS AND DISCUSSION 1: MIXING AND COMPACTION PROBLEMS

The results of this research are divided into three categories. In the first category, a criterion to identify the specimens that show mixing and compaction problems was established. This was achieved by varying SA in the specimens and studying the trends in dynamic moduli, tensile strength, compressive strength, gross porosity, and density, accompanied with SEM investigation of polished specimens. For several critical conditions, the average thickness of water film for individual fraction of aggregate size was calculated, and a criterion was developed for identifying the starting of mixing and compaction problems. This procedure will allow removal of the data of samples that had mixing and compaction problems. In the second category, the development of a theoretical model used to interpret dynamic moduli data of this research is presented. One of the limitations of this proposed theoretical model is also discussed. In the third category, the mechanical properties of interfacial transition zones are presented. The effects of silica fume and aggregate type on mechanical properties of transition zones are discussed. In addition, the influence of percolation of transition zones on mechanical properties of specimens is investigated as well.

5.1 Introduction

This chapter discusses issues related to identification of mixing and compaction problems. These problems can be detected by varying Va in the mortar specimens and observing the change of trends in dynamic moduli, tensile strength, compressive strength, and bulk density of the mortars. In addition, a higher gross porosity was observed when the mixing and compaction problems occurred in the specimen. By analyzing the BEI

micrographs of polished specimens, SEM investigation reveals the micro mechanism that causes the mixing and compaction problems.

Based on the average thickness of water film that virtually coats the aggregate surface, a criterion is established to judge whether a specimen has mixing and compaction problems or not. Further, an optimum water content for the mixture proportioning can be estimated from this criterion. This information may help in determining the lowest possible W/C that can be used without resulting in mixing and compaction problems in the specimens. This is useful information in designing high-strength concrete since W/C used tends to be as low as possible for high-strength concrete.

5.2 Abnormal Change of Trends in Dynamic Moduli

Usually, if the Va in the mortar increases, the elastic moduli of the mortar increase too. However, some researchers [Ishai 1961, Hansen 1965, and Swamy and Rigby 1971] obtained the experimental results and suggested that when the Va increases beyond the 0.52 - 0.60 range, the elastic moduli decrease rapidly.

In order to evaluate the moduli-decrease mechanism, an experiment was designed to investigate the relationship between dynamic moduli and Va. Five fractions of aggregate were used for the mortar specimens. Each specimen contained a single fraction of aggregate size. The results of dynamic modulus of elasticity are shown in Figure 5.1, and that of dynamic shear modulus are shown in Figure 5.2. These figures show that the decrease of elastic moduli may not only depend on Va, but may also depend on aggregate size. The moduli of mortars made of finer sand drop at a relatively lower Va, while the moduli of mortars made of coarser sand drop at a higher Va. For instance, the moduli of mortar containing aggregate size #50~#100 start to drop at point A. Its corresponding Va is 0.40. For the mortar containing aggregate size #4~#8, the drop happens at point D with a corresponding Va of 0.55. In other mixtures, the critical point C is corresponding to Va=0.50 for the mortar containing aggregate size #8~#16, and the critical point B is corresponding to Va=0.45 for the mortar containing aggregate size #30~#50. The mortar containing aggregate size #16~#30 does not show an apparent peak on either dynamic

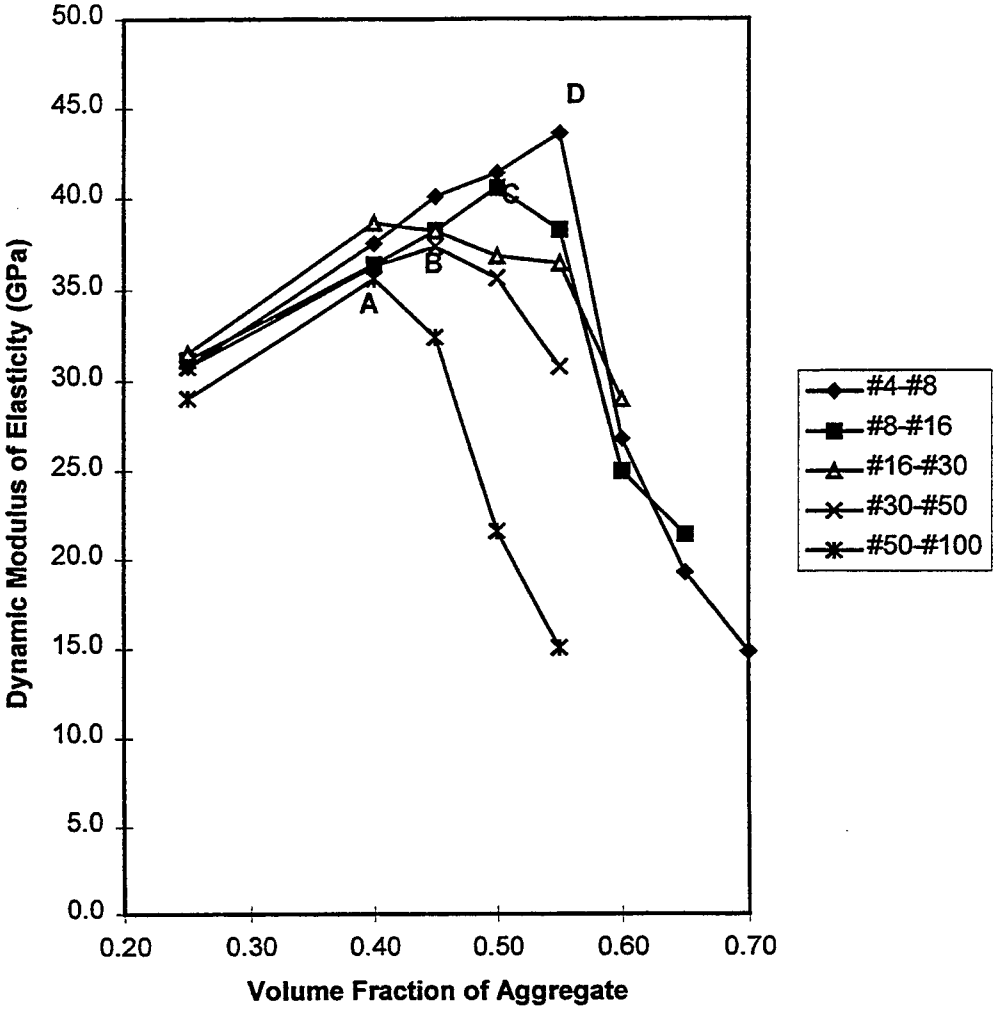

Figure 5.1 Dynamic Modulus of Elasticity vs. Va for dolomite mortars at 28 days old having one of five fractions (ASTM sieve no.: #4~#8, #8~#16, #16~#30, #30~#50, and #50~#100) of aggregate size and W/C=0.42.

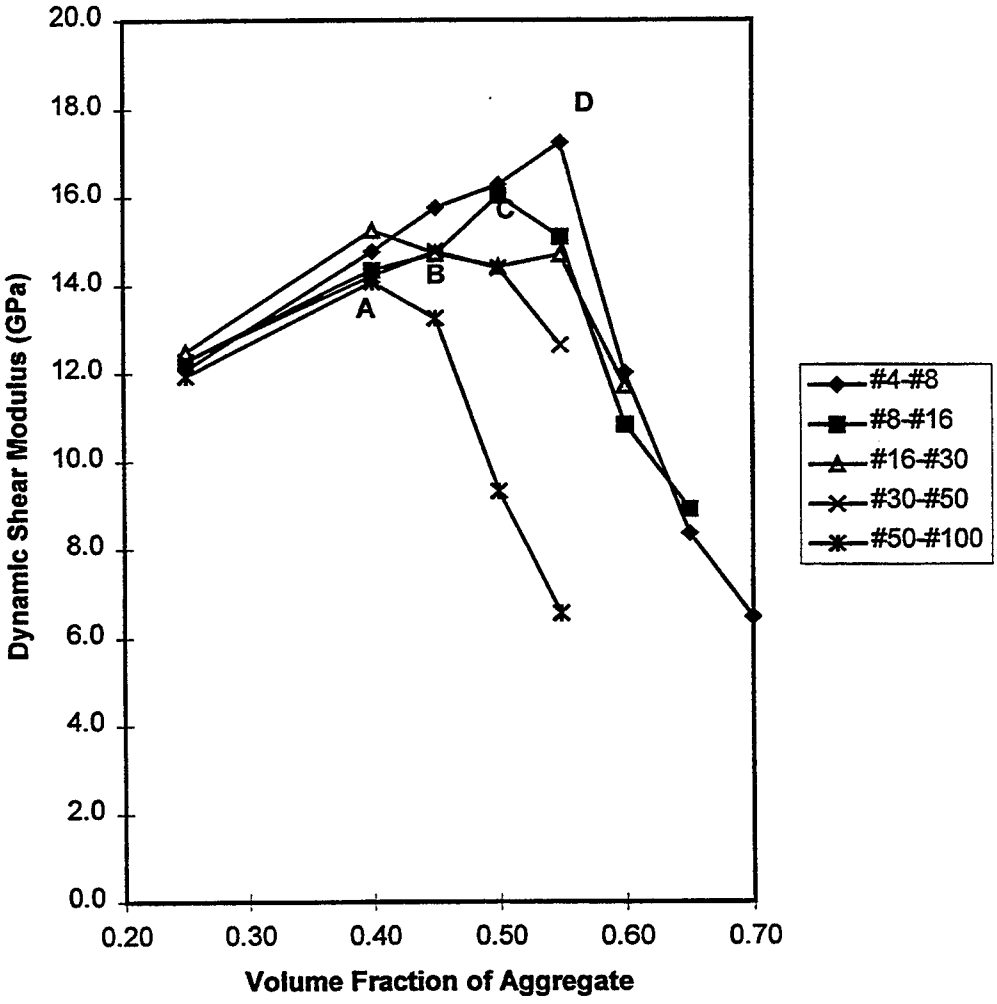

Figure 5.2 Dynamic Shear Modulus vs. Va for dolomite mortars at 28 days old having one of five fractions (ASTM Sieve No.: #4~#8, #8~#16, #16~#30, #30~#50, and #50~#100) of aggregate size and W/C=0.42.

modulus of elasticity or dynamic shear modulus. Thus, the critical points selected for further analysis were these marked as A, B, C, and D.

5.3 Abnormal Change of Trends in Tensile Strength and Compressive Strength

The graphs of tensile strength and compressive strength vs. SA are presented in Figures 5.3 and 5.4 respectively. The trends in these graphs are similar to that of dynamic elastic moduli vs. SA. Points A, B, C, and D in Figures 5.3 and 5.4 correspond to the critical points A, B, C, and D in Figures 5.1 and 5.2 respectively. It is observed that these four points are not only the critical points for dynamic moduli, but also are the critical points for tensile strength and compressive strength. Thus, it can be inferred that perhaps similar mechanisms are responsible for the unique behavior of the specimens in losing their moduli and strengths.

5.4 Abnormal Change of Trends in Gross Porosity and Bulk Density

Figures 5.5 and 5.6 show the graphs of gross porosity and SSD bulk density vs. Va respectively. Points A, B, C, and D in Figures 5.5 and 5.6 correspond to the critical points A, B, C, and D in Figures 5.1 and 5.2 respectively. It is observed that these four points are also the critical points in the graphs of gross porosity and SSD bulk density. The SSD bulk density shows the same trend as the dynamic elastic moduli, while the gross porosity presents an inverse trend. It is known that more compacted and less porous means denser and denser material usually behaves stiffer.

The reason why these critical points exist may be explained by the analysis of BEI micrographs of the SEM samples below.

5.5 Microscopic Image Analysis

Three samples, containing Va=0.25, 0.45, and 0.55, were prepared for SEM study. All have the same W/C of 0.42 and aggregate size #50~#100. After cutting the prismatic specimens for making SEM samples, many dark blue spots were observed on the

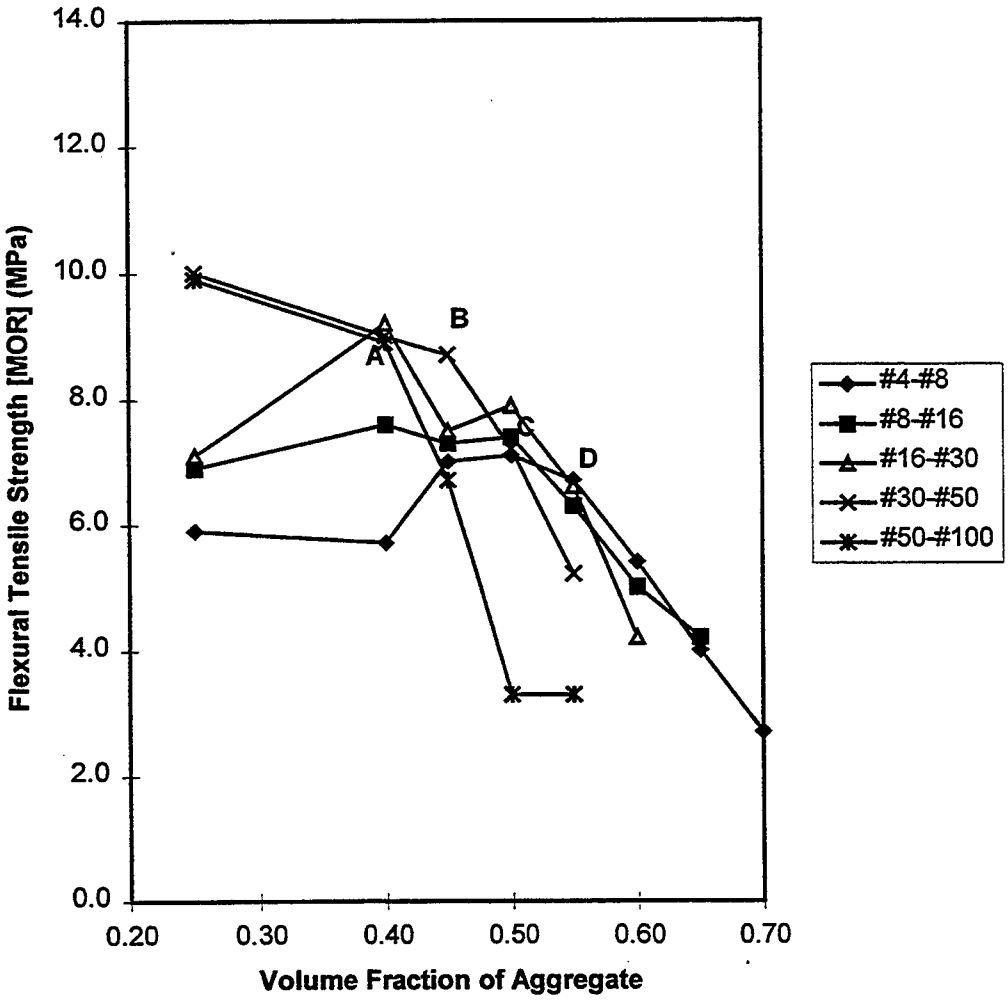

Figure 5.3 Flexural Tensile Strength vs. Va for dolomite mortars having one of five fractions (ASTM sieve no.: #4~#8, #8~#16, #16~#30, #30~#50, and #50~#100) of aggregate size and W/C=0.42.

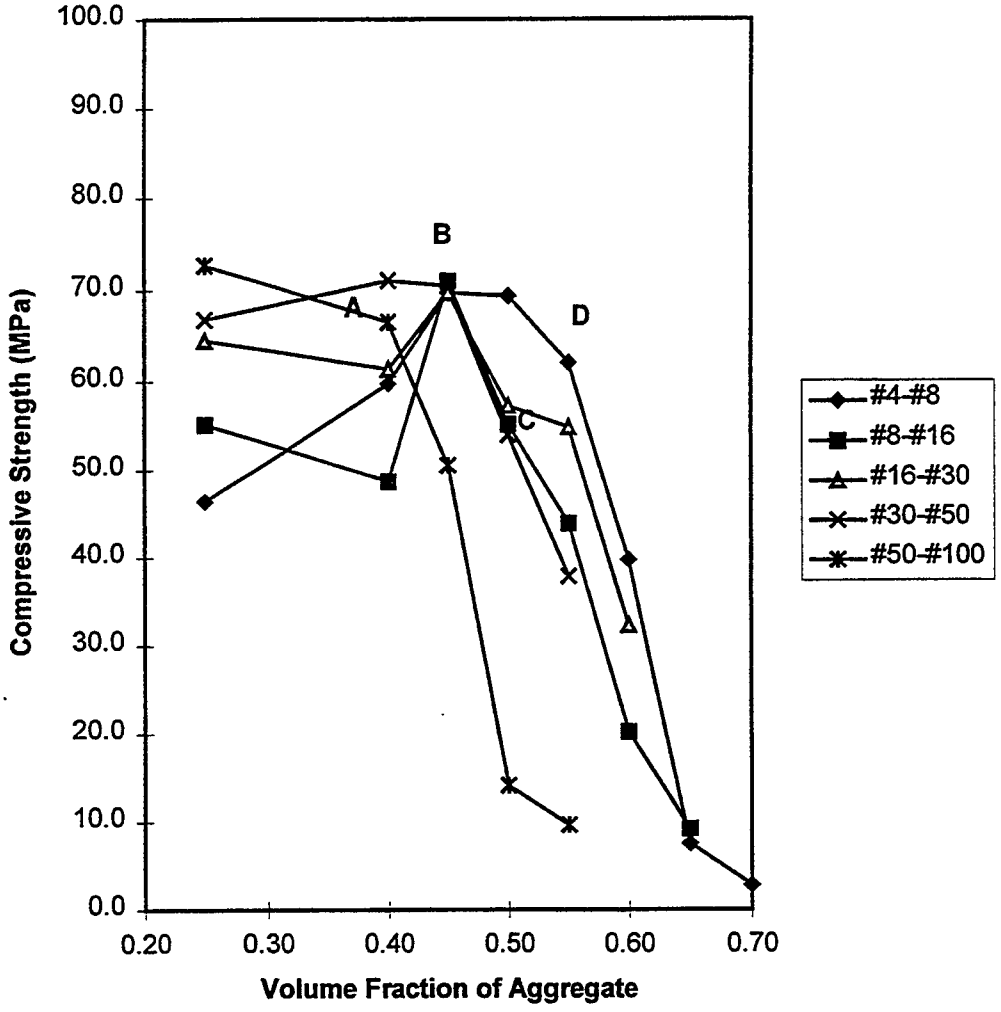

Figure 5.4 Compressive Strength vs. Va for dolomite mortars having one of five fractions (ASTM sieve no.: #4~#8, #8~#16, #16~#30, #30~#50, and #50~#100) of aggregate size and W/C=0.42.

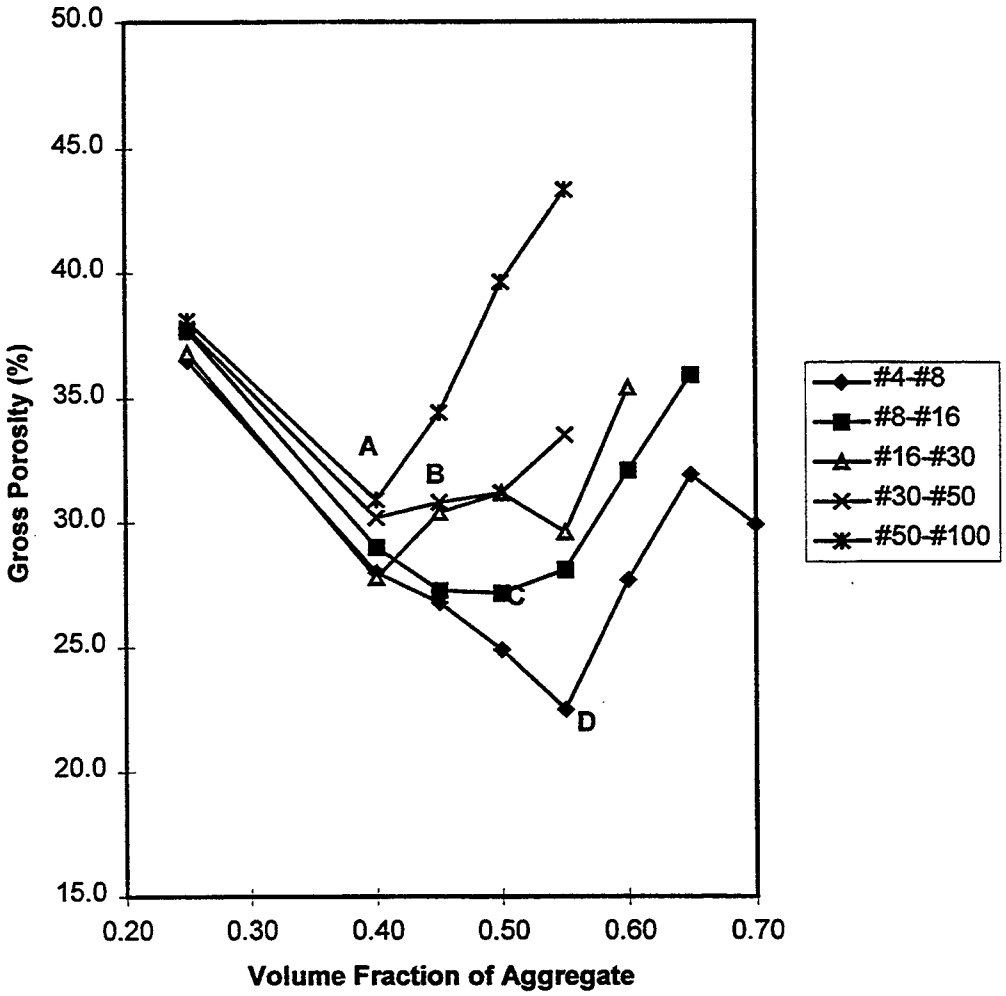

Figure 5.5 Gross Porosity vs. Va for dolomite mortars having one of five fractions (ASTM sieve no.: #4~#8, #8~#16, #16~#30, #30~#50, and #50~#100) of aggregate size and W/C=0.42.

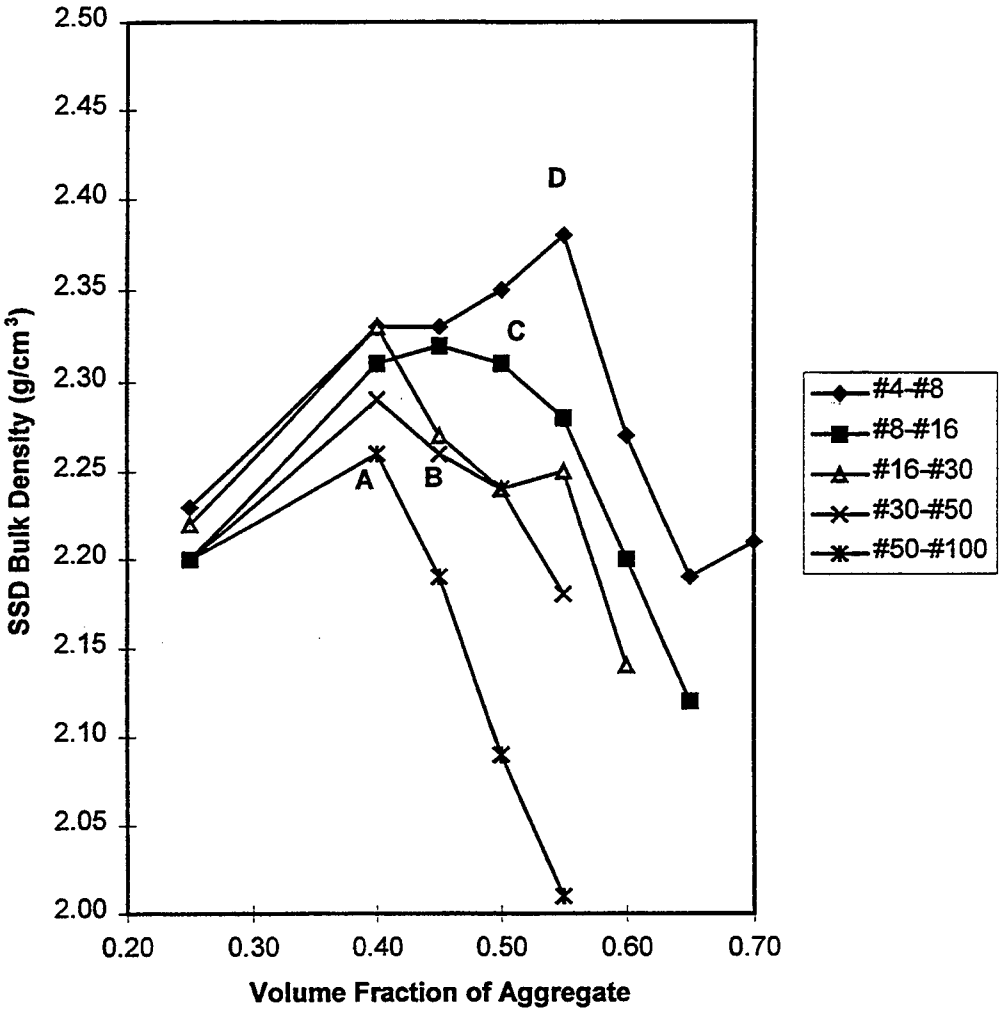

Figure 5.6 Saturated Surface Dry Bulk Density vs. Va for dolomite mortars having one of five fractions (ASTM sieve no.: #4~#8, #8~#16, #16~#30, #30~#50, and #50~#100) of aggregate size and W/C=0.42.

profile of the specimen with Va=0.55. For the specimen with Va=0.45, the dark blue spots were less intense, although they still could be recognized.

After the investigation of SEM, the secrets that cause the trends' alternation in moduli, strength, porosity, and density were gradually revealed. Figure 5.7 shows the BEI micrograph of dolomite mortar made of aggregate size #50~#100, magnification 60×, and mixture proportion 55_42_00. The first two digits in the mixture proportion represent the volume fraction of aggregate in hundredths. The second two digits represent W/C in hundredths as well. The third two digits are the percentage of cement weight substituted by silica fume. Judging from this micrograph, it is known that the dark blue spots in the specimen are the agglomerated cement grains. Taking a closer look at the cement cluster shown in Figure 5.8 with magnification 500×, it can be seen that there is no shell-like hydration product surrounding the unhydrated cement grains. Thus, the hydration process here may be somewhat abnormal. Because cement grains could not be dispersed and mixed well with aggregate particles, a large void space was observed between aggregate particles. A high gross porosity of the specimen was therefore measured. In addition, the bonding between aggregates was weak due to lack of paste. Thus, the values of dynamic moduli, tensile strength, and compressive strength become low. In the mortar with Va=0.45, the phenomenon of agglomerated cement grains and pores is not so crucial as that in the mortar with Va=0.55. However, this phenomenon still can be found. For instance, the phenomenon of agglomerated cement grains can be observed in Figure 5.9, and the phenomenon of agglomerated pores can be found at the bottom of Figure 5.10. Comparison of the BEI micrographs of mortars containing Va=0.55 and 0.45 with that of mortar containing Va=0.25 shown in Figure 5.11 indicates that the latter has a more normal image of mixture.

Three other samples, containing Va=0.25, 0.50, and 0.65 respectively, were also prepared and studied by SEM. All have the same W/C 0.42 and aggregate size #8~#16.

The phenomenon of agglomerated cement grains and pores was again observed in the samples with Va=0.65 shown in Figure 5.12. Moreover, large pores were also observed in Figure 5.13. While for the samples with Va=0.50 and 0.25, the BEI

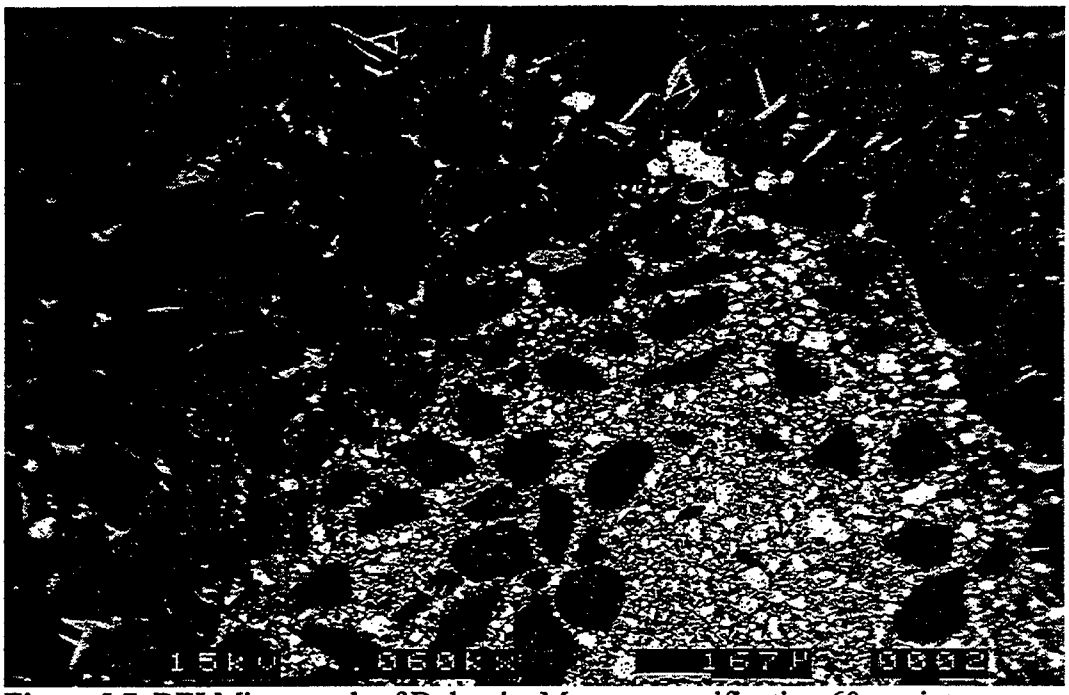

Figure 5.7 BEI Micrograph of Dolomite Mortar, magnification 60×, mixture proportion 55_42_00, aggregate size #50~#100.

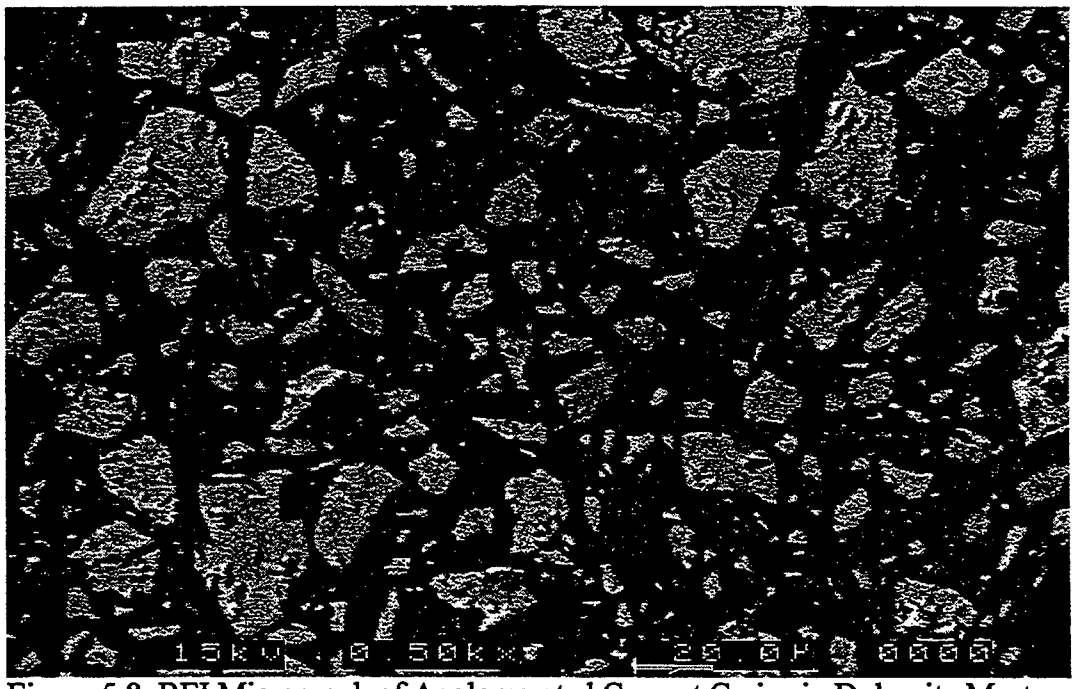

Figure 5.8 BEI Micrograph of Agglomerated Cement Grains in Dolomite Mortar, magnification 500×, mixture proportion 55_42_00, aggregate size #50~#100.

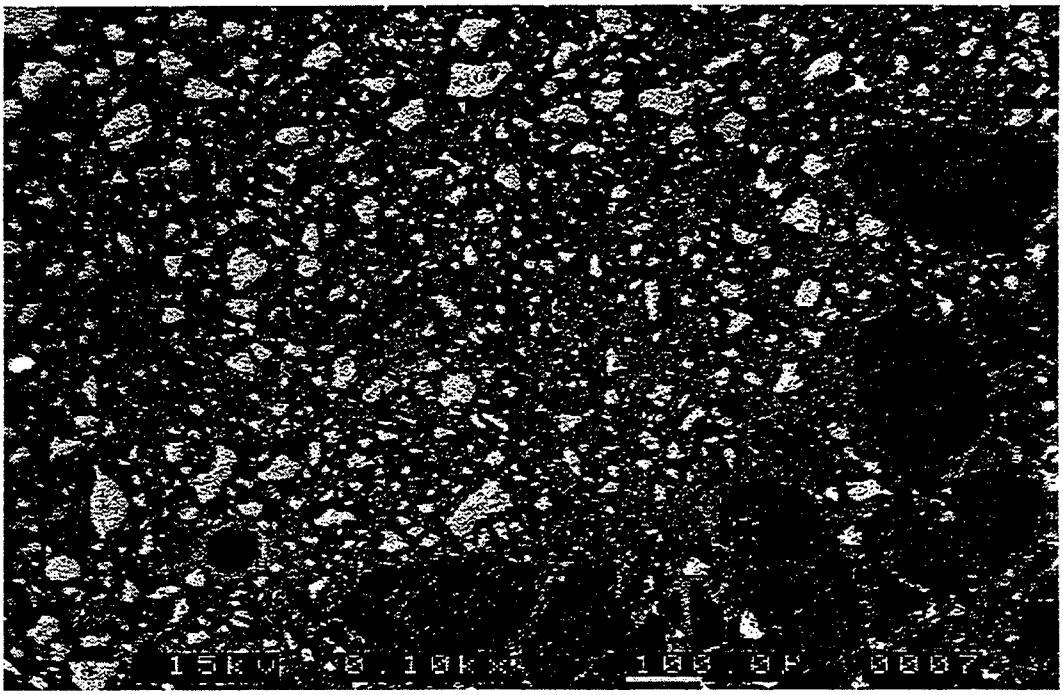

Figure 5.9 BEI Micrograph of Agglomerated Cement Grains in Dolomite Mortar, magnification 100×, mixture proportion 45_42_00, aggregate size #50~#100.

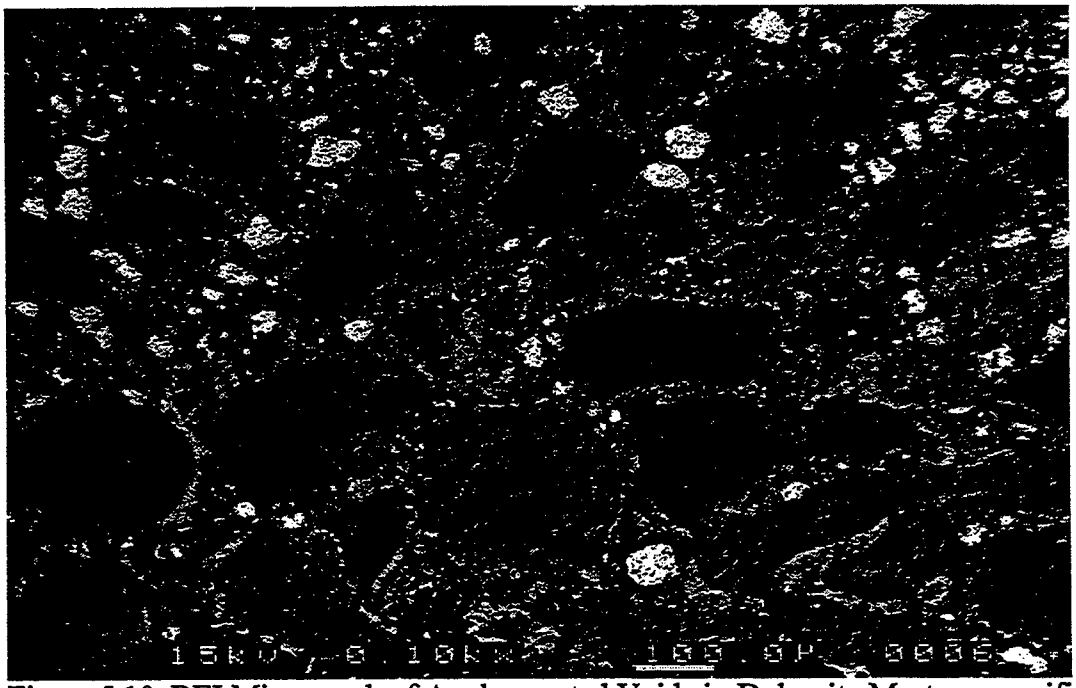

Figure 5.10 BEI Micrograph of Agglomerated Voids in Dolomite Mortar, magnification 100×, mixture proportion 45_42_00, aggregate size #50~#100.

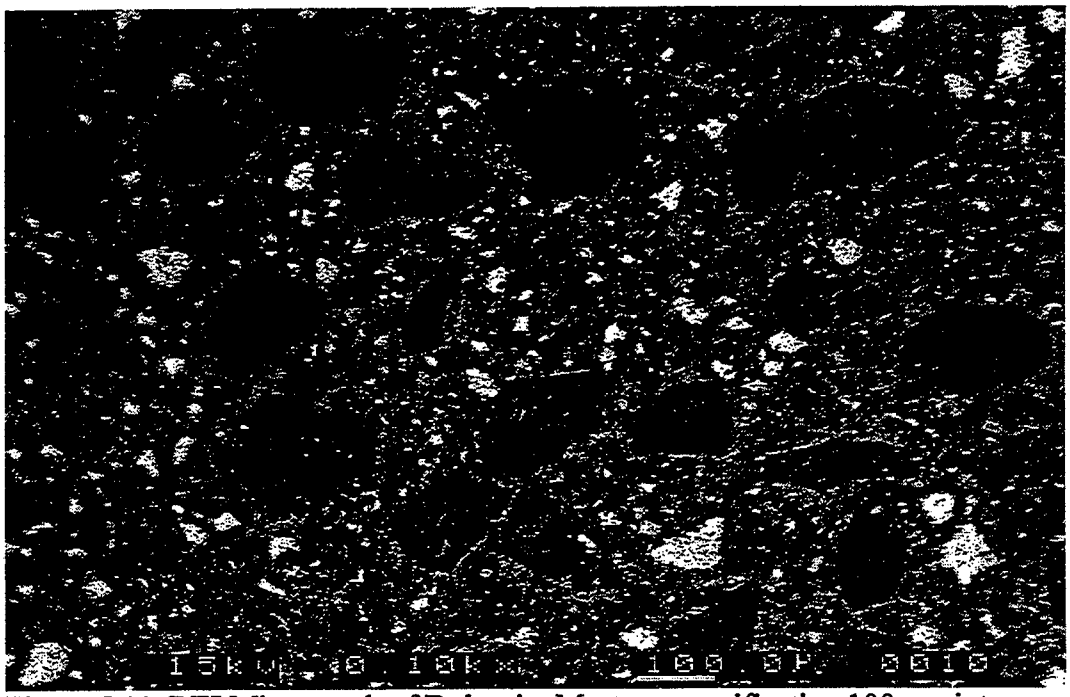

Figure 5.11 BEI Micrograph of Dolomite Mortar, magnification 100×, mixture proportion 25_42_00, aggregate size #50~#100.

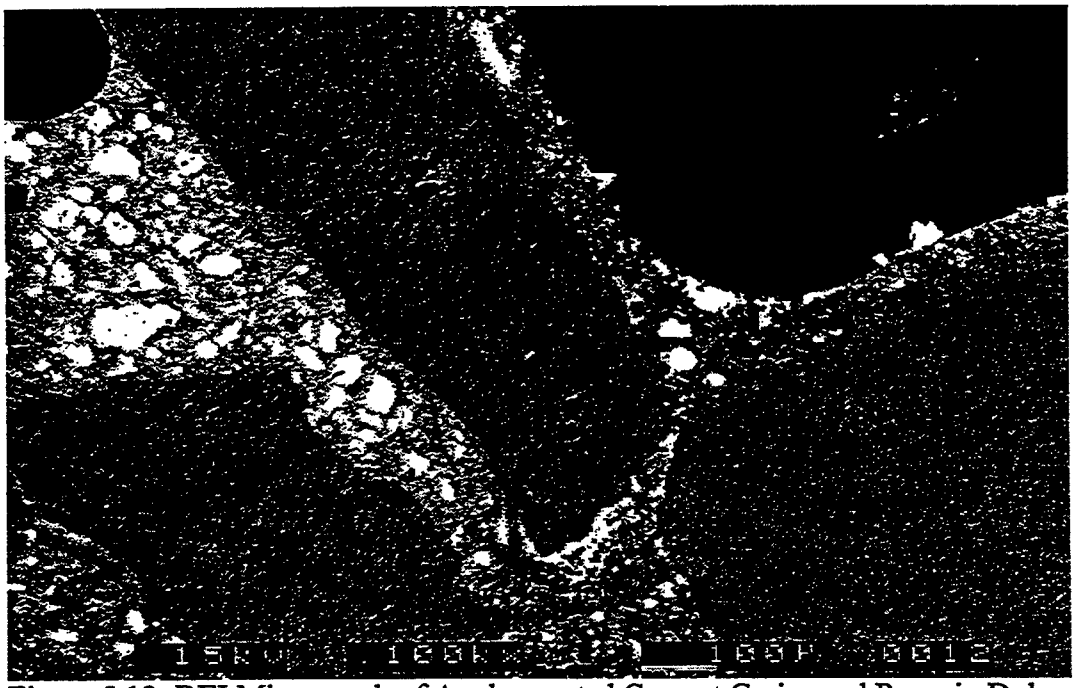

Figure 5.12 BEI Micrograph of Agglomerated Cement Grains and Pores in Dolomite Mortar, magnification 100×, mixture proportion 65_42_00, aggregate size #8~#16.

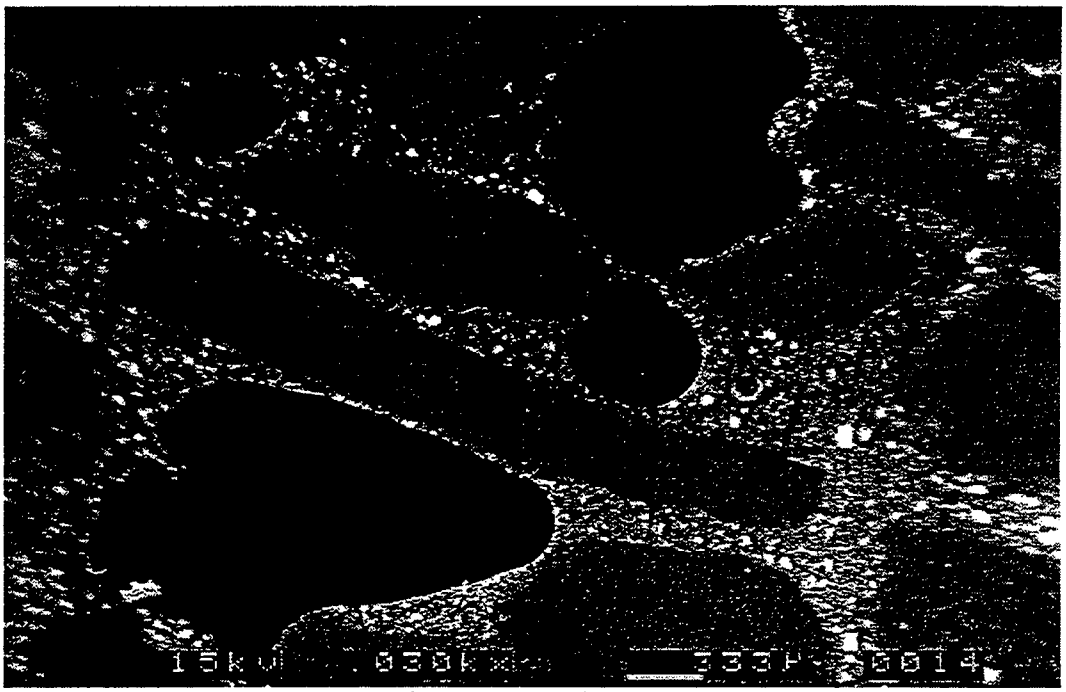

Figure 5.13 BEI Micrograph of Large Pores in Dolomite Mortar, magnification 30×, mixture proportion 65_42_00, aggregate size #8~#16.

micrographs show that they are normal mixtures as can be seen from Figures 5.14 and 5.15. However, some agglomerated small pores can be observed in some portions, especially within transition zones as shown in Figures 5.16 and 5.17.

In summary, because cement grains become agglomerated and cannot be effectively dispersed and mixed well with aggregates, the gross porosity is high and the dynamic moduli and strengths are low. The factor responsible for the cement grains to be agglomerated is closely related to the water availability for cement grains, because when Va increases, the total surface area of aggregate increases too. Thus, more water is held on the surface of the aggregate during mixing. If there is sufficient water to fill the voids between solid particles during casting, the mixture is normal. Under this condition, the W/C in the bulk paste is still the same as the designated one in mixture proportioning. However, if SA in the mortar increases beyond a critical value, an abnormal mechanism may begin to occur, which is discussed below. The solid grains have the higher priority to acquire water on their surface. Consequently, if the aggregate surface is increased, less water will remain for cement grains to participate by hydration. Under this condition, W/C of the bulk paste will be less than the designated value in mixture proportioning. Although near the aggregate surface the local W/C may be higher than the designated one in mixture proportioning, the overall W/C of paste including bulk paste and transition zones may show a lower value than that in the mortar with SA below the critical value. This concept may be explained by the data of LOI below.

5.6 LOI and W/C of Paste

The LOI shown in Figure 5.18 is the sum of non-evaporable water kept in hydrated cement and loss of carbon dioxide in dolomite due to dedolomization. Each point stands for the average value of three specimens' data. Since the volume of aggregate is kept constant, the loss of carbon dioxide is regarded as the same for all specimens. Thus, the difference in LOI data is due to the difference of loss of non-evaporable water. Less LOI means less non-evaporable water, and therefore a lesser

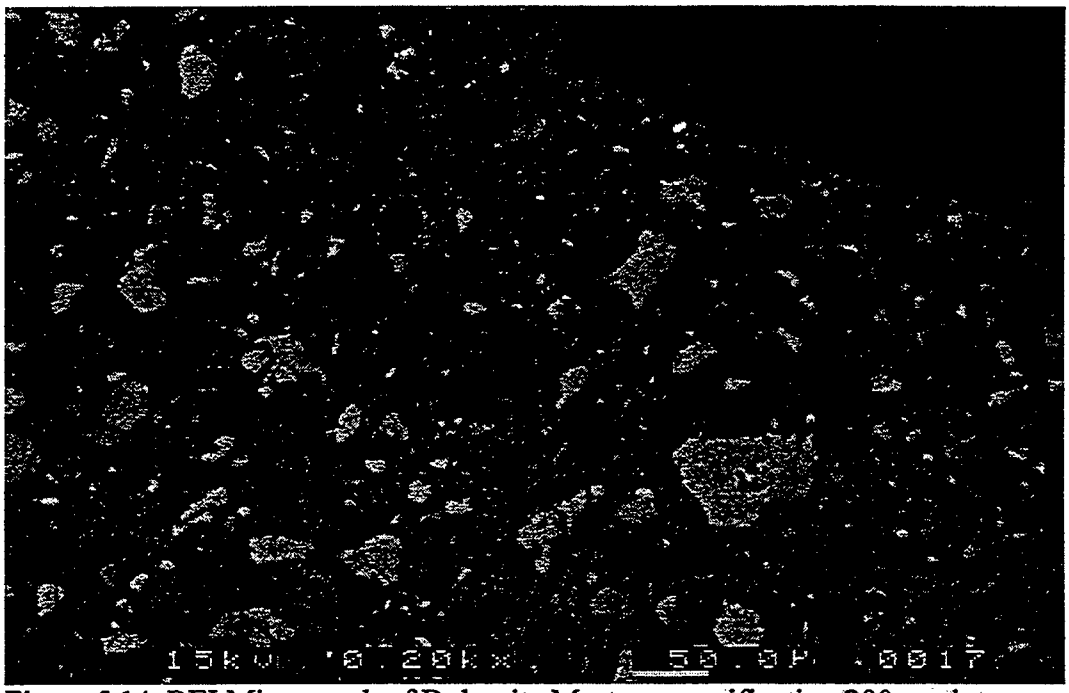

Figure 5.14 BEI Micrograph of Dolomite Mortar, magnification 200×, mixture proportion 50_42_00, aggregate size #8~#16.

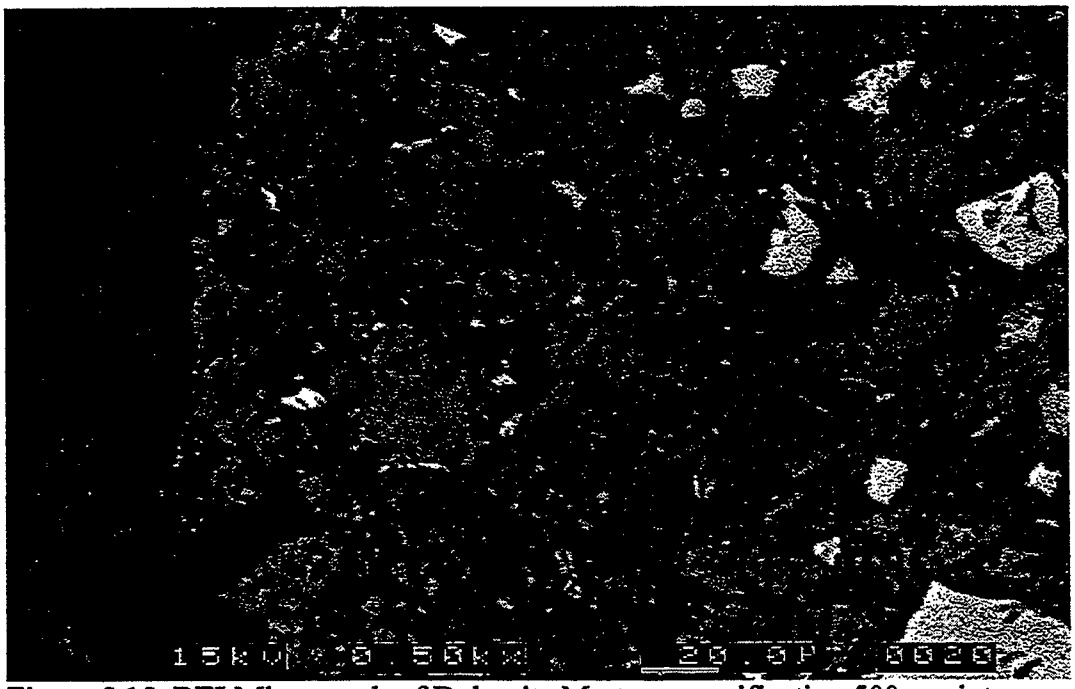

Figure 5.15 BEI Micrograph of Dolomite Mortar, magnification 500×, mixture proportion 25_42_00, aggregate size #8~#16.

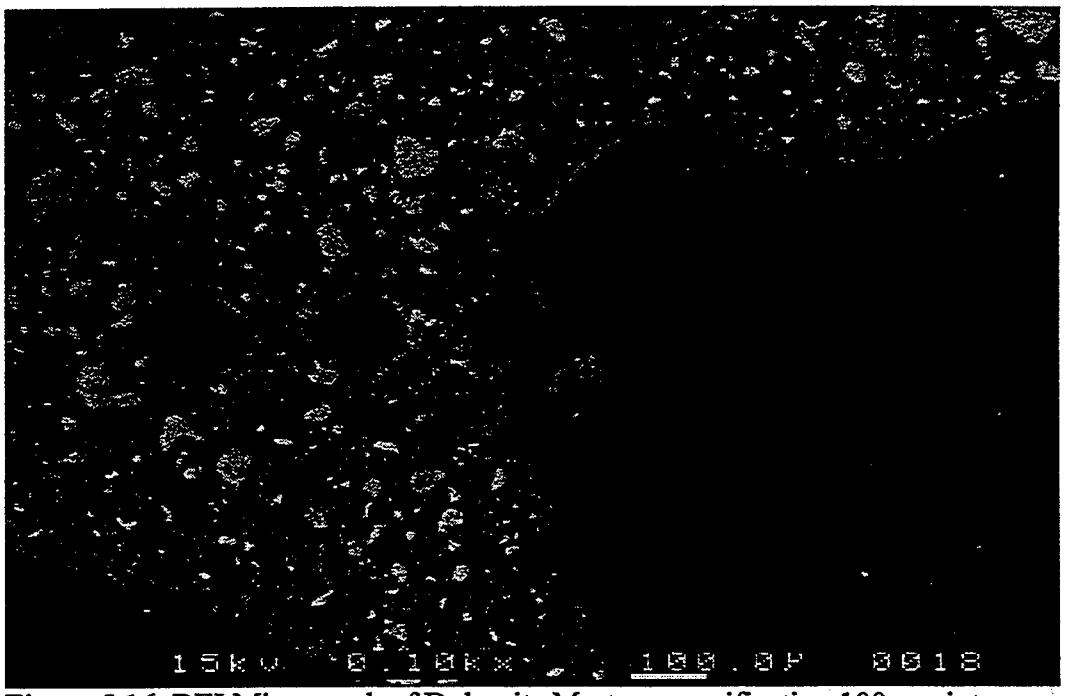

Figure 5.16 BEI Micrograph of Dolomite Mortar, magnification 100×, mixture proportion 50_42_00, aggregate size #8~#16.

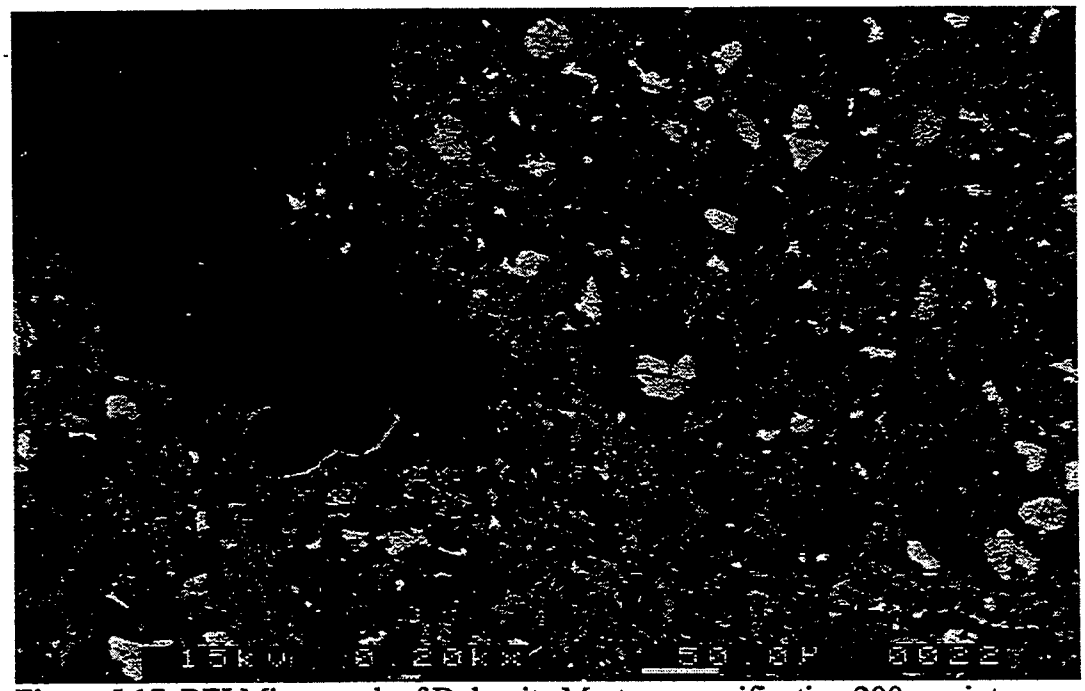

Figure 5.17 BEI Micrograph of Dolomite Mortar, magnification 200×, mixture proportion 25_42_00, aggregate size #8~#16.

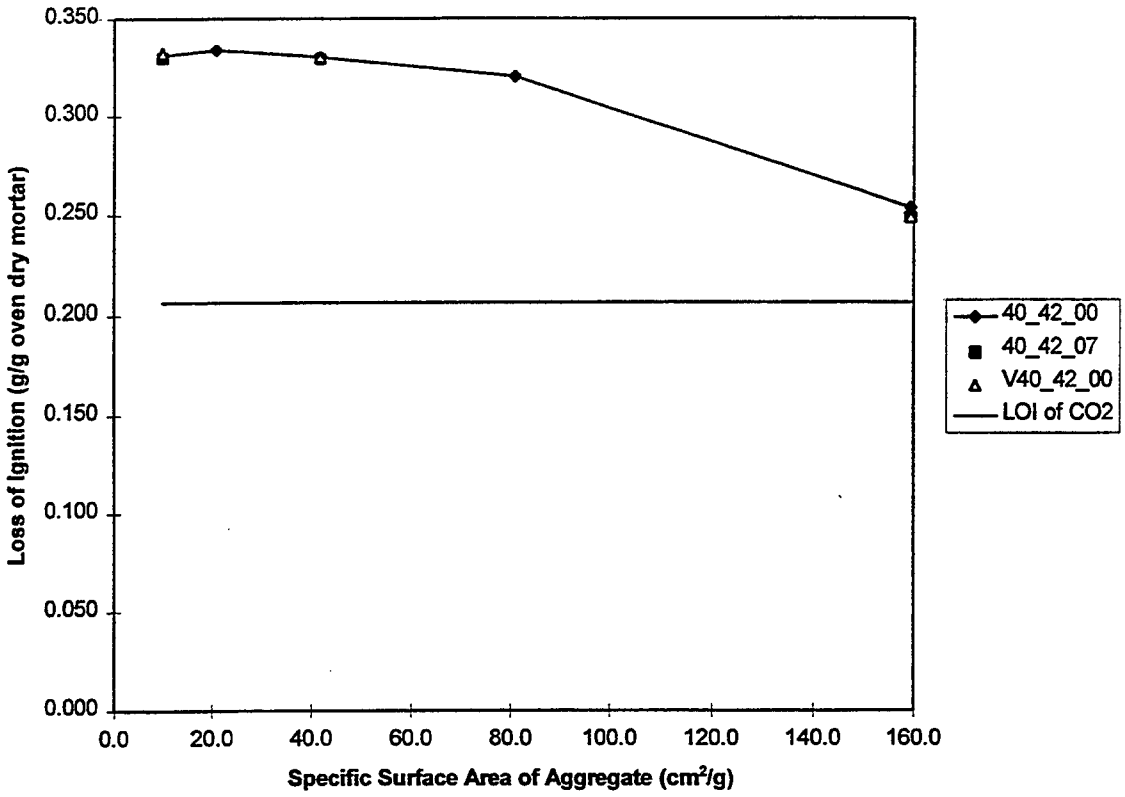

Figure 5.18 Loss-on-Ignition vs. SA for Dolomite Mortars. Five points of -◆- represent LOI of PC mortars having one of five fractions (ASTM Sieve No.: #4~#8, #8~#16, #16~#30, #30~#50, and #50~#100) of aggregate size, mixture proportions of 40_42_00, and normal mixing process. Three points: 1st, 3rd, and 5th of ■ represent LOI of SF mortars having mixture proportions of 40_42_07. Another three points: 1st, 3rd, and 5th of Δ represent LOI of PC mortars having mixture proportions of 40_42_00 and applying vacuum in mixing. LOI of CO_2 is the loss of carbon dioxide due to dedolomization.

degree of hydration. The samples for the five points marked by -♦- in Figure 5.18 are the same samples as those with Va=0.40 in Figure 5.1. The last one with SA around 160 cm^2/g corresponds to Point A in Figure 5.1. It is observed from Figure 5.18 that the specimen with the finest aggregate has a lower LOI compared to the others. Thus, it is less hydrated, while the others may hydrate at the same degree. This indicates that when there is enough water, the W/C of the bulk paste may still be the same as indicated by mixture proportions. It is not influenced by the increasing aggregate surface. However, if the aggregate surface increases in the mixture and approaches that of the critical point in Figure 5.1, the W/C of bulk paste decreases below its designed value. Thus, the overall degree of hydration of paste including bulk paste and transition zone becomes smaller. In addition, it is noted in Figure 5.18 that the LOI data of vacuum mixing mortars and 7% SF mortars are quite closer to the corresponding values of PC mortars. This indicates that vacuum mixing, or 7% of portland cement weight replaced by silica fume, does not influence the degree of hydration of mature mortar much.

The increase in the surface area of aggregate leads to an increase in the amount of water on the aggregate surface and may introduce two opposite effects on the mechanical properties of mortar. Firstly, the increase in the aggregate surface will also increase the volume of transition zones, while the volume of bulk paste will be decreased. As a result, the stiffness and rigidity of mortar will be reduced if the transition zone is less stiff and less rigid than bulk paste. Secondly, holding water on the aggregate surface will result in reduced W/C in the bulk paste, thus strengthening the bulk paste. This has a positive effect on the stiffness and rigidity of mortar. However, this mechanism happens only if the mixture proportioning has the aggregate surface area similar to or beyond that of the critical point in Figure 5.1.

If the aggregate surface area increases beyond that of the critical point, it will lead to a condition where there is not sufficient water for the cement grains to rinse. Thus, it results in cement grains being agglomerated, and they cannot disperse and hydrate well in the mixture. Under this condition, the mixture is harsh and difficult to compact. Therefore, based on the water availability and the total surface area of aggregate particles,

a criterion should be determined for identifying these mixing and compaction problems. It is noted that water, not paste, is the controlling factor. This is because in these problems it is lack of water to make paste. It is not a problem that paste itself cannot be dispersed into the space between aggregate particles.

5.7 Criterion for Identification of Mixing and Compaction Problems

Dividing the water volume by the total surface area of aggregate particles in the mixture leads to a water film thickness. This is actually a virtual value, because water does not coat on the aggregate surface at this thickness during mixing. However, this thickness indicates the maximum water available for each aggregate particle and is used as the criterion for identifying the mixing and compaction problems. Figure 5.19 shows the calculated water film thickness for the same mixtures used for Figure 5.1. Points A, B, C, and D correspond to Points A, B, C, and D in Figure 5.1 respectively. A regression curve, passing through Points A, B, C, and D and redrawn in Figure 5.20, is used to determine the criterion for identifying the mixing and compaction problems. The equation for this regression is

$$y = 0.11x^{-0.80} \tag{5.1}$$

where x is the specific surface area of aggregate in cm^2/g, and
y is the critical water film thickness in cm.

In Figure 5.19, any point located above the regression curve falls in the curve-descending region in Figure 5.1, and mixing and compaction problems may occur in the specimen. On the other hand, any point located below this regression curve falls in the curve-ascending region in Figure 5.1, and no mixing and compaction problems may occur in the specimen. Thus, this regression curve may be used to identify whether there are mixing and compaction problems within the specimen or not.

Figure 5.21 is obtained from Figure 5.20 by transforming the abscissa SA into the aggregate size. It shows a linear relationship between critical water film thickness and aggregate size by the regression line:

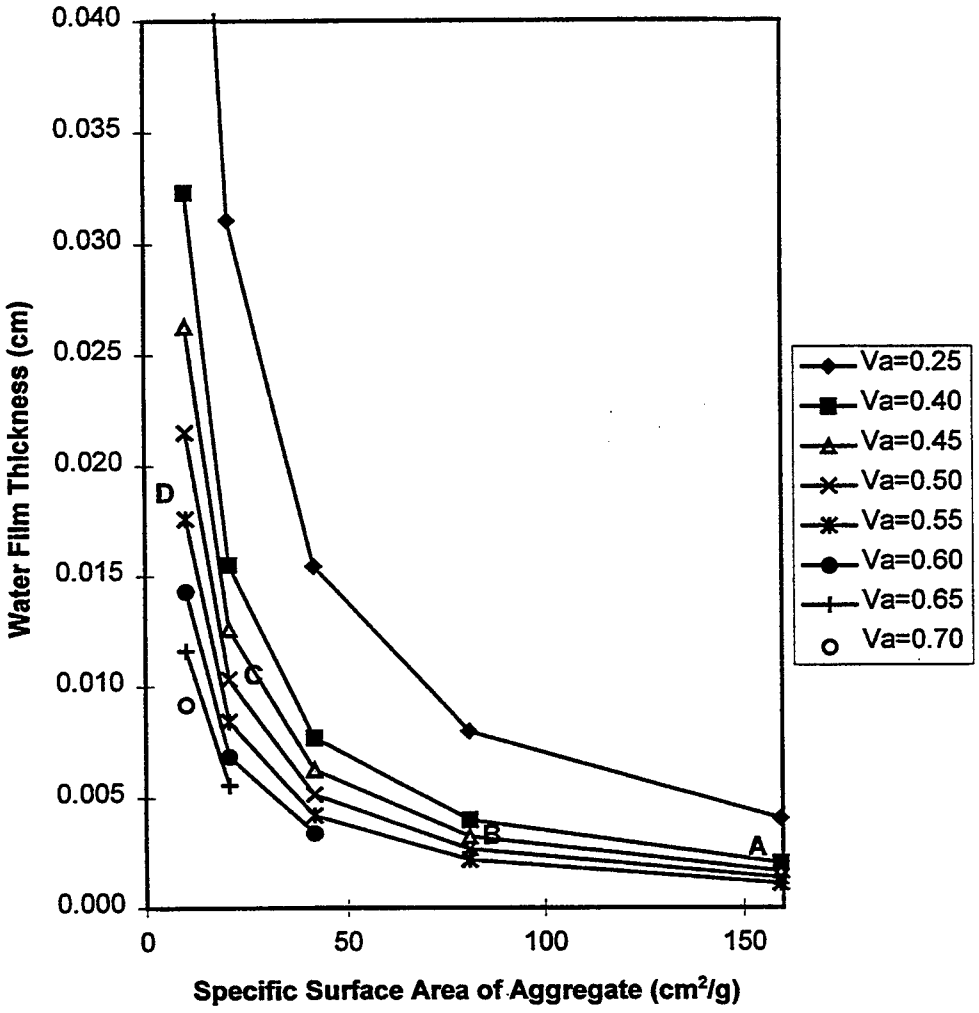

Figure 5.19 Water Film Thickness vs. SA for dolomite mortars having the same W/C 0.42 but various Va of 0.25, 0.40, 0.45, 0.50, 0.55, 0.60, 0.65, and 0.70.

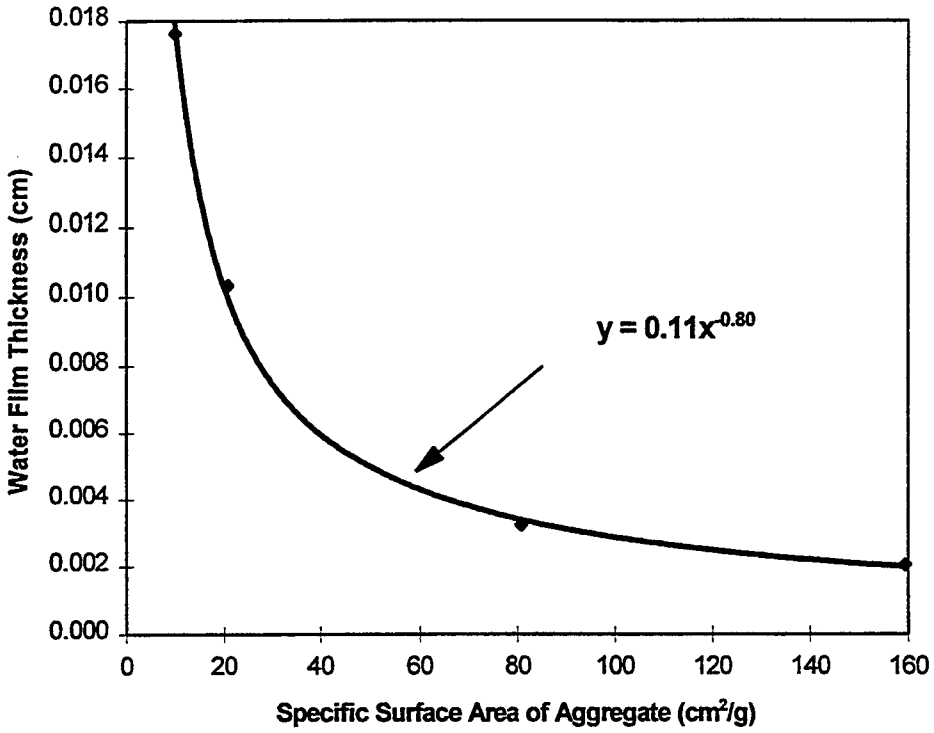

Figure 5.20 Water Film Thickness vs. SA for critical points: A, B, C, and D in Figure 5.19. Abscissa x stands for the specific surface area of aggregate in cm^2/g. Ordinate y stands for water film thickness in cm.

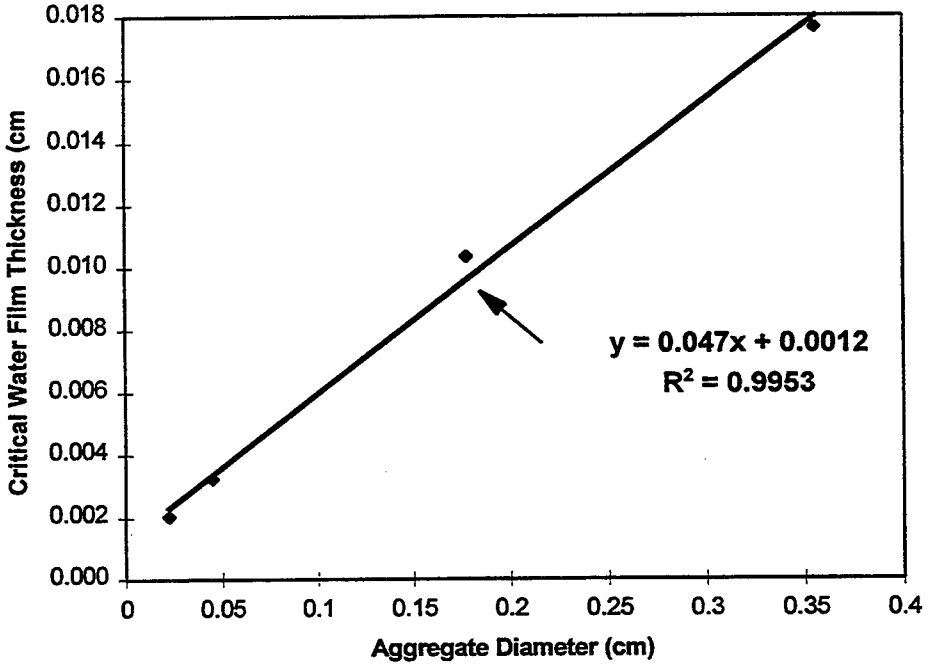

Figure 5.21 Critical Water Film Thickness vs. Aggregate Diameter. Abscissa x stands for aggregate diameter in cm. Ordinate y stands for the critical water film thickness also in cm. R is correlation coefficient.

$$y = 0.047x + 0.0012 \tag{5.2}$$

where x is aggregate diameter in cm, and
y is critical water film thickness in cm.

This regression line is the final form of criterion used for identifying the mixing and compaction problems. Equation (5.2) is derived based on the testing on mortar specimens with W/C=0.42. Thus, the aggregate diameter is effective for fine aggregate only and selection of a different W/C may influence the constants in this equation. In addition, some admixtures like silica fume or a commonly used agent such as superplasticizer may change the location of the regression line. However, it should be possible to determine the critical thickness of water film by following the same procedure.

5.8 Optimization of Water in Mixture Proportioning to Avoid Mixing and Compaction Problems

Recently, a lot of work has been done in trying to reduce W/C in order to obtain high-strength concrete, but the ability to reduce the water has a limit. The regression line in Figure 5.21 potentially provides a way to check the optimum quantity of water demanded for mixture proportioning. The optimum water quantity provided for mixture should be more than, and close to, the value calculated by Equation (5.2) in order to let the mixture gain its highest density, stiffness, rigidity, and strengths.

CHAPTER 6

RESULTS AND DISCUSSION 2: DEVELOPMENT OF A THEORETICAL MODEL TO INTERPRET DYNAMIC MODULI DATA

Many theories have been proposed to study the mechanical behavior of concrete. They can be roughly divided into two categories. One type of theory attempts to study the local stress or strain distribution inside and among aggregate particles, and thus may be called micro-mechanics approach. The other regards concrete as a statistically homogeneous and isotropic material and tries to find the effective moduli or other mechanical properties for a typical unit cell of concrete called the representative volume element. Basically, the latter method is an approach of rule of mixture, and its results can be directly incorporated into finite element code as a material property.

In the above two theoretical approaches, some researchers have focused their work on the evolution of moduli (e.g., stiffness and rigidity) models, while others have been trying to establish strength models with yielding or damage criteria embedded in their theoretical frameworks.

Since one of the experimental work tasks of this study is testing the dynamic moduli of elasticity of transition zones, the theoretical work will focus on developing a moduli model for concrete and mortar. Based on the rule of mixture, many models have been proposed for studying the elastic moduli of concrete and mortar. These models include the model of Voigt [1928], Reuss [1929], Hirsch [1962], Counto [1964], Hansen [1965], Bache and Nepper-Christensen [1965], Popovics [1970], and Hashin-Shtrikman (HS bounds) [1963], etc. Among these models, the last one represents a powerful approach to the analysis of composite materials. It deals with the bonding of the effective elastic properties between upper and lower bounds. For statistically isotropic and

homogeneous material, Hashin and Shtrikman applied the variational principal to derive the improved bounds that are much narrower than the Voigt-Reuss bounds. Up to now, most of the previous models of concrete were two-phase models. The theoretical framework of this study is to adopt HS bounds in three phases and then transform this three-phase model into another form in order to aid in explaining the experimental results of this study.

Two recent works of Hashin [1991 and 1992], using the variational method to derive bounds for the elastic properties of two-phase composites with imperfect interfaces, have been adopted by Simeonov and Ahmad [1995] for simulating the elastic modulus of transition zones of cement-based composites. The results of these two works have not been considered in developing the theoretical model of this study.

6.1 Hashin-Shtrikman Bounds of Three Phases

At the beginning, the main frame of the theoretical model of this study is established by adopting HS bounds extended in three phases. Subsequently, with manipulation of this model in a mathematical way, a suggestion is proposed for interpreting the experimental results.

Hashin and Shtrikman [1963], using variation principles in the linear theory of elasticity, derived upper and lower bounds for the effective elastic moduli (i.e., bulk modulus K, and shear modulus G) of quasi-isotropic and quasi-homogeneous multiphase material with arbitrary phase geometry. Let the smallest K and G of the components in a composite be denoted by K_1 and G_1, and the largest by K_n and G_n. The volume fraction of the rth component is denoted by v_r. With n phases in composite, the upper and lower bounds of K and G are read as:

the lower bound of bulk modulus of composite is

$$K_{LC} = K_1 + \frac{A_1}{1+\alpha_1 A_1} \tag{6.1}$$

the upper bound of bulk modulus of composite is

$$K_{UC} = K_n + \frac{A_n}{1+\alpha_n A_n} \tag{6.2}$$

where

$$\alpha_1 = -\frac{3}{3K_1 + 4G_1} \tag{6.3}$$

$$\alpha_n = -\frac{3}{3K_n + 4G_n} \tag{6.4}$$

$$A_1 = \sum_{r=2}^{r=n} \frac{v_r}{\frac{1}{K_r - K_1} - \alpha_1} \tag{6.5}$$

$$A_n = \sum_{r=1}^{r=n-1} \frac{v_r}{\frac{1}{K_r - K_n} - \alpha_n} \tag{6.6}$$

the lower bound of shear modulus of composite is

$$G_{LC} = G_1 + \frac{B_1}{2(1+\beta_1 B_1)} \tag{6.7}$$

the upper bound of shear modulus of composite is

$$G_{UC} = G_n + \frac{B_n}{2(1+\beta_n B_n)} \tag{6.8}$$

where

$$\beta_1 = -\frac{3(K_1 + 2G_1)}{5G_1(3K_1 + 4G_1)} \tag{6.9}$$

$$\beta_n = -\frac{3(K_n + 2G_n)}{5G_n(3K_n + 4G_n)} \tag{6.10}$$

$$B_1 = \sum_{r=2}^{r=n} \frac{v_r}{\frac{1}{2(G_r - G_1)} - \beta_1} \tag{6.11}$$

$$B_n = \sum_{r=1}^{r=n-1} \frac{v_r}{\frac{1}{2(G_r - G_n)} - \beta_n} \tag{6.12}$$

By definition, the lower bound of modulus of elasticity of composite is given by

$$E_{LC} = \frac{9K_{LC}G_{LC}}{(3K_{LC} + G_{LC})} \tag{6.13}$$

and the upper bound of modulus of elasticity of composite is given by

$$E_{UC} = \frac{9K_{UC}G_{UC}}{(3K_{UC} + G_{UC})} \tag{6.14}$$

Extend K_{UC}, K_{LC}, G_{UC}, and G_{LC} in three phases: 1, 2, 3 to obtain

$$K_{UC} = K_3 + \frac{\frac{v_1}{K_2 - K_3} + \frac{v_2}{K_1 - K_3} + \frac{3(1-v_3)}{3K_3 + 4G_3}}{\frac{1}{(K_1 - K_3)(K_2 - K_3)} + \frac{3(1-v_1)}{(K_2 - K_3)(3K_3 + 4G_3)} + \frac{3(1-v_2)}{(K_1 - K_3)(3K_3 + 4G_3)} + \frac{9v_3}{(3K_3 + 4G_3)^2}} \tag{6.15}$$

$$K_{LC} = K_1 + \frac{\frac{v_2}{K_3 - K_1} + \frac{v_3}{K_2 - K_1} + \frac{3(1-v_1)}{3K_1 + 4G_1}}{\frac{1}{(K_2 - K_1)(K_3 - K_1)} + \frac{3(1-v_2)}{(K_3 - K_1)(3K_1 + 4G_1)} + \frac{3(1-v_3)}{(K_2 - K_1)(3K_1 + 4G_1)} + \frac{9v_1}{(3K_1 + 4G_1)^2}} \tag{6.16}$$

$$G_{UC} = G_3 + \frac{\frac{v_1}{G_2 - G_3} + \frac{v_2}{G_1 - G_3} + \frac{6(1-v_3)(K_3 + 2G_3)}{5G_3(3K_3 + 4G_3)}}{\frac{1}{(G_1 - G_3)(G_2 - G_3)} + \frac{6(1-v_1)(K_3 + 2G_3)}{5G_3(G_2 - G_3)(3K_3 + 4G_3)} + \frac{6(1-v_2)(K_3 + 2G_3)}{5G_3(G_1 - G_3)(3K_3 + 4G_3)} + \frac{36v_3(K_3 + 2G_3)^2}{25G_3^2(3K_3 + 4G_3)^2}} \tag{6.17}$$

$$G_{LC} = G_1 + \frac{\frac{v_2}{G_3 - G_1} + \frac{v_3}{G_2 - G_1} + \frac{6(1-v_1)(K_1 + 2G_1)}{5G_1(3K_1 + 4G_1)}}{\frac{1}{(G_2 - G_1)(G_3 - G_1)} + \frac{6(1-v_2)(K_1 + 2G_1)}{5G_1(G_3 - G_1)(3K_1 + 4G_1)} + \frac{6(1-v_3)(K_1 + 2G_1)}{5G_1(G_2 - G_1)(3K_1 + 4G_1)} + \frac{36v_1(K_1 + 2G_1)^2}{25G_1^2(3K_1 + 4G_1)^2}} \tag{6.18}$$

where $K_3 > K_2 > K_1$ and $G_3 > G_2 > G_1$. Rewrite equations (6.15) ~ (6.18) to be

$$K_{UC} = K_3 - \frac{R}{S} \tag{6.19}$$

$$K_{LC} = K_1 + \frac{P}{Q} \tag{6.20}$$

$$G_{UC} = G_3 - \frac{V}{W} \tag{6.21}$$

$$G_{LC} = G_1 + \frac{T}{U} \tag{6.22}$$

where

$$R = v_1(K_3 - K_1)(3K_3 + 4G_3)^2 + (1 - v_1 - v_3)(K_3 - K_2)(3K_3 + 4G_3)^2 - 3(1 - v_3)(K_3 - K_1)(K_3 - K_2)(3K_3 + 4G_3) \tag{6.23}$$

$$S = (3K_3 + 4G_3)^2 - 3(1 - v_1)(K_3 - K_1)(3K_3 + 4G_3) - 3(v_1 + v_3)(K_3 - K_2)(3K_3 + 4G_3) + 9v_3(K_3 - K_1)(K_3 - K_2) \tag{6.24}$$

$$P = v_3(K_3 - K_1)(3K_1 + 4G_1)^2 + (1 - v_1 - v_3)(K_2 - K_1)(3K_1 + 4G_1)^2 + 3(1 - v_1)(K_3 - K_1)(K_2 - K_1)(3K_1 + 4G_1) \tag{6.25}$$

$$Q = (3K_1 + 4G_1)^2 + 3(1 - v_3)(K_3 - K_1)(3K_1 + 4G_1) + 3(v_1 + v_3)(K_2 - K_1)(3K_1 + 4G_1) + 9v_1(K_3 - K_1)(K_2 - K_1) \tag{6.26}$$

$$V = 25v_1G_3^2(G_3 - G_1)(3K_3 + 4G_3)^2 + 25(1 - v_1 - v_3)G_3^2(G_3 - G_2)(3K_3 + 4G_3)^2 - 30(1 - v_3)G_3(G_3 - G_1)(G_3 - G_2)(3K_3 + 4G_3)(K_3 + 2G_3) \tag{6.27}$$

$$W = 25G_3^2(3K_3 + 4G_3)^2 - 30(1 - v_1)G_3(G_3 - G_1)(3K_3 + 4G_3)(K_3 + 2G_3) - 30(v_1 + v_3)G_3(G_3 - G_2)(3K_3 + 4G_3)(K_3 + 2G_3) + 36v_3(G_3 - G_1)(G_3 - G_2)(K_3 + 2G_3)^2 \tag{6.28}$$

$$T = 25v_3G_1^2(G_3 - G_1)(3K_1 + 4G_1)^2 + 25(1 - v_1 - v_3)G_1^2(G_2 - G_1)(3K_1 + 4G_1)^2 + 30(1 - v_1)G_1(G_2 - G_1)(G_3 - G_1)(3K_1 + 4G_1)(K_1 + 2G_1) \tag{6.29}$$

$$U = 25G_1^2(3K_1 + 4G_1)^2 + 30(v_1 + v_3)G_1(G_2 - G_1)(3K_1 + 4G_1)(K_1 + 2G_1) + 30(1 - v_3)G_1(G_3 - G_1)(3K_1 + 4G_1)(K_1 + 2G_1) + 36v_1(G_2 - G_1)(G_3 - G_1)(K_1 + 2G_1)^2 \tag{6.30}$$

In reference to Appendix A, it is proved that R, S, P, Q, V, W, T, and U are all positive if $K_3 > K_2 > K_1$ and $G_3 > G_2 > G_1$. Under this circumstance, the relationships of $K_{UC} < K_3$, $K_{LC} > K_1$, $G_{UC} < G_3$, and $G_{LC} > G_1$ are always sustained. Based on Equations (6.19) through (6.30), it is not easy to describe the model for lower and upper bounds of K and G. Nevertheless, a description of the model based on three-dimensional geometry will make this model easier to understand.

6.2 Characteristics of Proposed Three-Phase Model

In reference to Figure 6.1, an equilateral triangle with length $2/\sqrt{3}$ on each side is taken as a ternary coordinate system used to express the volume fractions of three constituents in a composite. For the three sides of a triangle, there are three perpendicular distances for any point within this equilateral triangle. These three distances, representing the volume fractions of three constituents, have their total equal to one. Thus, although the geometric length on each side of the equilateral triangle is $2/\sqrt{3}$, the volume fraction values represented on each side of triangle are between 0 and 1 and vary linearly. Furthermore, each vertex of the triangle stands for one of the three constituents.

If the ternary coordinate system is set to be the base as shown in Figure 6.2, the upper and lower bounds of K (or G) are the two triangular curved surfaces between the three vertical axes. K_1, K_2, and K_3 (or G_1, G_2, and G_3) are the intersections between the triangular curved surfaces and the three vertical axes. If the volume fraction of aggregate is fixed at v_3, the upper bound is curve a$\frown$b and the lower bound is curve f$\frown$c. They are the intercepted curves between plane abde and two triangular curved surfaces. The gap between the upper and lower bounds increases with increasing relative K (or G) among the three constituents.

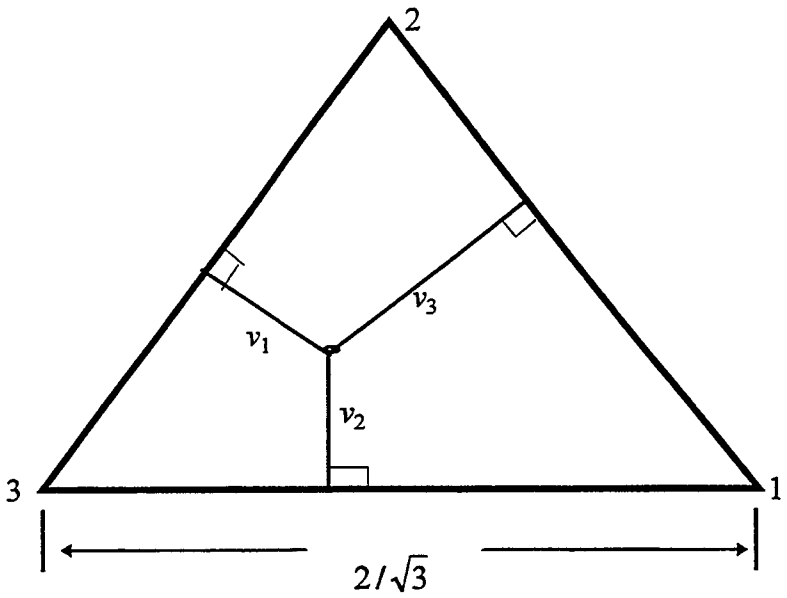

Figure 6.1 Base of Ternary Coordinate System

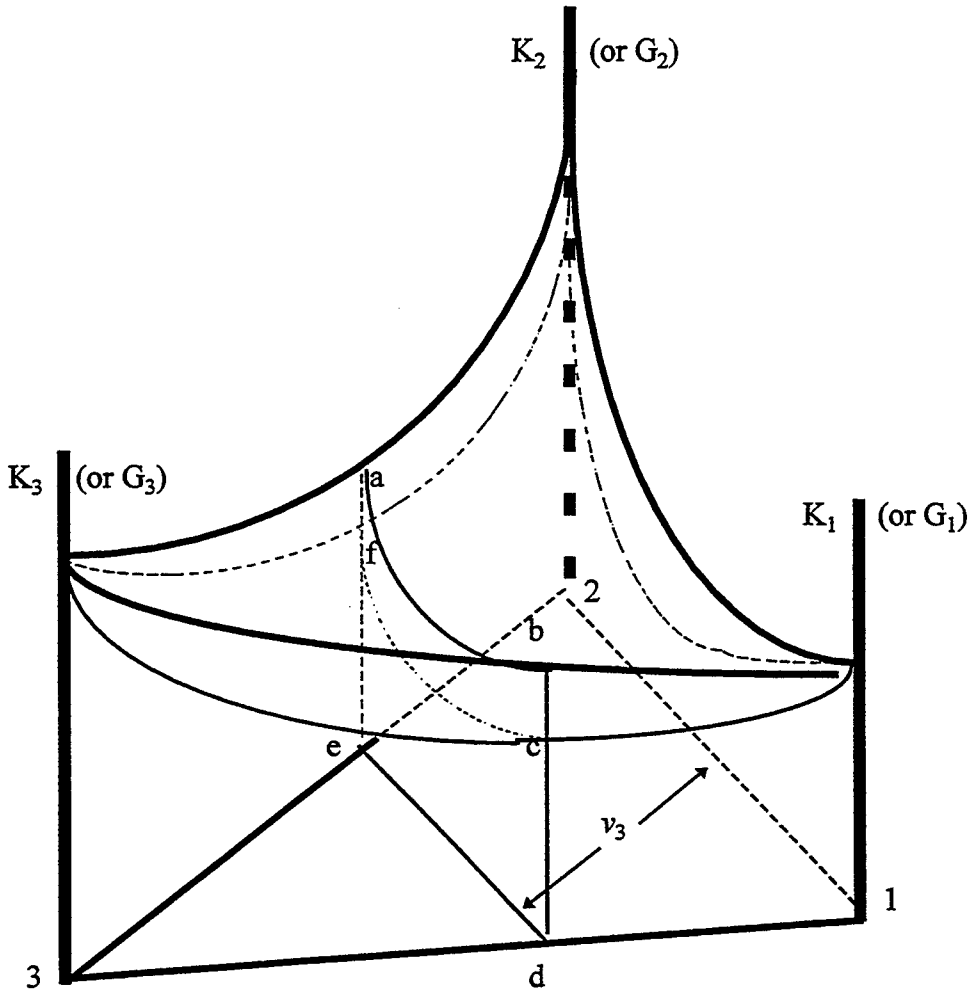

Figure 6.2 Ternary Coordinate System

6.3 Applicable Limitation of Proposed Model

There is a limitation when applying this model to mortar. The experimental results of Ishai [1961] and Swamy [1971] showed that the modulus of elasticity decreases if v_3 in mortar is somewhere around 0.52 or 0.60. Figure 5.1 also shows a similar trend. Consequently, the triangular region of Δ3ed in Figure 6.2 with v_3 near or exceeding a critical value will show a moduli-drop phenomenon. Practically, this region is not applicable for simulating the elastic moduli of mortar.

In Chapter 5.7, the criterion for identifying the mixing and compaction problems in mortar is established based on the thickness of virtual water film surrounding aggregate particles. This criterion can also be used to judge if the experimental data is suitable for the proposed model to simulate. In other words, this criterion is used to find the limitation of the proposed model. The proposed model cannot be applied to simulate the elastic moduli if the mixing and compaction problems occur in the specimen because the structures of constituents in the specimen have been changed contradicting the basic assumption of HS bounds.

6.4 Verification of Proposed Model

In order to check the validation of the proposed Hashin-Shtrikman 3-D model for mortar, a procedure of mathematical manipulation using some experimental data as input is presented below.

Equations (6.19) ~ (6.30) give a mathematical expression for 3-D HS bounds. Assume phase 3 is aggregate, phase 2 is bulk paste, phase 1 is transition zones, v_3 is the volume fraction of aggregate, v_2 is the volume fraction of bulk paste, and v_1 is the volume fraction of transition zones. In the equations, the moduli of elasticity and shear moduli for mortar, aggregate, and bulk paste (E_c, G_c, E_3, G_3, E_2, and G_2) can be determined from testing on mortar, aggregate, and pure paste having the same W/C ratio as mortar. Subsequently, the bulk moduli for mortar, aggregate, and bulk paste can be calculated from the measured moduli of elasticity and shear moduli by $K=EG/(9G-3E)$. v_3 can be acquired from mixture proportions. v_2 and v_1 can be calculated from an assumed

thickness of transition zones and the specific surface area and quantity of the aggregate used for mixtures.

Since the four equations (6.19) ~ (6.22) represent the upper and lower bounds of both bulk modulus and shear modulus, the solutions of bulk and shear moduli may theoretically fall between these upper and lower bounds. Assume each solution is the average of its associated upper bound and lower bound. Then, the bulk modulus (K_1) and shear modulus (G_1) of transition zones can be determined. Let K_c and G_c be the average values of their associated upper bounds and lower bounds. Equation (6.31) is obtained by taking the average of Equations (6.19) and (6.20), and Equation (6.32) is obtained by taking the average of Equations (6.21) and (6.22);

$$K_C = \frac{1}{2}(K_{UC} + K_{LC}) = f_1(K_1, G_1) \tag{6.31}$$

$$G_C = \frac{1}{2}(G_{UC} + G_{LC}) = f_2(K_1, G_1) \tag{6.32}$$

where f_1, and f_2 are two functions.

Eventually, there are two equations: (6.31) and (6.32), and two unknowns: K_1 and G_1. Thus, the unknowns can be determined. The solutions for K_1 and G_1 do not need to be very accurate since they can be anywhere between their associated upper bounds and lower bounds. With a few iterations, a trial-and-error method has been used to solve these two nonlinear equations. Results show that this method works well and it will be discussed later.

Subsequently, the question is how to choose the data to verify the proposed model. Among the experimental data of this study, there are two groups of data that can be used for verification of the proposed model. The first group includes the dynamic modulus of elasticity and dynamic shear modulus data for mixtures which are 28 days old with mixture proportions W/C=0.42, no silica fume, and volume fractions of aggregate 0.25, 0.40, and 0.55. The values of dynamic modulus of elasticity and dynamic shear modulus for various SA are presented in Figures 6.3 and 6.4 respectively. The other group includes the dynamic modulus of elasticity and dynamic shear modulus of mixtures

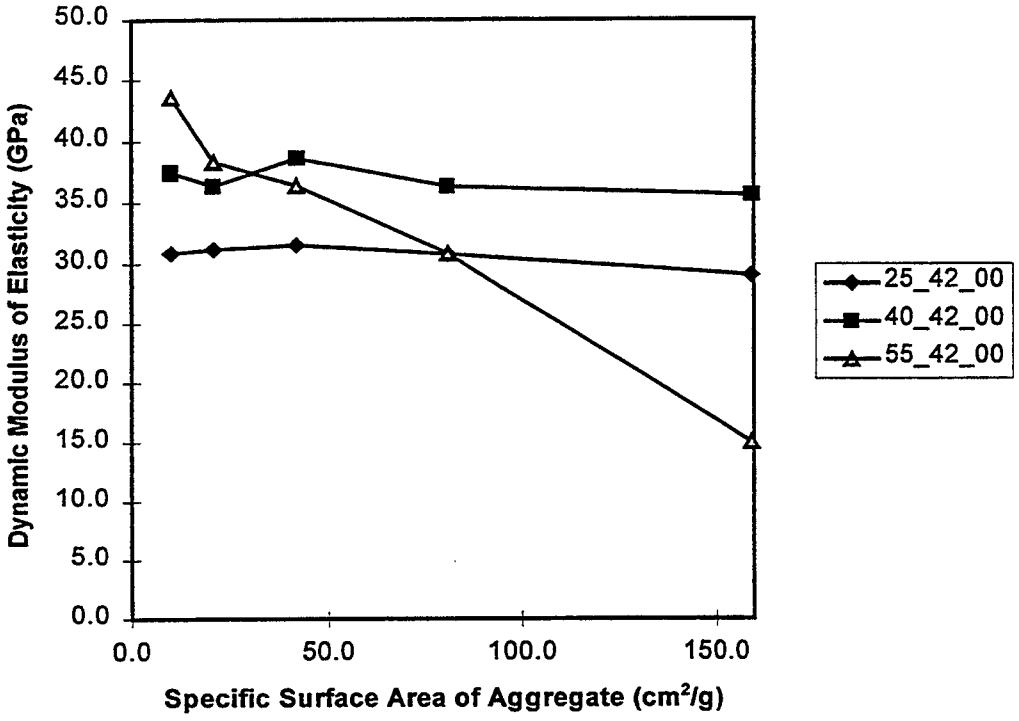

Figure 6.3 Dynamic Modulus of Elasticity vs. SA for PC mortars having mixture proportions of 25_42_00, 40_42_00, and 55_42_00.

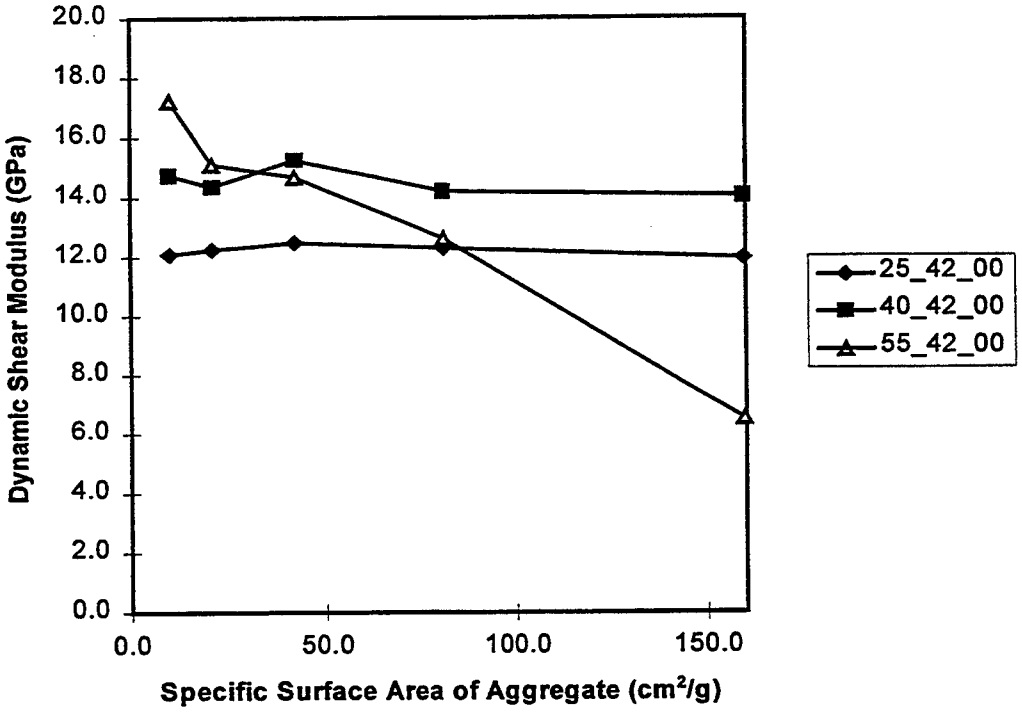

Figure 6.4 Dynamic Shear Modulus vs. SA for PC mortars having mixture proportions of 25_42_00, 40_42_00, and 55_42_00.

that have the mixture proportions similar to the former group, except 7% of cement weight is substituted by silica fume. Their values of dynamic modulus of elasticity and dynamic shear modulus, which correspond to various values of SA, are presented in Figures 6.5 and 6.6 respectively.

The reason for choosing these two groups of data was the constant W/C used with these mixtures. Thus, the mechanical properties of the three constituents of mortars: aggregate, bulk paste, and transition zones, can be maintained and are not dependent on changing the relative quantities of constituents. The only change is the relative quantities of constituents when varying SA in the mortar, and this satisfies the basic assumption of the Hashin-Shtrikman bounds theory.

To validate the proposed model, the experimental data must be investigated before it can be used. If the mixing and compaction problems occur in the specimen, the data of this specimen must be discarded. Thus, the "sieve" used is the critical water film surrounding the aggregate, which is Equation (5.2) in Chapter 5.7. Figures 6.7 and 6.8 present the water film thickness with the variation of aggregate diameter for the two groups of mixtures mentioned above. The criterion line represents Equation (5.2). Any mixture with its associated water film thickness falling below this line may have mixing and compaction problems. Judging from Figures 6.7 and 6.8, it is inferred that whether the mixtures contain silica fume or not, all of the ten mixtures with a ν_3=0.55 have mixing and compaction problems. The others with a ν_3 of 0.25 and 0.40 seem normal.

The proposed model is tested as follows. The dynamic moduli of aggregate presented in Table 6.1 were determined by testing rock prisms with the resonant frequency method. Also, using the resonant frequency method, the dynamic moduli of bulk paste were determined by testing pure paste prisms having a W/C of 0.42.

By applying the measured dynamic moduli of mortars which contain the finer aggregates, i.e., #30-#50, or #50-#100, and have mixture proportions of 40_42_00 and 40_42_07, and assuming the thickness of transition zones to be 50 μm, the dynamic moduli of transition zones can be calculated by Equations (6.31) and (6.32). During this calculating process, $E=9KG/(3K+G)$ is used. The reason to choose the data of finer

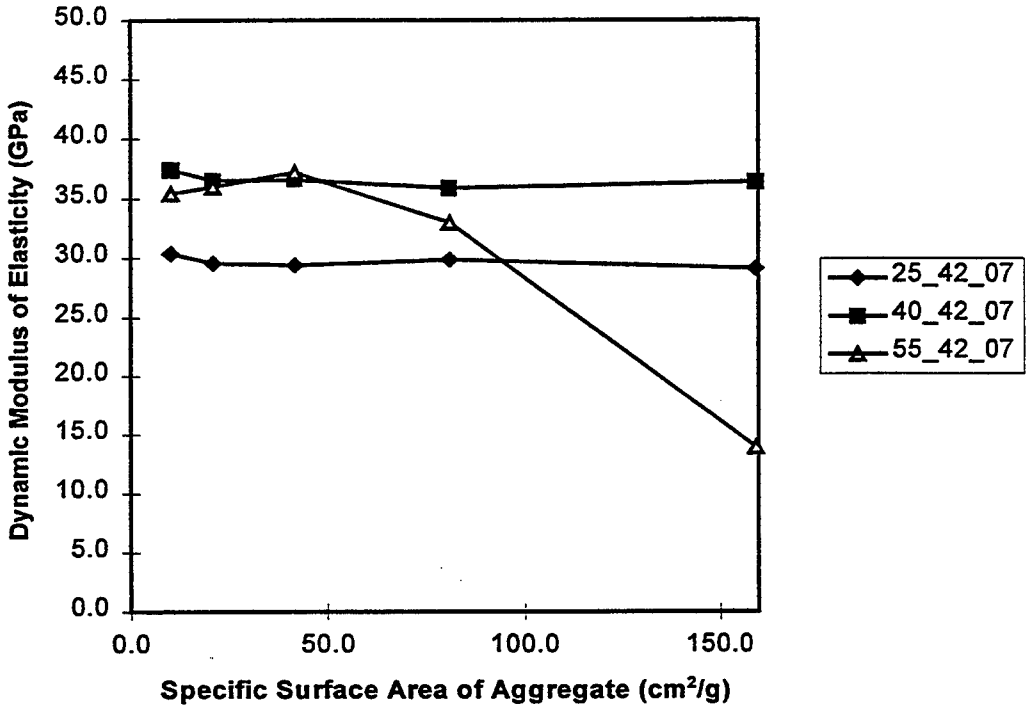

Figure 6.5 Dynamic Modulus of Elasticity vs. SA for SF mortars having mixture proportions of 25_42_07, 40_42_07, and 55_42_07.

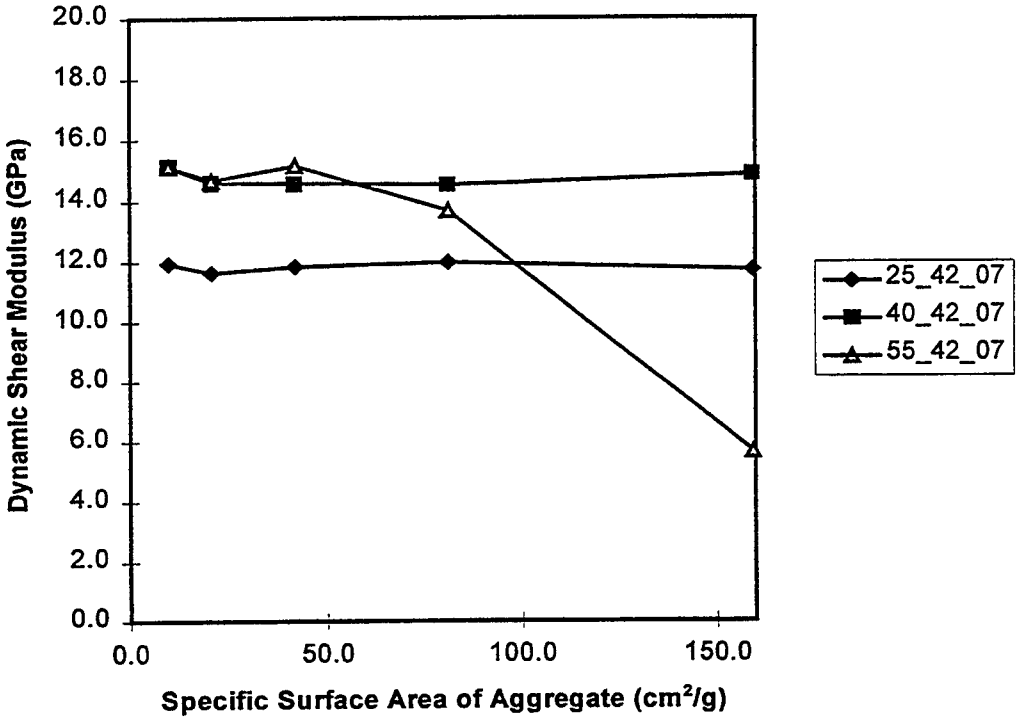

Figure 6.6 Dynamic Shear Modulus vs. SA for SF mortars having mixture proportions of 25_42_07, 40_42_07, and 55_42_07.

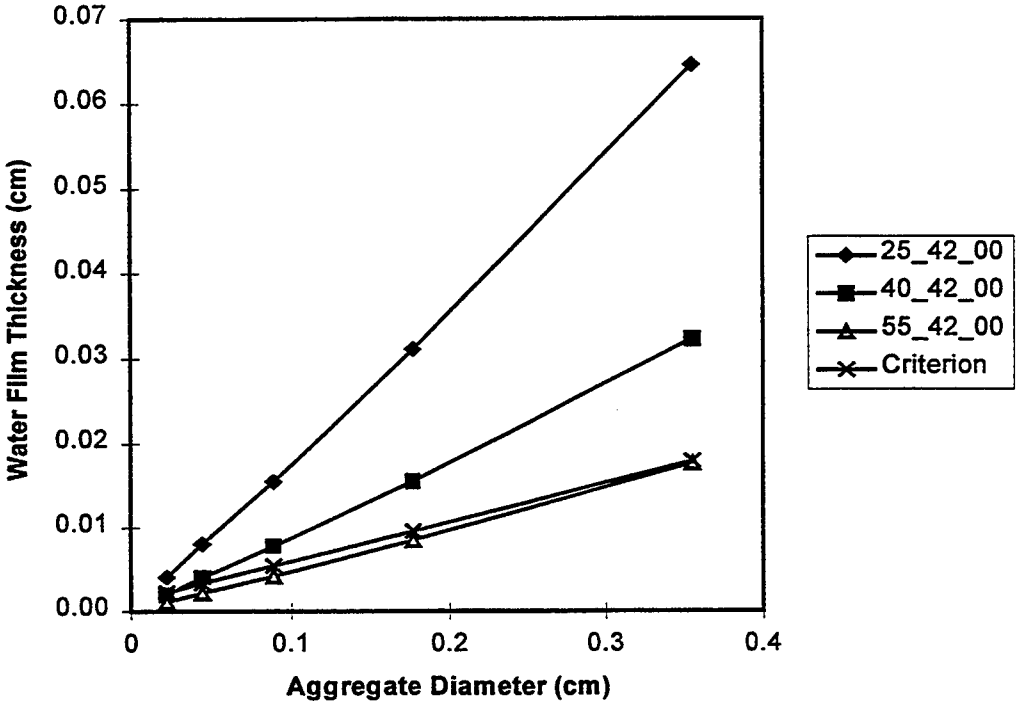

Figure 6.7 Water Film Thickness vs. Aggregate Diameter for the criterion and PC mortars having mixture proportions of 25_42_00, 40_42_00, and 55_42_00.

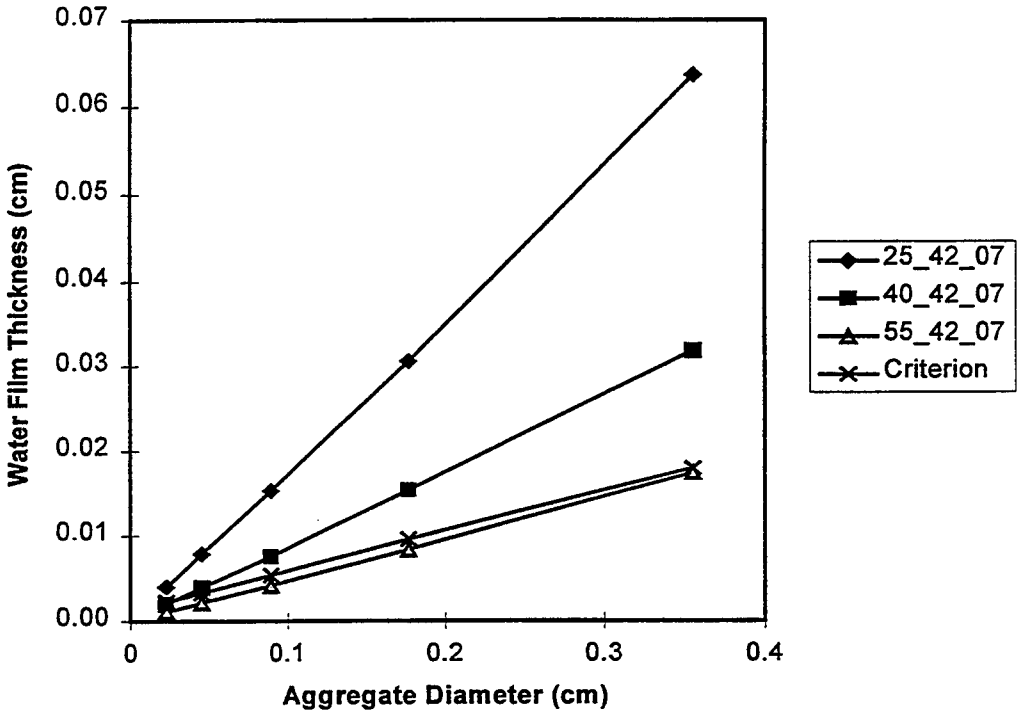

Figure 6.8 Water Film Thickness vs. Aggregate Diameter for the criterion and SF mortars having mixture proportions of 25_42_07, 40_42_07, and 55_42_07.

Table 6.1 Measured Dynamic Modulus of Elasticity (Ed) and Dynamic Shear Modulus (Gd) for Aggregate and Bulk Paste, and Calculated Values for Transition Zones in PC Mortars and 7% SF Mortars. (The thickness of transition zones is assumed to be 50μm.)

	Aggregate	Bulk Paste	Transition Zones (50μm)
PC Mortars			
Ed (GPa)	86.9	21.7	18.5
Gd (GPa)	37.2	8.3	7.0
SF Mortars			
Ed (GPa)	86.9	21.2	19.4
Gd (GPa)	37.2	7.8	7.7

aggregate mortars for calculation is that only these specimens contain enough volume of transition zones and this can reduce the error propagated via calculation.

In accordance with the data in Table 6.1, it is possible to predict the upper bounds and lower bounds of dynamic modulus of elasticity and dynamic shear modulus by using Equations (6.13), (6.14), and (6.19) ~ (6.22). Figures 6.9 and 6.10 show the calculated upper and lower bounds and measured data of dynamic modulus of elasticity and dynamic shear modulus for the mortars with mixture proportions of 40_42_00. For a v_3 of 0.25, the calculated upper and lower bounds and measured data in dynamic modulus of elasticity and dynamic shear modulus for the mortars with mixture proportions of 25_42_00 are shown in Figures 6.11 and 6.12. The measured data all fall between the upper and lower bounds.

In an extreme case, if v_3 is increased to 0.55, the calculated upper and lower bounds and measured data for dynamic modulus of elasticity and dynamic shear modulus for the mortars with mixture proportions of 55_42_00 are shown in Figures 6.13 and 6.14. The measured data are out of bounds. As mentioned before, at this high aggregate concentration, the mixing and compaction problems that occurred in the mixtures may have caused this result.

In another case, 7% of the cement weight in the specimen was substituted by silica fume. Figures 6.15 and 6.16 show the calculated upper and lower bounds and measured data for dynamic modulus of elasticity and dynamic shear modulus for the mortars having mixture proportions of 40_42_07. If v_3 is changed to 0.25, the calculated upper and lower bounds and measured data for dynamic modulus of elasticity and dynamic shear modulus for the mortars having mixture proportions of 25_42_07 are presented in Figures 6.17 and 6.18. The measured data also fall between the upper and lower bounds.

However, if v_3 is changed to 0.55, the calculated upper and lower bounds and the measured data in dynamic modulus of elasticity and dynamic shear modulus for the mortars having mixture proportions of 55_42_07 are presented in Figures 6.19 and 6.20. Again, the measured data are out of bounds. This may be also due to the mixtures having mixing and compaction problems.

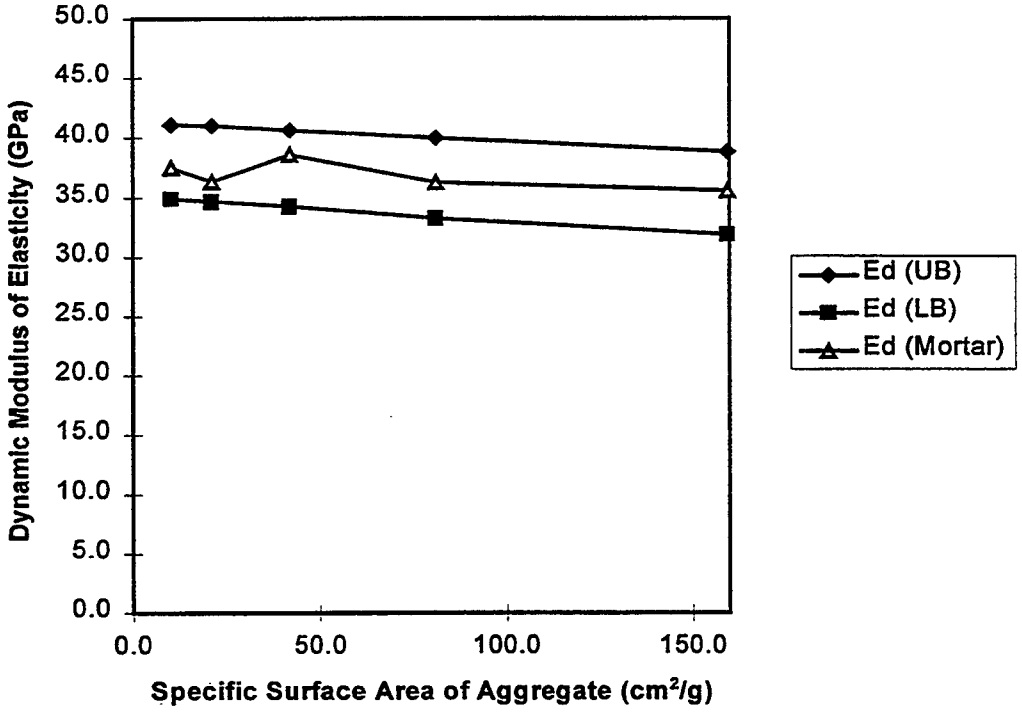

Figure 6.9 Dynamic Modulus of Elasticity vs. SA for calculated Hashin-Shtrikman bounds (UB: upper bound, LB: lower bound) and measured data for PC mortars having mixture proportions of 40_42_00.

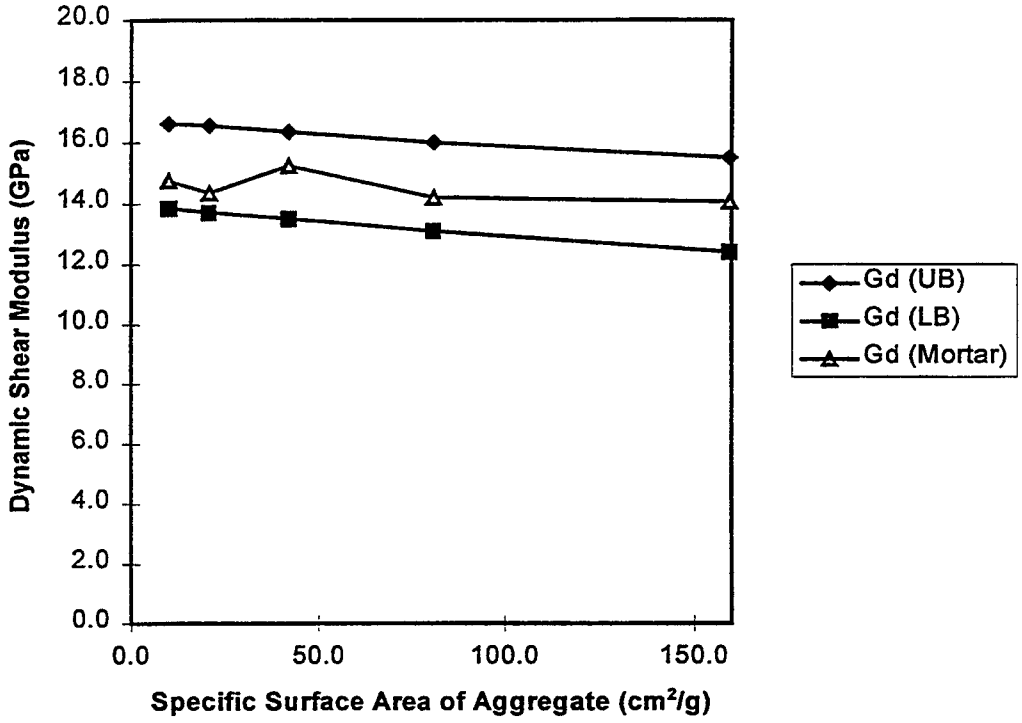

Figure 6.10 Dynamic Shear Modulus vs. SA for calculated Hashin-Shtrikman bounds (UB: upper bound, LB: lower bound) and measured data for PC mortars having mixture proportions of 40_42_00.

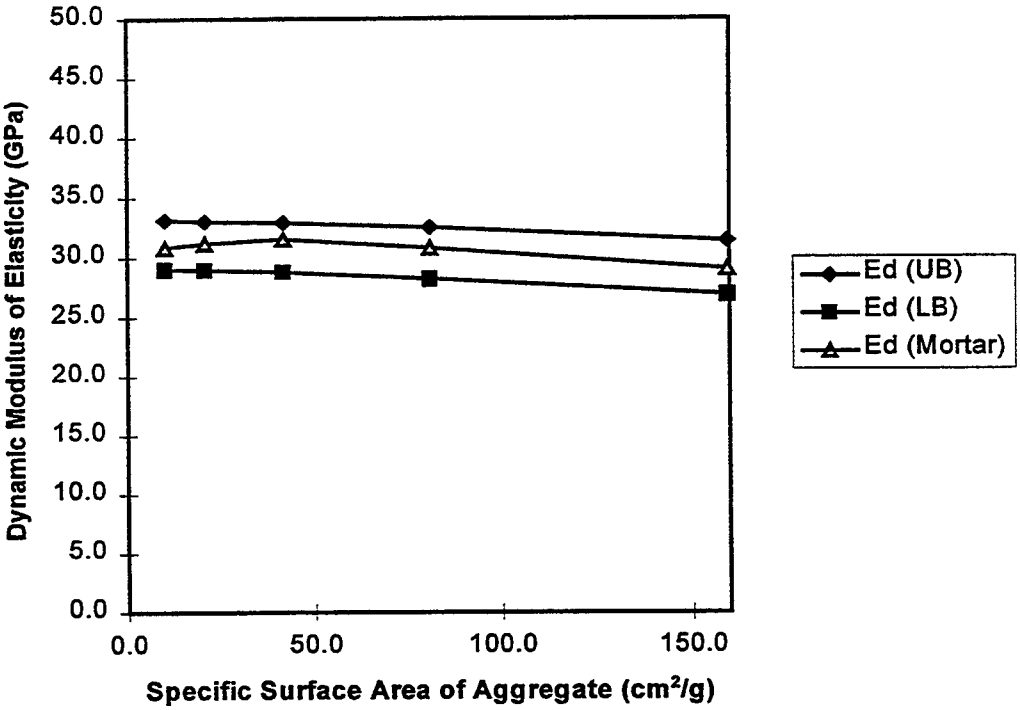

Figure 6.11 Dynamic Modulus of Elasticity vs. SA for calculated Hashin-Shtrikman bounds (UB: upper bound, LB: lower bound) and measured data for PC mortars having mixture proportions of 25_42_00.

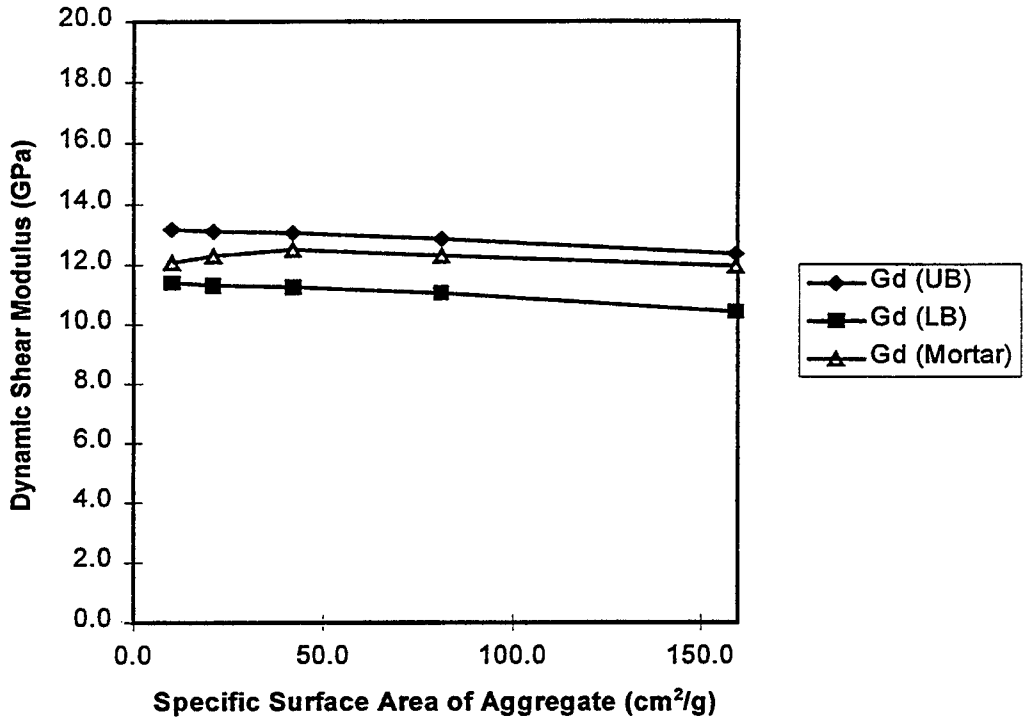

Figure 6.12 Dynamic Shear Modulus vs. SA for calculated Hashin-Shtrikman bounds (UB: upper bound, LB: lower bound) and measured data for PC mortars having mixture proportions of 25_42_00.

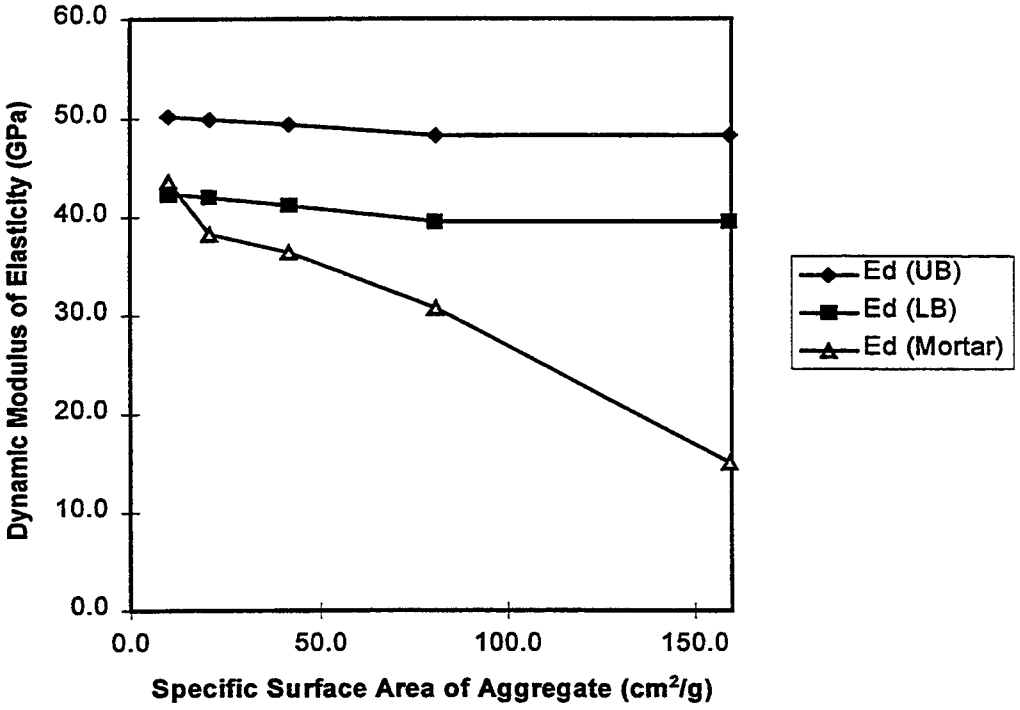

Figure 6.13 Dynamic Modulus of Elasticity vs. SA for calculated Hashin-Shtrikman bounds (UB: upper bound, LB: lower bound) and measured data for PC mortars having mixture proportions of 55_42_00.

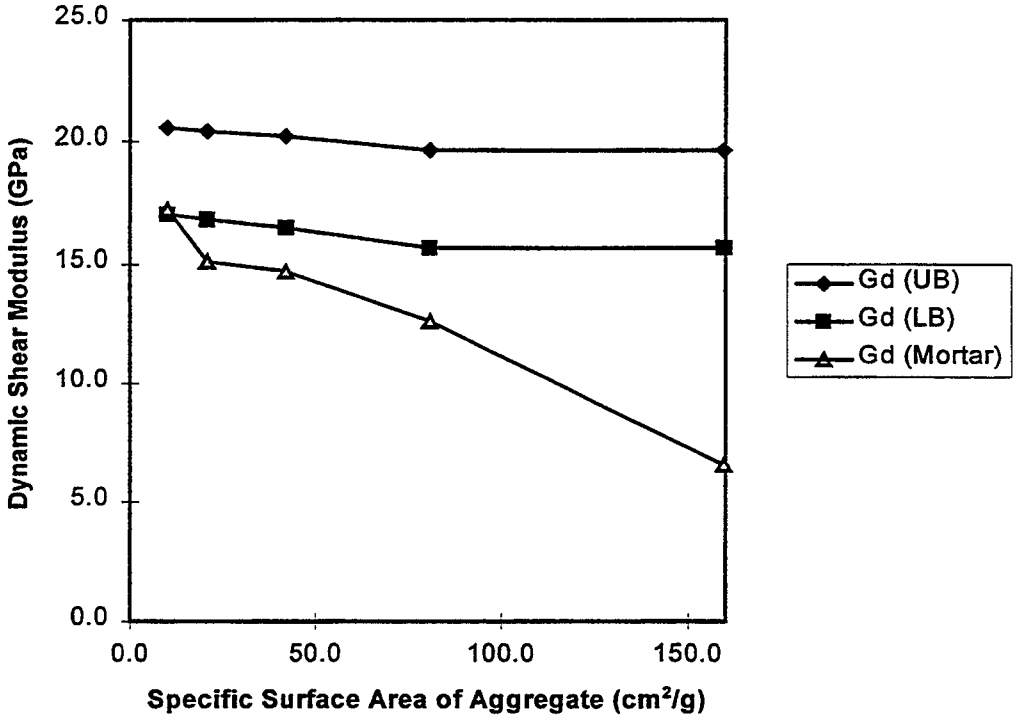

Figure 6.14 Dynamic Shear Modulus vs. SA for calculated Hashin-Shtrikman bounds (UB: upper bound, LB: lower bound) and measured data for PC mortars having mixture proportions of 55_42_00.

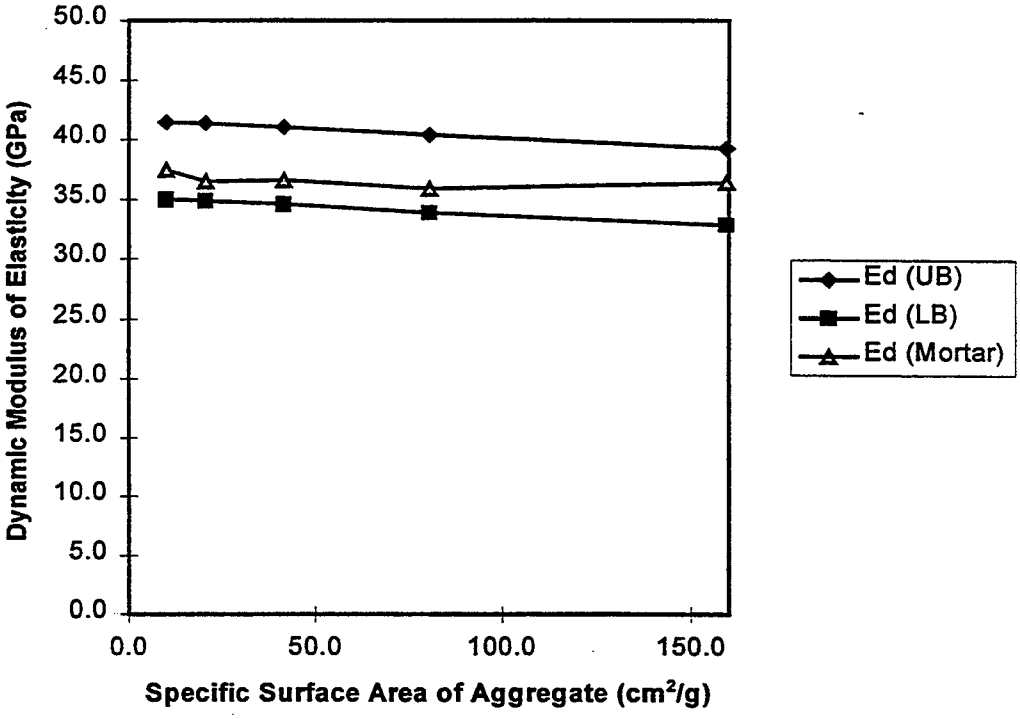

Figure 6.15 Dynamic Modulus of Elasticity vs. SA for calculated Hashin-Shtrikman bounds (UB: upper bound, LB: lower bound) and measured data for SF mortars having mixture proportions of 40_42_07.

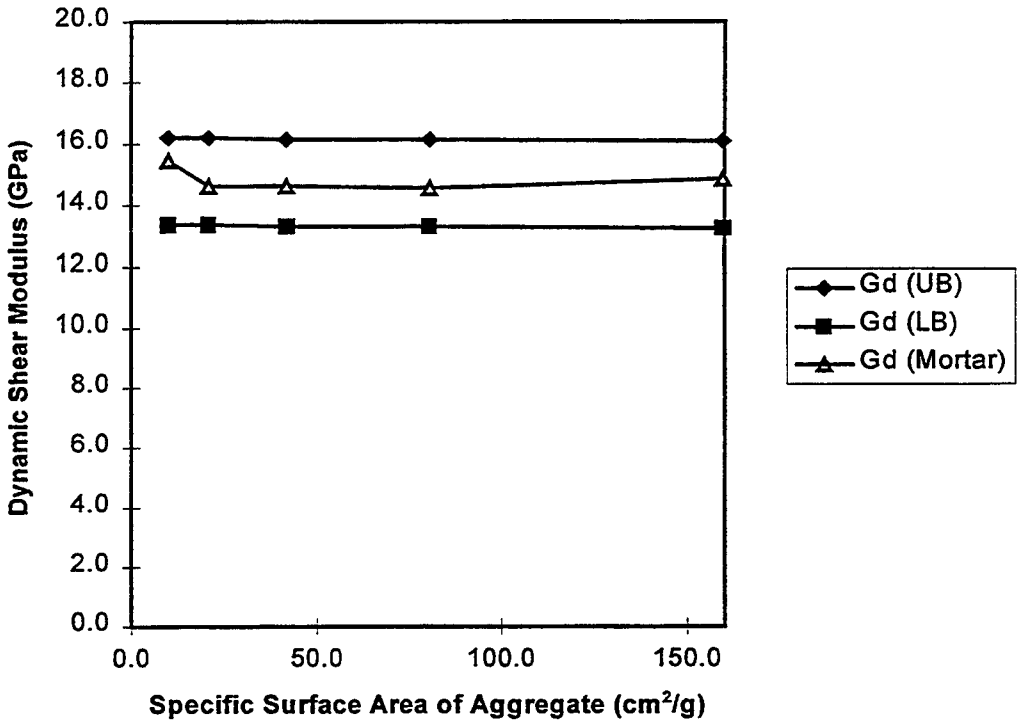

Figure 6.16 Dynamic Shear Modulus vs. SA for calculated Hashin-Shtrikman bounds (UB: upper bound, LB: lower bound) and measured data for SF mortars having mixture proportions of 40_42_07.

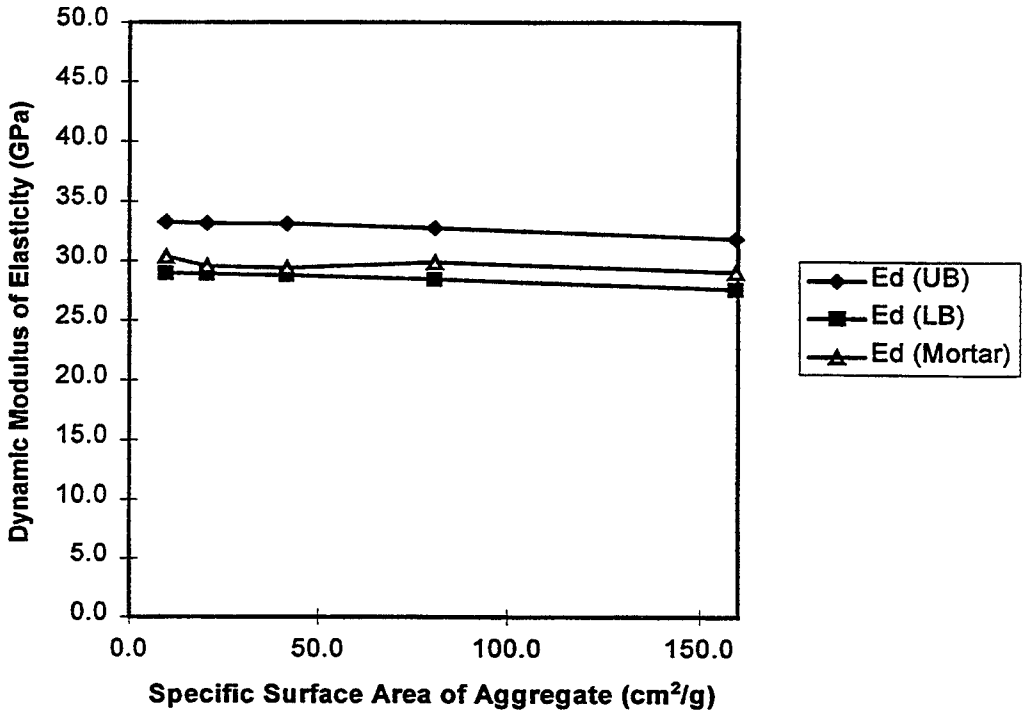

Figure 6.17 Dynamic Modulus of Elasticity vs. SA for calculated Hashin-Shtrikman bounds (UB: upper bound, LB: lower bound) and measured data for SF mortars having mixture proportions of 25_42_07.

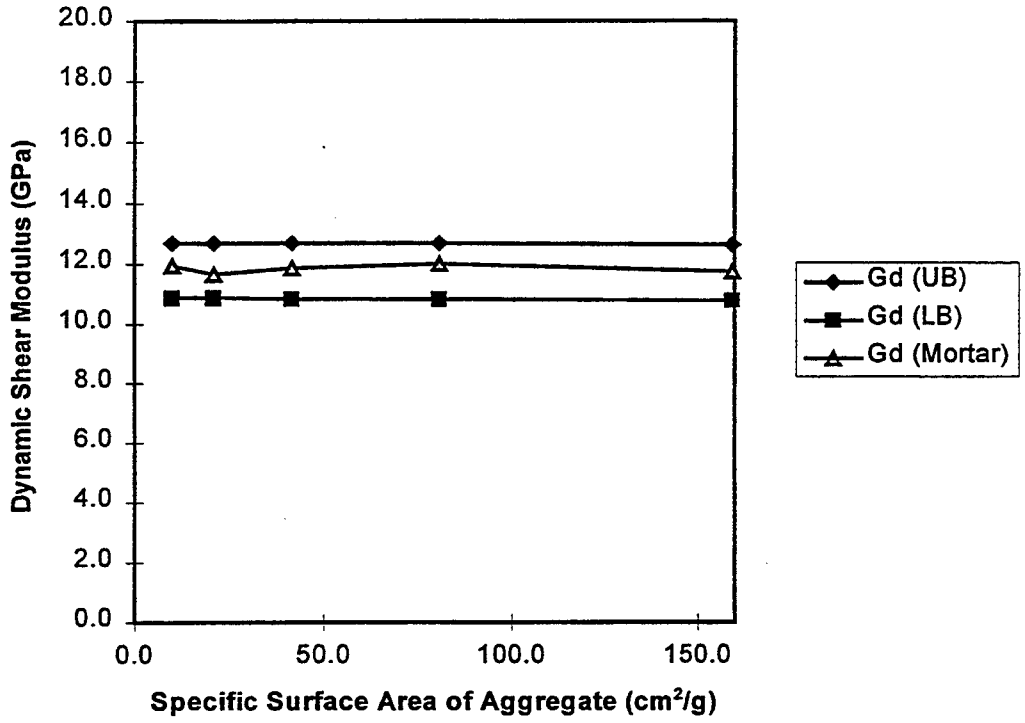

Figure 6.18 Dynamic Shear Modulus vs. SA for calculated Hashin-Shtrikman bounds (UB: upper bound, LB: lower bound) and measured data for SF mortars having mixture proportions of 25_42_07.

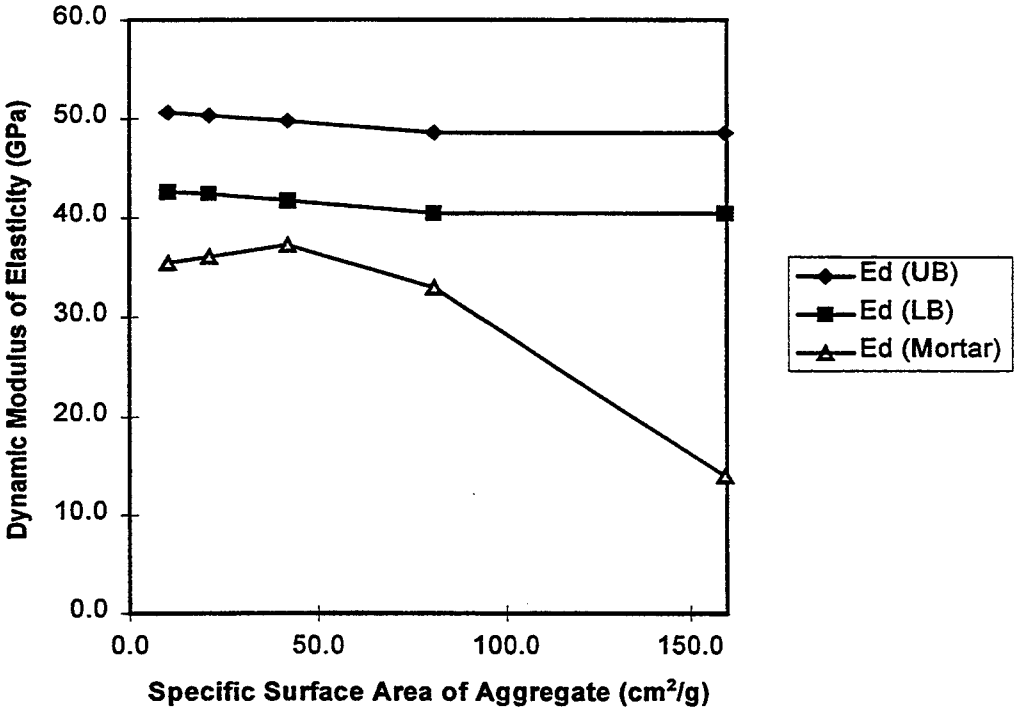

Figure 6.19 Dynamic Modulus of Elasticity vs. SA for calculated Hashin-Shtrikman bounds (UB: upper bound, LB: lower bound) and measured data for SF mortars having mixture proportions of 55_42_07.

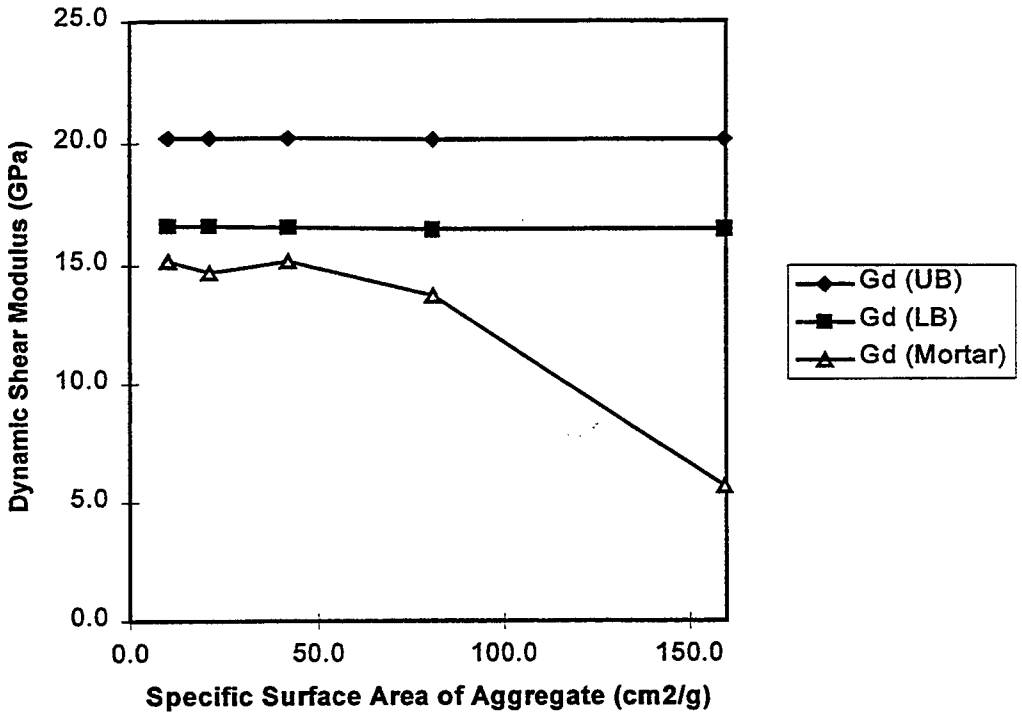

Figure 6.20 Dynamic Shear Modulus vs. SA for calculated Hashin-Shtrikman bounds (UB: upper bound, LB: lower bound) and measured data for SF mortars having mixture proportions of 55_42_07.

Cohen et al. [1995] tried to estimate the average stiffness and rigidity of the cement paste-aggregate transition zone by using the logarithmic mixture rule. In another study, Lutz and Monteiro [1995] tried to determine the bulk and shear moduli of the transition zone by introducing a power law. The results of both studies show that the stiffness, rigidity, and bulk modulus of the transition zone may be less than those of the bulk paste. Ordinarily, among the three constituents of concrete or mortar, aggregate has the highest stiffness, rigidity, and bulk modulus. If Va is increasing, the volume fraction of transition zones will also increase. The increasing volume of transition zones will lower the elastic moduli of concrete or mortar matrix. On the other hand, the increasing volume of aggregate will raise the elastic moduli of concrete or mortar. Thus, it would become a confounded problem by designing an experiment this way. Therefore, the volume fractions of constituents, the abscissas in the ternary coordinate system of the proposed model, are not suitable for studying the elastic moduli of transition zones in concrete or mortar. Before applying the proposed model to study the transition zone, it needs to be transformed from the relationship between elastic moduli and volume fractions of constituents into the relationship between elastic moduli and SA. The reason was explained in detail in Chapter 1.3.

6.5 Modification of Proposed Model

The transformation is basically a mathematical manipulation. Assume ρ is the density of aggregate particle and t is the average thickness of transition zones. The total mass and volume of the aggregate are kept constant for each mixture proportion of this study. Aggregate size is the only variable. Under this circumstance, the equations for taking the derivatives of moduli E_{LC}, E_{UC}, G_{LC}, and G_{UC} to the specific surface area of aggregate by mass S_{agg} are expressed as:

for the lower bound of modulus of elasticity $$\frac{dE_{LC}}{dS_{agg}} = \frac{dE_{LC}}{dv_1} t\rho \qquad (6.33)$$

for the upper bound of modulus of elasticity $$\frac{dE_{UC}}{dS_{agg}} = \frac{dE_{UC}}{dv_1} t\rho \qquad (6.34)$$

for the lower bound of shear modulus $$\frac{dG_{LC}}{dS_{agg}} = \frac{dG_{LC}}{dv_1} t\rho \quad (6.35)$$

for the upper bound of shear modulus $$\frac{dG_{UC}}{dS_{agg}} = \frac{dG_{UC}}{dv_1} t\rho \quad (6.36)$$

In Equations (6.33) ~ (6.36), t and ρ both act as magnification factors for the derivatives in the right hand side. However, if S_{agg} stands for the specific surface area of aggregate by volume, then the derivatives of E_{LC}, E_{UC}, G_{LC}, and G_{UC} are expressed as:

for the lower bound of modulus of elasticity $$\frac{dE_{LC}}{dS_{agg}} = \frac{dE_{LC}}{dv_1} tv_3 \quad (6.37)$$

for the upper bound of modulus of elasticity $$\frac{dE_{UC}}{dS_{agg}} = \frac{dE_{UC}}{dv_1} tv_3 \quad (6.38)$$

for the lower bound of shear modulus $$\frac{dG_{LC}}{dS_{agg}} = \frac{dG_{LC}}{dv_1} tv_3 \quad (6.39)$$

for the upper bound of shear modulus $$\frac{dG_{UC}}{dS_{agg}} = \frac{dG_{UC}}{dv_1} tv_3 \quad (6.40)$$

Similarly, t and v_3 in Equations (6.37) ~ (6.40) are two magnification factors. By simple deriving from Equations (6.13), (6.14) and (6.19) ~ (6.30), Equations (6.41) ~ (6.54) can be obtained.

$$\frac{dE_{LC}}{dv_1} = \frac{9(3K_{LC}^2 \frac{dG_{LC}}{dv_1} + G_{LC}^2 \frac{dK_{LC}}{dv_1})}{(3K_{LC} + G_{LC})^2} \quad (6.41)$$

$$\frac{dE_{UC}}{dv_1} = \frac{9(3K_{UC}^2 \frac{dG_{UC}}{dv_1} + G_{UC}^2 \frac{dK_{UC}}{dv_1})}{(3K_{UC} + G_{UC})^2} \quad (6.42)$$

From the geometric relationship, it is observed that dK_{LC}/dv_1, dG_{LC}/dv_1, dK_{UC}/dv_1, and dG_{UC}/dv_1 in Equations (6.41) and (6.42) are the slopes of curves f∩c and a∩b in Figure 6.2 expressed in its associated K or G coordinate system.

In this study, v_3 is fixed and $v_2+v_3=1-v_1$. Thus,

$$\frac{dK_{UC}}{dv_1} = -\frac{1}{S}\frac{dR}{dv_1} + \frac{R}{S^2}\frac{dS}{dv_1} \tag{6.43}$$

$$\frac{dR}{dv_1} = (K_2 - K_1)(3K_3 + 4G_3)^2 \tag{6.44}$$

$$\frac{dS}{dv_1} = 3(K_2 - K_1)(3K_3 + 4G_3) \tag{6.45}$$

$$\frac{dK_{LC}}{dv_1} = \frac{1}{Q}\frac{dP}{dv_1} - \frac{P}{Q^2}\frac{dQ}{dv_1} \tag{6.46}$$

$$\frac{dP}{dv_1} = (K_1 - K_2)(3K_1 + 4G_1)(3K_3 + 4G_1) \tag{6.47}$$

$$\frac{dQ}{dv_1} = 3(K_2 - K_1)(3K_3 + 4G_1) \tag{6.48}$$

$$\frac{dG_{UC}}{dv_1} = -\frac{1}{W}\frac{dV}{dv_1} + \frac{V}{W^2}\frac{dW}{dv_1} \tag{6.49}$$

$$\frac{dV}{dv_1} = 25G_3^2(G_2 - G_1)(3K_3 + 4G_3)^2 \tag{6.50}$$

$$\frac{dW}{dv_1} = 30G_3(G_2 - G_1)(3K_3 + 4G_3)(K_3 + 2G_3) \tag{6.51}$$

$$\frac{dG_{LC}}{dv_1} = \frac{1}{U}\frac{dT}{dv_1} - \frac{T}{U^2}\frac{dU}{dv_1} \tag{6.52}$$

$$\frac{dT}{dv_1} = 5G_1(G_1 - G_2)(3K_1 + 4G_1)[6G_3(K_1 + 2G_1) + G_1(9K_1 + 8G_1)] \tag{6.53}$$

$$\frac{dU}{dv_1} = 6(G_2 - G_1)(K_1 + 2G_1)[6G_3(K_1 + 2G_1) + G_1(9K_1 + 8G_1)] \tag{6.54}$$

One of the typical graphs of this study is similar to Figure 6.21, the relationship between dynamic modulus of elasticity and SA, which is adopted from the experiment by Cohen et al. [1994]. In the same experiment, the data of dynamic shear modulus with a varying SA are presented in Figure 6.22. These two graphs are good examples of how to apply the above modified model in the process of interpretation of the experimental data.

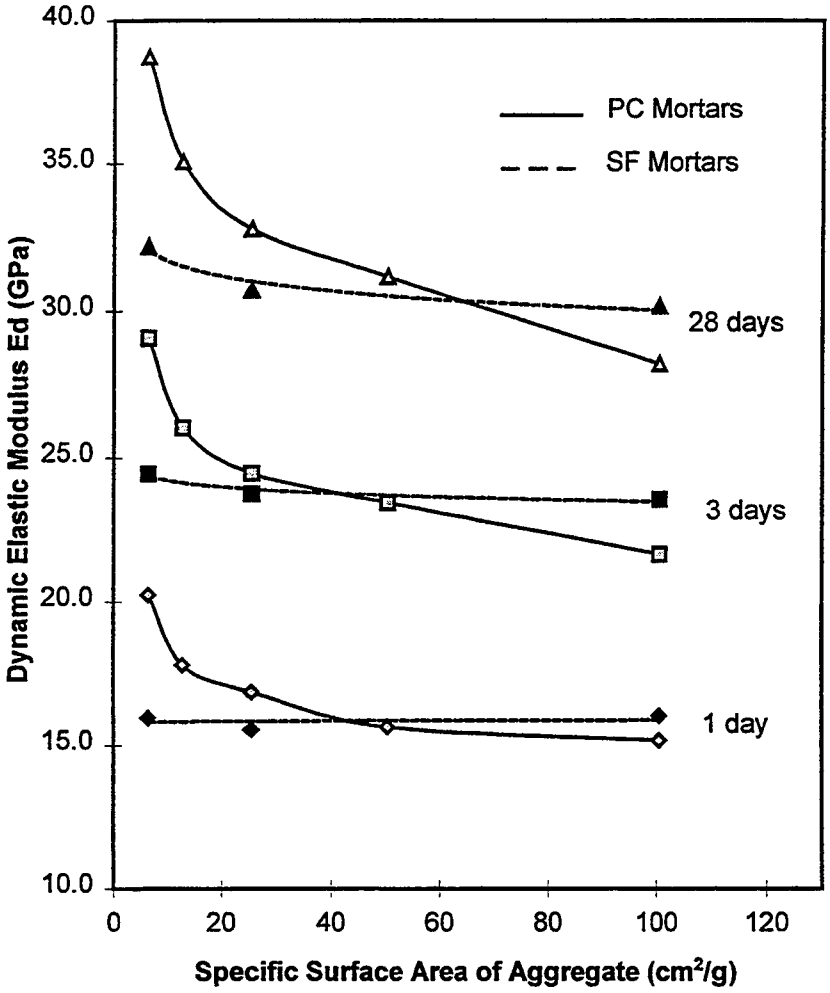

Figure 6.21 Dynamic Elastic Modulus vs. SA from Cohen et al. [1994].

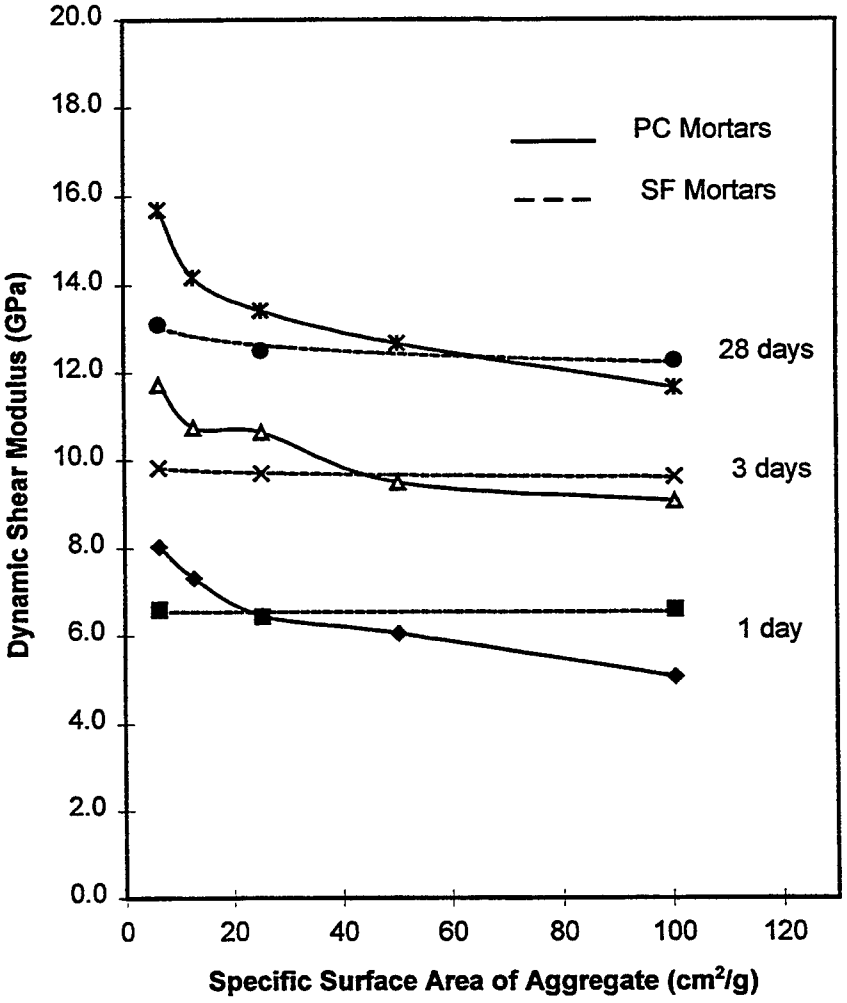

Figure 6.22 Dynamic Shear Modulus vs. SA from the same experiment as for Figure 6.21.

6.6 Interpretation of Experimental Data by Using Modified Model

Equations (6.33) ~ (6.36) are suitable for describing the characteristics of the curves in Figures 6.21 and 6.22. Two cases are described below.

1. K and G of transition zones are both less than those of bulk paste ($K_1 < K_2$ and $G_1 < G_2$).

Under this condition, it can be assumed that

$$K_2 = xK_1 \tag{6.55}$$

and

$$G_2 = yG_1 \tag{6.56}$$

where $x, y > 1$.

From the similar relationship as Equation (6.13), it is obtained

$$E_2 = \frac{9K_2G_2}{3K_2 + G_2} \tag{6.57}$$

and

$$E_1 = \frac{9K_1G_1}{3K_1 + G_1} \tag{6.58}$$

By subtracting Equation (6.58) from Equation (6.57) and substituting K_2 and G_2 in Equations (6.55) and (6.56) into Equation (6.57), it is obtained

$$E_2 - E_1 = \frac{9K_1G_1}{(3K_1 + G_1)(3xK_1 + yG_1)}[3xK_1(y-1) + yG_1(x-1)] > 0 \tag{6.59}$$

Thus, E_1 also will be less than E_2. In reference to Appendix B, the right hand sides of Equations (6.43), (6.46), (6.49), and (6.52) are all negative if $K_3 > K_2 > K_1$ and $G_3 > G_2 > G_1$. Therefore, the right hand sides of Equations (6.41) and (6.42) are both negative. Thus, the right hand sides of Equations (6.33) and (6.34), which are corresponding to the slopes of lower and upper bounds for the data of solid curves in Figure 6.21, are both negative too. A mechanical interpretation for the solid curves in Figure 6.21 is suggested by the fact that the dynamic modulus of elasticity of bulk paste is larger than that of the transition zone. Also, the right hand sides of Equations (6.49) and (6.52) are both negative. Thus, the right hand sides of Equations (6.35) and (6.36), which correspond to the slopes of lower and upper bounds for the data of solid curves in Figure 6.22, are both negative as well. This may also suggest a mechanical interpretation for the solid curves

in Figure 6.22 that the dynamic shear modulus of bulk paste is larger than that of the transition zone.

2. K and G are the same for transition zones and bulk paste ($K_1 = K_2$ and $G_1 = G_2$). Under this condition, E is the same for transition zones and bulk paste too ($E_1 = E_2$). This can be proven by applying $E=9KG/(3K+G)$. Therefore, the right hand sides of Equations (6.44), (6.45), (6.47), (6.48), (6.50), (6.51), (6.53) and (6.54) will all equal to zero. Thus, the right hand sides of Equations (6.43), (6.46), (6.49), and (6.52) are all equal to zero too. Furthermore, the right hand sides of Equations (6.41) and (6.42) are both equal to zero. Thus, the right hand sides of Equations (6.33) and (6.34), which are corresponding to the slopes of lower and upper bounds for the data of dashed curves in Figure 6.21, are both equal to zero as well. This may suggest a mechanical interpretation for the dashed curves in Figure 6.21 that the dynamic modulus of elasticity of bulk paste may be equal to that of the transition zone. Also, the right hand sides of Equations (6.49) and (6.52) are both equal to zero. Thus, the right hand sides of Equations (6.35) and (6.36), which correspond to the slopes of lower and upper bounds for the data of dashed curves in Figure 6.22, are both equal to zero too. This may also suggest a mechanical interpretation for the dashed curves in Figure 6.22 that the dynamic shear modulus of bulk paste may be equal to that of the transition zone.

By physical inference, it also makes sense. In this study, since the aggregate volume is fixed, the increasing volume of transition zones will replace the bulk paste by the same amount. If the stiffness and rigidity of the transition zone are less than those of bulk paste, then the dynamic modulus of elasticity and dynamic shear modulus, the smeared-average properties in the mortar matrix, will be reduced when the volume of transition zones is increasing. However, if the stiffness and rigidity are the same for both the transition zone and bulk paste, the composite matrix will retain the same stiffness and rigidity no matter how the relative quantity between the transition zone and bulk paste is varied.

CHAPTER 7

RESULTS AND DISCUSSION 3: SIGNIFICANCE OF TRANSITION ZONES ON PHYSICAL AND MECHANICAL PROPERTIES OF PORTLAND CEMENT MORTAR

7.1 Introduction

The major objective of this chapter is to analyze the significance of cement paste-aggregate interfacial transition zones on the physical and mechanical properties of mortar presented in five sections.

1. Based on the experimental results of MIP and SEM, the porosity of transition zones is described and how the influence of vacuum mixing on this porosity is discussed. In addition, a problem found in applying MIP data to study the porosity of transition zones is also discussed.

2. How the aggregate type and silica fume affect the dynamic moduli of transition zones is investigated. Also, the results of EDS performed on aggregate, bulk paste, and transition zones, are presented.

3. The effects of W/C and Va on the dynamic moduli of transition zones are discussed.

4. With the percolation mechanism in mortar specimens, the tensile and compressive strengths of transition zones are studied.

5. The values of logarithmic decrement of damping for transition zones in flexural, longitudinal, and torsional modes are estimated.

It is known that the degree of compaction of the specimen directly impacts its elastic moduli. The higher the compaction in the specimen, the more rigid and stiffer its behavior. In Chapter 4.2.1, it is discussed that the gross porosity is an index of

compaction for the specimens. Thus, the relationship between gross porosity and dynamic moduli, such as dynamic modulus of elasticity and dynamic shear modulus, is studied. Some researchers may raise the question that entrapped air in some harsh specimens may result in erroneous interpretation of the experimental data. Therefore, the effect of vacuum mixing on the porosity and dynamic moduli of transition zones is also studied with the aid of MIP and microscopic examination.

7.2 The Effects of Vacuum Mixing on Compaction, Porosity, Dynamic Moduli of the Transition Zone

A harsh mixture may contain much entrapped air, and thus the dynamic moduli of the mixture may be reduced. In studying the dynamic moduli of transition zones, it is essential to separate the influence of this entrapped air from that of the transition zone. It is known that vacuum mixing may eliminate entrapped air or reduce its amount. Therefore, the effect of vacuum mixing on the dynamic moduli of mortar specimens can be used to study the influence of entrapped air on the dynamic moduli. In this study, differences in porosity and in the degree of compaction are studied between specimens having the same mixture proportion but mixed with and without vacuum being applied during mixing. In addition, the microstructural effects associated with the vacuum mixing are studied by MIP and SEM methods.

Figure 7.1 shows the relationship between gross porosity and SA for dolomite mortars having mixture proportions of 40_42_00. Data are presented with and without vacuum mixing. It is observed that the gross porosity for the vacuum-mixed mixture is lower, i.e., the mixture is more compact. Consequently, both the dynamic modulus of elasticity and the dynamic shear modulus are found to increase slightly as shown in Figures 7.2 and 7.3. It is seen that the vacuum mixing process does not alter any of the trends of porosity, dynamic modulus of elasticity, and dynamic shear modulus. This implies that these mixtures do not have a compaction problem that is due to entrapping extremely large amounts of air.

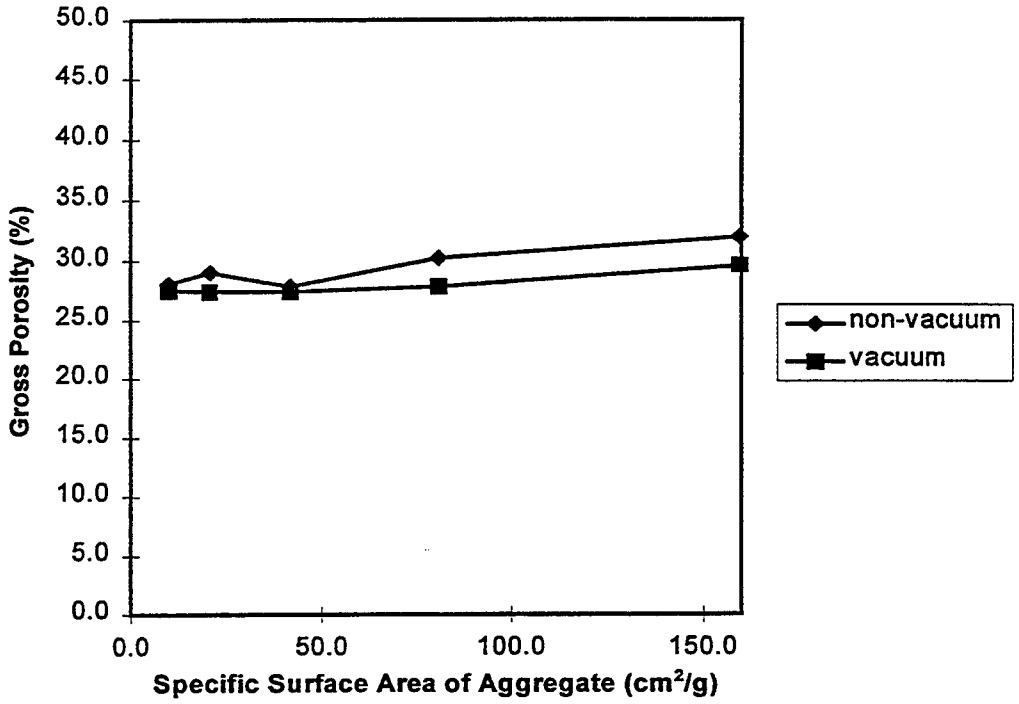

Figure 7.1 Gross Porosity vs. SA for dolomite mortars having mixture proportions of 40_42_00, with and without vacuum applied in mixing.

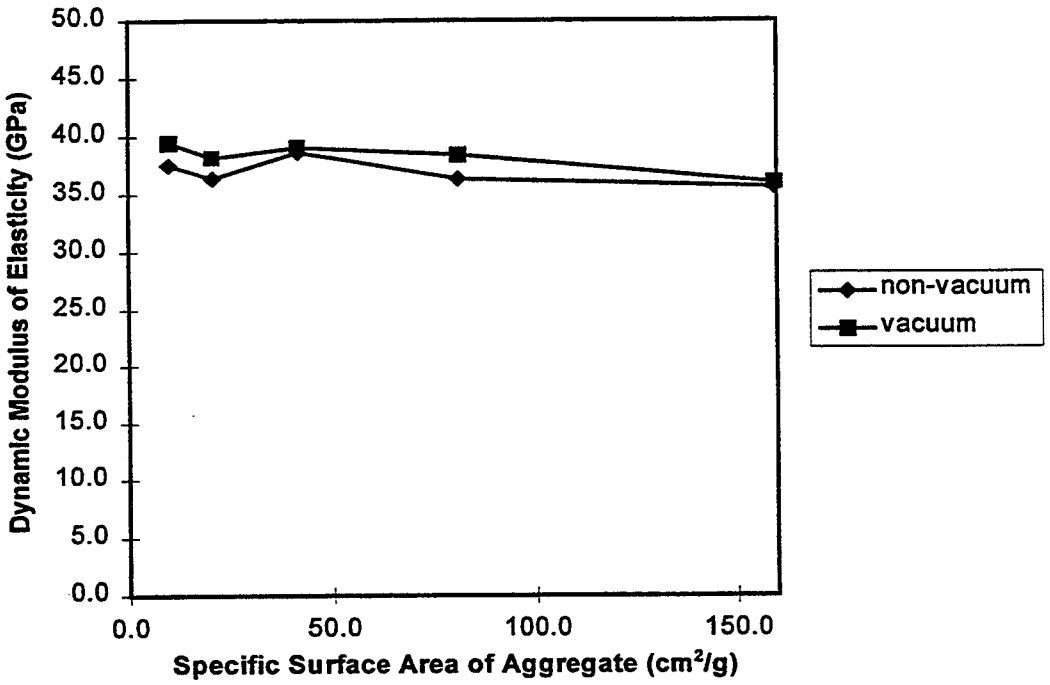

Figure 7.2 Dynamic Modulus of Elasticity vs. SA for dolomite mortars at 28 days old having mixture proportions of 40_42_00, with and without vacuum applied in mixing.

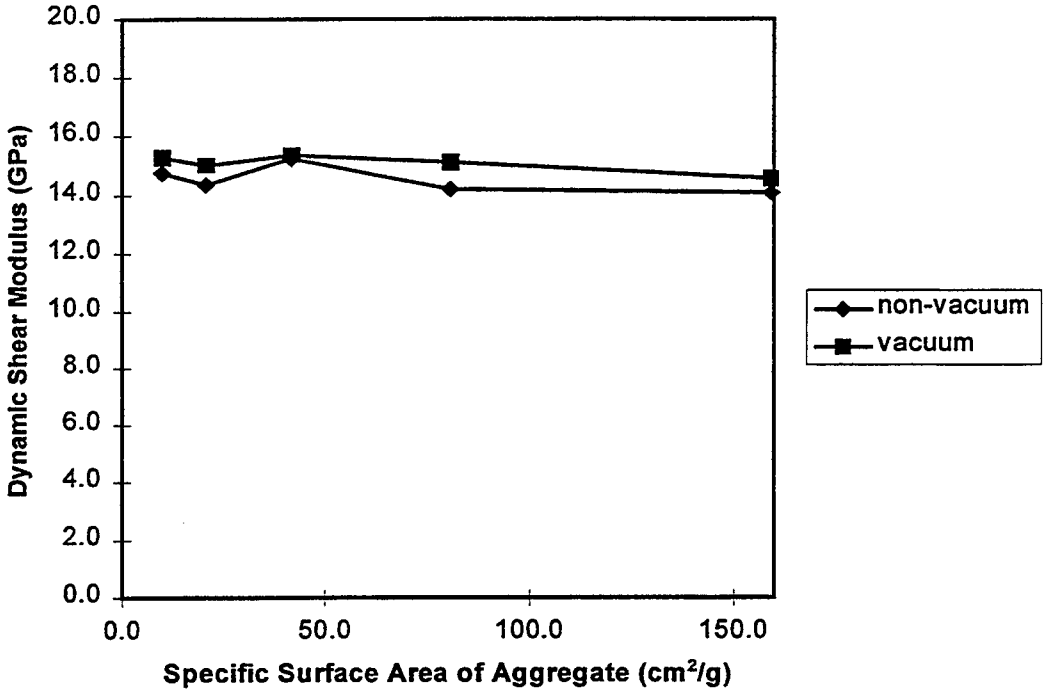

Figure 7.3 Dynamic Shear Modulus vs. SA for dolomite mortars at 28 days old having mixture proportions of 40_42_00, with and without vacuum applied in mixing.

For other mixtures having mixture proportions of 40_50_00, it is observed that vacuum mixing has similar modest effect on gross porosity as shown in Figure 7.4. For the mixtures having mixture proportions of 55_42_00, vacuum mixing has essentially no effect on the gross porosity as shown in Figure 7.5. Also, the associated dynamic modulus of elasticity and dynamic shear modulus are both observed to be uninfluenced by the vacuum mixing as shown in Figures 7.6 and 7.7. As indicated in Chapter 5.5, it is known that this group of specimens may all have mixing and compaction problems due to insufficient water added for mixing. It is therefore inferred that this kind of mixing and compaction problem cannot be solved by vacuum mixing, although such mixing can reduce the content of entrapped air.

MIP is notorious for its "ink-bottle" effect. However, the information concerning threshold pore size and the total cumulative intruded volume provided by MIP is still regarded as valid. Figure 7.8 presents the MIP result for PC mortars having mixture proportions of 40_42_00, without vacuum mixing. It is observed that the mortars with finer aggregate contain more intruded pore volume. In contrast, if vacuum is applied during mixing, the total volume of pores decreases to a stable value (about 0.06 cm^3/g) regardless of the aggregate size in the mixture, as shown in Figure 7.9. These MIP results are consistent with the gross porosity results shown in Figures 7.1 and 7.4 in that vacuum mixing reduces the pore volume and the specimens become more compact. In addition, no abnormally large volume of pores is detected in Figure 7.8. Thus, the specimens used are deemed to be free of compaction problem.

Results from investigating BEI micrographs in SEM analysis may support the viewpoint that the increase of pore volume with fineness of aggregate, as shown in Figure 7.8, is due to the progressively increasing volume of transition zones. This is discussed as follows. Figure 7.10 presents a BEI micrograph of a transition zone around a dolomite aggregate having a size between ASTM Sieve No. #4 and #8. The mixture proportion for this specimen is 40_42_00. The magnification of this image is 200×. Figure 7.11 taken at 500× is a magnified view of the rectangular region in Figure 7.10. There appear to be a porous region near the calcium hydroxide deposit at the surface of the

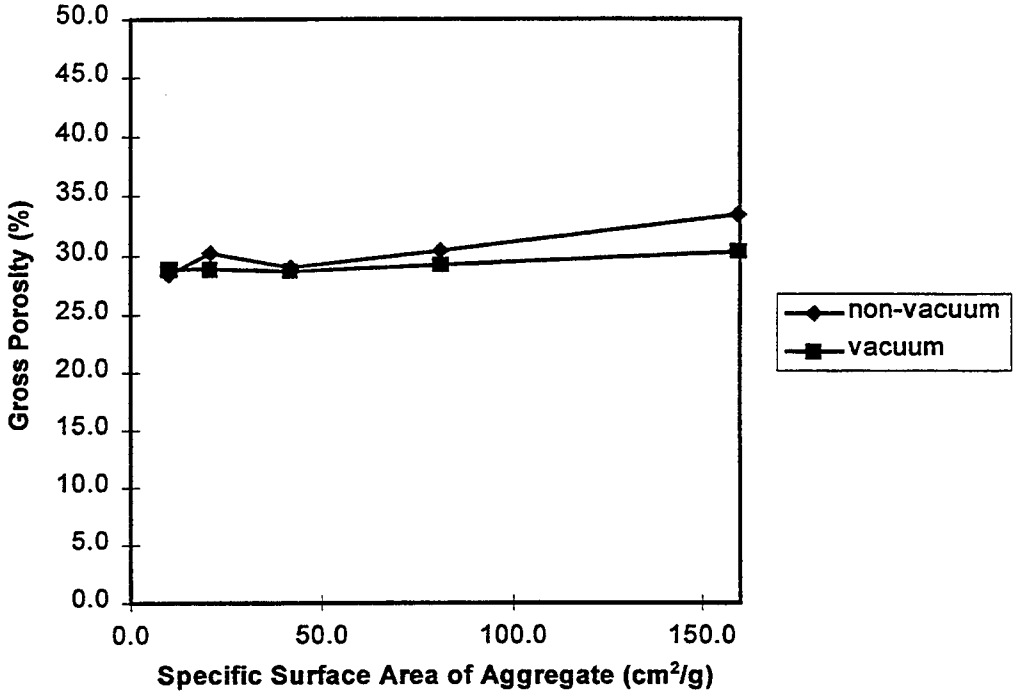

Figure 7.4 Gross Porosity vs. SA for dolomite mortars having mixture proportions of 40_50_00, with and without vacuum applied in mixing.

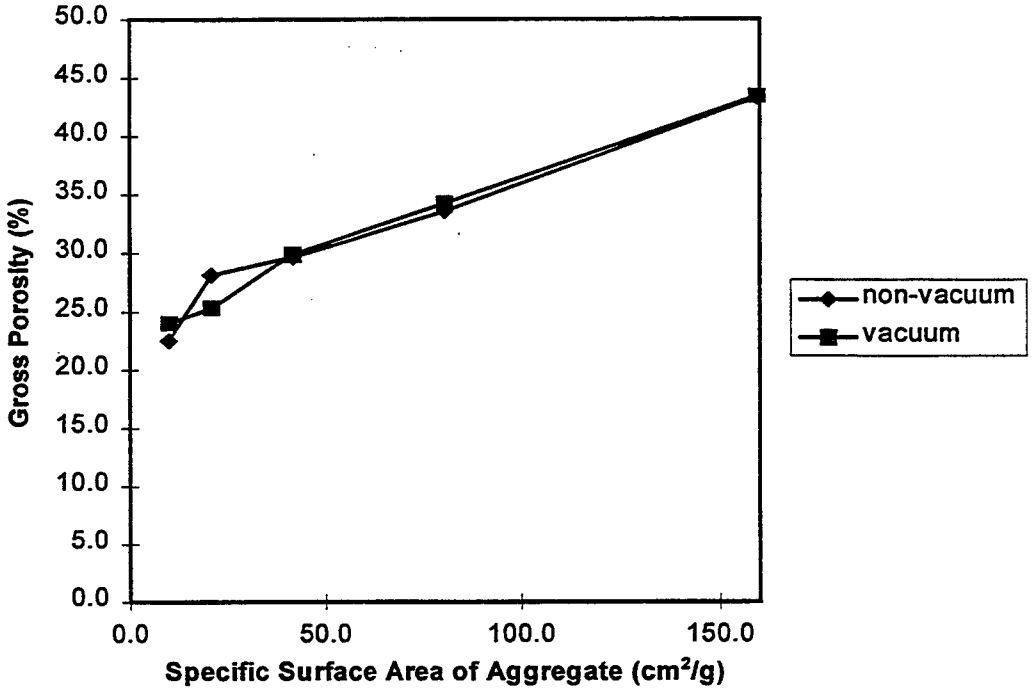

Figure 7.5 Gross Porosity vs. SA for dolomite mortars having mixture proportions of 55_42_00, with and without vacuum applied in mixing.

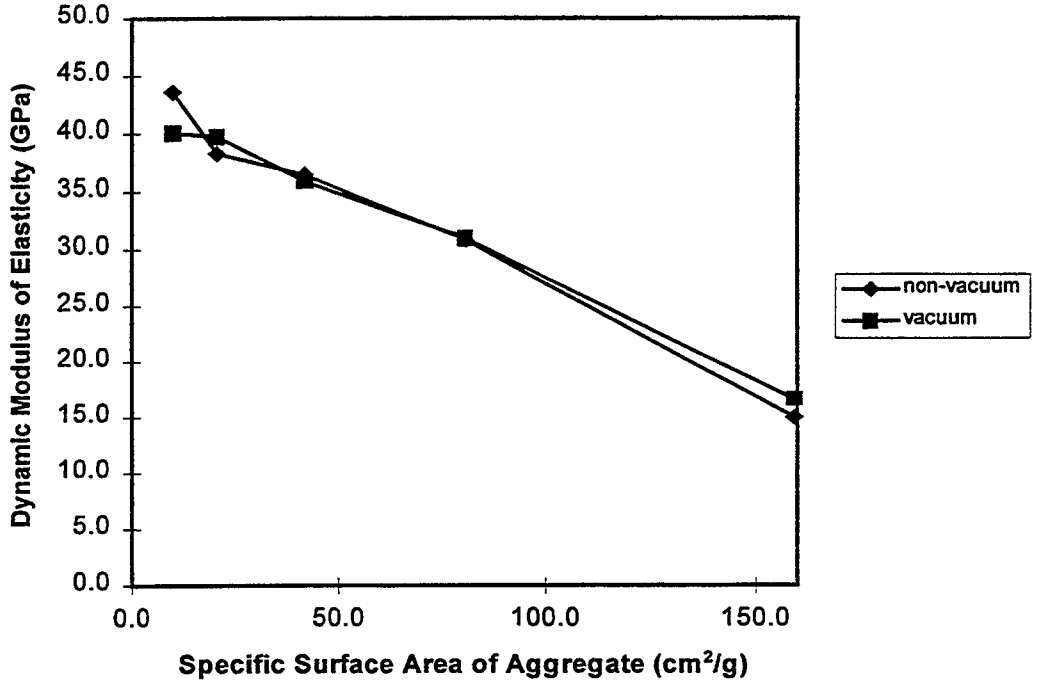

Figure 7.6 Dynamic Modulus of Elasticity vs. SA for dolomite mortars at 28 days old having mixture proportions of 55_42_00, with and without vacuum applied in mixing.

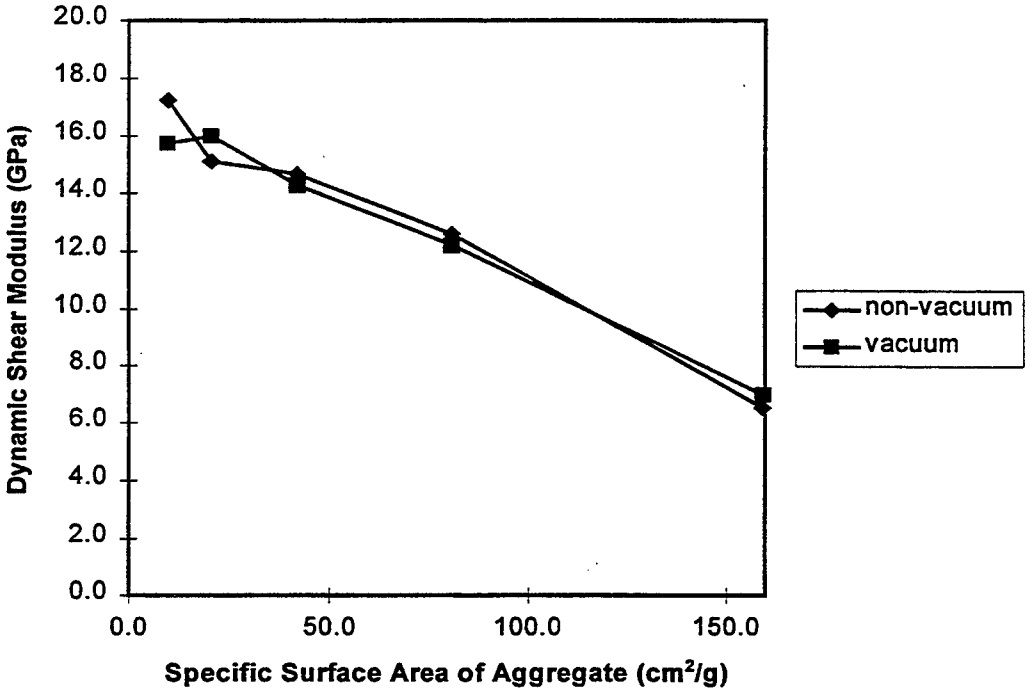

Figure 7.7 Dynamic Shear Modulus vs. SA for dolomite mortars at 28 days old having mixture proportions of 55_42_00, with and without vacuum applied in mixing.

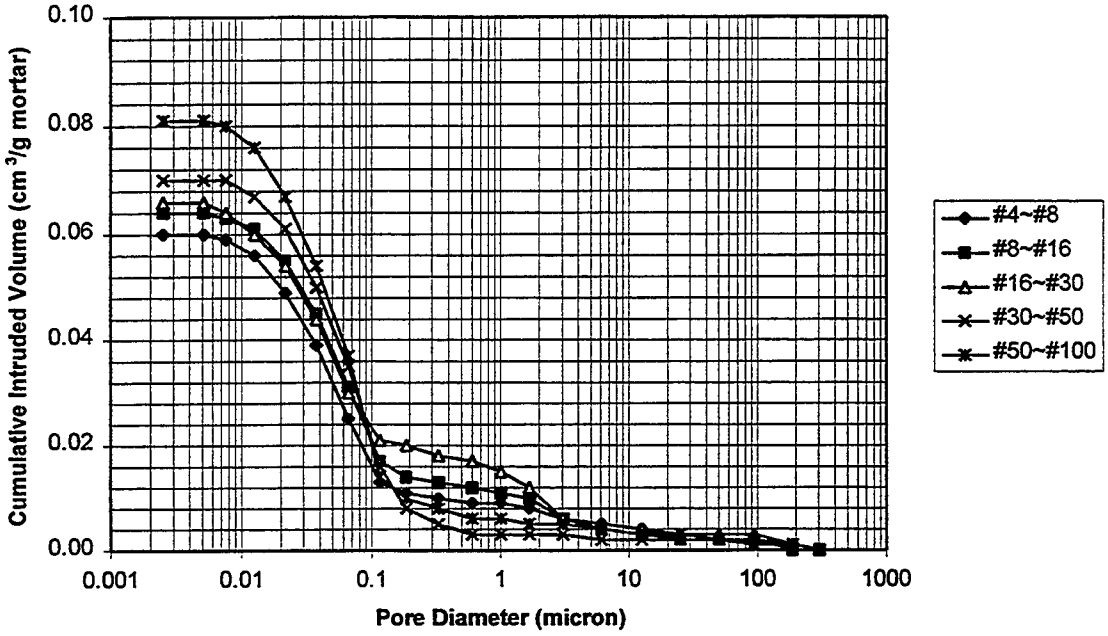

Figure 7.8 MIP Cumulative Intruded Volume vs. Pore Diameter for mortars having one of the five fractional sizes (ASTM sieve no.: #4~#8, #8~#16,#16~#30, #30~#50, and #50~#100) of aggregate, mixture proportions of 40_42_00, and no vacuum applied in mixing.

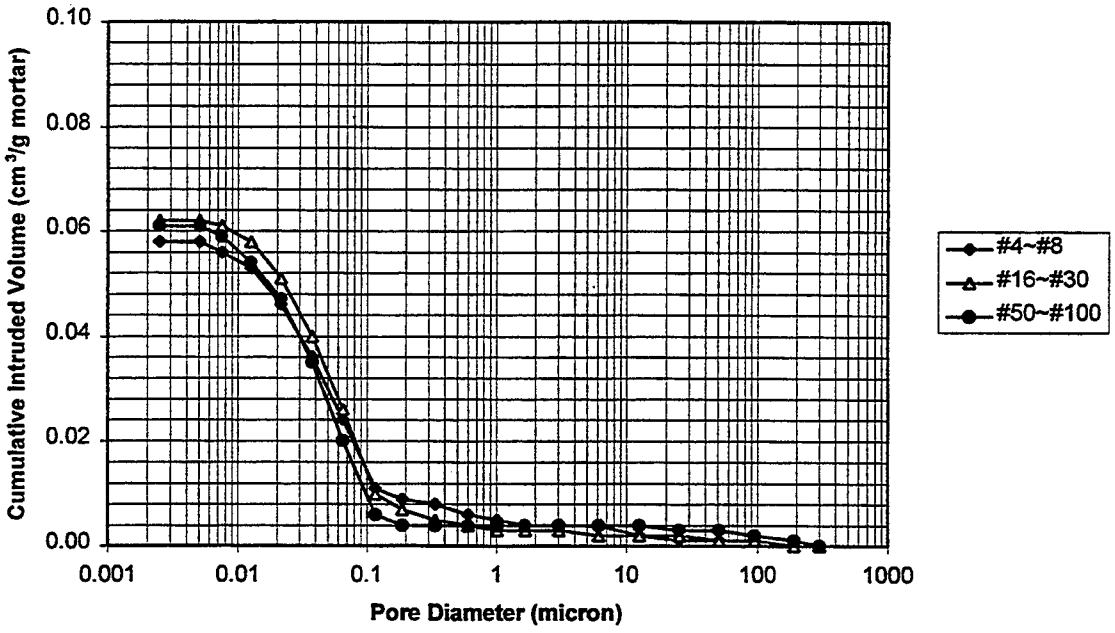

Figure 7.9 MIP Cumulative Intruded Volume vs. Pore Diameter for mortars having one of the three fractional sizes (ASTM Sieve No.: #4~#8, #16~#30, and #50~#100) of aggregate, mixture proportions of 40_42_00, and vacuum applied in mixing.

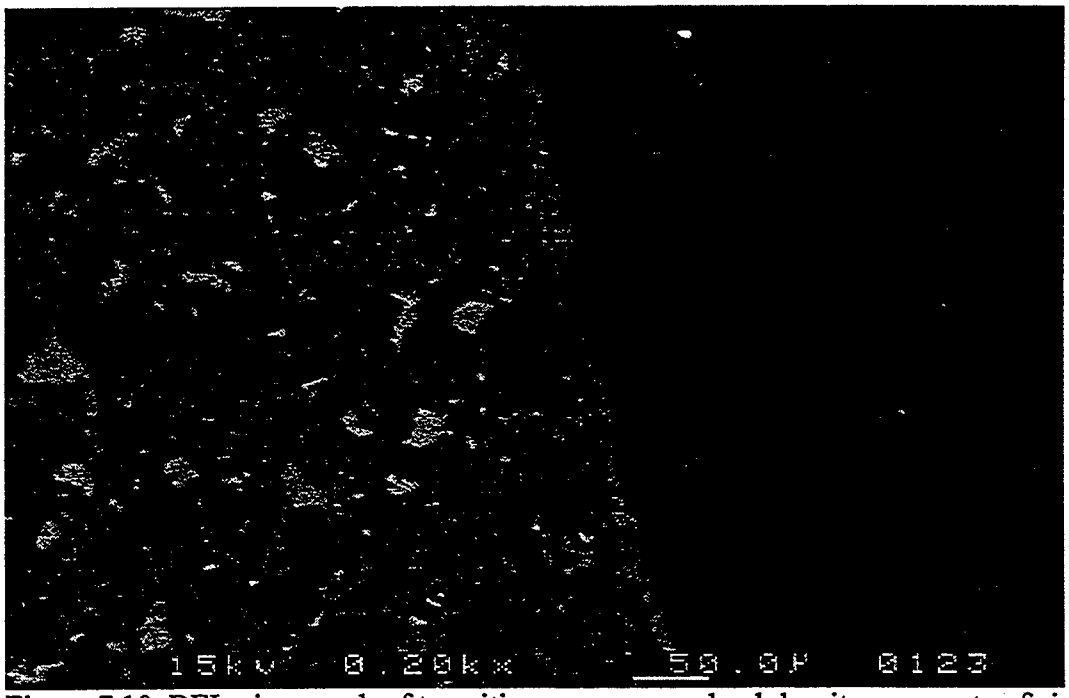

Figure 7.10 BEI micrograph of transition zones around a dolomite aggregate of size between ASTM sieve no. #4 and #8, magnification 200×, mixture proportion 40_42_00.

Figure 7.11 A magnified view of the rectangular region in Figure 7.10, magnification 500×.

aggregate. Therefore, it may be suggested that increasing the volume of transition zones may also increase the pore volume, thus porosity, in the specimen. However, the phenomenon of porous region was not uniformly observed in the specimens and the porosity may vary from place to place. This SEM investigation is consistent with one of the conclusions by Scrivener and Gartner [1988]. Based on SEM image analysis, they measured porosity by varying the distance from aggregate surface and proposed that porosity became higher when approaching the aggregate surface.

Figure 7.12 is a BEI micrograph of a specimen having the same mixture proportion and magnification as the one for Figure 7.11, except that vacuum mixing was applied for this specimen. In comparison with Figure 7.11, it appears that the quantity of pores is much diminished, especially, the number of smaller pores, less than 10 μm, is significantly reduced. This observation is consistent with the MIP result that vacuum mixing reduces the pore volume in the specimen. It is also noticed that many pores near the aggregate surface are either eliminated or reduced in size due to the vacuum mixing.

In summary, porosity plays an important role in determining the dynamic moduli of a specimen. Vacuum mixing can efficiently reduce the number of small pores, thus lowering the porosity in both the bulk paste and the transition zones and making them more compact. Therefore, the dynamic moduli of specimen are increased.

7.2.1 A Reconsideration on Studying Porosity of the Transition Zone by MIP

An interesting and essential attempt is made to determine the porosity of transition zones. Intuitively, the solution may fall on the quantitative analysis of MIP data for aggregate, paste, and mortar. Basically, this quantitative analysis is according to the following concept. Mortar is composed of aggregate, bulk paste, and transition zones. One can measure the porosities of aggregate particles, bulk paste, and mortar by MIP. Then, by subtracting the porosities of aggregate particle and bulk paste from the porosity of mortar in accordance with the volume fraction of each constituent, the porosity of the transition zone may be able to be determined.

Figure 7.12 BEI micrograph with magnification 500×. The mixture proportion for this specimen is the same as the one for Figure 7.11; 40_42_00 except that vacuum mixing was applied for this specimen.

Unfortunately, the issue of the average thickness of the transition zone is still controversial and is the subject of several studies. Thus, the exact volume fractions for bulk paste and transition zones in the mortar cannot be determined. An alternate method to avoid using the thickness or volume of the transition zone is to present the result as the extra volume of pores in the cement paste of mortar by comparing it to the volume of pores in bulk paste. The bulk paste used for comparison must have the same W/C and volume as the cement paste of mortar. Conceptually, this extra volume of pores expressed in per unit volume of transition zones and bulk paste may be induced by transition zones. This method can be expressed by the following equation:

$$\frac{\Delta V_{TZ-BP}}{v_{TZ+BP}} = \frac{V_{Mortar} \times D_{Mortar} - V_{Agg} \times D_{Agg} \times v_{Agg}}{1 - v_{Agg}} - V_{BP} \times D_{BP} \qquad (7.1)$$

where ΔV_{TZ-BP} is the difference in pore volume between transition zones and bulk paste,

v_{TZ+BP} is the combine volume of transition zones and bulk paste,

V_{Mortar}, V_{BP}, and V_{Agg} represent the pore volume measured by MIP and expressed in per unit weight of 105°C oven dry mortar, bulk paste, and aggregate particle respectively,

D_{Mortar}, D_{BP}, and D_{Agg} are the bulk densities of mortar, bulk paste, and aggregate particle respectively, the weight of specimen was measured after a 105°C oven dry process, and

v_{Agg} is the volume fraction of aggregate in mortar.

The extra porosity induced into mortar by the transition zone is presented by the numerator of the left hand side of Equation (7.1), while the denominator represents the combined volume of the bulk paste and the transition zones.

In the following, it is explained how the variables in the right hand side of Equation (7.1) are determined from experiment. Because the included aggregate particle is regarded as having no influence on the properties of bulk paste, the porosity of bulk paste can be assumed to be the same as that of plain paste with the same W/C. Thus, V_{BP} and D_{BP} can be determined by measuring on the plain paste with the same W/C as mortar. With the variation of pore diameter, the cumulative volume of pores is shown in Figure

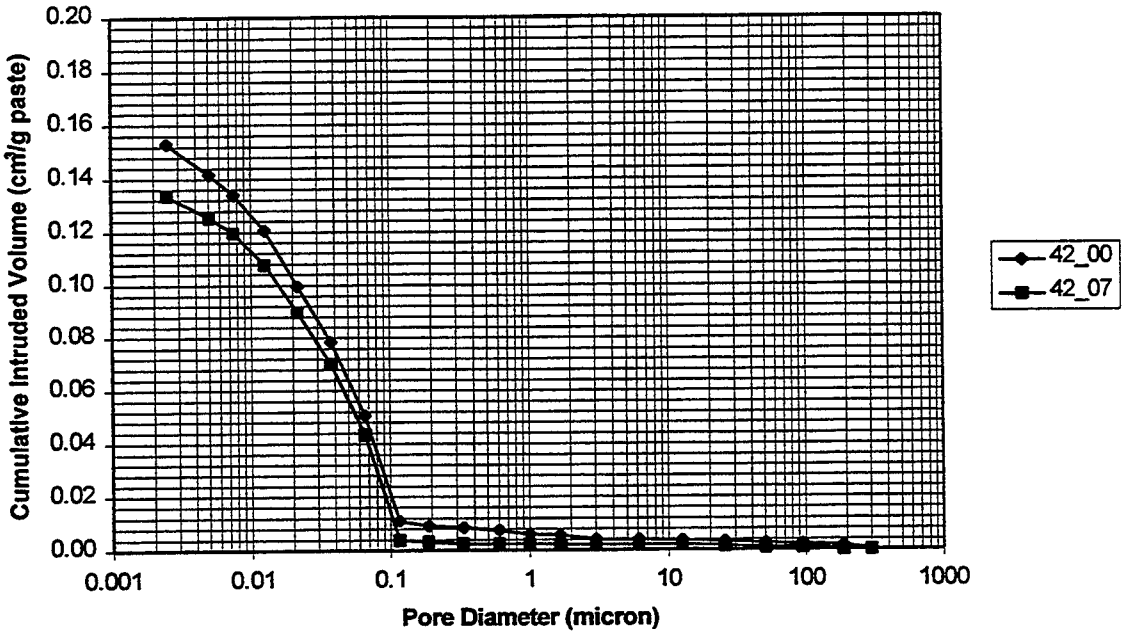

Figure 7.13 MIP Cumulative Intruded Volume vs. Pore Diameter for plain paste, having mixture proportion W/C=0.42, with 7% and without silica fume, and without vacuum applied in mixing.

7.13 for plain paste (V_{BP}) having a W/C of 0.42, none and 7% silica fume content. The point in the far left hand side of each curve has its largest volume. This largest volume represents the total volume of pores inside the specimen and is used for calculation.

In addition, V_{Mortar}, D_{Mortar}, V_{Agg}, and D_{Agg} can be determined by performing MIP and density tests on mortars and aggregate particles. The relationship between pore diameter and the cumulative volume of pores (V_{Mortar}) is shown in Figure 7.8 for dolomite mortars having five fractions of aggregate sizes (ASTM Sieve No.: #4~#8, #8~#16, #16~#30, #30~#50, and #50~#100), mixture proportion 40_42_00. The relationship between pore diameter and the cumulative volume of pores is shown in Figure 7.14 for dolomite mortars having three fractions of aggregate sizes (ASTM Sieve No.: #4~#8, #16~#30, and #50~#100), mixture proportion 40_42_07. v_{Agg} can be determined from mixture proportion. The relationship between the cumulative volume of pores and pore diameter is shown in Figure 7.15 for five fractional sizes (ASTM sieve no.: #4~#8, #8~#16, #16~#30, #30~#50, and #50~#100) of dolomite aggregate particles. To the right hand side of five critical points: A, B, C, D, and E, ascendant regions are observed in the curves when pore diameter becomes smaller. In accordance with the discussion by Olek et al. [1990], this may be due to the rearrangement and compaction of the clumps or agglomerates of aggregate particles. Nevertheless, due to the lack of a second slope-transforming region in the curves, the rearrangement and compaction phenomenon are not obvious for each individual aggregate particle. Thus, the plateau region, the left hand side of each critical point, represents the cumulative intruded volume for aggregate particle in each fractional size. By subtracting the volume due to rearrangement and compaction, Figure 7.15 is transformed into Figure 7.16. Thus, the intruded volume of aggregates (V_{Agg}) can be determined from the point in the far left hand side of each curve in Figure 7.16. It is noted that the pore volume in this kind of dolomite aggregate particle

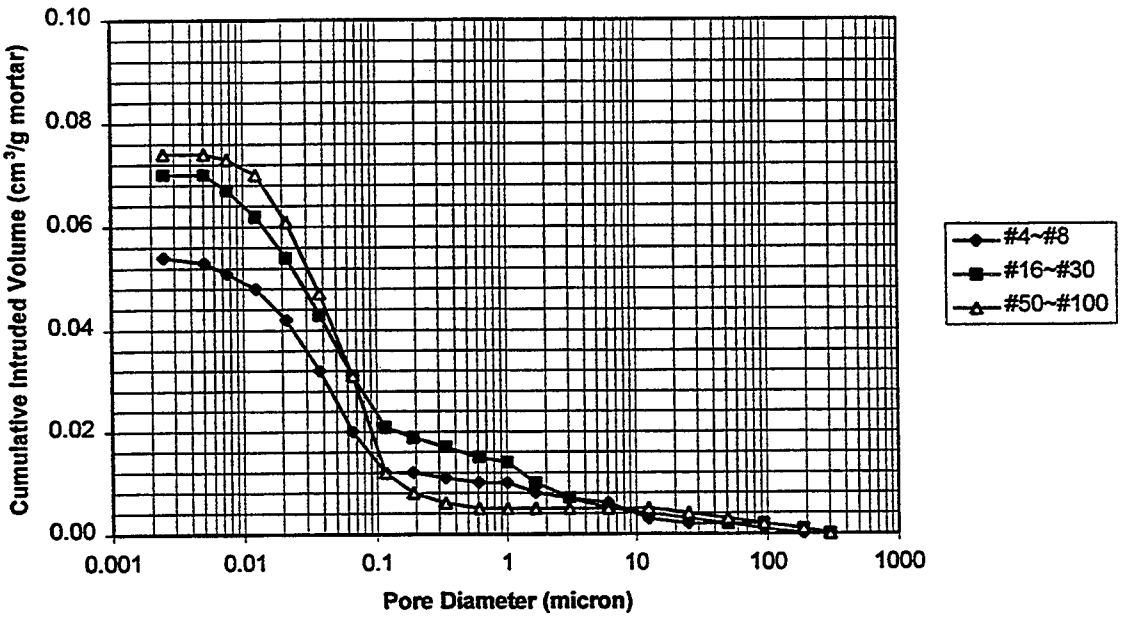

Figure 7.14 MIP Cumulative Intruded Volume vs. Pore Diameter for mortars having one of the three fractional sizes (ASTM Sieve No.: #4~#8, #16~#30, and #50~#100) of aggregate, mixture proportions of 40_42_07, and without vacuum applied in mixing.

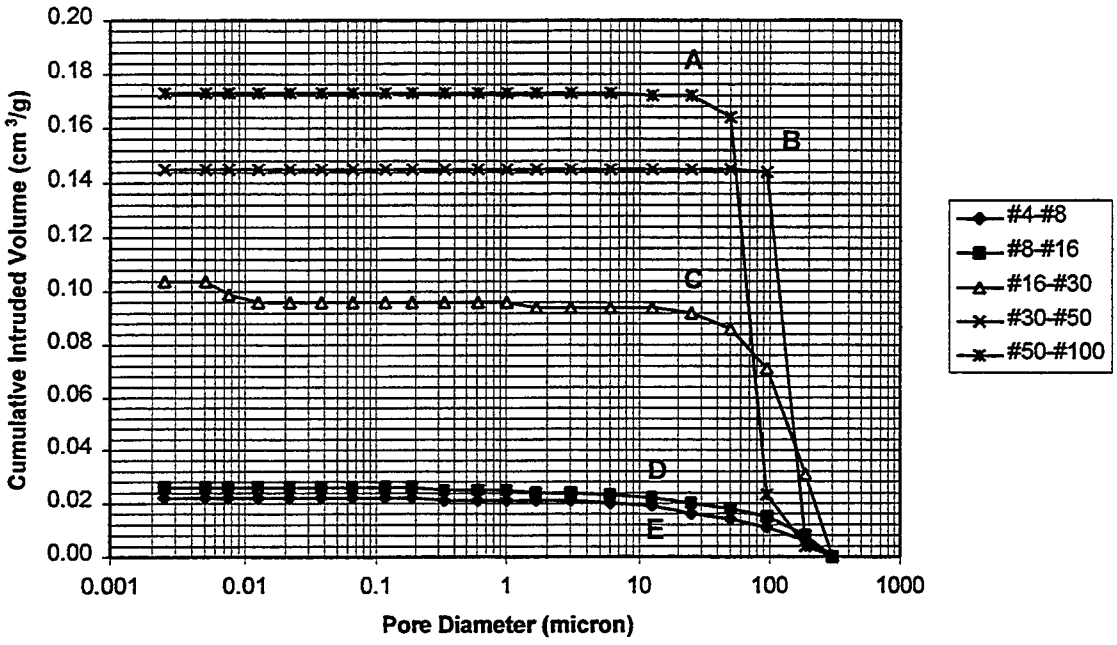

Figure 7.15 MIP Cumulative Intruded Volume vs. Pore Diameter for five fractional sizes (ASTM Sieve No.: #4~#8, #8~#16, #16~#30, #30~#50, and #50~#100) of dolomite sand particles. Include the effects of rearrangement and compaction of sand particles.

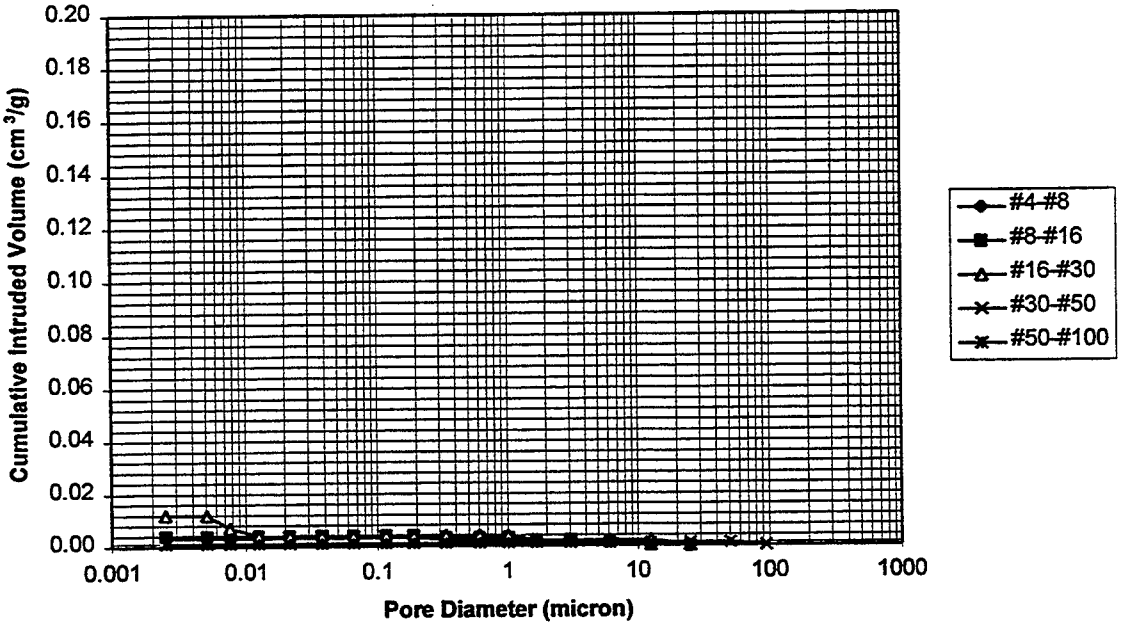

Figure 7.16 MIP Cumulative Intruded Volume vs. Pore Diameter for five fractional sizes (ASTM Sieve No.: #4~#8, #8~#16, #16~#30, #30~#50, and #50~#100) of dolomite sand particles. Exclude the effects of rearrangement and compaction of sand particles.

is quite small; close to zero, regardless of aggregate size. Thus, all of the variables in the right hand side of Equation (7.1) are able to be determined.

In this study, data for two groups of dolomite mortars were used for calculation in the right hand side of Equation (7.1). One is the group for the PC mortars having five fractions of aggregate sizes (ASTM Sieve No.: #4~#8, #8~#16, #16~#30, #30~#50, and #50~#100) and mixture proportion 40_42_00. The other group is for the SF mortars having three fractions of aggregate sizes (ASTM Sieve No.: #4~#8, #16~#30, and #50~#100) and mixture proportion 40_42_07. The calculated results are shown in Figure 7.17. The calculated values of $\Delta V_{TZ-BP} / v_{TZ+BP}$ are negative for the PC mortars having individual aggregate size fraction #4~#8, #8~#16, #16~#30, or #30~#50 included. In addition, the calculated values of $\Delta V_{TZ-BP} / v_{TZ+BP}$ are also negative for the 7% SF mortar having aggregate size fraction #4~#8 included. Does this mean the porosity of the transition zone is less than that of bulk paste? A discussion of this question is presented below.

A similar experiment was conducted by Kayyali [1985, 1987] and similar results were obtained. In his work, a conclusion was drawn that the porosity of the transition zone is lower than that of bulk paste. Another conclusion he made is that the porosity of the transition zone is so low as to mask the pores in aggregate particles from being intruded.

However, judging from the MIP data of this study in Figures 7.8 and 7.14, it may be concluded that the porosity of the mortar increases when the volume of the transition zone increases. In addition, Figure 7.17 shows a trend that when SA increases, the volume of transition zone increases, as well as the value of $\Delta V_{TZ-BP} / v_{TZ+BP}$. These results may support the viewpoint that the transition zone is more porous than the bulk paste. Furthermore, as shown in BEI micrographs of Figures 7.10 and 7.11, the large amount of tiny pores residing in transition zones may also support this point of view. But why are some of the calculated values of $\Delta V_{TZ-BP} / v_{TZ+BP}$ negative? An explanation suggests that the pore volume of bulk paste in mortar may be lower than that of plain paste with the same W/C. This is based on the concept that if the W/C of the region

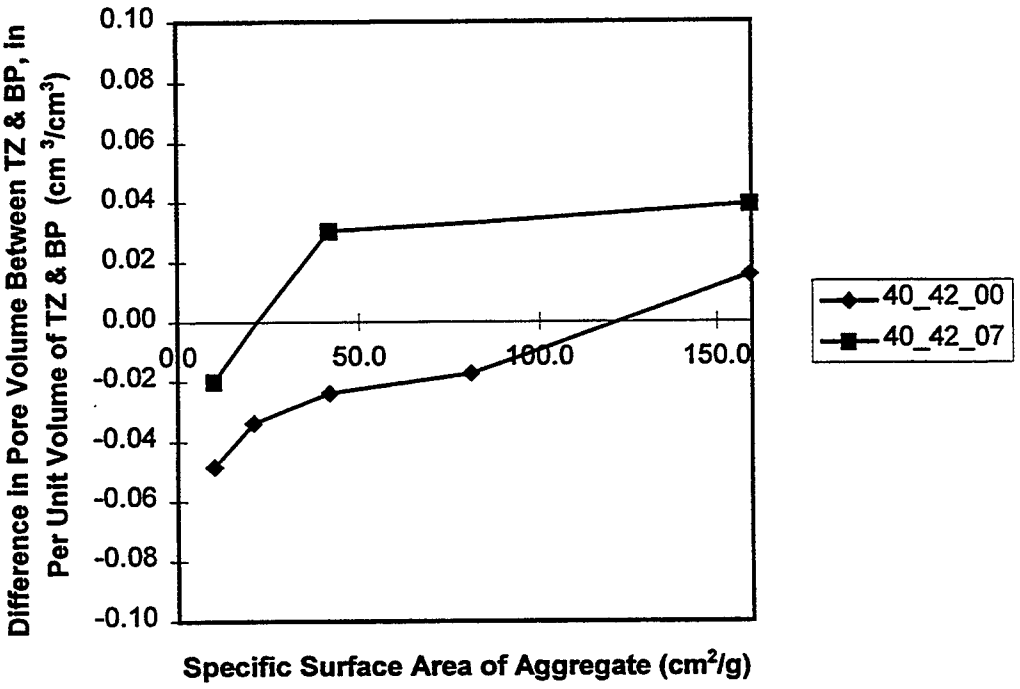

Figure 7.17 Difference in Pore Volume Between the Transition Zone (TZ) and Bulk Paste (BP) vs. SA in Per Unit Volume of the Transition Zone and Bulk Paste ($\Delta V_{TZ-BP} / \upsilon_{TZ+BP}$) for PC and SF dolomite mortars having Va=0.40, W/C=0.42. PC mortars have one of the five fractional sizes (ASTM sieve no.: #4~#8, #8~#16, #16~#30, #30~#50, and #50~#100) of aggregate. 7% SF mortars have one of the three fractional sizes (ASTM sieve no.: #4~#8, #16~#30, and #50~#100) of aggregate. No vacuum was applied in mixing.

around the aggregate surface is higher than the denoted value, the W/C of bulk paste must be lower, resulting in less pore volume. Another explanation suggests that aggregate particle in the mortar plays a role as a barrier to the pore channel system that is the intruded path of mercury. Thus, the pores induced by the aggregate particles located in the center portion of the specimen may be isolated and cannot be intruded by mercury, although the volume of these pores ought to be counted in the porosity of mortar. Therefore, the MIP data for the mortar specimen is lower than its real value.

The suspicion on the masked effect of aggregate is based on the results of three other experiments. Firstly, Figure 2 in Bourdette et al. [1995] shows that the incremental volume intruded by mercury with pore diameter between 0.03 and 0.05 μm in the plain paste is much larger (almost twice) than that in the cement paste of mortar. Thus, the masked effect may mainly happen on the pores of 0.03 to 0.05 μm size.

Secondly, the BEI micrographs in Figures 2 and 3 of Scrivener and Nemati [1996] show that although Wood's metal fills into the pores around aggregate, a lot of pores in the bulk paste are still not intruded by Wood's metal. This may indicate that some pore channels may be either isolated or masked in the specimen. However, the penetrating capacity of their technique is 0.08 μm. This is not enough substantiation to prove the masking effect. A penetrating capacity of at least 0.03 μm is necessary, and the intruding material ought to be capable of being "frozen" in the pores like Wood's metal for investigation.

Finally, a delicate experiment by Winslow and Liu [1990] addressed the difference in pore volume between plain cement paste and the cement paste in mortar or concrete. Their experiment compared the data of specimens at an equal degree of hydration, and not at equal hydration time. In addition, by applying an optical microscope, the volume of entrapped air could be estimated and subtracted from the total pore volume in the specimen measured by MIP. Thus, their results may be regarded as more reasonable in reflecting the pore volume of the specimen. A relationship between cumulative extra intruded volume and pore diameter is shown as Figure 5 in their paper. The extra intruded volume is the difference obtained by subtracting the pore volume of

plain paste from that of cement paste in concrete. Two curves are shown in Figure 5; one is for the more hydrated pastes and the other is for the less hydrated pastes. For the curve of more hydrated pastes, there is a descendent region for the cumulative extra intruded volume if the pore diameter is smaller than 0.1 μm. For the curve of less hydrated pastes, there are two descendent regions in the curve. The descendent region in the curve of more hydrated pastes may indicate that the pore volume having a pore diameter of less than 0.1 μm in the plain paste is larger than that of the concrete paste. Both pastes used for comparison are at the same degree of hydration. Another explanation may suggest that some of the pore channels with a pore diameter of less than 0.1 μm are masked by the aggregate particles. Thus, part of the pore volume, corresponding to pore diameter less than 0.1 μm, measured in the concrete paste is less than that measured in the plain paste. Therefore, this descendent region is observed in the curve of more hydrated pastes.

A question may be raised that, with the maximum pressure of 60,000 psi in the MIP experiment of this study, the intruded capability of mercury is about 25 **Å**. However, this value is calculated according to Washburn relation. In the complex channel system of pores similar to that in the mortar, the channel is tortuous and the shape of the cross section is irregular. This could cause a large loss of pressure head. Therefore, the intruded capacity of mercury in the inner portion of mortar specimen will be reduced, especially if some of the channel system of pores happen to be intercepted by aggregate particles, the porosity measured by MIP on the mortar will be lower than its true value. Thus, some of the negative values of $\Delta V_{TZ-BP} / v_{TZ+BP}$ were obtained. However, this point of view needs to be verified by more advanced instruments and experimental techniques.

7.3 Dynamic Moduli of Transition Zones for Various Aggregate Types and the Influence of Silica Fume

Based on analyzing the slopes of the curves in Figures 6.21 and 6.22, it is suggested in Chapter 6.6 that dynamic modulus of elasticity and dynamic shear modulus of transition zones surrounding quartzite aggregate particles may be less than those of

bulk paste. Another suggestion is that silica fume may modify the transition zone to possess a level of dynamic moduli equal to that of the bulk paste. In this section, a discussion is presented on the dynamic moduli of transition zones around other types of aggregates such as dolomite and perlite.

Figures 7.18 and 7.19 present the dynamic modulus of elasticity and dynamic shear modulus with varying SA for dolomite mortars having mixture proportions 37_52_00 and 37_52_10. These mixture proportions are the same as those of quartzite mortars having their dynamic moduli shown in Figures 6.21 and 6.22.

Before performing analysis on the experimental data, an attempt was made to check the validity of these data. With reference to Chapter 5.6, invalid data due to the compaction problem may be found by checking whether or not the average thickness of water film around the aggregate particle exceeds the criterion. Figure 7.20 presents the thickness of water film for the two groups of specimens having mixture proportions 37_52_00 and 37_52_10. It is observed that the water films are always thicker than the criterion. Thus, there are probably no mixing and compaction problems in these two groups of specimens. Therefore, the data for these two groups of specimens are considered to be valid for analysis.

By comparing Figures 7.18 and 7.19 with Figures 6.21 and 6.22, it is noticed that the dynamic modulus of elasticity and dynamic shear modulus of PC dolomite mortars are relatively flat in comparison with those of PC quartzite mortars. In accordance with the interpretation in Chapter 6.6, this may suggest that the transition zone around dolomite sand particles is stiffer and more rigid than that around quartzite sand particles. This conclusion is in accord with the conclusion of Monteiro and Mehta [1986, (1)], who concluded that the carbonate rock reacts with the cement paste in the transition zone and may strengthen the transition zone.

By observing the curves in Figures 7.18 and 7.19, it may be suggested that silica fume has an effect of reducing the dynamic modulus of elasticity and the dynamic shear modulus of mortars. In order to evaluate the mechanism resulting in this effect, it is better to analyze the data of gross porosity and to investigate the microstructure in the

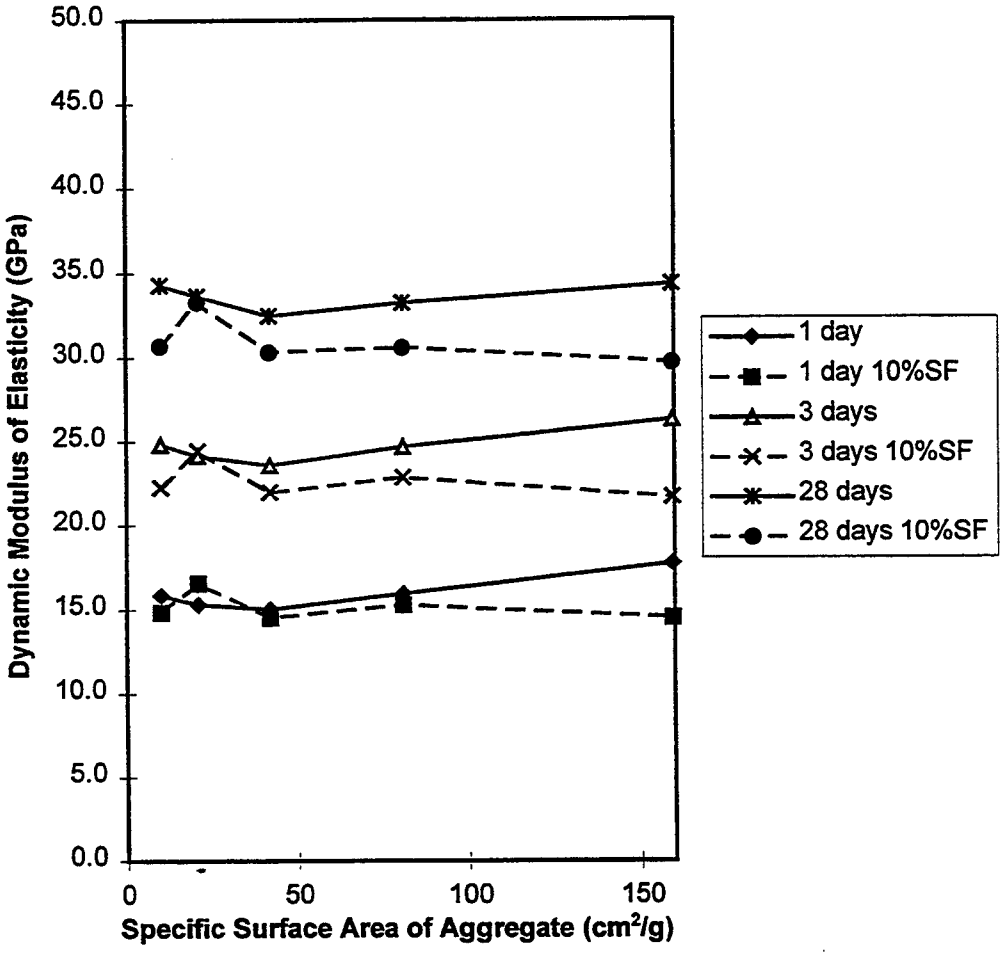

Figure 7.18 Dynamic Modulus of Elasticity vs. SA for dolomite mortars at 1, 3, and 28 days old having mixture proportions of 37_52_00 and 37_52_10.

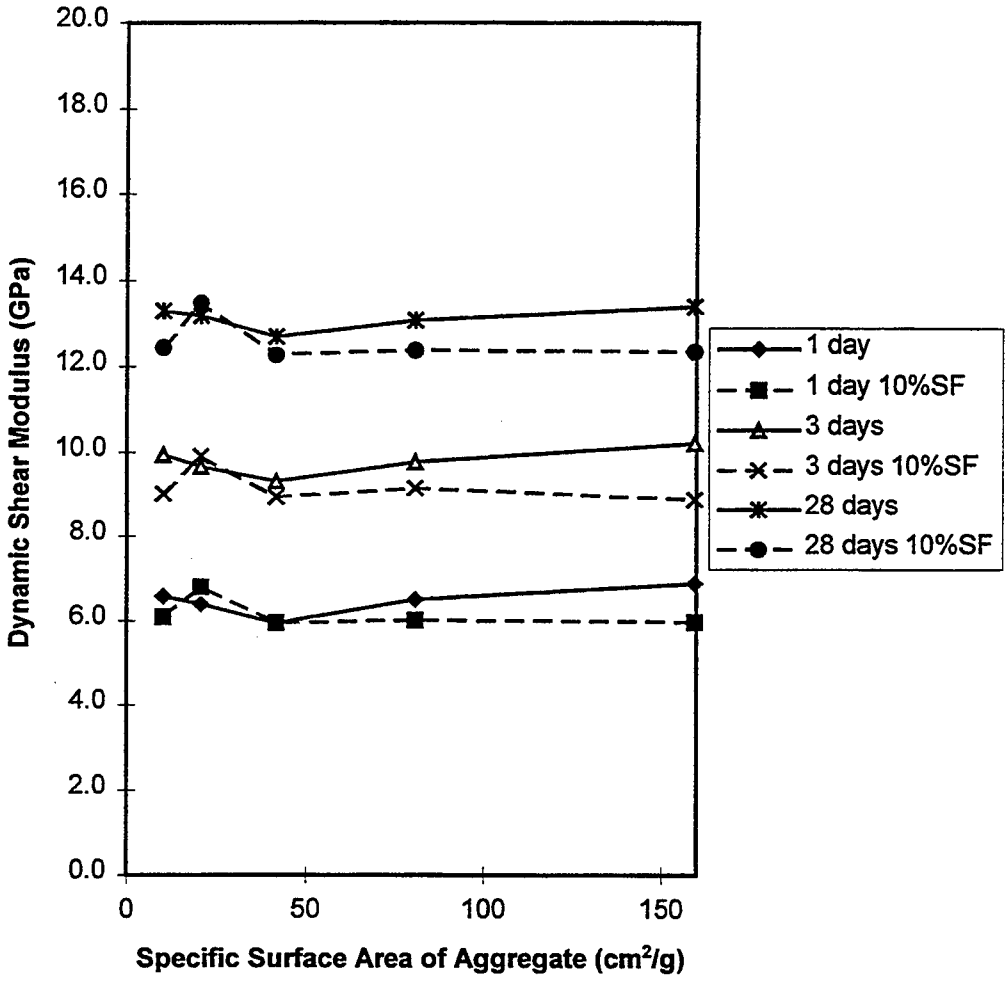

Figure 7.19 Dynamic Shear Modulus vs. SA for dolomite mortars at 1, 3, and 28 days old having mixture proportions of 37_52_00 and 37_52_10.

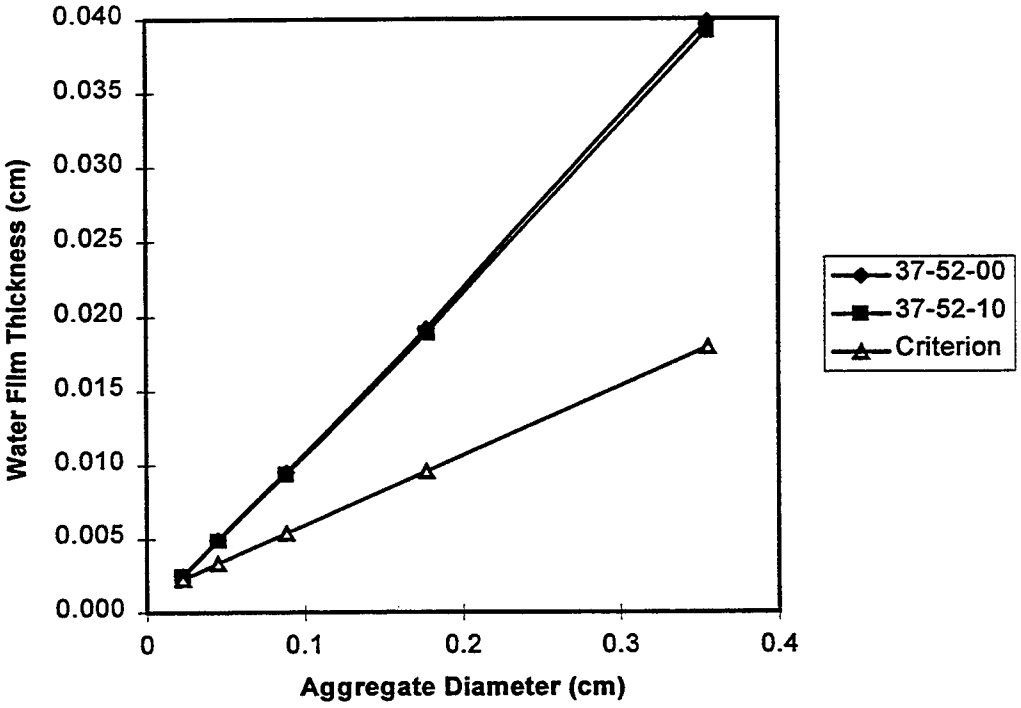

Figure 7.20 Water Film Thickness vs. Aggregate Diameter for the criterion and dolomite mortars having mixture proportions of 37_52_00 and 37_52_10.

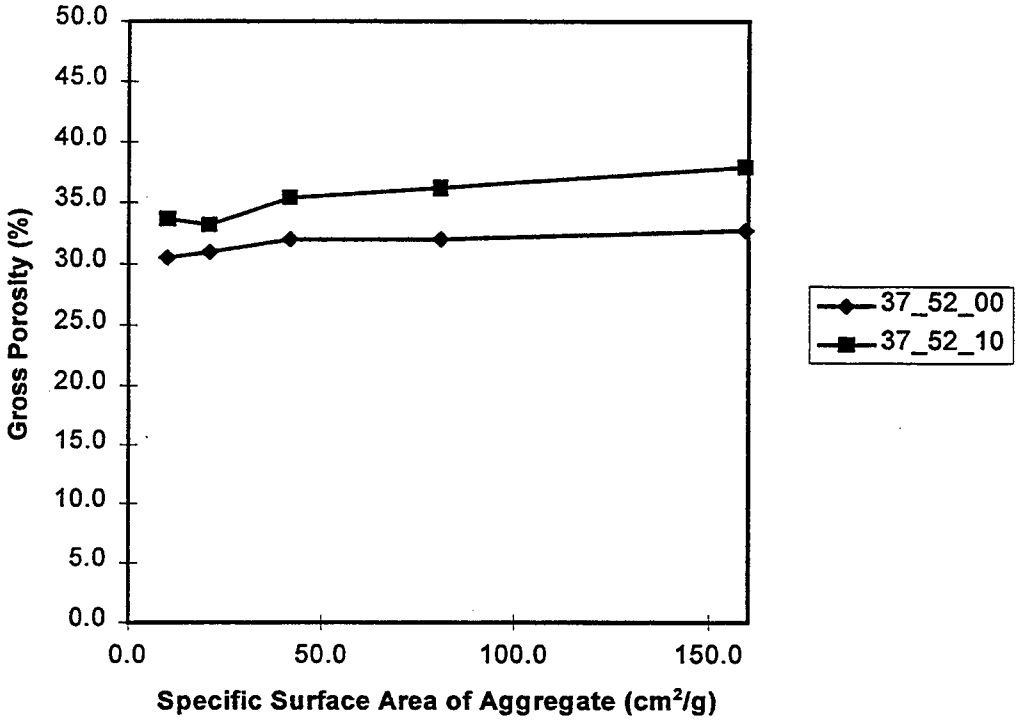

Figure 7.21 Gross Porosity vs. SA for dolomite mortars having mixture proportions of 37_52_00 and 37_52_10.

associated mortar specimens. Figure 7.21 presents the trend in gross porosity with the variation of SA for two groups of dolomite mortars having mixture proportions 37_52_00 and 37_52_10 respectively. The SF mortar group shows a higher gross porosity than the PC mortar group. It is known from Chapter 4.2.1 that this gross porosity represents the space between the solid particles in the fresh mortar mixture, which consists of sand particles, cement grains, and silica fume particles. Thus, gross porosity is an index of compaction. With reference to Figure 7.21, it may be concluded that when part of the cement is replaced by silica fume, the space between solid particles in the mortar becomes larger. In other words, the SF mortar is less compact immediately after casting.

In order to discuss the changes that develop in the space between solid particles in the SF mortar, a BEI micrograph of PC dolomite mortar at 28 days old is presented in Figure 7.22. Since most of the clear distances between aggregate particles are less than 100 μm, all of the space between aggregate particles may be regarded as transition zones. In other words, this is a percolation case. A magnified view of the rectangular region in Figure 7.22 is shown in Figure 7.23. It is observed that many pores less than 10 μm, exist in the pore system. If the mixture proportion is kept the same, except that 10% of cement weight is replaced by silica fume, the pore system is significantly changed. Figures 7.24~7.26 present this changed pore system under three levels of magnifications: 200×, 500×, and 1000×. It is observed that many of the visible pores presented in Figure 7.23 are not present in Figure 7.25. On the other hand, many pores are found between 10 and 20 μm, rather larger than the pores found in Figures 7.22 and 7.23. Therefore, it may be concluded that the pore system of the transition zone is changed by silica fume.

Does silica fume also change the pore system of the bulk paste? Figure 7.27 shows BEI micrograph of PC dolomite mortar having mixture proportion 37_52_00, sand particle size #16~#30, a magnified view of which is presented in Figure 7.28. Most of the pores are less than 10 μm. If 10% of the cement weight is replaced by silica fume, most of the pores less than 10 μm are missing, as shown in the BEI micrograph in Figure 7.29. The sizes of remaining pores are mostly between 10 and 20 μm. Therefore, the

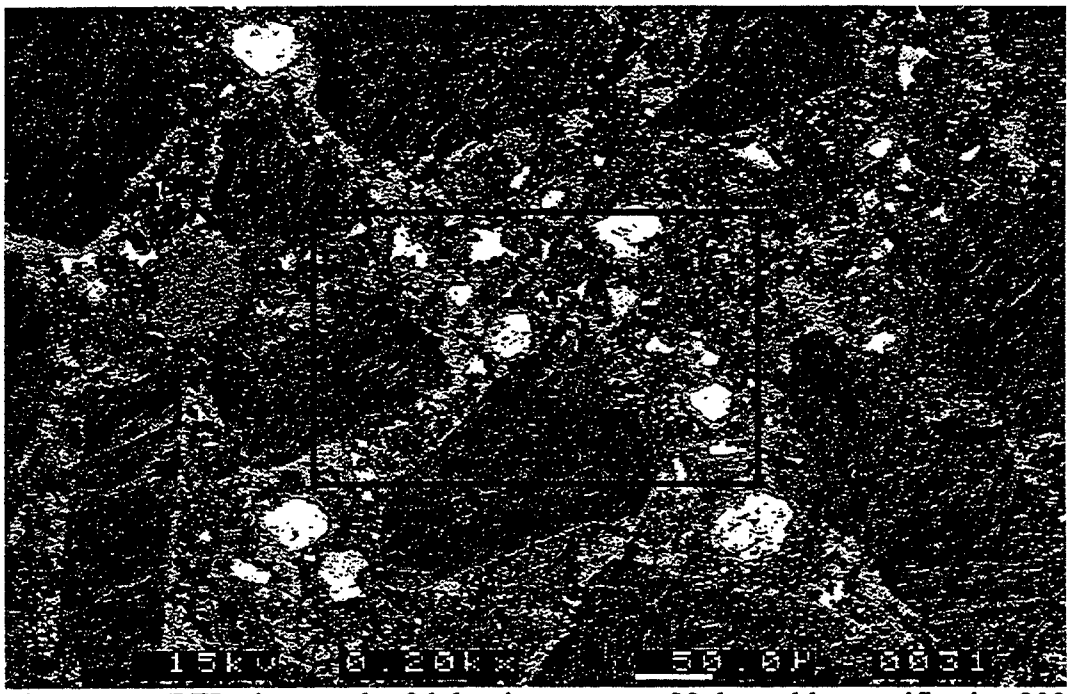

Figure 7.22 BEI micrograph of dolomite mortar at 28 days old, magnification 200×, mixture proportion 37_52_00, aggregate size #50~#100.

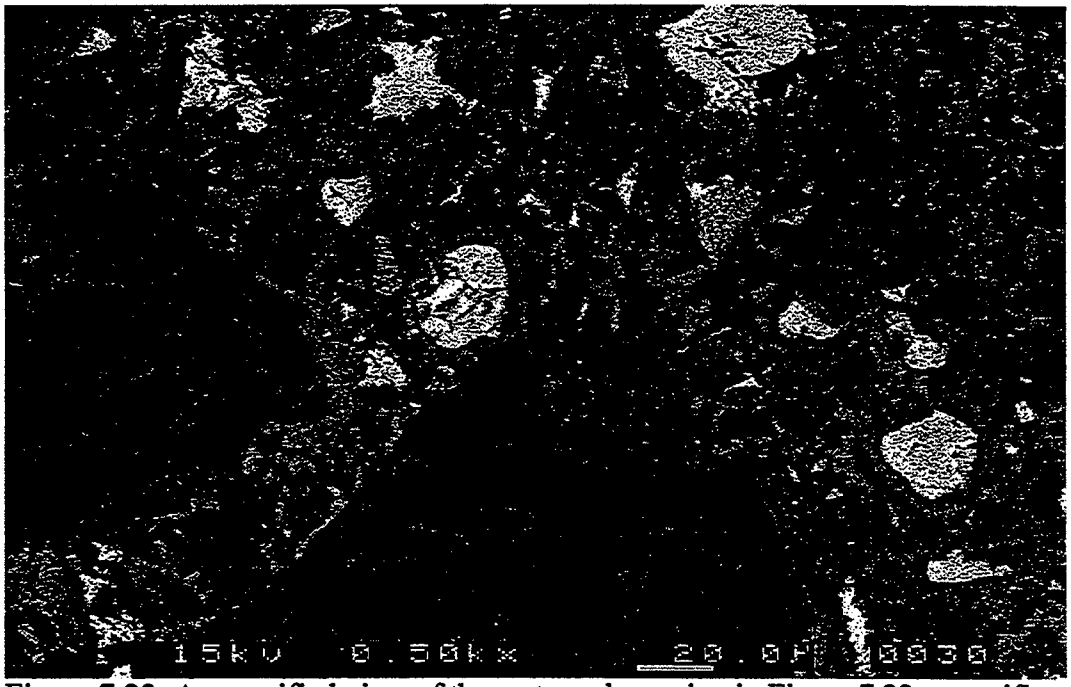

Figure 7.23 A magnified view of the rectangular region in Figure 7.22, magnification 500×.

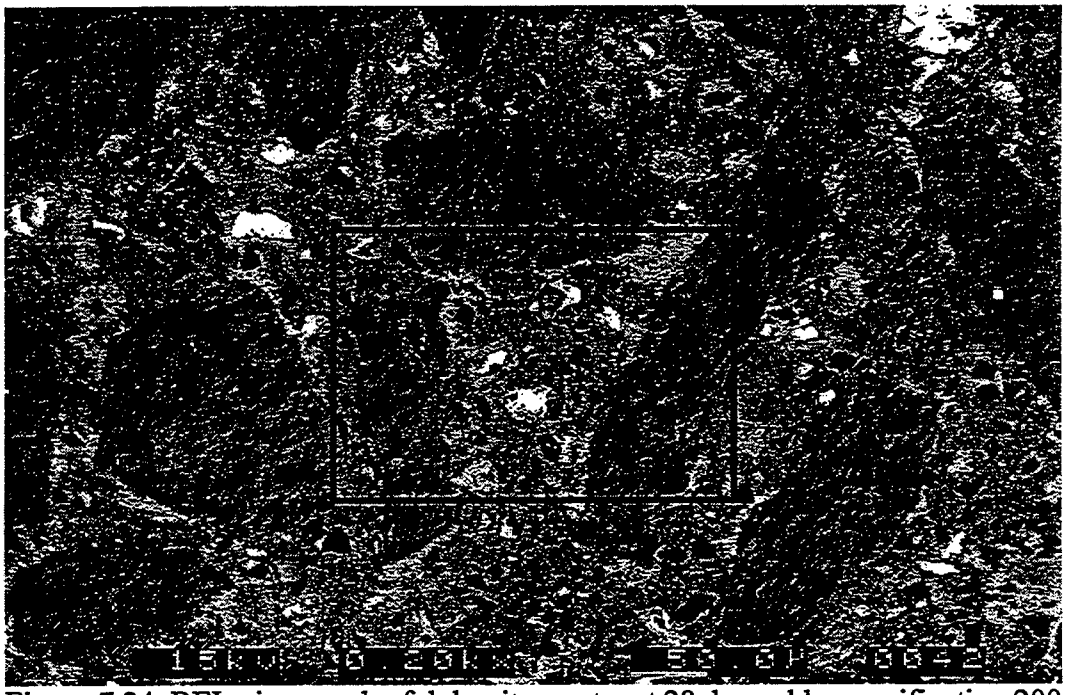

Figure 7.24 BEI micrograph of dolomite mortar at 28 days old, magnification 200×, mixture proportion 37_52_10, aggregate size #50~#100.

Figure 7.25 A magnified view of the rectangular region in Figure 7.24, magnification 500×.

Figure 7.26 A magnified view of the rectangular region in Figure 7.25, magnification 1000×.

Figure 7.27 BEI micrograph of dolomite mortar at 28 days old, magnification 500×, mixture proportion 37_52_00, aggregate size #16~#30.

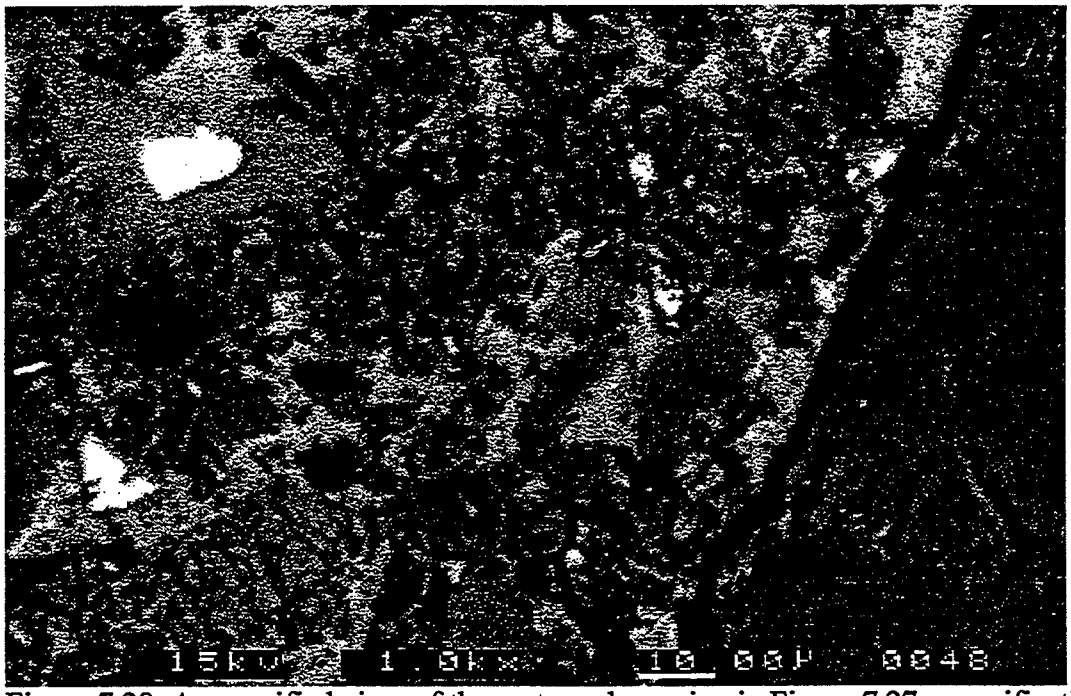

Figure 7.28 A magnified view of the rectangular region in Figure 7.27, magnification 1000×.

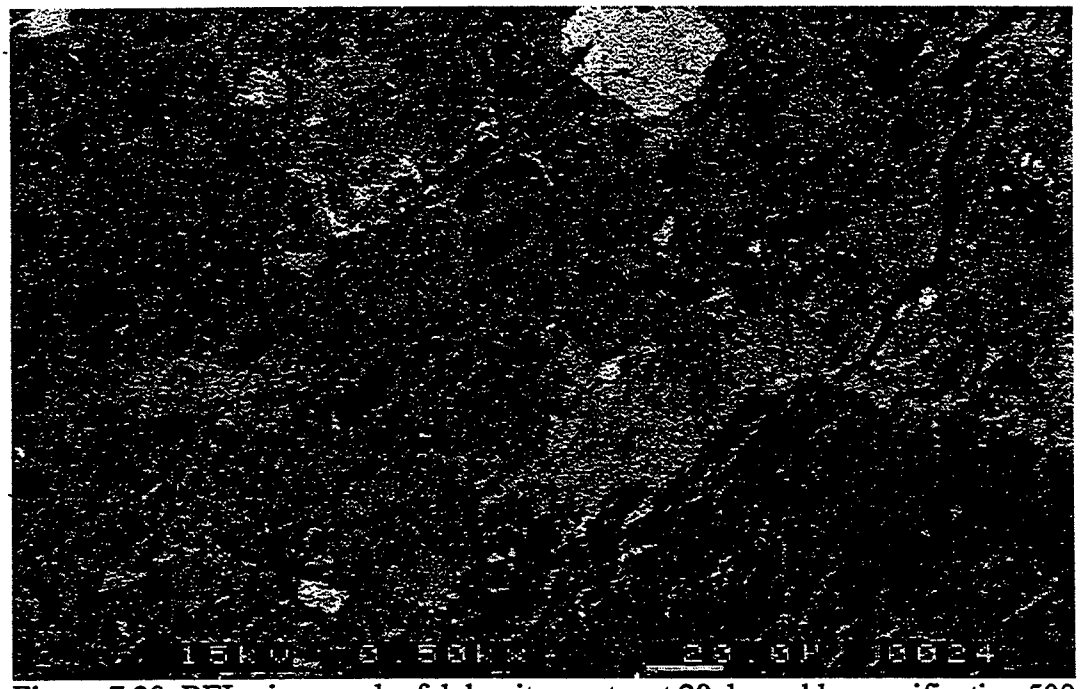

Figure 7.29 BEI micrograph of dolomite mortar at 28 days old, magnification 500×, mixture proportion 37_52_10, aggregate size #16~#30.

modification in the pore system happens not only in the transition zone, but also in bulk paste.

The above discussion may suggest that silica fume has the micro-filler effect, especially to the pores of size less than 10 μm. However, inevitably it also has side effects on the mortar, making solid particles become less compact and altering the pore size distribution by introducing many pores of size 10 to 20 μm. The micro-filler effect may increase the bulk density of mortar, while the effects of less compaction and of producing larger pores may decrease the bulk density. In addition, silica fume itself has a lower bulk density than that of cement. Thus, the addition of silica fume will tend to decrease the bulk density of mortar. In reality, the decreasing effect overwhelms the increasing effect. Thus, as shown in Figure 7.30, the bulk density of SF mortar is less than that of PC mortar having the same Va and W/C. For the same class of material, materials with higher bulk density will show higher dynamic moduli. Therefore, the PC mortars show higher dynamic moduli than the SF mortars in Figures 7.18 and 7.19.

With reference to Figures 6.21 and 6.22, the reduction in dynamic moduli by silica fume also happens in quartzite mortar. However, the mechanism is somewhat different between quartzite mortar and dolomite mortar. Unlike what happen in dolomite mortar, silica fume may have a larger strengthening effect on the transition zone of quartzite mortar. Therefore, by comparing the far right hand side points in the PC mortar curve with those of the corresponding SF mortar curve in Figures 6.21 and 6.22, it is seen that the dynamic moduli of SF mortar exceed those of PC mortar. While both mortars possess a large number of transition zones, dolomite mortar does not show this characteristic. The reason may be revealed by investigating the microstructure and porosity of the mortar as follows.

Two of the BEI micrographs of quartzite mortar are shown in Figures 7.31 and 7.32. Since most of the distances between aggregate particles are less than 100 μm, the space between aggregate particles may be regarded as the transition zone. By comparing the BEI micrograph in Figure 7.31 with that in Figure 7.23, it is noticed that the transition zone of quartzite mortar is more porous than that of dolomite mortar when both mortars

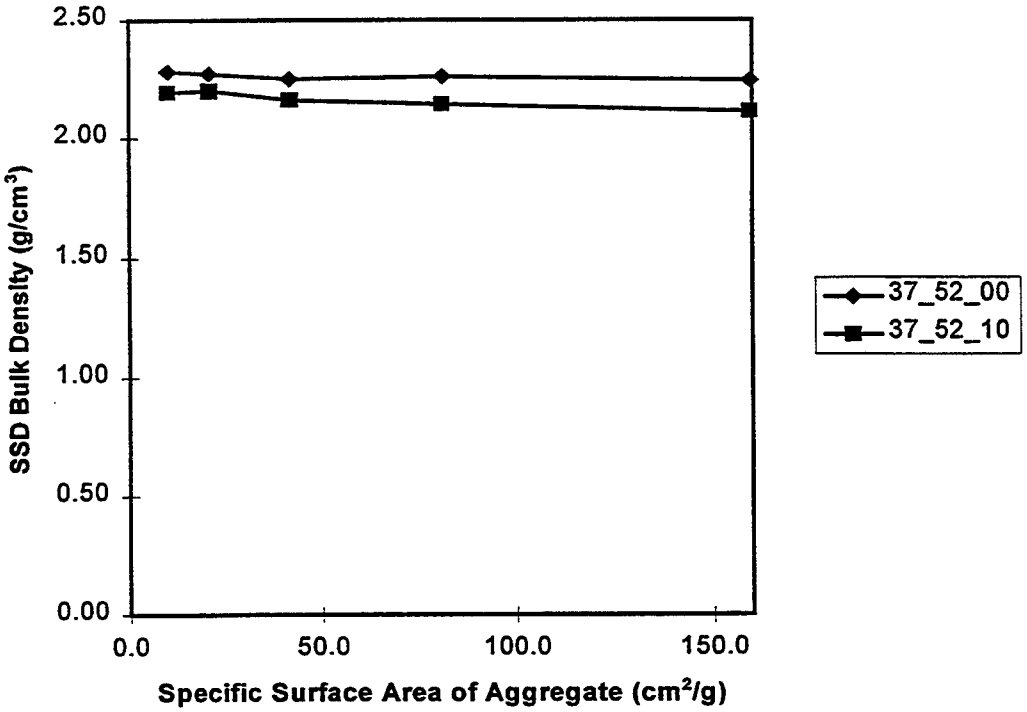

Figure 7.30 SSD Bulk Density vs. SA for dolomite mortars having mixture proportions of 37_52_00 and 37_52_10.

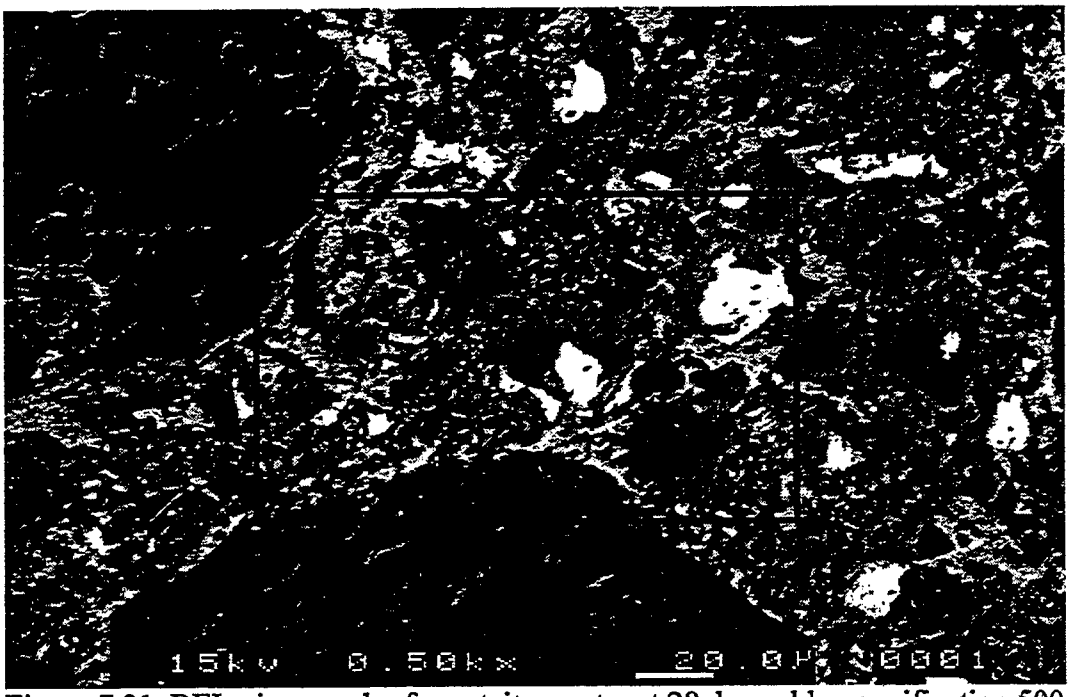

Figure 7.31 BEI micrograph of quartzite mortar at 28 days old, magnification 500×, mixture proportion 37_52_00, aggregate size #50~#100.

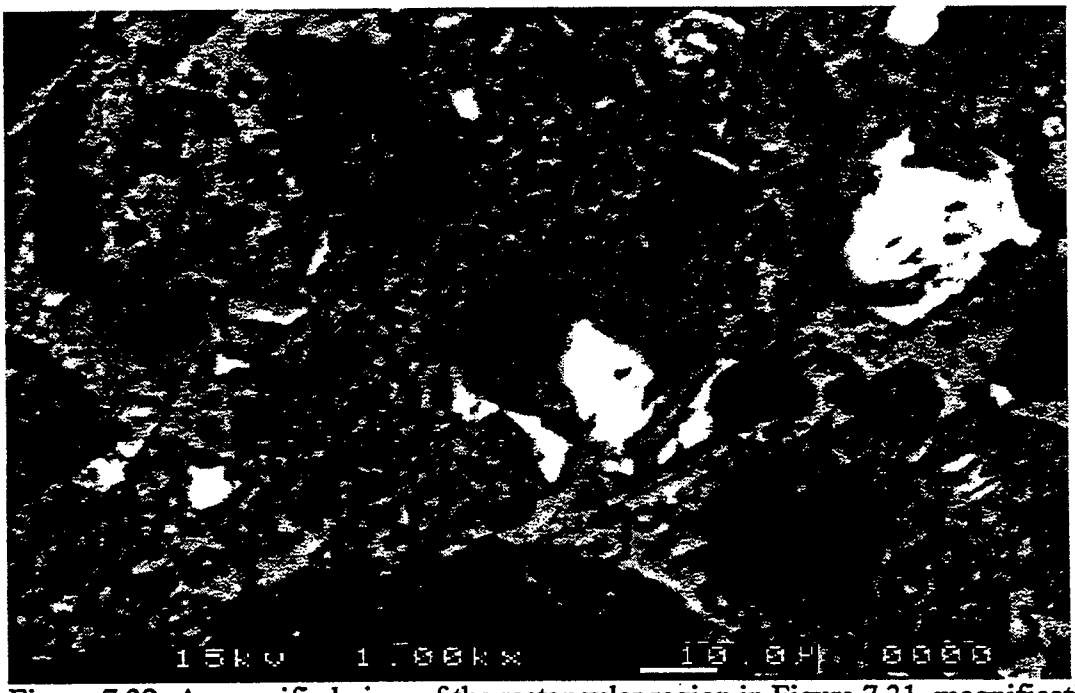

Figure 7.32 A magnified view of the rectangular region in Figure 7.31, magnification 1000×.

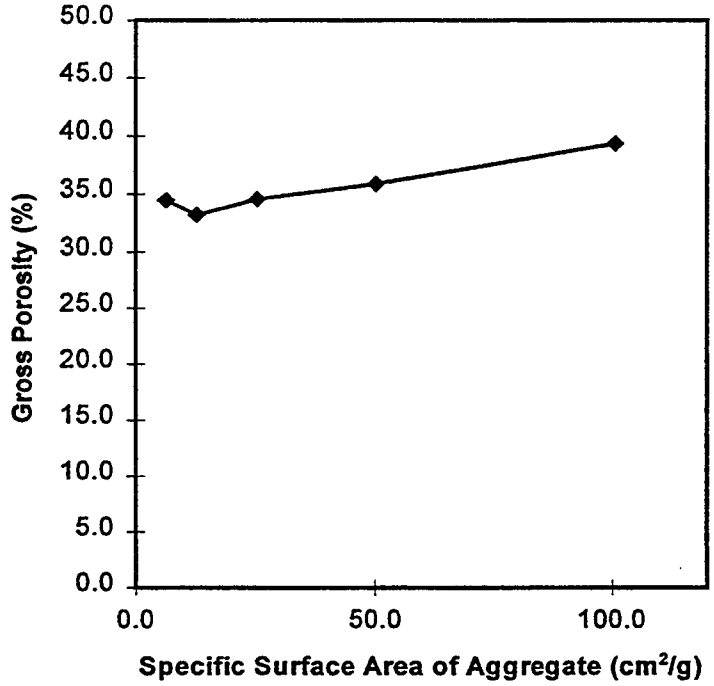

Figure 7.33 Gross Porosity vs. SA for quartzite mortars at 28 days old, having one of five fractions of aggregate sizes (ASTM Sieve No.: #4~#8, #8~#16, #16~#30, #30~#50, and #50~#100), mixture proportions of 37_52_00.

have the same mixture proportion. Thus, for quartzite mortar the trend is that gross porosity increases correspondingly to SA increases, as shown in Figure 7.33; the corresponding trend for dolomite mortar is relatively flat as shown in Figure 7.21. Therefore, for quartzite mortar the relationship between dynamic modulus of elasticity and SA shows a decreasing trend in Figure 7.34. The graph in Figure 7.34 presents two five-point curves. One is the relationship between dynamic modulus of elasticity measured by the resonant frequency method and the SA. The other is the same relationship, but the dynamic modulus of elasticity was measured by pulse velocity method. Both curves are quite close. This may strengthen the suggestion that the trend in dynamic modulus of elasticity with varying SA for quartzite mortar is a decreasing trend. This trend is different from that for dolomite mortar which shows a relatively flat trend in Figure 7.18. In Figure 7.34, the data of the two points connected by a short line represent the dynamic modulus of elasticity of the mortar made of one of the ASTM standard quartz sands, C-190 and C-109. The purpose of presenting these data is to provide an impression of the trend in dynamic modulus of elasticity with varying SA for quartz mortar.

By comparing Figure 7.35 with Figure 7.29, it is noticed that similar to what happens in dolomite mortar, silica fume also has a micro-filler effect in quartzite mortar. In Figure 7.35, few pores of sizes less than 10 μm are found; most of the pores observed are of sizes between 10 and 20 μm.

In summary, the transition zone of dolomite mortar is seen as being as stiff and rigid as bulk paste, which may be due to two effects. One is the chemical strengthening effect proposed by Monteiro and Mehta [1986, (1)]. The other is the effect of the less porous transition zone of dolomite mortar compared to that of quartzite mortar. In addition, because the transition zone of quartzite mortar is quite porous, it may be thus less stiff and less rigid than bulk paste. Silica fume has the same effects on the transition zones of dolomite and quartzite mortars. One effect is that the amount of pores of size less than 10 μm are significantly reduced, and another is that the amount of pores of size between 10 and 20 μm is increased. The last effect is that the mortar become less

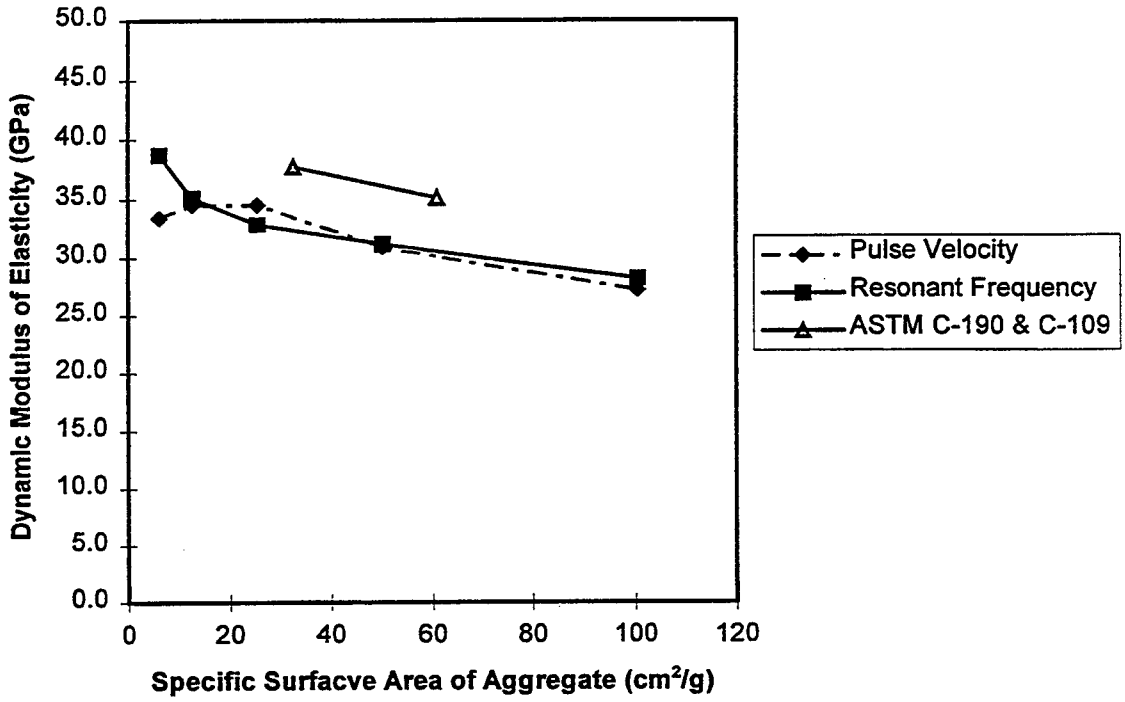

Figure 7.34 Dynamic Modulus of Elasticity vs. SA for quartzite and quartz mortars. The quartzite mortars are at 28 days old, having one of the five fractions of aggregate sizes (ASTM Sieve No.: #4~#8, #8~#16, #16~#30, #30~#50, and #50~#100), mixture proportions of 37_52_00. Two different measuring methods were performed on these quartzite mortars. One is Resonant Frequency method performed by Cohen et al. [1994], the other is Pulse Velocity method. Quartz mortars were made of one of ASTM Ottawa standard quartz sands: C-190 and C-109, having mixture proportions of 40_50_00 and measured by Resonant Frequency method.

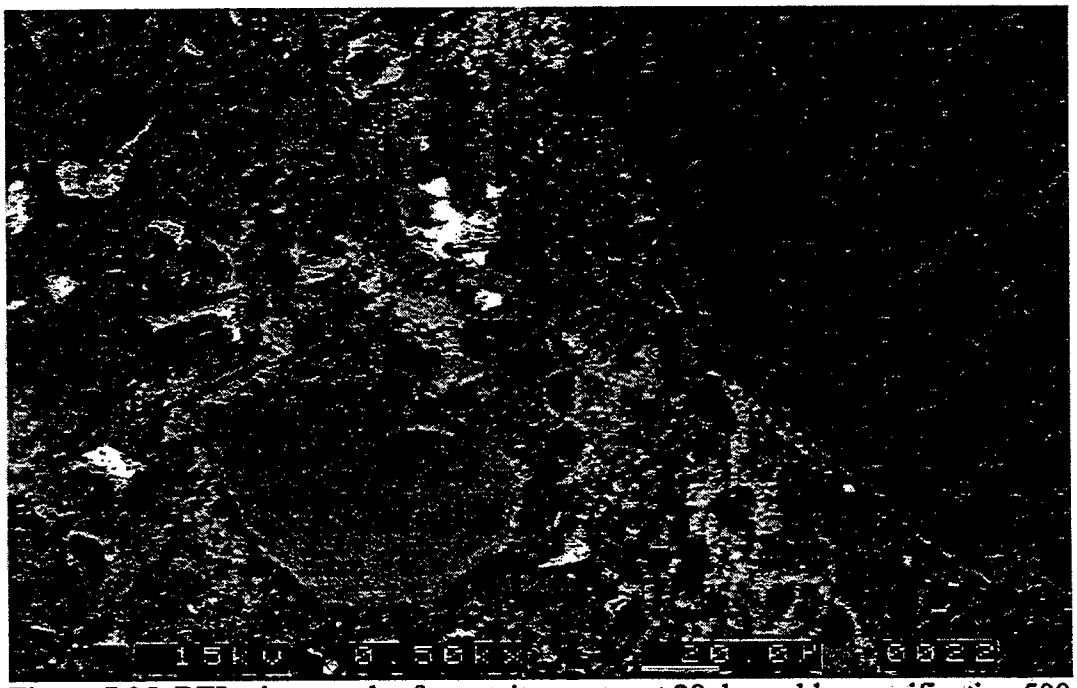

Figure 7.35 BEI micrograph of quartzite mortar at 28 days old, magnification 500×, mixture proportion 37_52_10.

compact. These three effects may lower the dynamic moduli of dolomite mortar but do not alter the trend in dynamic moduli with varying SA. For quartzite mortars, the trend in dynamic moduli with varying SA is changed from leaning to flat after adding silica fume. In other words, unlike what happens in the transition zone of dolomite mortar, silica fume shows a stiffening effect on the transition zone of quartzite mortar. Based on the data in Figures 6.21 and 6.22, an explanation is suggested below.

Due to the fact that the transition zone of quartzite mortar is quite porous, the trend in dynamic moduli with varying SA was decreasing. Silica fume can effectively modify this porous transition zone and this micro-filler effect overwhelms the other two effects; i.e., the less compact mortar and the introduction of larger pores. Thus, the dynamic moduli of SF quartzite mortar having a large number of transition zones are higher than those of similar PC quartzite mortar. However, when there are fewer transition zones (e.g., SA is smaller), the effect of micro-filler suppresses the effects of less compact pores and introducing larger ones. Under this circumstance, the dynamic moduli of SF quartzite mortar are lower than those of PC quartzite mortar.

With regard to the microstructural study on the transition zone of perlite mortar, the BEI micrographs of perlite mortar are presented in Figures 7.36 and 7.37. Figures 7.23, 7.31, and 7.37 show the transition zone images of dolomite, quartzite, and perlite mortars respectively having the same mixture proportion 37_52_00, aggregate size #50~#100, and taken at magnification 500×. By comparing the images in these three figures, it may be concluded that the transition zones of dolomite and perlite mortars are denser, while the transition zone of quartzite mortar is porous. With reference to Figures 7.38 and 7.39, the relationship between dynamic moduli and SA for perlite mortar shows a flat trend as that for dolomite mortars. This may also suggest that the transition zone of perlite mortar is as stiff and rigid as bulk paste. However, there are some differences between perlite mortar and dolomite mortar. Silica fume only has a minor influence on the dynamic moduli of perlite mortar, which may be due to two reasons. Firstly, the dynamic moduli of perlite mortar is only about one-third of those of dolomite or quartzite mortar. Thus, for perlite mortar, the effect of lowering the dynamic moduli by silica fume

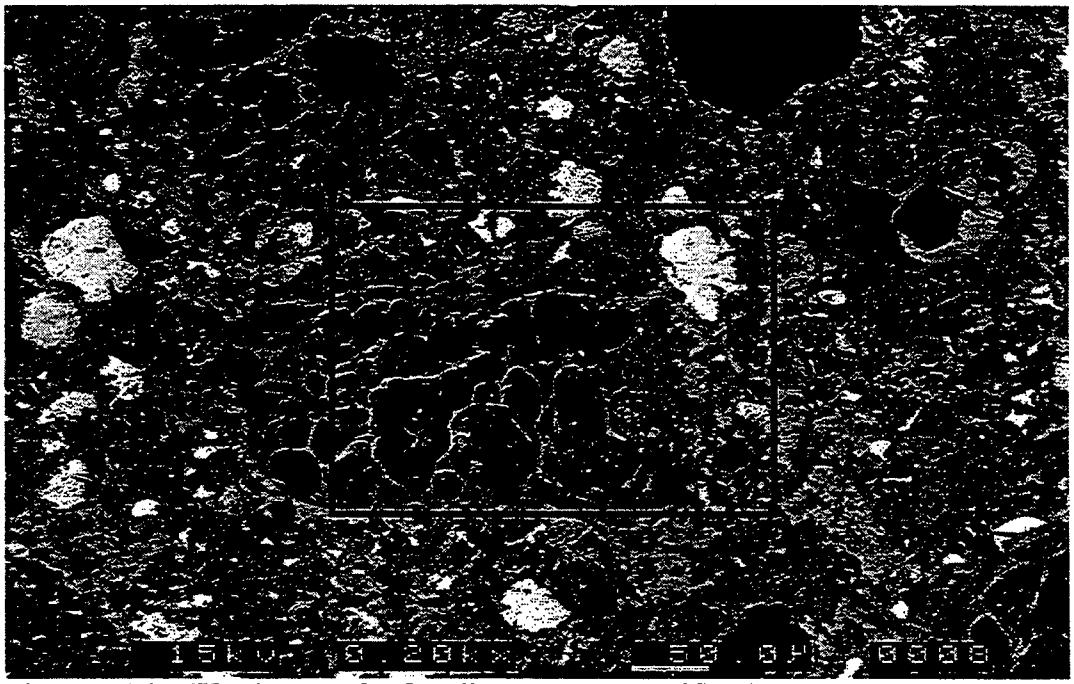

Figure 7.36 BEI micrograph of perlite mortar, magnification 200×, mixture proportion 37_52_00, aggregate size #50~#100.

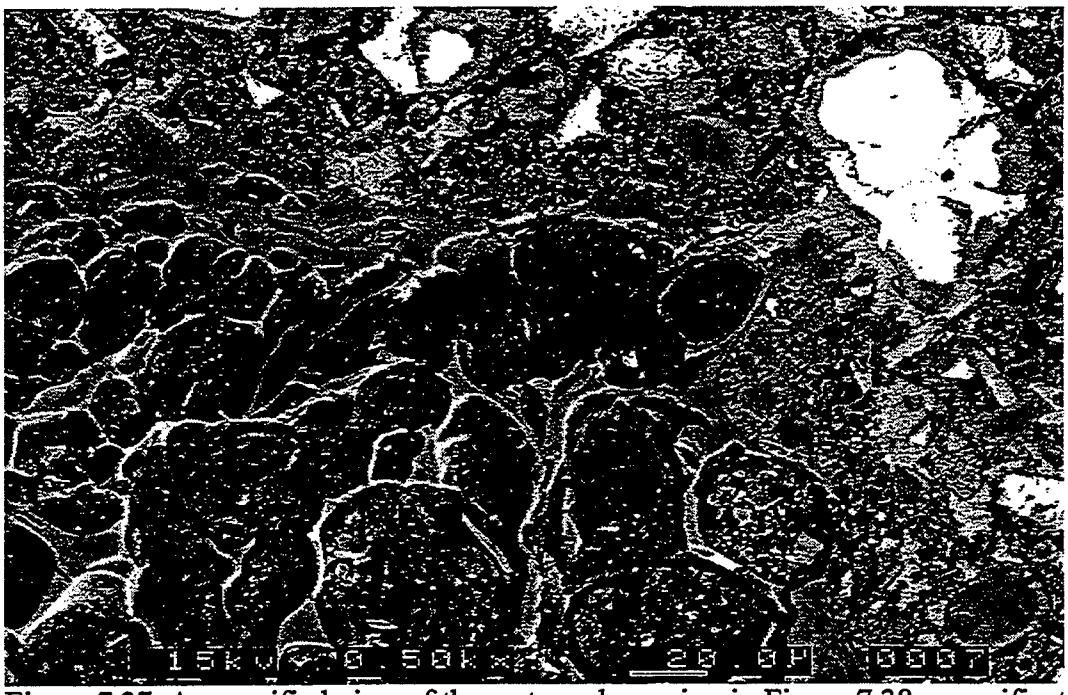

Figure 7.37 A magnified view of the rectangular region in Figure 7.38, magnification 500×.

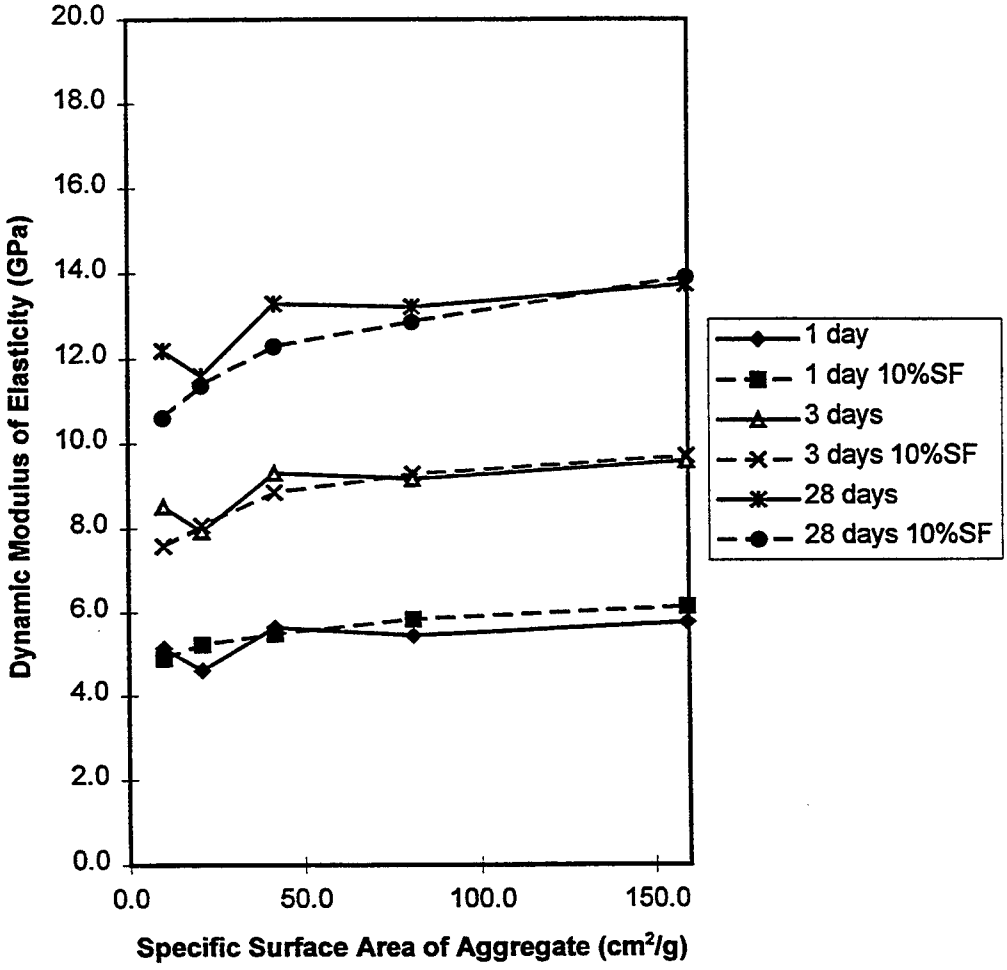

Figure 7.38 Dynamic Modulus of Elasticity vs. SA for perlite mortars at 1, 3, and 28 days old having mixture proportions of 37_52_00 and 37_52_10.

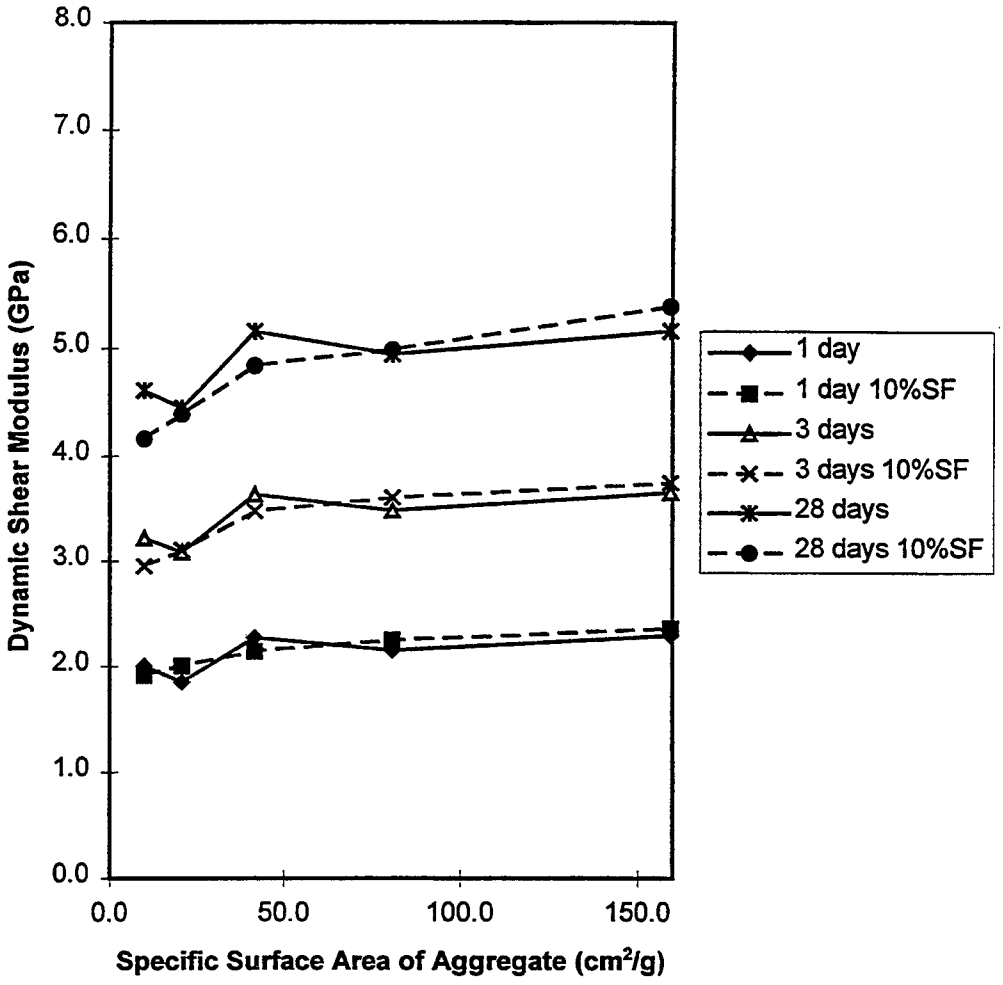

Figure 7.39 Dynamic Shear Modulus vs. SA for perlite mortars at 1, 3, and 28 days old having mixture proportions of 37_52_00 and 37_52_10.

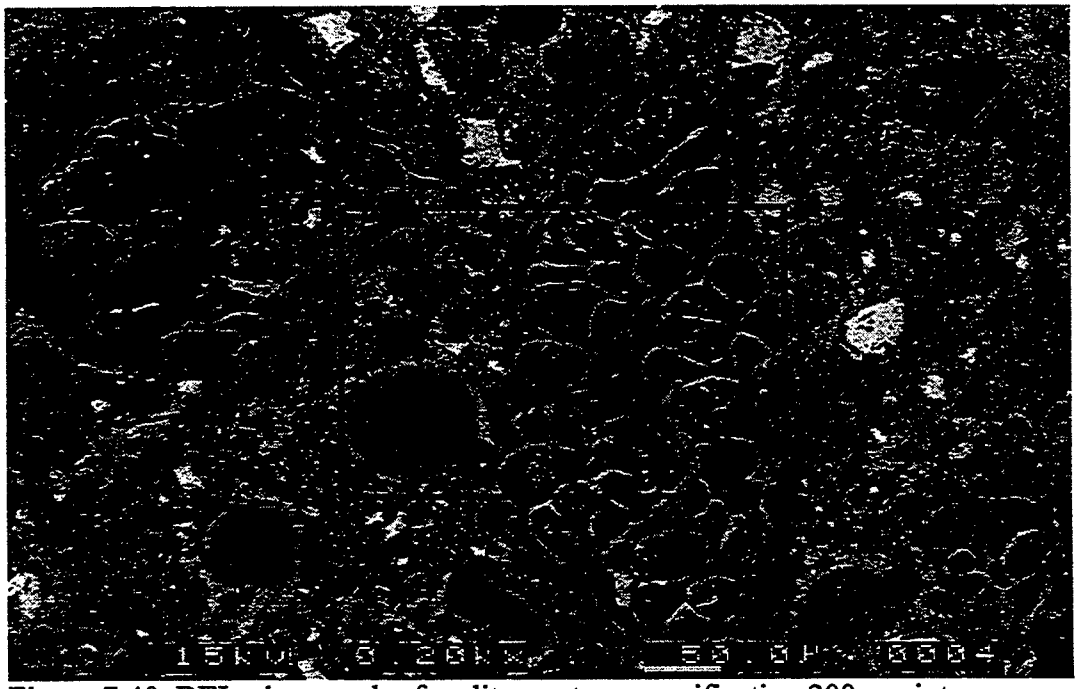

Figure 7.40 BEI micrograph of perlite mortar, magnification 200×, mixture proportion 37_52_10, aggregate size #50~#100.

Figure 7.41 A magnified view of the rectangular region in Figure 7.40, magnification 500×.

may be less obvious if the percentage of reduction is similar for perlite and dolomite mortars. Secondly, the pores in perlite mortar are not significantly influenced by silica fume as shown in Figures 7.40 and 7.41. With 10% of the cement weight replaced by silica fume, many pores of less than 10 μm in size still exist in the mortar. Even in the bulk paste, the modification by silica fume is also poor as shown in Figure 7.42. This mechanism is quite different from that of dolomite and quartzite mortars, where many pores of a size less than 10 μm are modified due to the addition of silica fume.

An alternate way to study the transition zones around these three types of aggregates is by applying EDS.

Figure 7.43 shows the BEI micrograph of dolomite mortar having a mixture proportion 37_52_00. A, B, C, and D as the four locations where EDS was performed. Their EDS results are shown in Figure 7.44. Judging from the number of elements detected, the following two conclusions may be drawn. Location A is a dolomite aggregate that is rich in magnesium. Location B is calcium hydroxide which is rich in calcium and has less silicon. In addition, judging from the distance between the points and the aggregate surface, the following conclusion may be made. Location C is in the transition zone, while location D is in the bulk paste of the dolomite mortar. It seems that the difference in chemical composition between the transition zone and the bulk paste is not obvious. Carbon is introduced due to the epoxy used in preparing the samples. Thus, the carbon information is meaningless in the EDS analysis. This makes it difficult to provide information to support the conclusion by Monteiro and Mehta [1986, (1)], namely, that there is etching of calcite in the carbonate rock and this calcite reacts with calcium in the transition zone to form compound of smaller crystal.

Figure 7.45 shows the BEI micrograph of quartzite mortar having mixture proportion 37_52_00. A, B, and C as the three locations where EDS was performed. Their EDS results are shown in Figure 7.46. In accordance with the amounts of elements detected, the following conclusion may be drawn. Location A is a quartzite aggregate that is rich in silicon. In addition, judging from the distance between the points and aggregate surface, the following conclusion may be made. Location B is in the transition

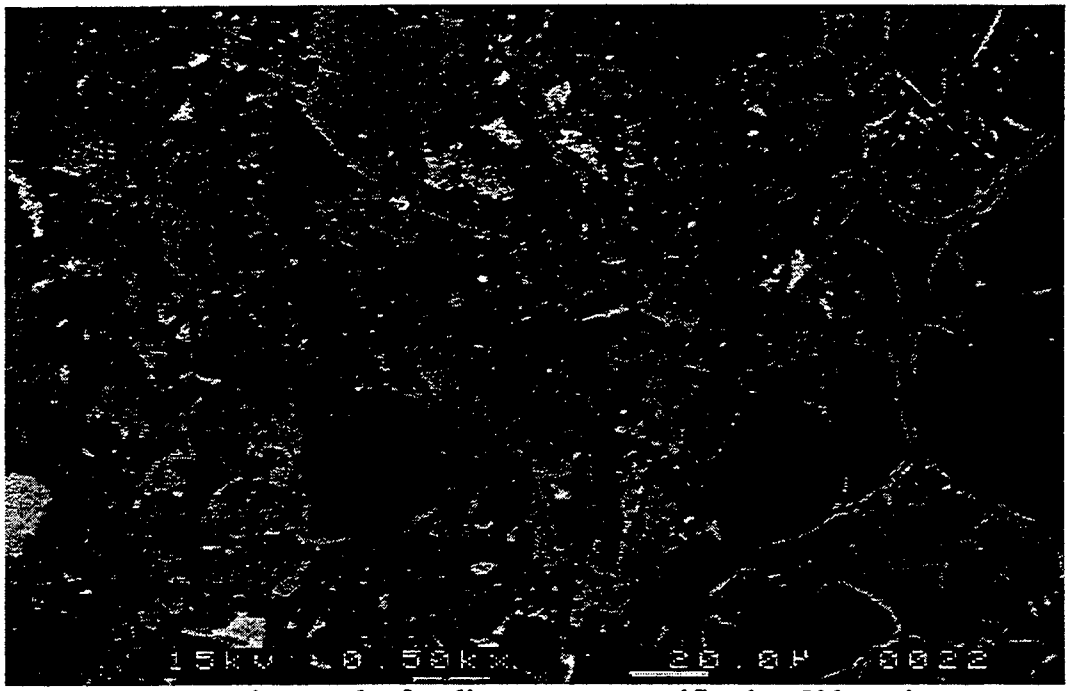

Figure 7.42 BEI micrograph of perlite mortar, magnification 500×, mixture proportion 37_52_10, aggregate size #16~#30.

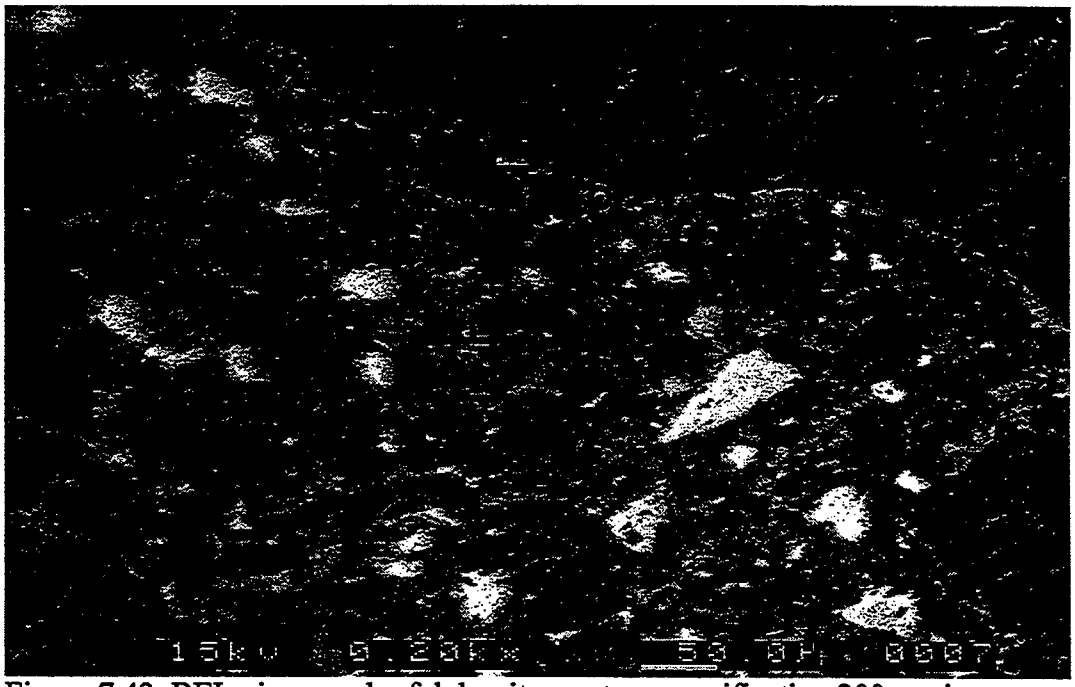

Figure 7.43 BEI micrograph of dolomite mortar, magnification 200×, mixture proportion 37_52_00, aggregate size #16~#30. The circles marked by A, B, C, and D are the four locations to apply EDS.

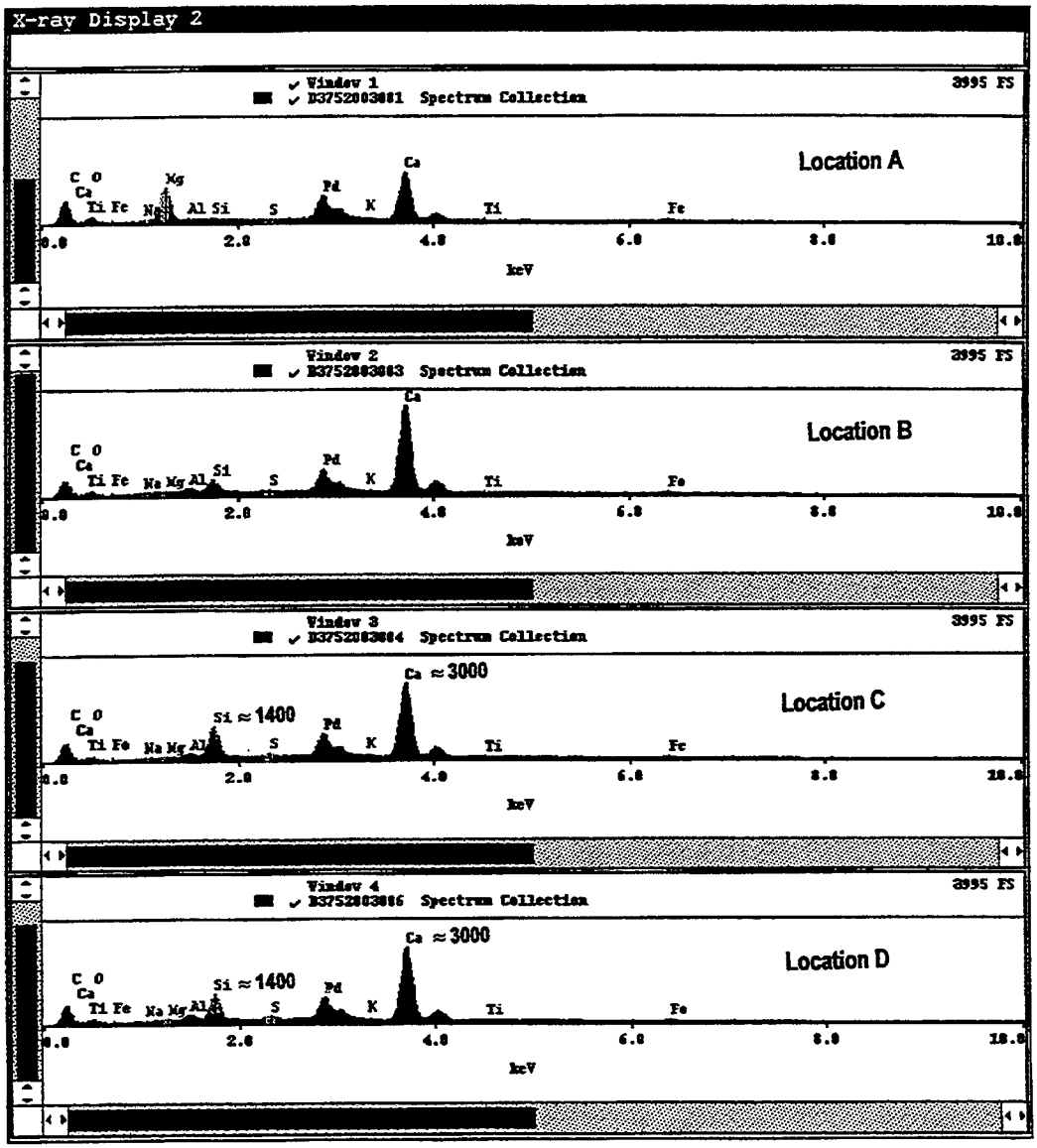

Figure 7.44 EDS results of the four locations: A, B, C, and D in Figure 7.43.

Figure 7.45 BEI micrograph of quartzite mortar, magnification 200×, mixture proportion 37_52_00, aggregate size #16~#30. The circles marked by A, B, and C are the three locations to apply EDS.

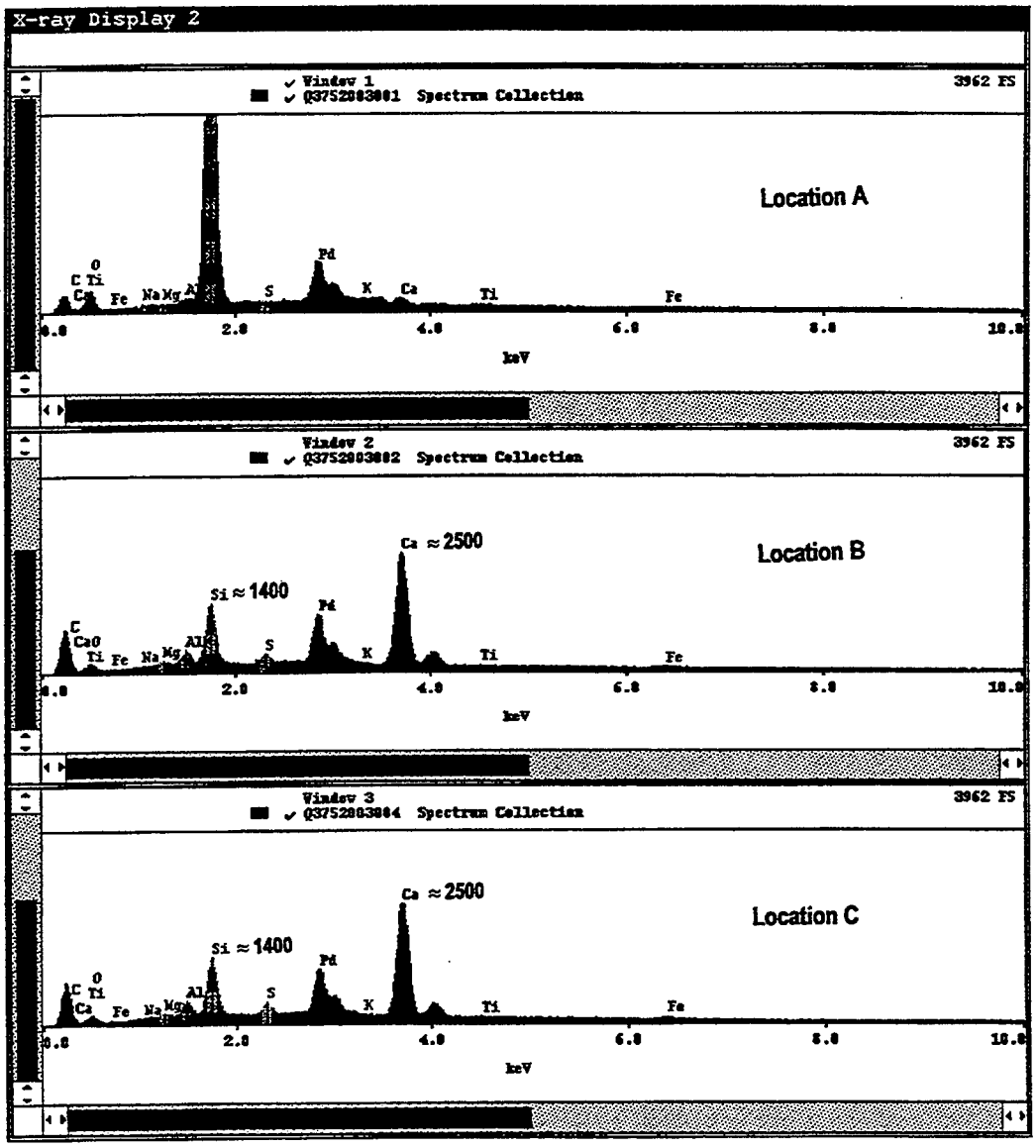

Figure 7.46 EDS results of the three locations: A, B, and C in Figure 7.45.

zone, while location C is in the bulk paste of the quartzite mortar. It also shows that the difference in chemical composition between the transition zone and the bulk paste is not obvious.

Figure 7.47 shows the BEI micrograph of perlite mortar having mixture proportion 37_52_00. A, B, and C at the three locations where EDS was performed. Their EDS results are shown in Figure 7.48. In accordance with the amounts of elements detected, the following conclusion may be drawn. Location A is a perlite aggregate that is rich in silicon. In addition, judging from the distance between the points and aggregate surface, the following conclusion may be made. Location B is in the transition zone, while location C is in the bulk paste of the perlite mortar. It also shows that the difference in chemical composition between the transition zone and the bulk paste is not obvious too.

7.4 The Effects of W/C and Volume Fraction of Aggregate on Dynamic Moduli of the Transition Zone

As indicated in Chapter 6.6, it is known that the relationship between dynamic moduli of mortar and SA in the mortar may reflect the relative values of dynamic moduli between the transition zone and bulk paste. Thus, in this study, the investigation of how W/C and Va affect the dynamic moduli of the transition zone is transformed into studying how the relationship between dynamic moduli and SA is affected by W/C and Va. If the trend in dynamic moduli with varying SA is affected by W/C, it may be proposed that the degree of influence by W/C on the dynamic moduli of the transition zone is different from its affect on the dynamic moduli of bulk paste. In addition, if the trend in dynamic moduli with varying SA is affected by Va, it may be inferred that the quantity of aggregate in mortar can alter the dynamic moduli of the transition zone. The latter inference is based on an assumption that the dynamic moduli of bulk paste are not affected by the quantity of aggregate in the mortar.

The trends in dynamic modulus of elasticity and dynamic shear modulus with varying SA are shown in Figures 7.49 and 7.50 respectively for PC dolomite mortars

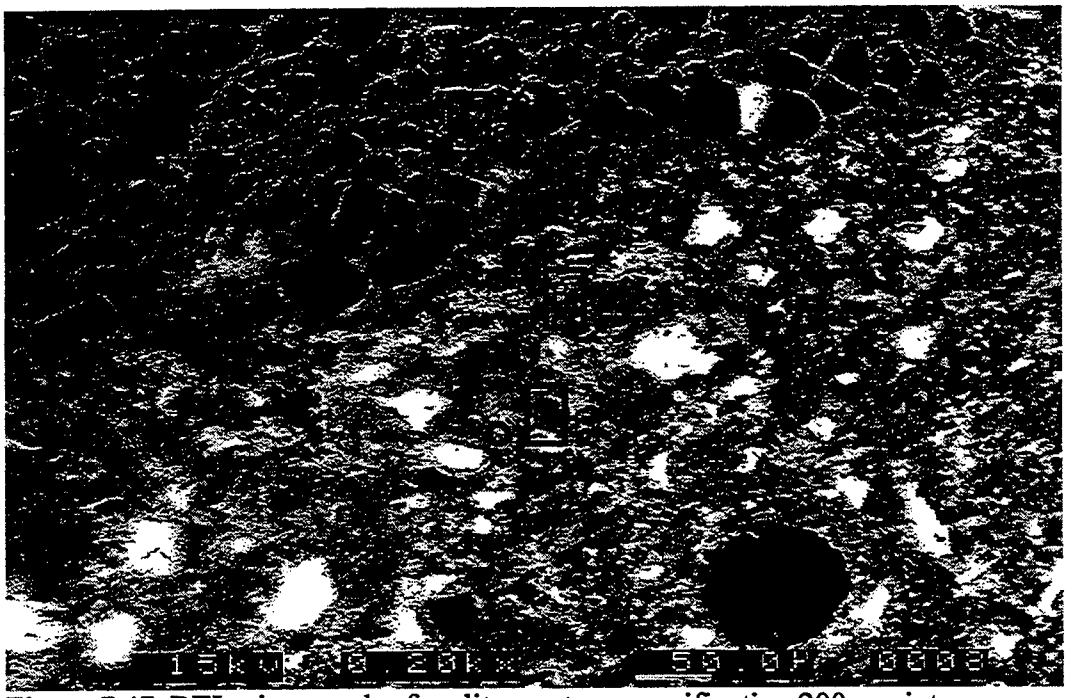

Figure 7.47 BEI micrograph of perlite mortar, magnification 200×, mixture proportion 37_52_00, aggregate size #16~#30. The circles marked by A, B, and C are the three locations to apply EDS.

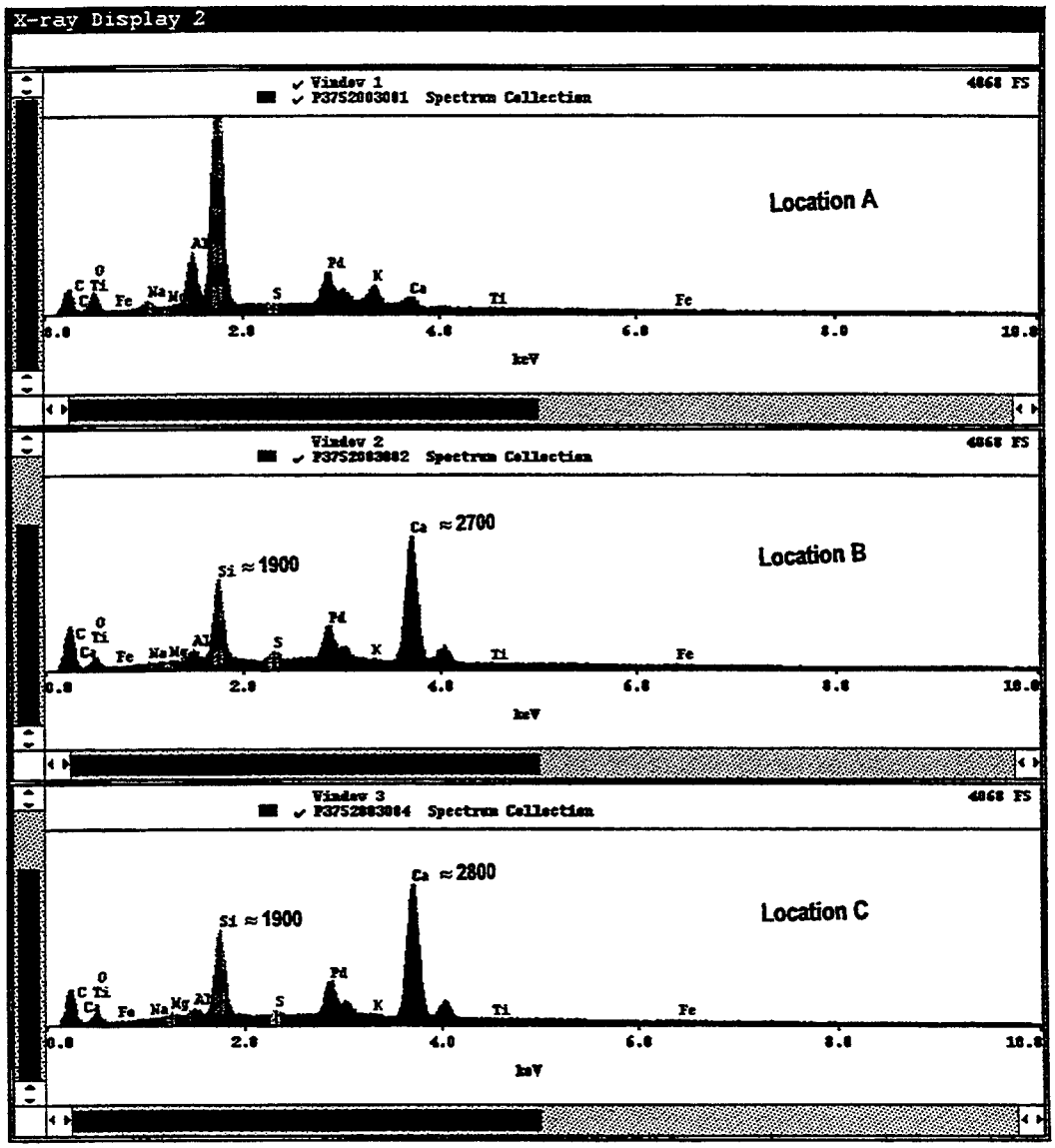

Figure 7.48 EDS results of the three locations: A, B, and C in Figure 7.47.

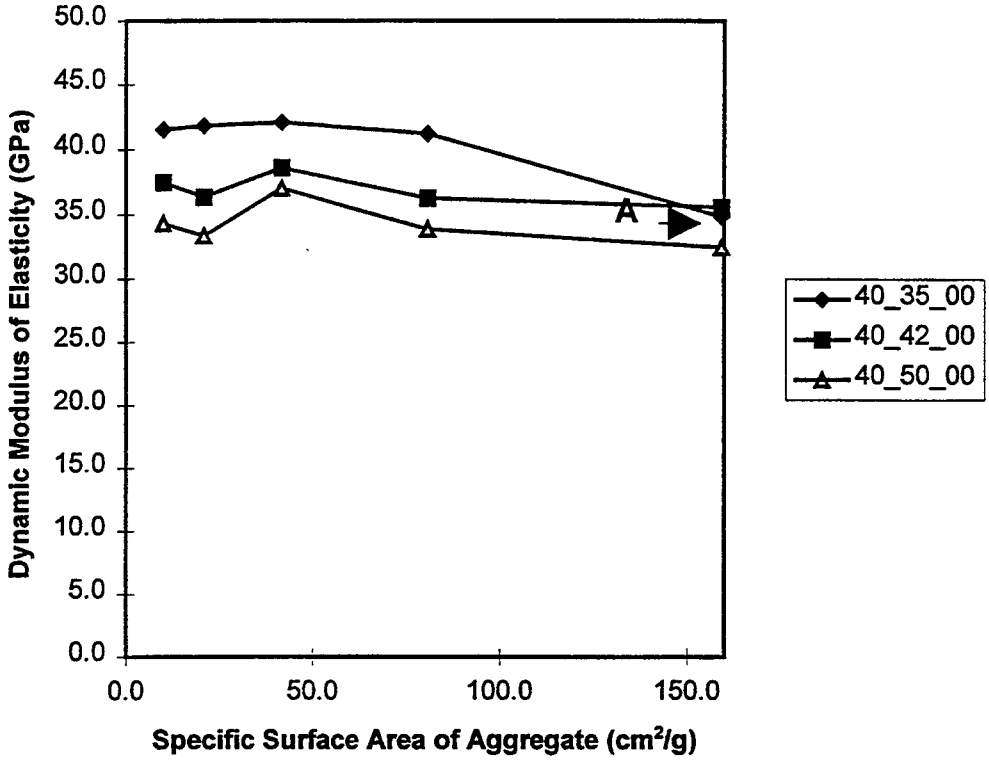

Figure 7.49 Dynamic Modulus of Elasticity vs. SA for dolomite mortars at 28 days old having mixture proportions of 40_35_00, 40_42_00, and 40_50_00.

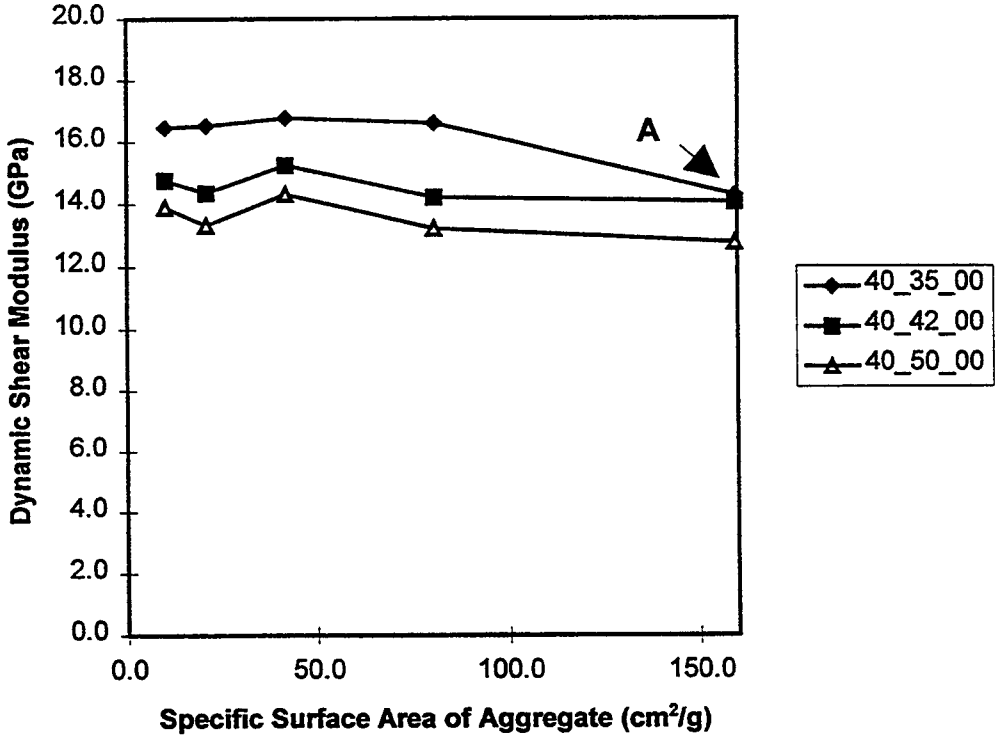

Figure 7.50 Dynamic Shear Modulus vs. SA for dolomite mortars at 28 days old having mixture proportions of 40_35_00, 40_42_00, and 40_50_00.

having mixture proportions 40_35_00, 40_42_00, and 40_50_00. In these two figures, the mixture for the data indicated by A shows relatively lower values in dynamic modulus of elasticity and dynamic shear modulus. Thus, for the group of mixtures, 40_35_00, both dynamic modulus of elasticity and dynamic shear modulus show decreasing trends with increasing SA. However, these decreasing trends may be due to the mixing and compaction problems that occurred in some of the specimens because of insufficient water for mixing. In Chapter 5.6, based on the water film around aggregate particles, a criterion is proposed for predicting the mixing and compaction problems. As shown in Figure 7.51, that criterion is used in this section to check whether or not the mixing and compaction problems occurred in the specimens having mixture proportions 40_35_00, 40_42_00, and 40_50_00.

Figures 7.52 and 7.53 present the dynamic modulus of elasticity and dynamic shear modulus with varying SA respectively for 7% SF mortars. The group of mixtures having mixture proportion 40_35_07 also show a decreasing trend in the dynamic moduli owing to the values being relatively low for B and C points. By comparing the average thickness of the water film around aggregate particles with the criterion as shown in Figure 7.54, the mixing and compaction problems may be detected in some of these SF mortars. Figures 7.51 and 7.54 show that some mixtures have water film thickness values closer to that of the criterion, and, consequently, they are more suitable for analysis.

Table 7.1 shows the data of thickness of water film for the criterion, PC mortars having mixture proportions 40_35_00, 40_42_00, and 40_50_00, and SF mortars having mixture proportions 40_35_07, 40_42_07, and 40_50_07. In accordance with the data in Table 7.1 and the curves in Figures 7.49, 7.50, 7.52 and 7.53, the following conclusion may be drawn. If the water film of an aggregate particle is within ±13% of the criterion, the mortar will probably have mixing and compaction problems. If it is 13% less than the criterion, mixing and compaction problems are more likely to occur; if it is 13% above the criterion, mixing and compaction problems likely may not happen.

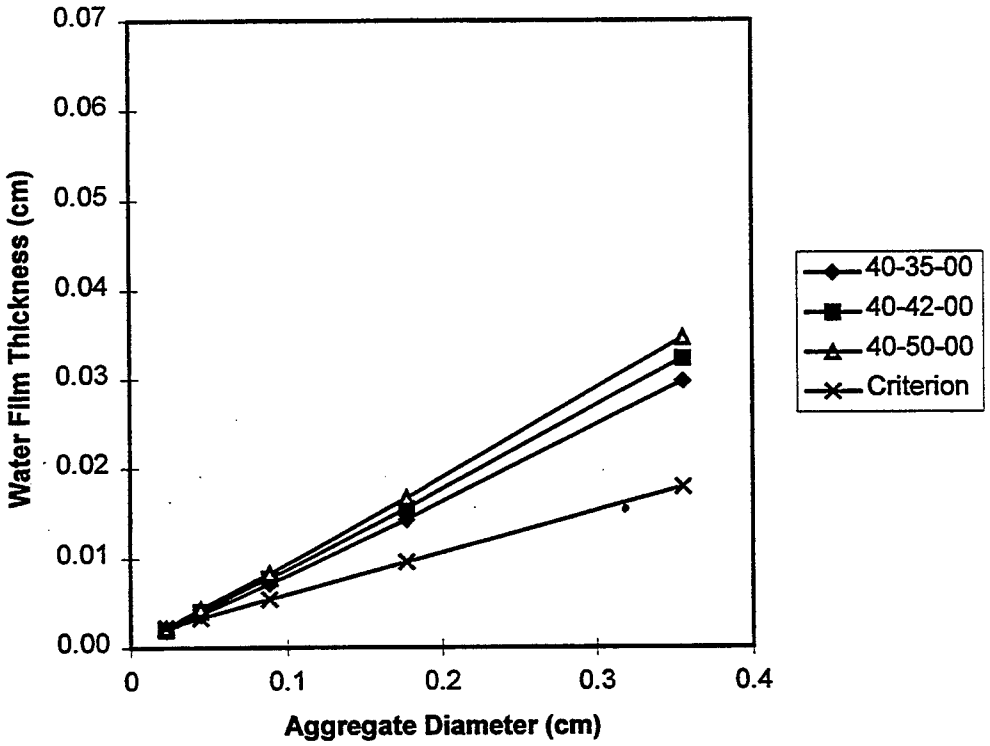

Figure 7.51 Water Film Thickness vs. Aggregate Diameter for dolomite mortars having mixture proportions of 40_35_00, 40_42_00, and 40_50_00. A criterion line is also plotted for comparison.

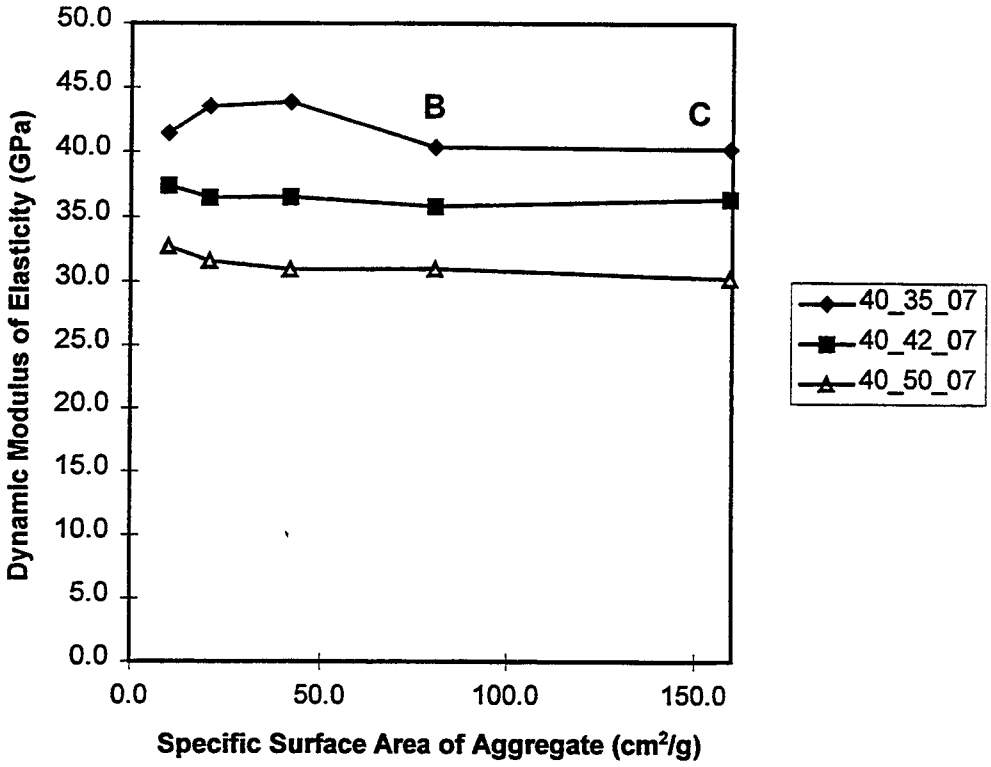

Figure 7.52 Dynamic Modulus of Elasticity vs. SA for dolomite mortars at 28 days old having mixture proportions of 40_35_07, 40_42_07, and 40_50_07.

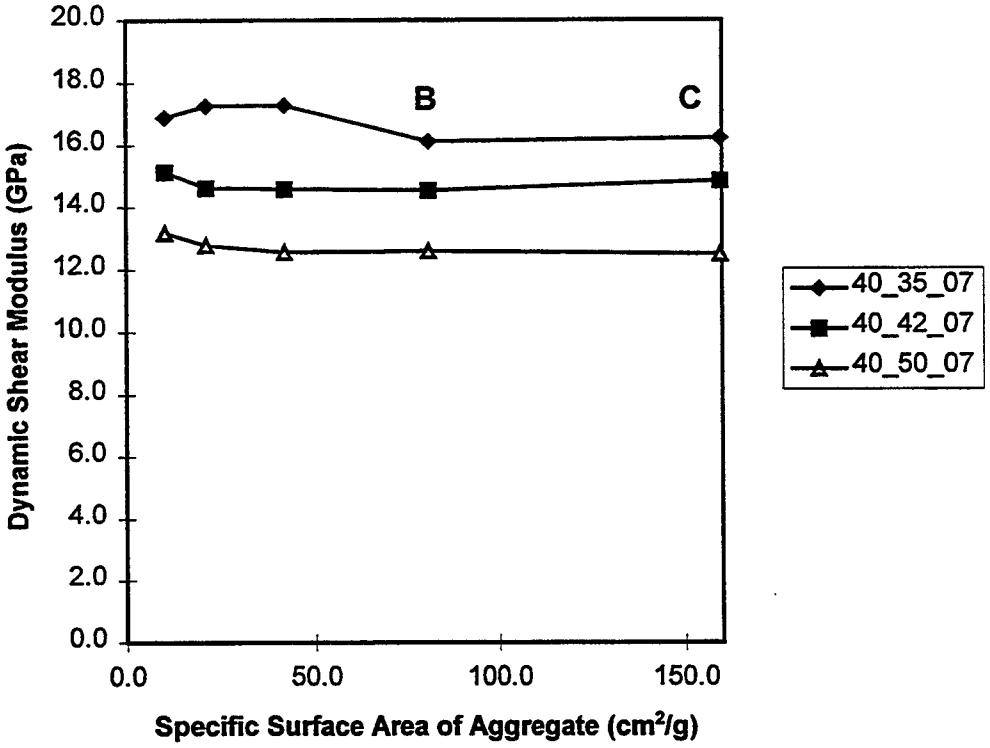

Figure 7.53 Dynamic Shear Modulus vs. SA for dolomite mortars at 28 days old having mixture proportions of 40_35_07, 40_42_07, and 40_50_07.

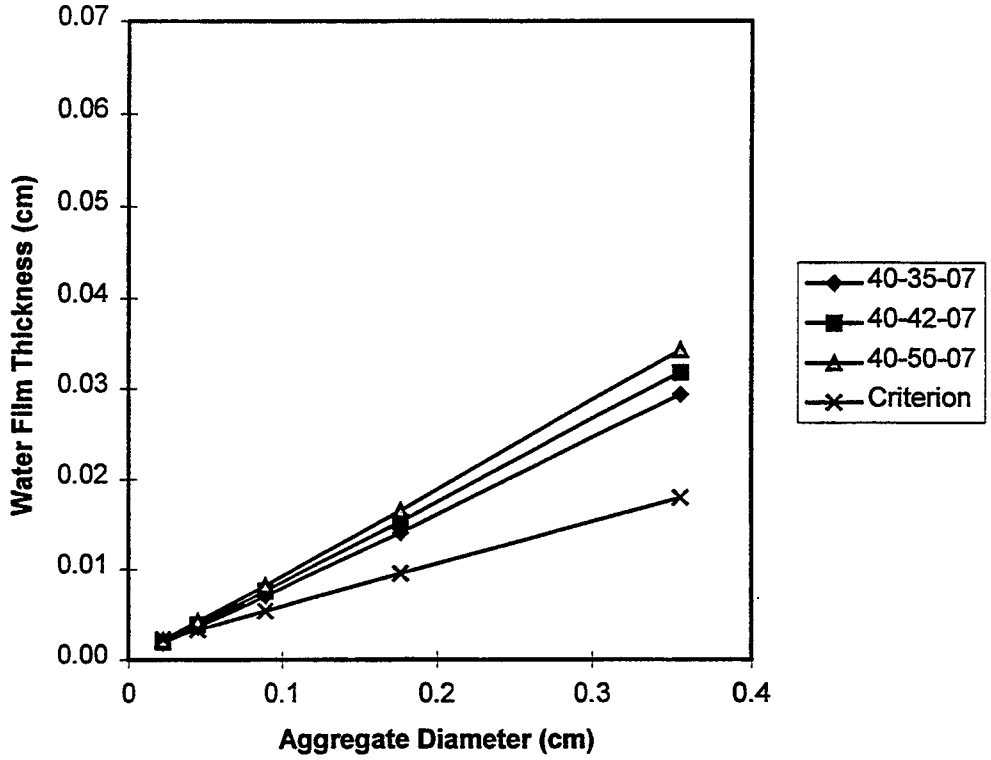

Figure 7.54 Water Film Thickness vs. Aggregate Diameter for dolomite mortars having mixture proportions of 40_35_07, 40_42_07, and 40_50_07. A criterion line is also plotted for comparison.

Table 7.1 Thickness of Water Film for Criterion, PC Mortars, and SF Mortars. PC mortars have mixture proportions of 40_35_00, 40_42_00, and 40_50_00. SF mortars have mixture proportions of 40_35_07, 40_42_07, and 40_50_07.

Aggregate size	Specific surface area of aggregate	Water film criterion	Water film for mixture 40_35_00	Compared with criterion	Water film for mixture 40_35_07	Compared with criterion
#4-#8	10.0	0.0179	0.0297	+65.9%	0.0293	+63.7%
#8-#16	20.8	0.0096	0.0143	+49.0%	0.0141	+46.9%
#16-#30	41.8	0.0054	0.0071	+31.5%	0.0070	+29.6%
#30-#50	80.9	0.0033	0.0037	+12.1%	0.0036(B)	+9.1%
#50-#100	159.4	0.0023	0.0019(A)	-17.4%	0.0018(C)	-21.7%
			Water film for mixture 40_42_00		Water film for mixture 40_42_07	
#4-#8	10.0	0.0179	0.0323	+80.4%	0.0318	+77.7%
#8-#16	20.8	0.0096	0.0155	+61.5%	0.0153	+59.4%
#16-#30	41.8	0.0054	0.0077	+42.6%	0.0076	+40.7%
#30-#50	80.9	0.0033	0.0040	+21.2%	0.0039	+18.2%
#50-#100	159.4	0.0023	0.0020	-13.0%	0.0020	-13.0%
			Water film for mixture 40_50_00		Water film for mixture 40_50_07	
#4-#8	10.0	0.0179	0.0346	+93.3%	0.0343	+91.6%
#8-#16	20.8	0.0096	0.0166	+72.9%	0.0165	+71.9%
#16-#30	41.8	0.0054	0.0083	+53.7%	0.0082	+51.9%
#30-#50	80.9	0.0033	0.0043	+30.3%	0.0042	+27.3%
#50-#100	159.4	0.0023	0.0022	-4.3%	0.0021	-8.7%

Note: The mixtures marked by A, B, and C may have mixing and compaction problems.

In comparison to the criterion, the thickness of water film for the three mixtures marked by A, B, and C are -17%, +9%, and -21.7% respectively. Therefore, they show the loss in dynamic moduli in Figures 7.49, 7.50, 7.52, and 7.53.

Since the mixtures marked by A, B, and C are more likely to exhibit mixing and compaction problems, their data should not be regarded as valid in interpreting the trend of dynamic moduli. Finally, the result is that the trends in dynamic modulus of elasticity and dynamic shear modulus with varying SA are quite flat for a different W/C in both PC mortars and SF mortars. In other words, the influence of W/C on bulk paste is equivalent to its influence on transition zones in dolomite mortar.

Can Va affect the dynamic moduli of transition zone? Figures 6.3, 6.4, 6.5, and 6.6 present the dynamic modulus of elasticity and dynamic shear modulus with varying SA for PC mortars having mixture proportions 25_42_00, 40_42_00, and 55_42_00, and SF mortars having mixture proportions 25_42_07, 40_42_07, and 55_42_07. Figures 6.7 and 6.8 present the thickness of water film for each mixture and criterion. The data of thickness of water film for the groups with mixture proportions 40_42_00 and 40_42_07 are presented in Table 7.1. The data for the groups with mixture proportions 25_42_00, 25_42_07, 55_42_00, and 55_42_07 are presented in Table 7.2. It is observed that all of the data in two groups having mixture proportions 55_42_00 and 55_42_07 are less than the criterion. Thus, the mixtures in these two groups are likely to have mixing and compaction problems. Therefore, the data of these two groups may be regarded as invalid. Finally, the result is that the trends in dynamic modulus of elasticity and dynamic shear modulus with varying SA are rather flat for a different Va. In other words, Va may not influence the dynamic moduli of the transition zone.

7.5 Percolation of Transition Zones and Its Influence on Mechanical Properties

It is generally considered that percolation of transition zones will accelerate the rate of deterioration and result in a durability problem in cementitious material. This is based on the understanding that water can go through cementitious material easier if percolation has formed inside the material. The water may bring in harmful substances,

Table 7.2 Thickness of Water Film for Criterion, PC Mortars, and SF Mortars. PC mortars have mixture proportions of 25_42_00 and 55_42_00. SF mortars have mixture proportions of 25_42_07 and 55_42_07.

Aggregate size	Specific surface area of aggregate	Water film criterion	Water film for mixture 25_42_00	Compared with criterion	Water film for mixture 25_42_07	Compared with criterion
#4-#8	10.0	0.0179	0.0646	+261%	0.0636	+255%
#8-#16	20.8	0.0096	0.0311	+224%	0.0306	+219%
#16-#30	41.8	0.0054	0.0155	+187%	0.0152	+181%
#30-#50	80.9	0.0033	0.0080	+142%	0.0079	+139%
#50-#100	159.4	0.0023	0.0041	+78.3%	0.0040	+73.9%
			Water film for mixture 55_42_00		Water film for mixture 55_42_07	
#4-#8	10.0	0.0179	0.0176	-1.7%	0.0174	-2.8%
#8-#16	20.8	0.0096	0.0085	-11.5%	0.0084	-12.5%
#16-#30	41.8	0.0054	0.0042	-22.2%	0.0042	-22.2%
#30-#50	80.9	0.0033	0.0022	-33.3%	0.0021	-36.4%
#50-#100	159.4	0.0023	0.0011	-52.2%	0.0011	-52.2%

dissolve, and then carry away soluble material, thus deteriorating the cementitious material.

An issue in this study is whether or not dynamic moduli of mortar will be affected by the percolation mechanism. The behavior of dynamic moduli is discussed in Chapters 7.2 and 7.3. It is suggested that porosity and the dynamic moduli of individual constituent control the dynamic moduli of mortar. By observing Figures 7.18 and 7.19, the data in the dynamic modulus of elasticity and the dynamic shear modulus show consistently flat trends, even for the percolated mixtures having mixture proportions of 37_52_00 and 37_52_10, and aggregate size #50~#100, which correspond to SA=159 cm^2/g. Thus, the percolation mechanism of transition zones may not affect dynamic moduli of mortar.

Another issue is whether or not tensile and compressive strengths of mortar will be influenced by the percolation mechanism. The experimental study on the strengths of transition zones meets the same problem as in the study of dynamic moduli of transition zones. That is, no instrument is available to measure the tensile or compressive strength of transition zones directly. Thus, the relationships of tensile and compressive strengths with varying SA were chosen to be studied. However, there are some differences between the study of dynamic moduli and the study of strength. Unlike dynamic moduli, the strength in mortar is controlled by the weakest link. This weakest link includes the weak points and the structure of these weak points, whichever link is the weakest. Based on the concept of probability, the strength of the material will be lower if there are more weak points, such as pores, in a homogeneous material. However, in a heterogeneous material, such as concrete or mortar, the strength is controlled not only by the probability of the weak points, but also the weakest structure of these points.

By keeping Va constant, increasing SA in the mortar by using finer aggregate particles may also increase the volume of transition zones, if the thickness of transition zones remains the same. Thus, the chance of a weak link in the mortar is increased if the volume of transition zones is increased. In addition, if the aggregate particles are crushed to a smaller size, they become stronger. This is because the crushing impact can

eliminate the weak links in aggregate particles. In this study, SA is increased by using finer aggregate particles. Thus, there will be two opposite effects in the mortar if the fracture cracks are transgranular (cleavage) in performing the strength test. The first effect is the chance that a weak link may become higher, thus lowering the strength of the mortar. The other is the included aggregate particles become stronger thus increase the strength of mortar. However, if the fracture cracks are intergranular (around aggregate particle), under a percolation condition, the strength of the mortar may be related to the strength of transition zones only because the fracture cracks are just propagated along the connected transition zones under this circumstance. Thus, the strength of the mortar will be significantly reduced if the strength of the transition zones is much lower than that of the bulk paste or aggregate particle. This is the concept used for studying the strength of transition zones.

Figure 7.55 presents the relationship between flexural tensile strength and SA for dolomite mortars having mixture proportions of 40_35_00, 40_42_00, 40_50_00, 40_35_07, 40_42_07, and 40_50_07. The data for the group of mixtures having mixture proportions of 40_50_00 have a hump-shaped trend, owing to two abnormally high points that correspond to SA=42 and 81 cm^2/g. In addition, Figure 7.56 shows that the compressive strengths for this group of mixtures are abnormally high. Another group of mixtures having mixture proportions of 37_52_00; close to 40_50_00, also shows a hump-shaped trend in tensile strength, as presented in Figure 7.57. The compressive strength is presented in Figure 7.58. With regard to dolomite mortars having mixture proportions of 40_50_00 and 37_52_00, the reason for their extraordinarily high tensile and compressive strengths is not yet known. However, this does not influence the analysis of the strength of the transition zone.

Figures 7.59, 7.60, and 7.61 present tensile cracks in the mortars having mixture proportions of 40_42_00 and aggregate sizes of #4~#8, #16~#30, and #50~#100 individually, which correspond to a SA of 10, 42, and 159 cm^2/g respectively. In addition, Figures 7.62, 7.63, and 7.64 present tensile cracks in the mortars having aggregate sizes of #4~#8, #16~#30, and #50~#100 respectively and the same mixture

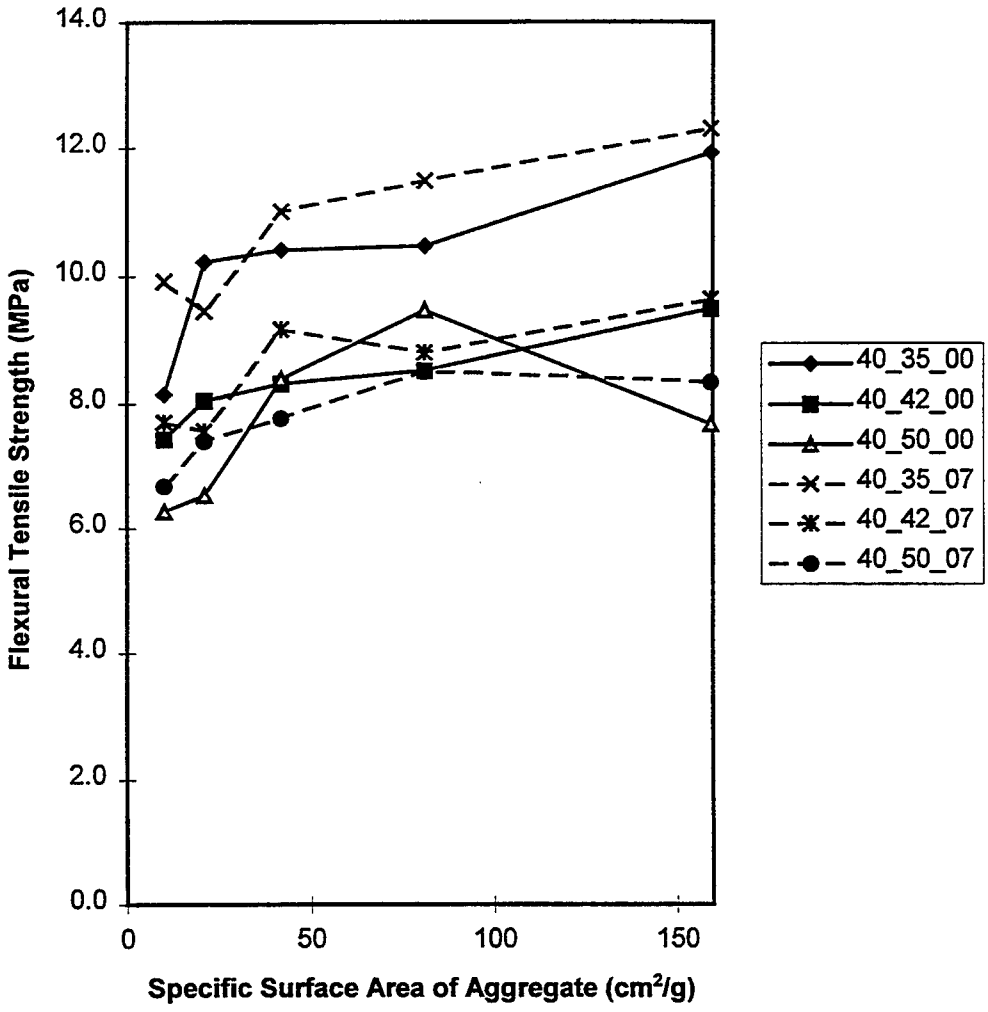

Figure 7.55 Flexural Tensile Strength vs. SA for dolomite mortars at 56 days old having mixture proportions of 40_35_00, 40_42_00, 40_50_00, 40_35_07, 40_42_07, and 40_50_07.

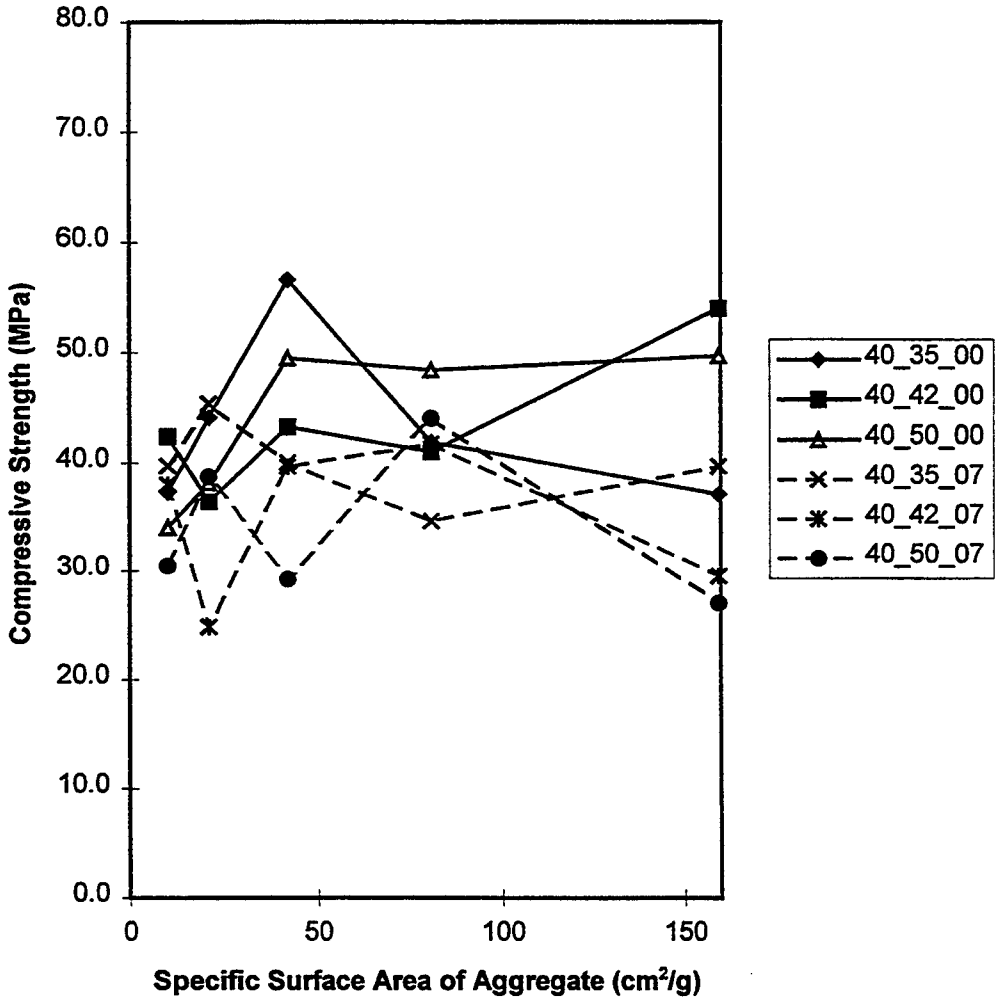

Figure 7.56 Compressive Strength vs. SA for dolomite mortars at 56 days old having mixture proportions of 40_35_00, 40_42_00, 40_50_00, 40_35_07, 40_42_07, and 40_50_07.

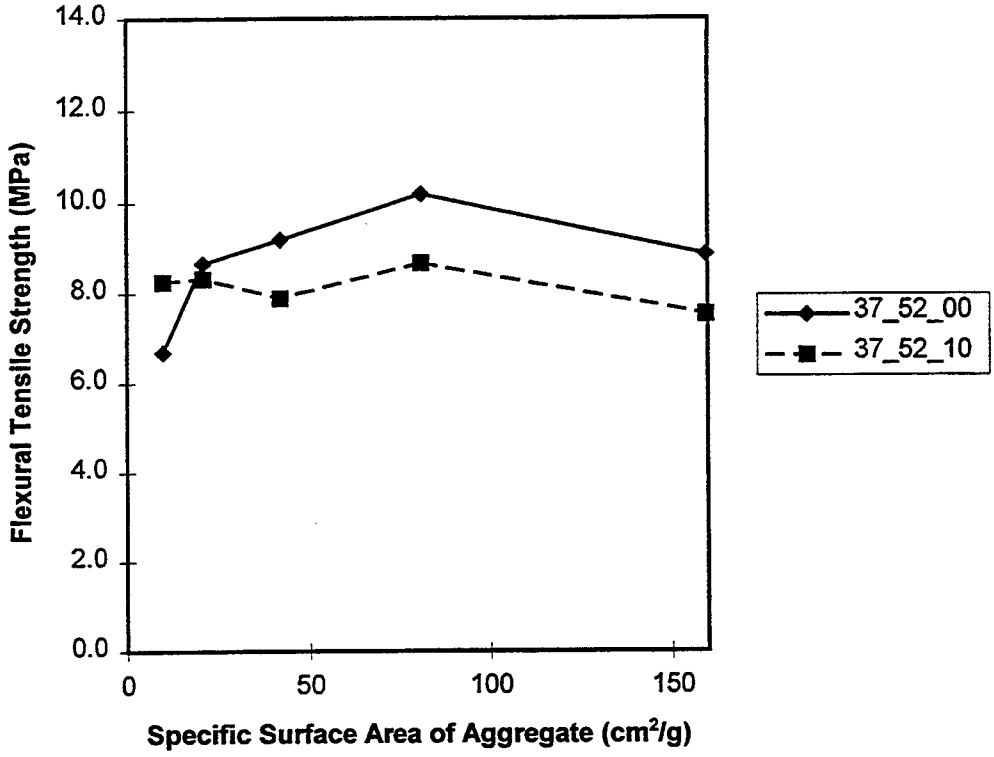

Figure 7.57 Flexural Tensile Strength vs. SA for dolomite mortars at 56 days old having mixture proportions of 37_52_00 and 37_52_10.

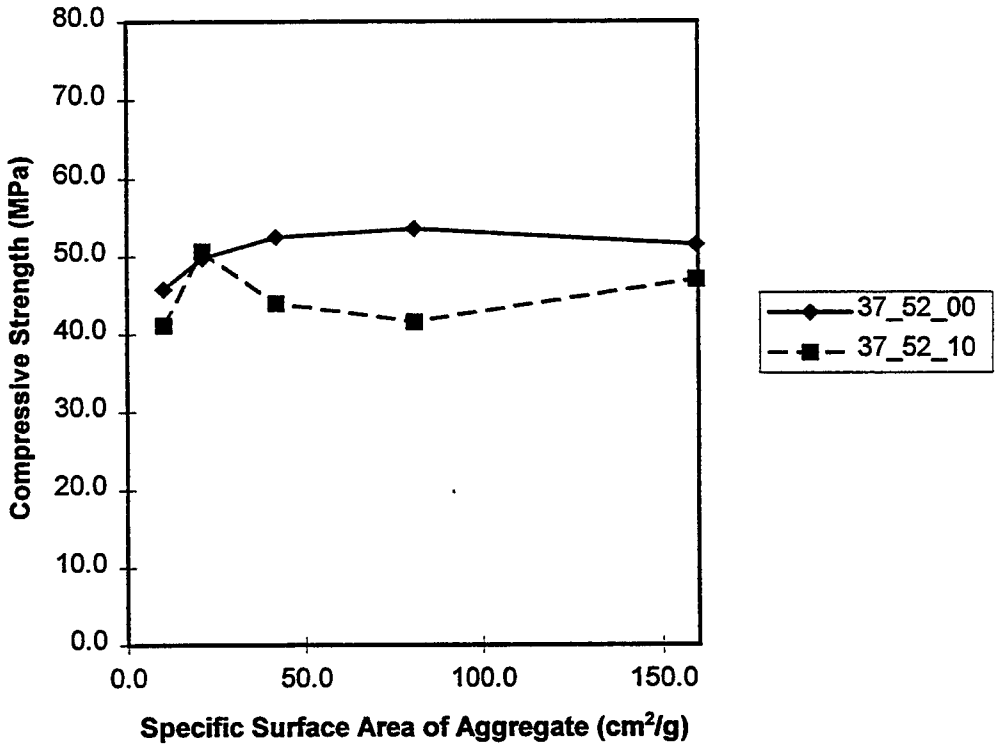

Figure 7.58 Compressive Strength vs. SA for dolomite mortars at 56 days old having mixture proportions of 37_52_00 and 37_52_10.

Figure 7.59 BEI micrograph of flexural tensile crack in dolomite mortar, magnification 30×, mixture proportion 40_42_00, aggregate size #4~#8.

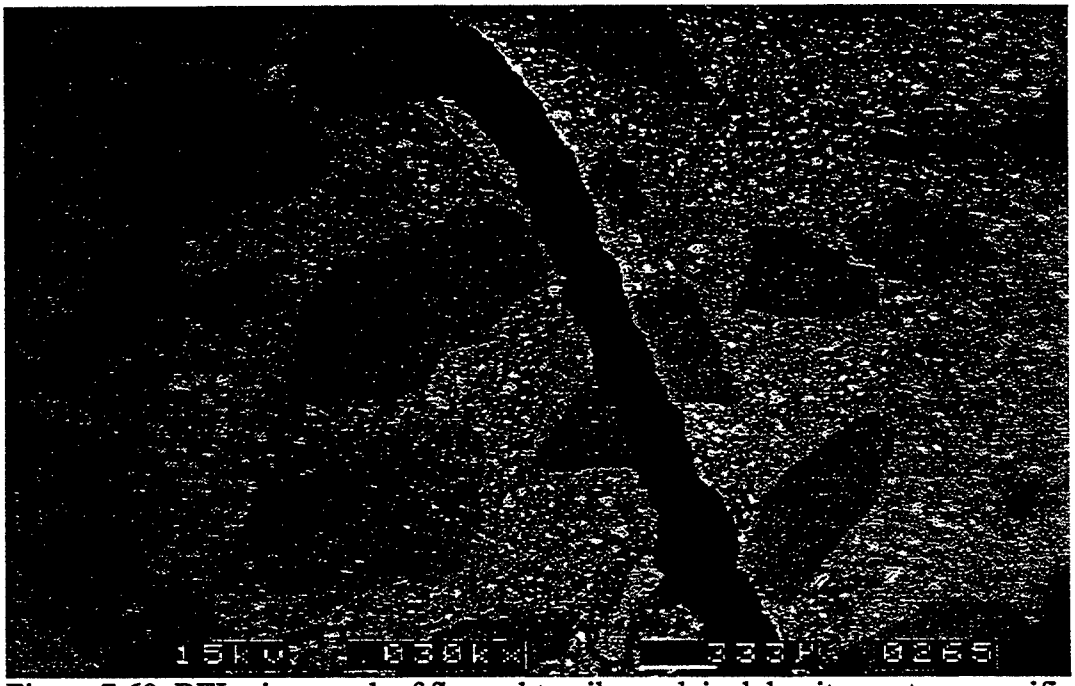

Figure 7.60 BEI micrograph of flexural tensile crack in dolomite mortar, magnification 30×. mixture proportion 40_42_00, aggregate size #16~#30

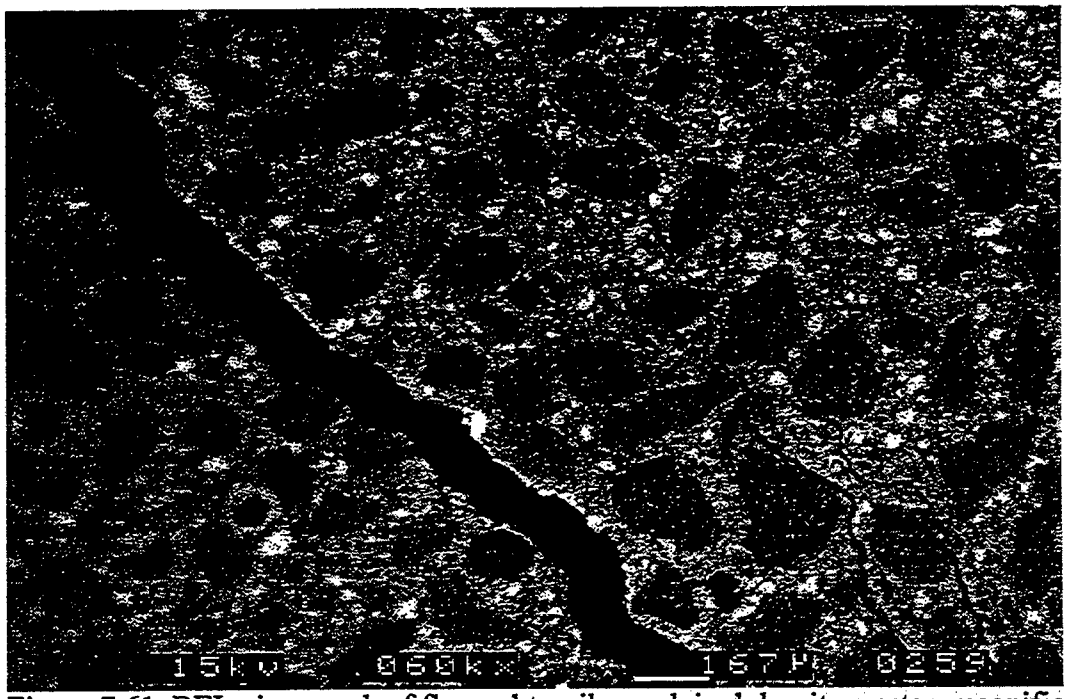

Figure 7.61 BEI micrograph of flexural tensile crack in dolomite mortar, magnification 60×, mixture proportion 40_42_00, aggregate size #50~#100.

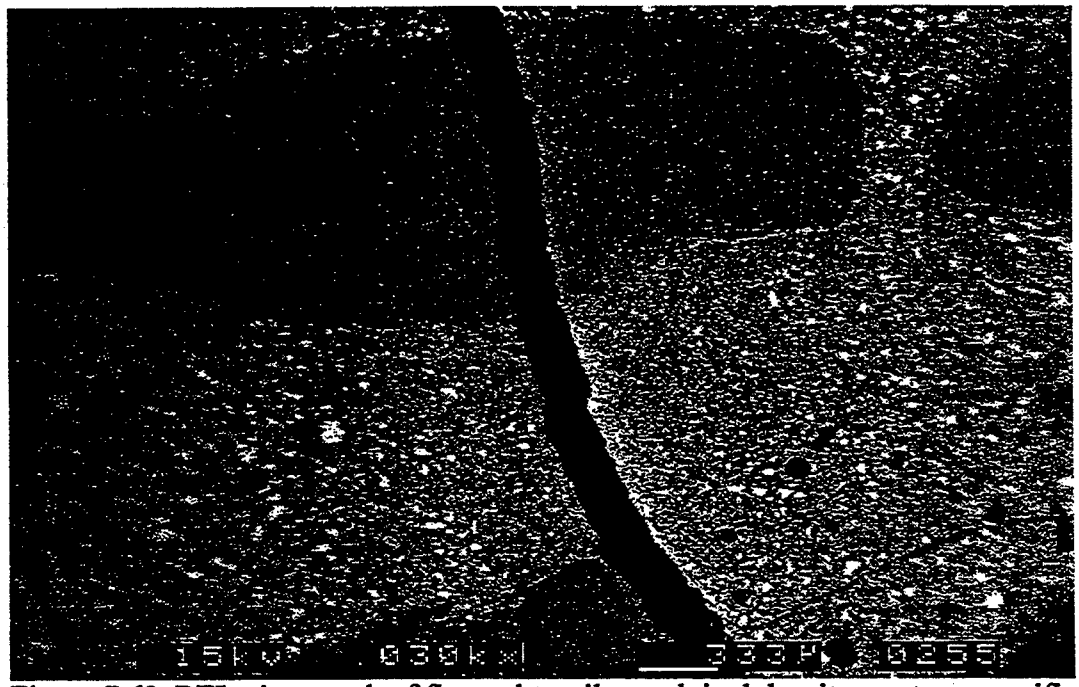

Figure 7.62 BEI micrograph of flexural tensile crack in dolomite mortar, magnification 30×, mixture proportion 40_42_07, aggregate size #4~#8.

Figure 7.63 BEI micrograph of flexural tensile crack in dolomite mortar, magnification 30×, mixture proportion 40_42_07, aggregate size #16~#30.

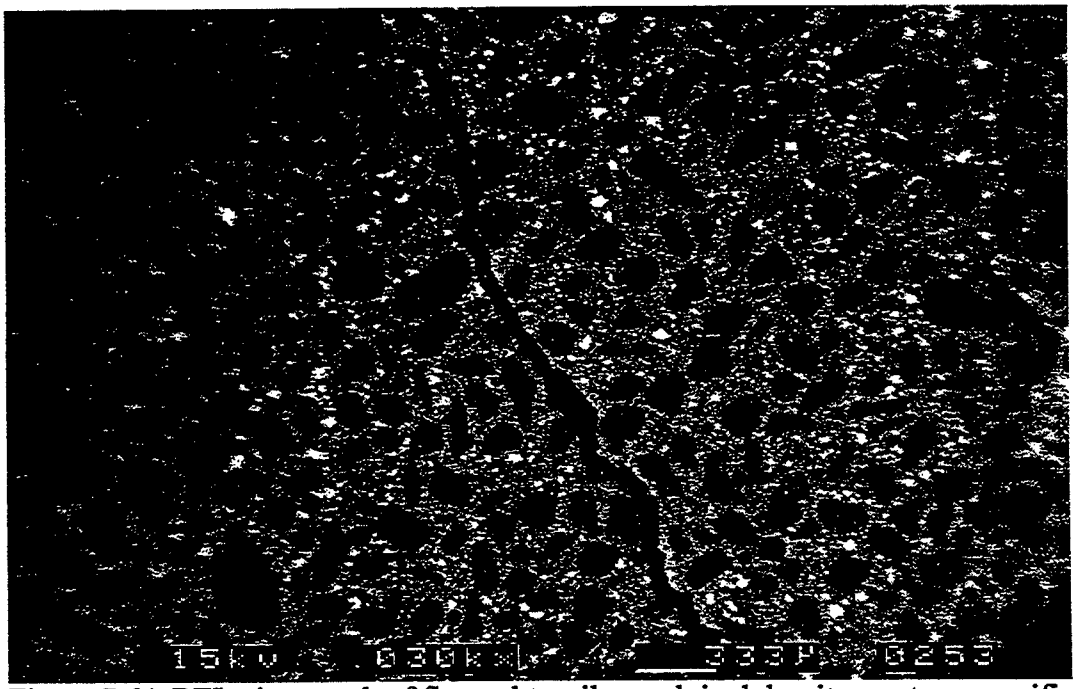

Figure 7.64 BEI micrograph of flexural tensile crack in dolomite mortar, magnification 30×, mixture proportion 40_42_07, aggregate size #50~#100.

proportions of 40_42_07. It is observed that when the included aggregate particles are larger, e.g., #4~#8 or #16~#30, the cracks are transgranular in both PC mortar and SF mortar. However, if the included aggregate particles are smaller, e.g., #50~#100, the cracks are intergranular in both PC mortar and SF mortar. A suggestion is that the tensile strength of transition zones in dolomite mortar is low. Thus, the tensile crack is intergranular under the percolation cases as shown in Figures 7.61 and 7.64. Nevertheless, based on different points of view, two reasons may be suggested to interpret the occurrence of the intergranular fracture cracks. One reason is that an aggregate particle is stronger when it is smaller, and thus, becomes harder to break hrough. The other reason is that it may take less energy for the crack to propagate around the smaller dolomite aggregate particle instead of breaking through it. Therefore, the intergranular cracks that occurred in the percolated mortars may not positively indicate that the tensile strength of transition zones is low. On the contrary, the tensile strength of transition zones in dolomite mortar may be on a similar level as that of bulk paste. This is based on the observation in Figure 7.55 that the trends in flexural tensile strength with a varying SA for two groups of mixtures having mixture proportions of 40_42_00 and 40_42_07 are still increasing slightly even though the percolation condition existed and intergranular fracture cracks formed inside the mortars.

Figures 7.65, 7.66, and 7.67 present the tensile fracture cracks in dolomite mortars having aggregate sizes of #4~#8, #16~#30, and #50~#100 respectively and the same mixture proportions of 37_52_00. In addition, Figures 7.68, 7.69, and 7.70 present the tensile fracture cracks in dolomite mortars having aggregate sizes of #4~#8, #16~#30, and #50~#100 respectively and the same mixture proportions of 37_52_10. By observing Figures 7.67 and 7.70, the intergranular cracks are found in both PC and SF mortars having aggregate size #50~#100 included. This phenomenon is similar to what happen in the two groups of mortars having mixture proportions of 40_42_00 and 40_42_07.

Figures 7.71, 7.72, and 7.73 present the tensile fracture cracks in quartzite mortars having aggregate sizes of #4~#8, #16~#30, and #50~#100 respectively and the same mixture proportions of 37_52_00. In addition, Figures 7.74, 7.75, and 7.76 present the

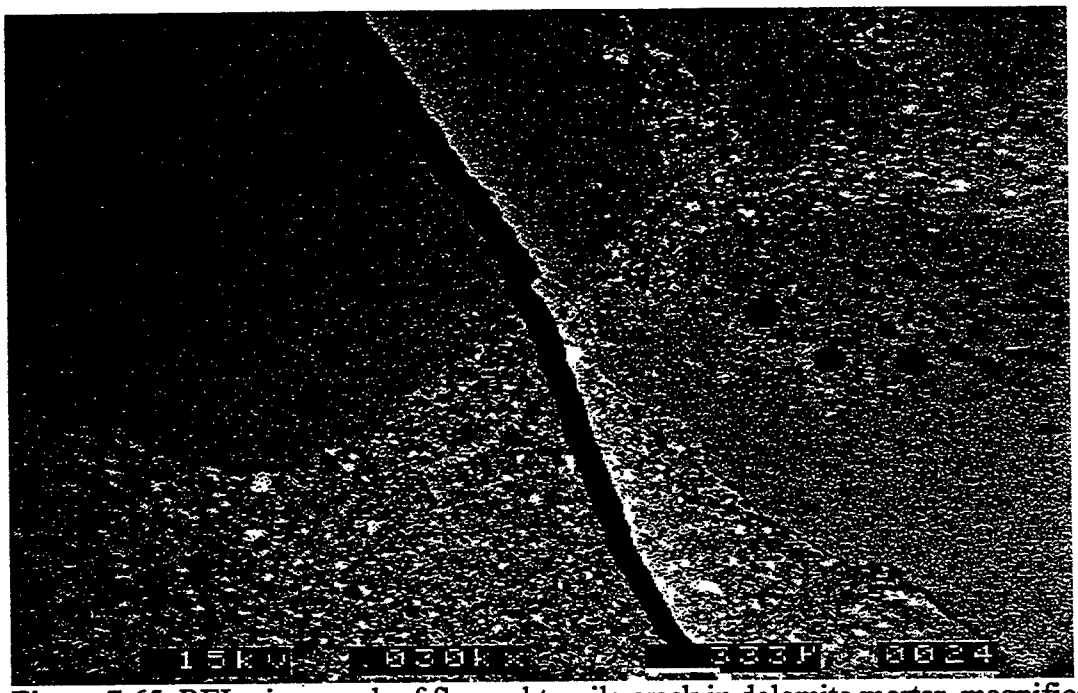

Figure 7.65 BEI micrograph of flexural tensile crack in dolomite mortar, magnification 30×, mixture proportion 37_52_00, aggregate size #4~#8.

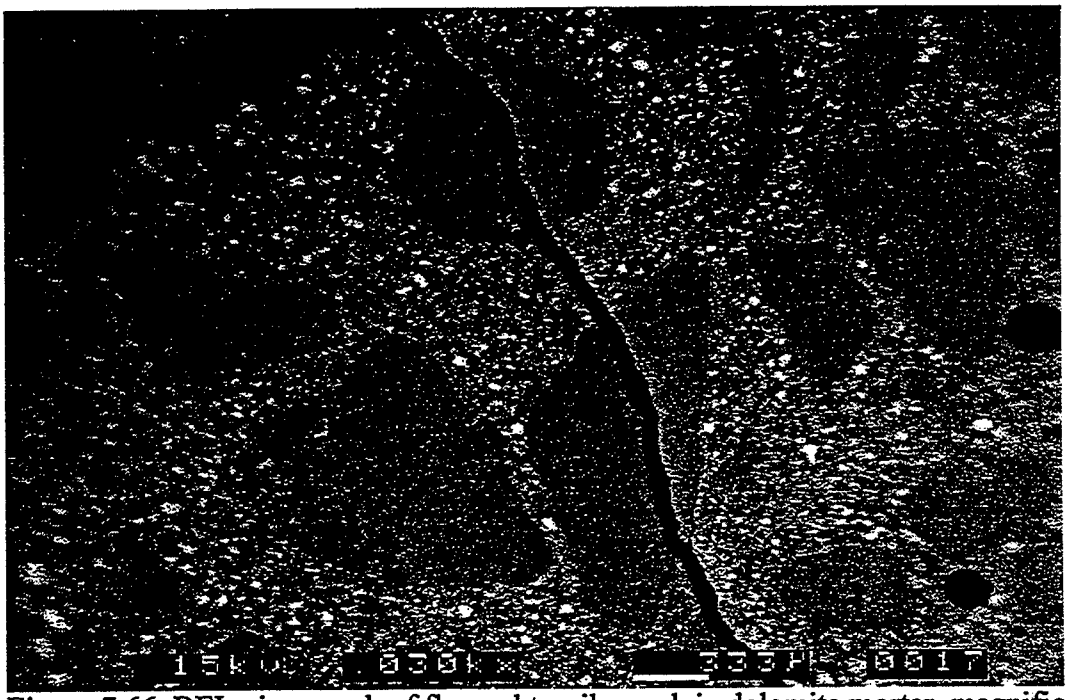

Figure 7.66 BEI micrograph of flexural tensile crack in dolomite mortar, magnification 30×, mixture proportion 37_52_00, aggregate size #16~#30.

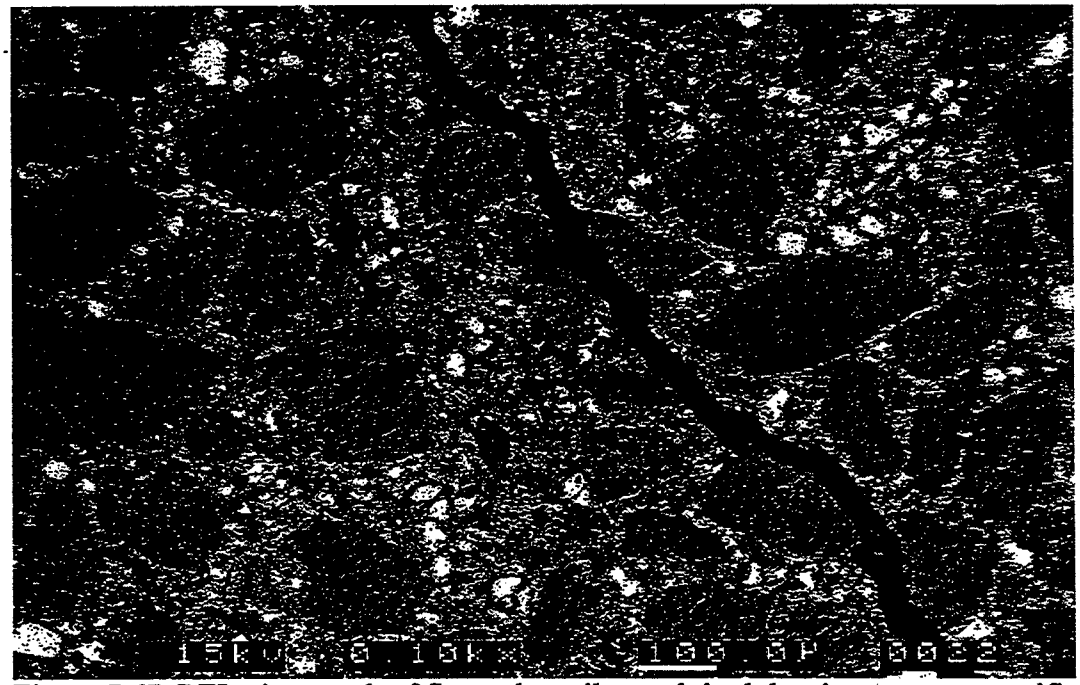

Figure 7.67 BEI micrograph of flexural tensile crack in dolomite mortar, magnification 100×, mixture proportion 37_52_00, aggregate size #50~#100.

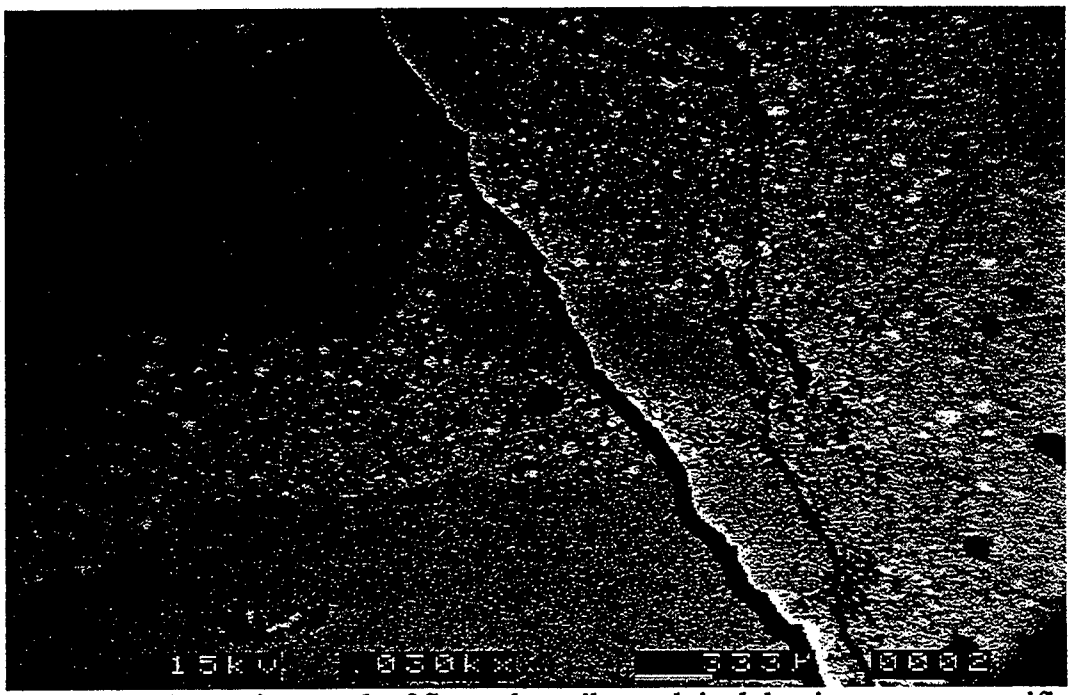

Figure 7.68 BEI micrograph of flexural tensile crack in dolomite mortar, magnification 30×, mixture proportion 37_52_10, aggregate size #4~#8.

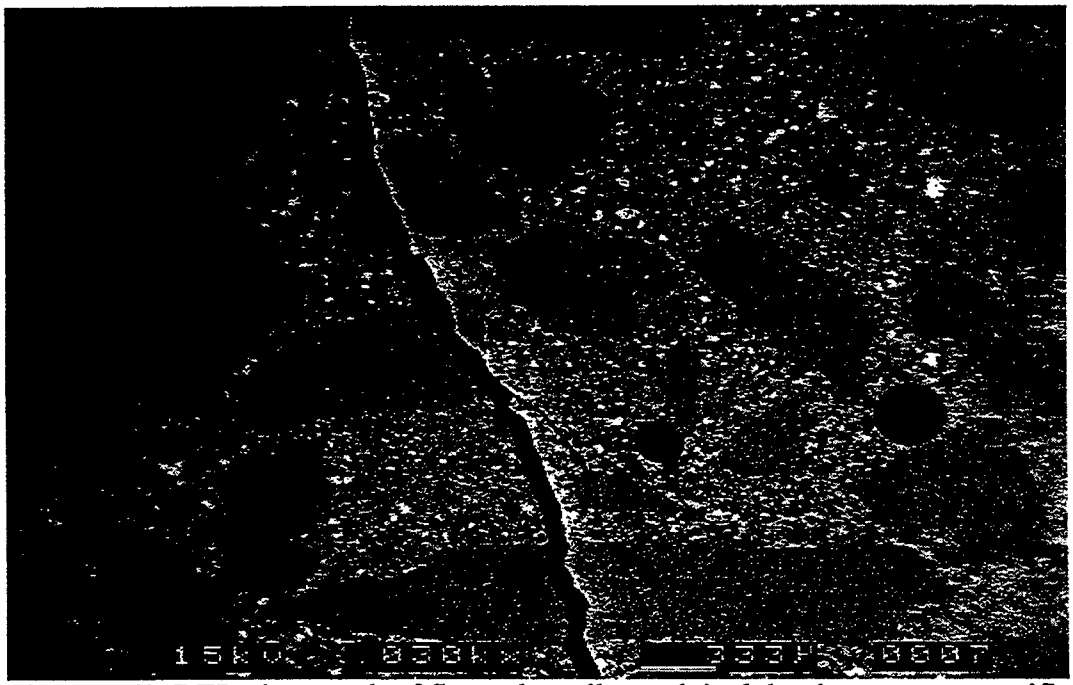

Figure 7.69 BEI micrograph of flexural tensile crack in dolomite mortar, magnification 30×, mixture proportion 37_52_10, aggregate size #16~#30.

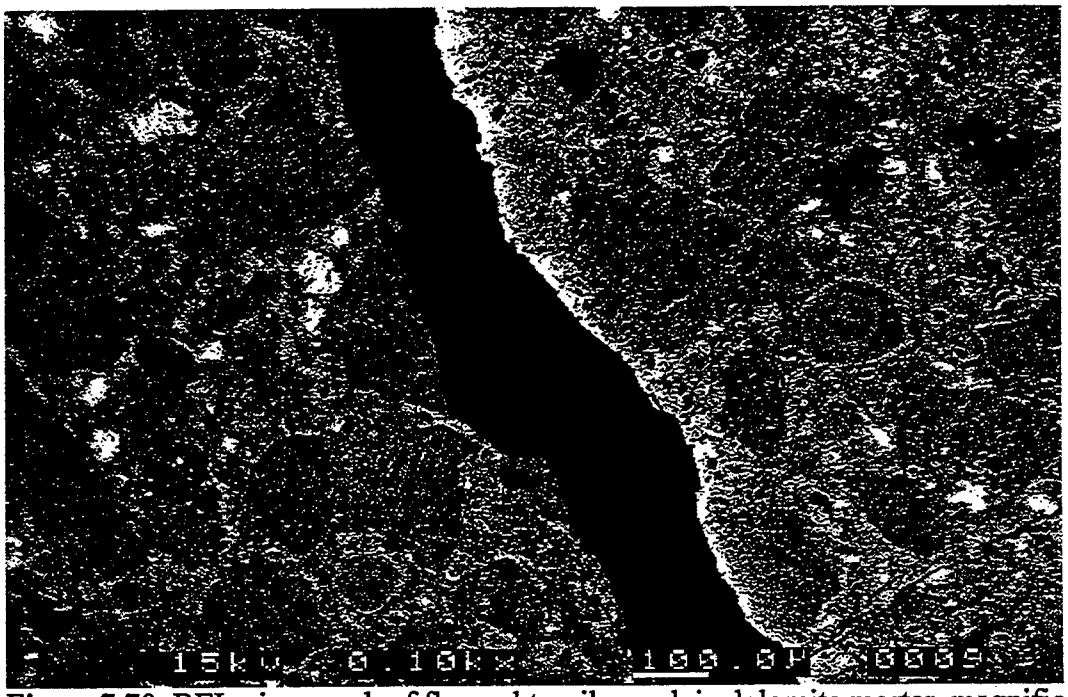

Figure 7.70 BEI micrograph of flexural tensile crack in dolomite mortar, magnification 100×, mixture proportion 37_52_10, aggregate size #50~#100.

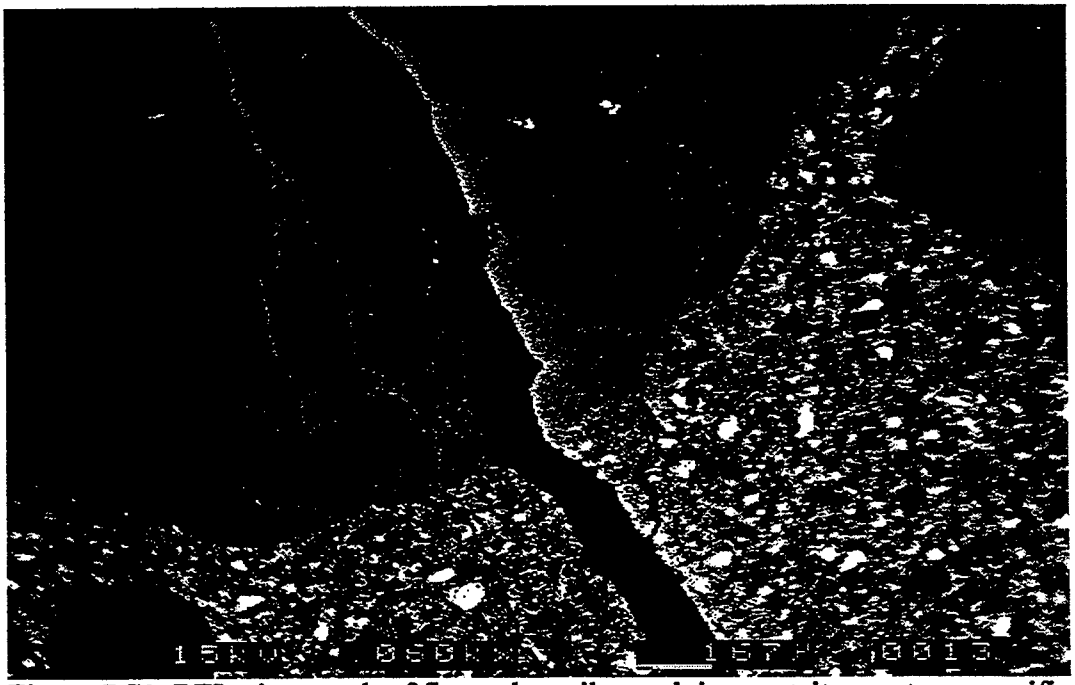

Figure 7.71 BEI micrograph of flexural tensile crack in quartzite mortar, magnification 60×, mixture proportion 37_52_00, aggregate size #4~#8.

Figure 7.72 BEI micrograph of flexural tensile crack in quartzite mortar, magnification 60×, mixture proportion 37_52_00, aggregate size #16~#30.

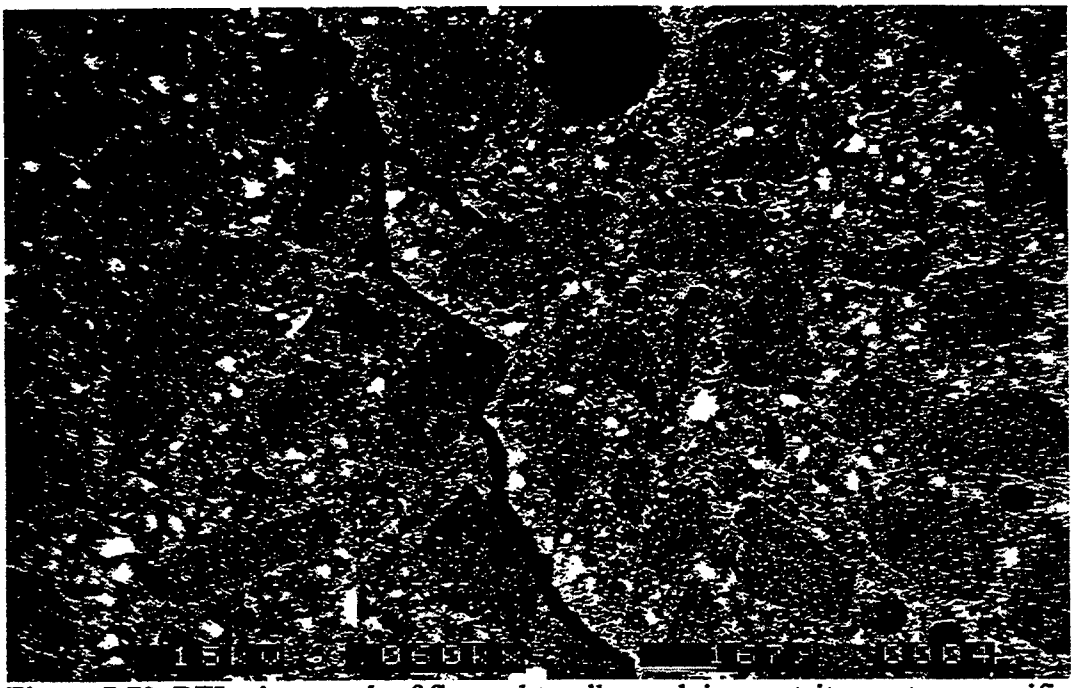

Figure 7.73 BEI micrograph of flexural tensile crack in quartzite mortar, magnification 60×, mixture proportion 37_52_00, aggregate size #50~#100.

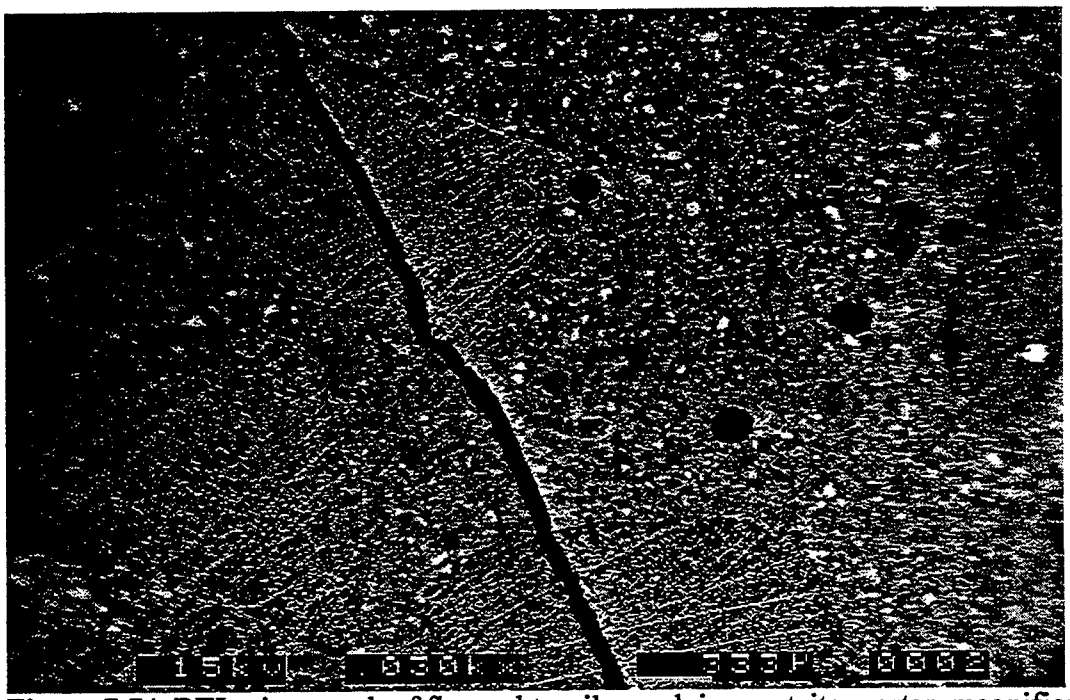

Figure 7.74 BEI micrograph of flexural tensile crack in quartzite mortar, magnification 30×, mixture proportion 37_52_10, aggregate size #8~#16.

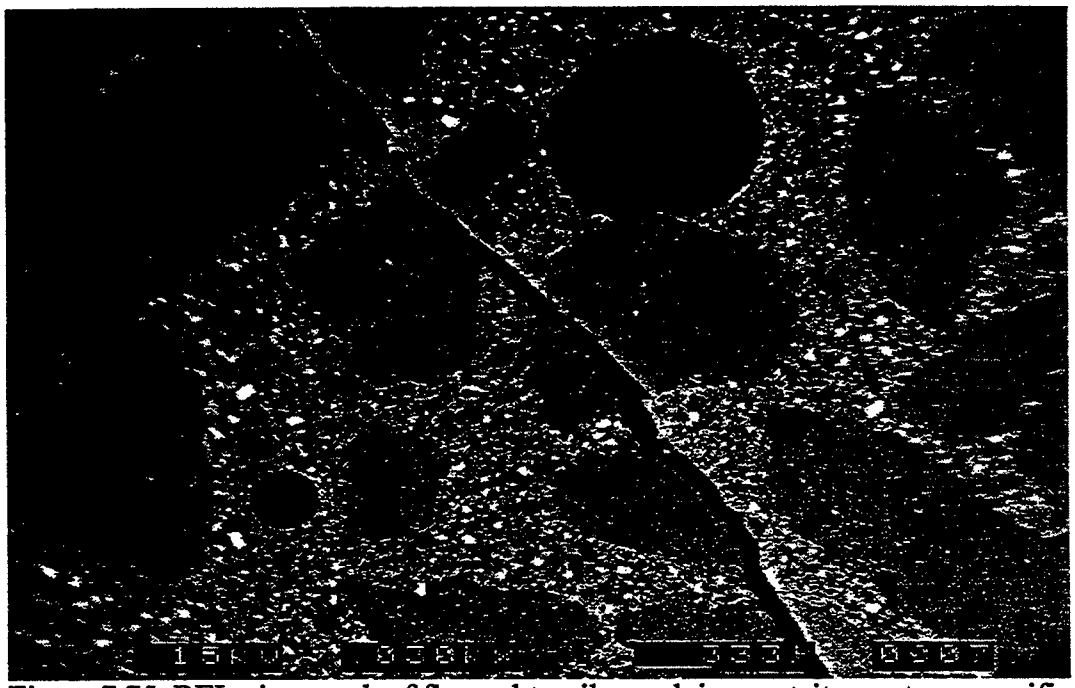

Figure 7.75 BEI micrograph of flexural tensile crack in quartzite mortar, magnification 30×, mixture proportion 37_52_10, aggregate size #16~#30.

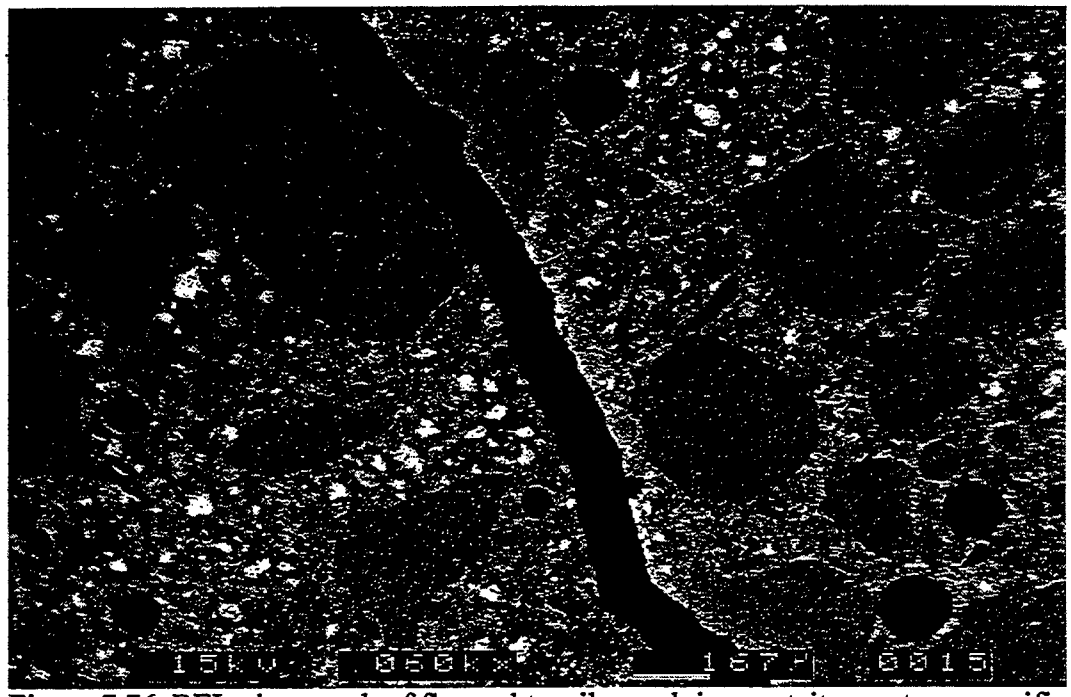

Figure 7.76 BEI micrograph of flexural tensile crack in quartzite mortar, magnification 60×, mixture proportion 37_52_10, aggregate size #30~#50.

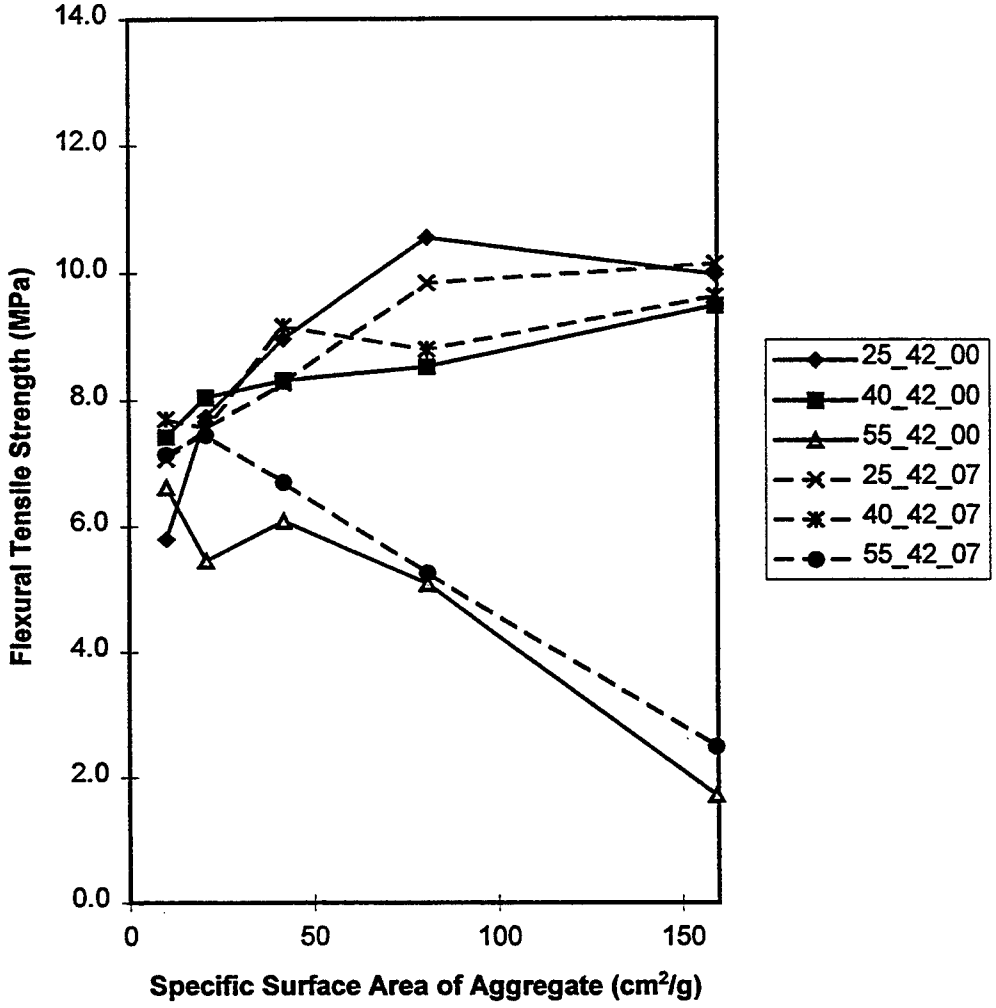

Figure 7.77 Flexural Tensile Strength vs. SA for dolomite mortars at 56 days old having mixture proportions of 25_42_00, 40_42_00, 55_42_00, 25_42_07, 40_42_07, and 55_42_07.

tensile fracture cracks in quartzite mortars having aggregate sizes of #8~#16, #16~#30, and #30~#50 respectively and the same mixture proportions of 37_52_10. By observing Figures 7.73 and 7.76, it is concluded that similar to dolomite mortars, the intergranular cracks are more likely to occur in quartzite mortars with smaller aggregate particles.

Figure 7.77 presents the relationship between flexural tensile strength and SA for dolomite mortars having mixture proportions of 25_42_00, 40_42_00, 55_42_00, 25_42_07, 40_42_07, and 55_42_07. In addition, Figure 7.78 presents the relationship between compressive strength and SA for dolomite mortars having mixture proportions of 25_42_00, 40_42_00, 55_42_00, 25_42_07, 40_42_07, and 55_42_07. It is observed that the values of tensile and compressive strengths are low for the two groups of mixtures having mixture proportions of 55_42_00 and 55_42_07. This may be due to the mixing and compaction problems that is discussed in Chapter 6.4.

The study of the influence of silica fume on the strength of dolomite mortar is based on the comparison of the data of tensile and compressive strengths in Figures 7.55~7.58, 7.77, and 7.78 between mortar groups in each pair, such as 40_35_00 and 40_35_07; 40_42_00 and 40_42_07; 40_50_00 and 40_50_07; 37_52_00 and 37_52_10; 25_42_00 and 25_42_07; and 55_42_00 and 55_42_07. Unlike the fact that silica fume usually has a reducing effect on the dynamic moduli of mortar as discussed in Chapter 7.3, the modifications induced by silica fume to the pore system can have either an increasing or a decreasing effect on the flexural tensile strength and compressive strength of dolomite mortar. This is also different from what happens in concrete, where silica fume usually has an increasing effect on its strength. The reason may be due to the different pore size distribution between mortar and concrete. Concrete usually has many pores that are greater in size than 20 μm. The pores that are 10 to 20 μm in size, introduced into mortar by silica fume, may not influence the pore system of concrete very much. Therefore, the micro-filler effect overwhelms the effect of introducing larger pores and thereby strengthens the concrete. However, these pores may significantly increase the amount of large pores in the mortar, and this effect may lower the strength of the mortar. Although the micro-filler effect may increase the strength of the mortar, the

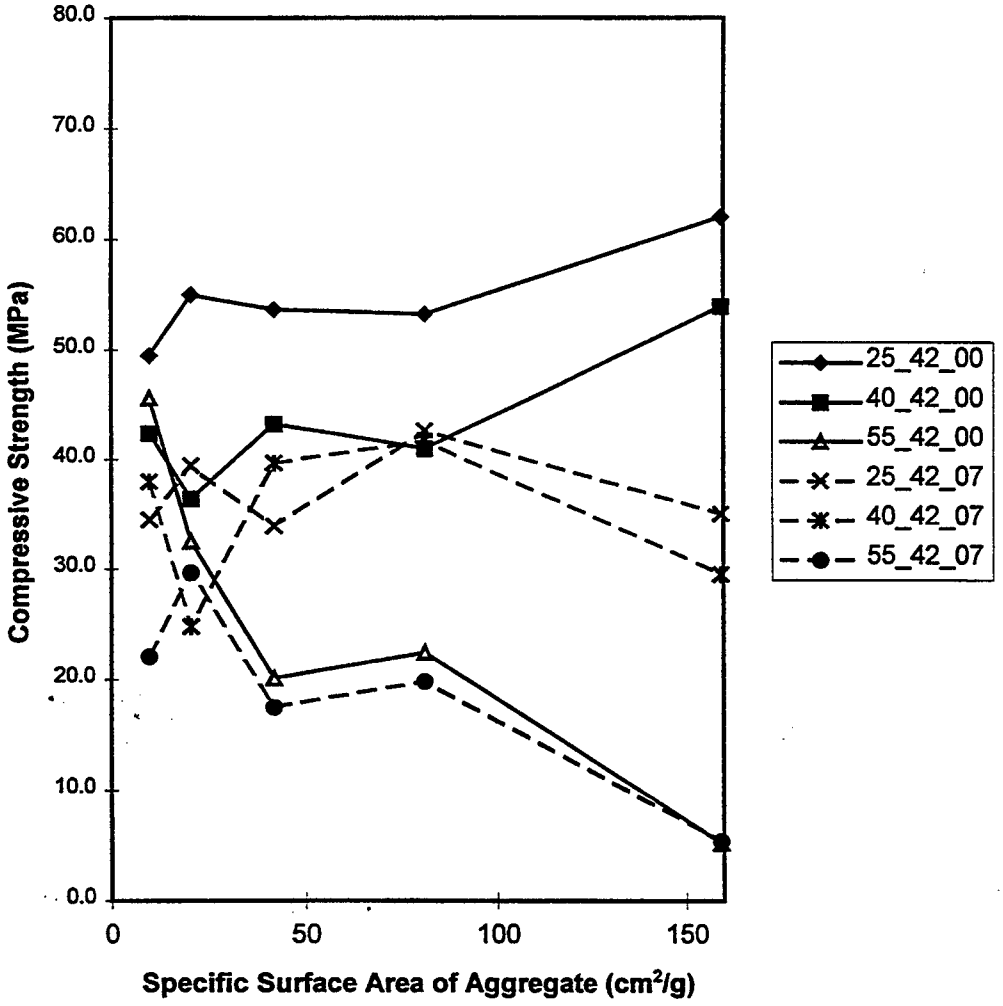

Figure 7.78 Compressive Strength vs. SA for dolomite mortars at 56 days old having mixture proportions of 25_42_00, 40_42_00, 55_42_00, 25_42_07, 40_42_07, and 55_42_07.

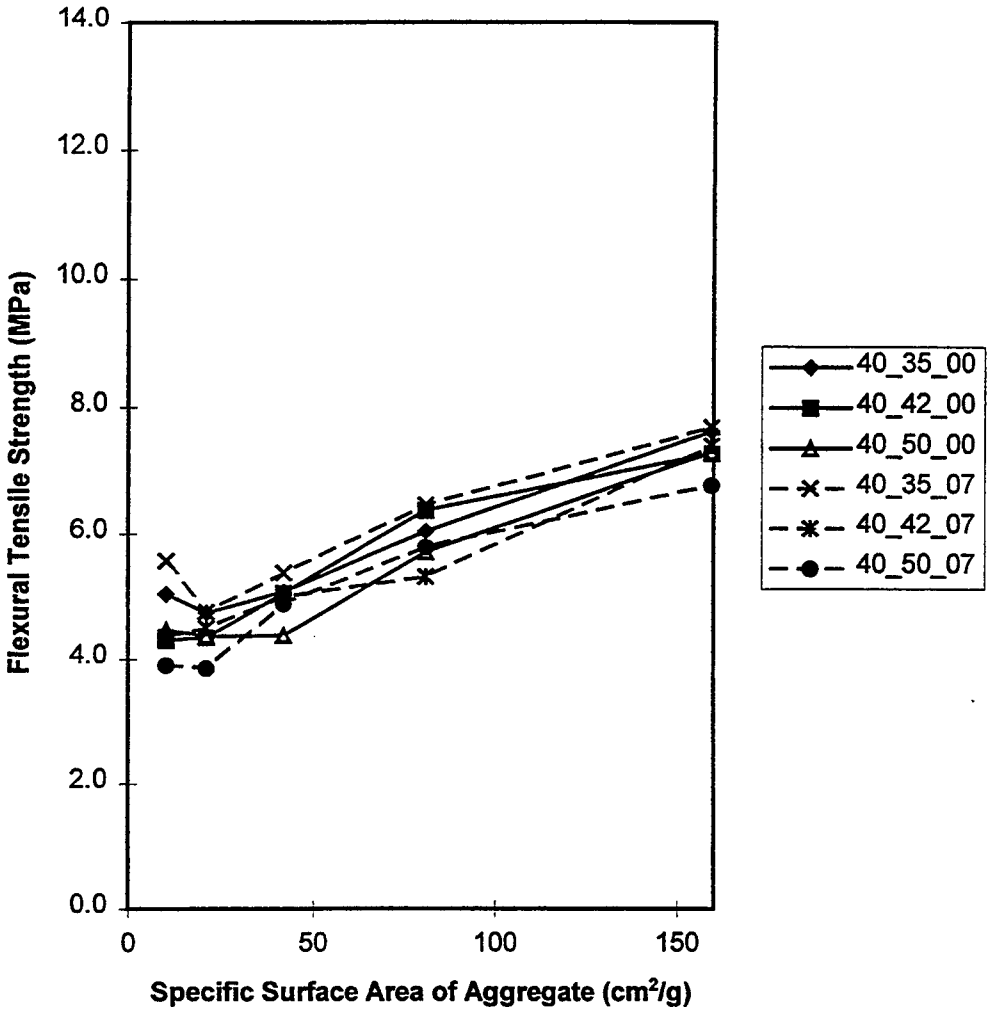

Figure 7.79 Flexural Tensile Strength vs. SA for perlite mortars at 56 days old having mixture proportions of 40_35_00, 40_42_00, 40_50_00, 40_35_07, 40_42_07, and 40_50_07.

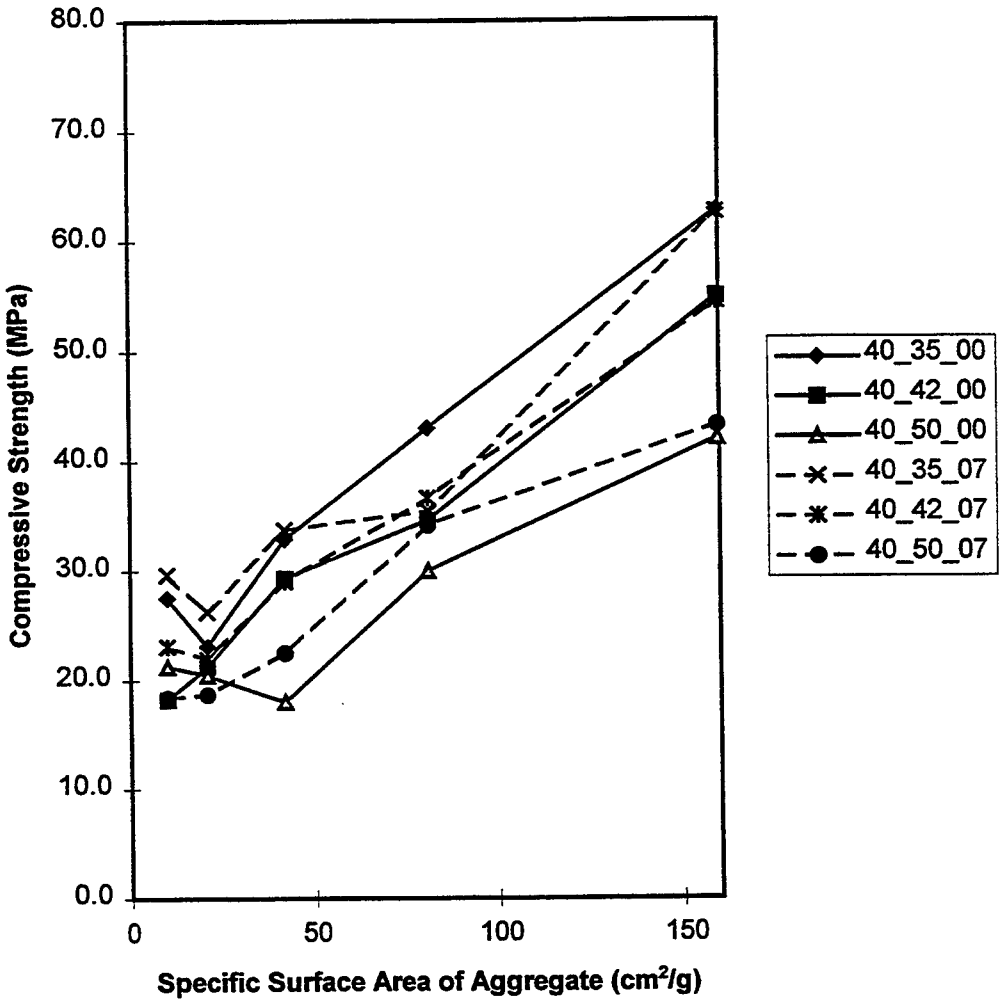

Figure 7.80 Compressive Strength vs. SA for perlite mortars at 56 days old having mixture proportions of 40_35_00, 40_42_00, 40_50_00, 40_35_07, 40_42_07, and 40_50_07.

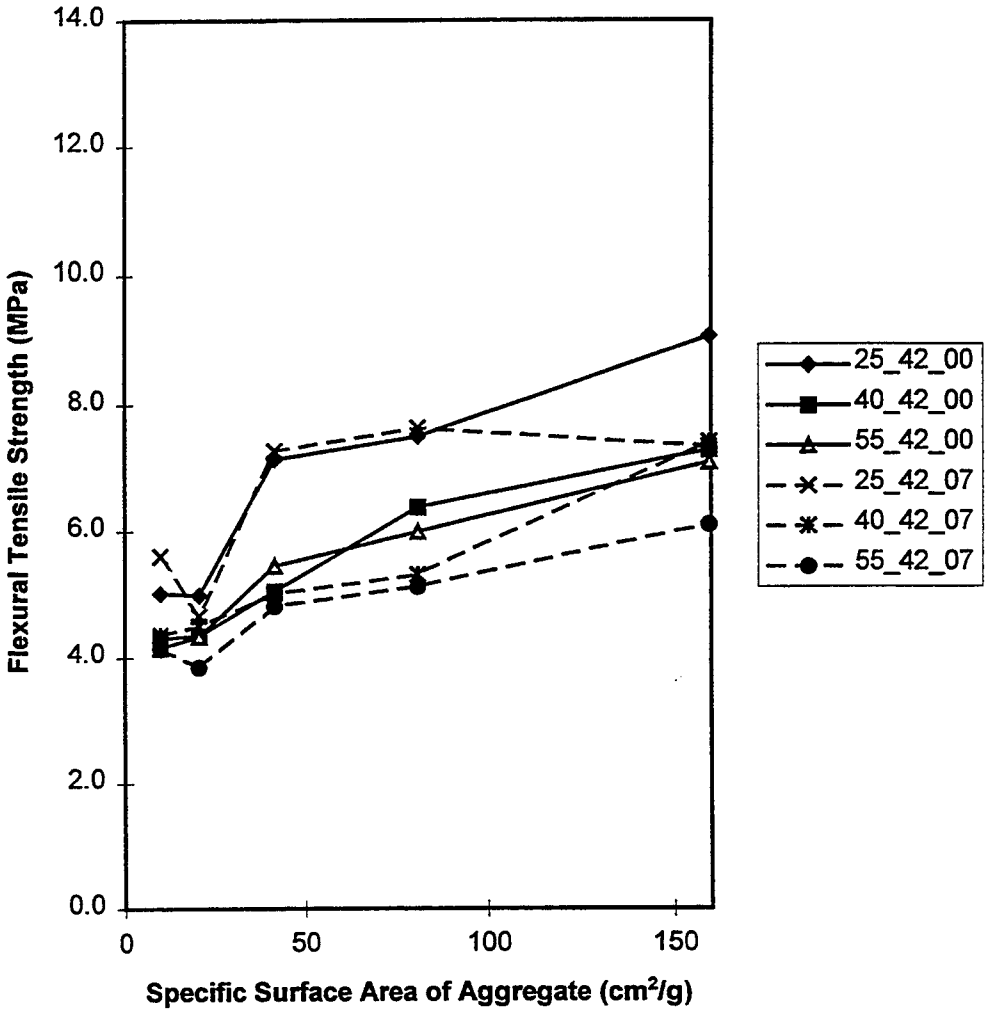

Figure 7.81 Flexural Tensile Strength vs. SA for perlite mortars at 56 days old having mixture proportions of 25_42_00, 40_42_00, 55_42_00, 25_42_07, 40_42_07, and 55_42_07.

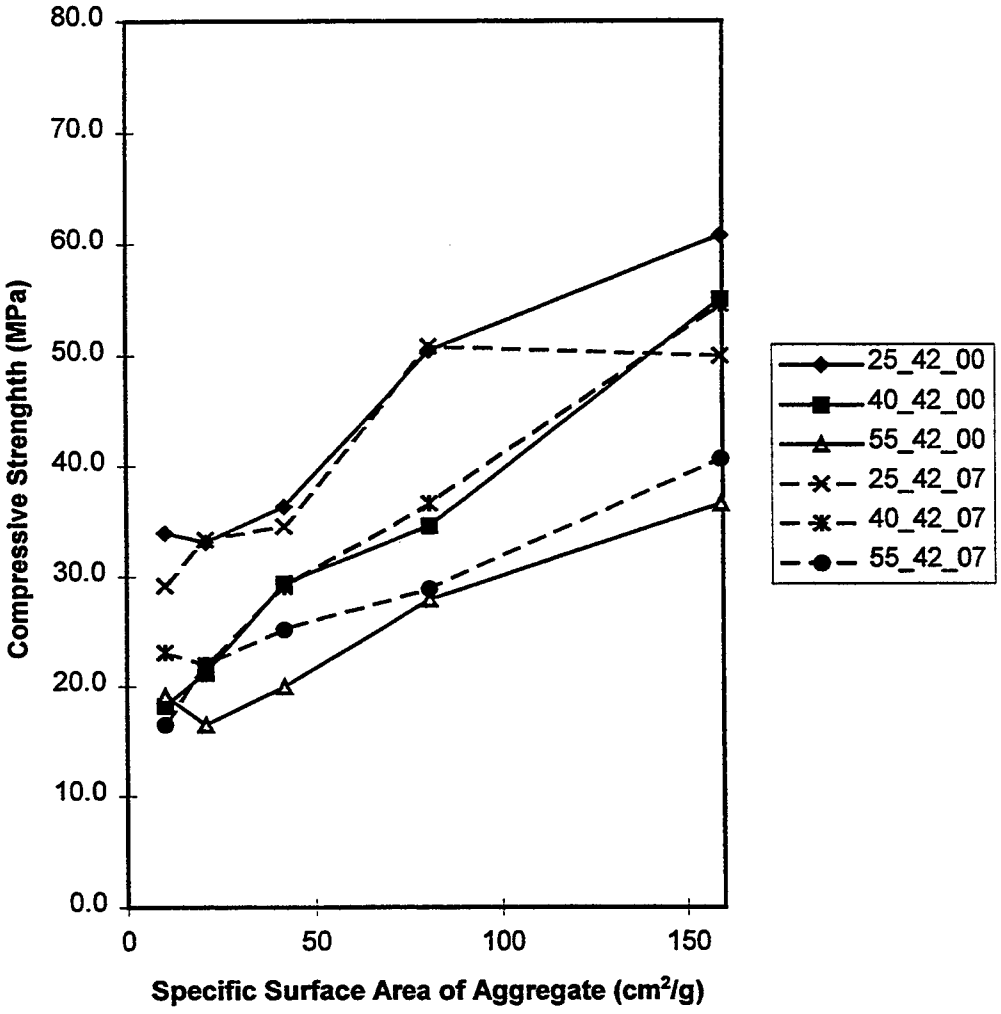

Figure 7.82 Compressive Strength vs. SA for perlite mortars at 56 days old having mixture proportions of 25_42_00, 40_42_00, 55_42_00, 25_42_07, 40_42_07, and 55_42_07.

power of these two opposite effects may be balanced. Therefore, silica fume does not show an obvious effect, either positive or negative, on the strength of mortar.

Figures 7.79 and 7.80 present flexural tensile strengths and compressive strengths with varying SA respectively for perlite mortars at 56 days old having mixture proportions of 40_35_00, 40_42_00, 40_50_00, 40_35_07, 40_42_07, and 40_50_07. In addition, Figures 7.81 and 7.82 present flexural tensile strengths and compressive strengths with varying SA respectively for perlite mortars at 56 days old having mixture proportions of 25_42_00, 40_42_00, 55_42_00, 25_42_07, 40_42_07, and 55_42_07. Moreover, Figures 7.83 and 7.84 present flexural tensile strengths and compressive strengths with varying SA for perlite mortars at 56 days old having mixture proportions of 37_52_00 and 37_52_10. It is observed that the tensile and compressive strengths of perlite mortars are higher if the aggregate particles included are finer. It is also observed that silica fume may only have a minor effect on the flexural tensile strength and compressive strength of perlite mortar. This is indicated by comparing the data of tensile and compressive strengths in Figures 7.79~7.84 between mortar groups in each pair, such as 40_35_00 and 40_35_07, 40_42_00 and 40_42_07, 40_50_00 and 40_50_07, 25_42_00 and 25_42_07, 55_42_00 and 55_42_07, and 37_52_00 and 37_52_10. As discussed in Chapter 7.3, silica fume does not have an apparent influence on the dynamic moduli of perlite mortar. One of the reasons why silica fume has a minor effect on the moduli or strengths of perlite mortars may be due to the fact that the transition zone of perlite mortar is not obvious. Silica fume cannot effectively modify this ambiguous transition zone.

Figures 7.85, 7.86, and 7.87 present the tensile fracture crack in perlite mortars having aggregate sizes of #4~#8, #16~#30, and #50~#100 respectively and the same mixture proportions of 37_52_00. In addition, Figures 7.88, 7.89, and 7.90 present the tensile fracture crack in perlite mortars having aggregate sizes of #4~#8, #16~#30, and #50~#100 respectively and the same mixture proportions of 37_52_10. The characteristics of the fracture cracks in perlite mortar are different from those in dolomite or quartzite mortars. In perlite mortar, the cracks are transgranular regardless of the size

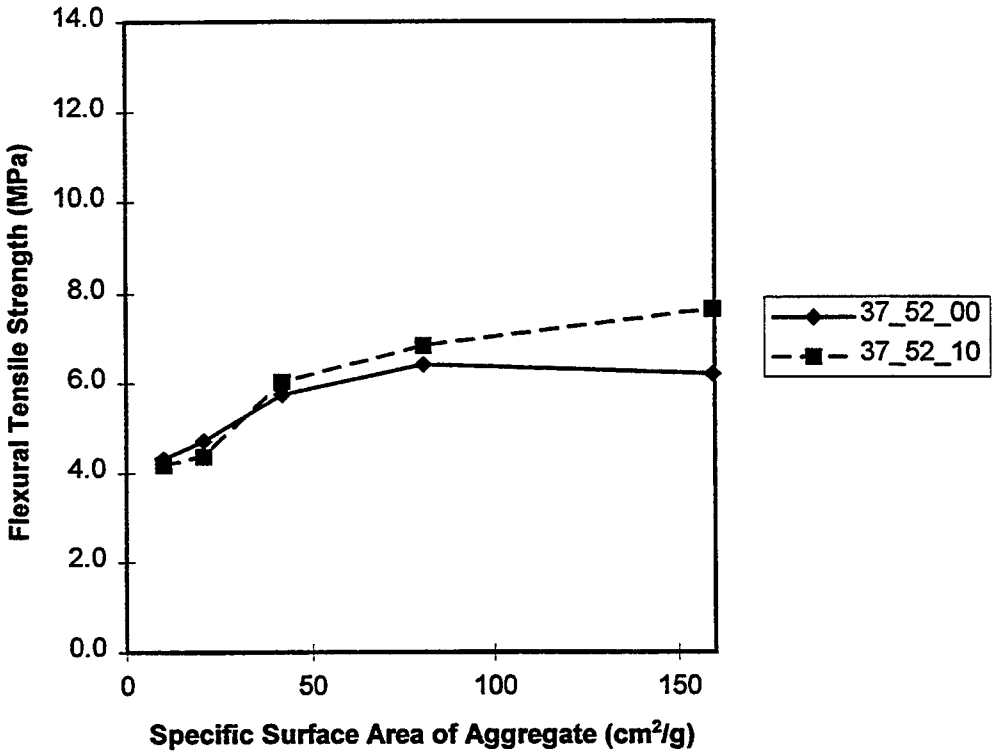

Figure 7.83 Flexural Tensile Strength vs. SA for perlite mortars at 56 days old having mixture proportions of 37_52_00 and 37_52_10.

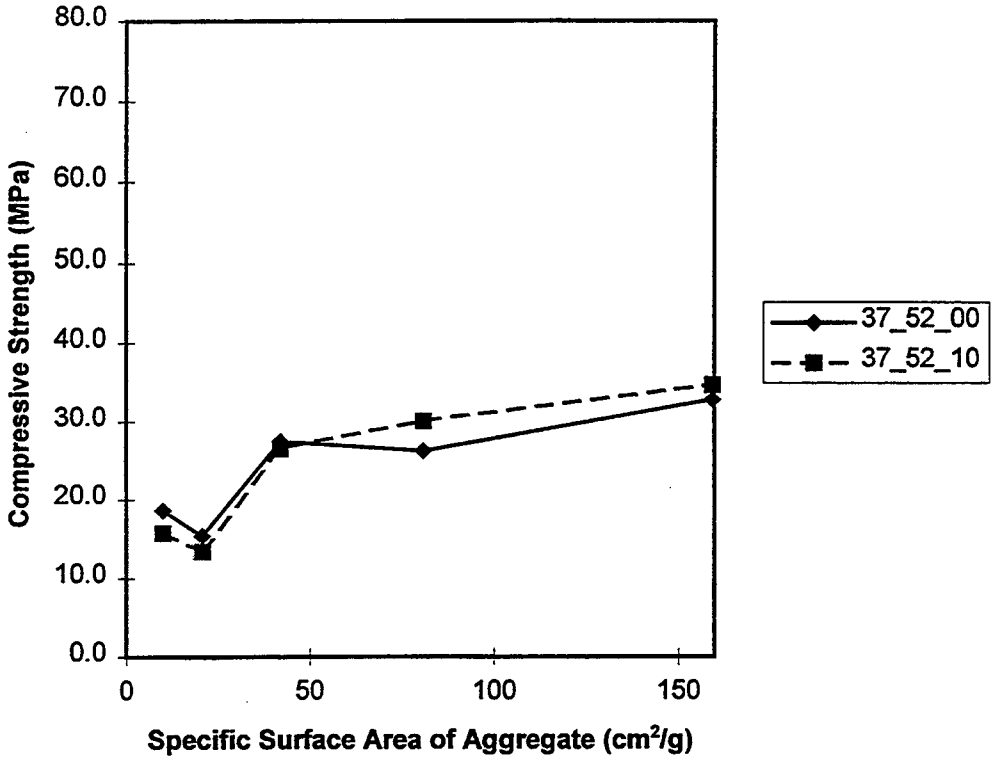

Figure 7.84 Compressive Strength vs. SA for perlite mortars at 56 days old having mixture proportions of 37_52_00 and 37_52_10.

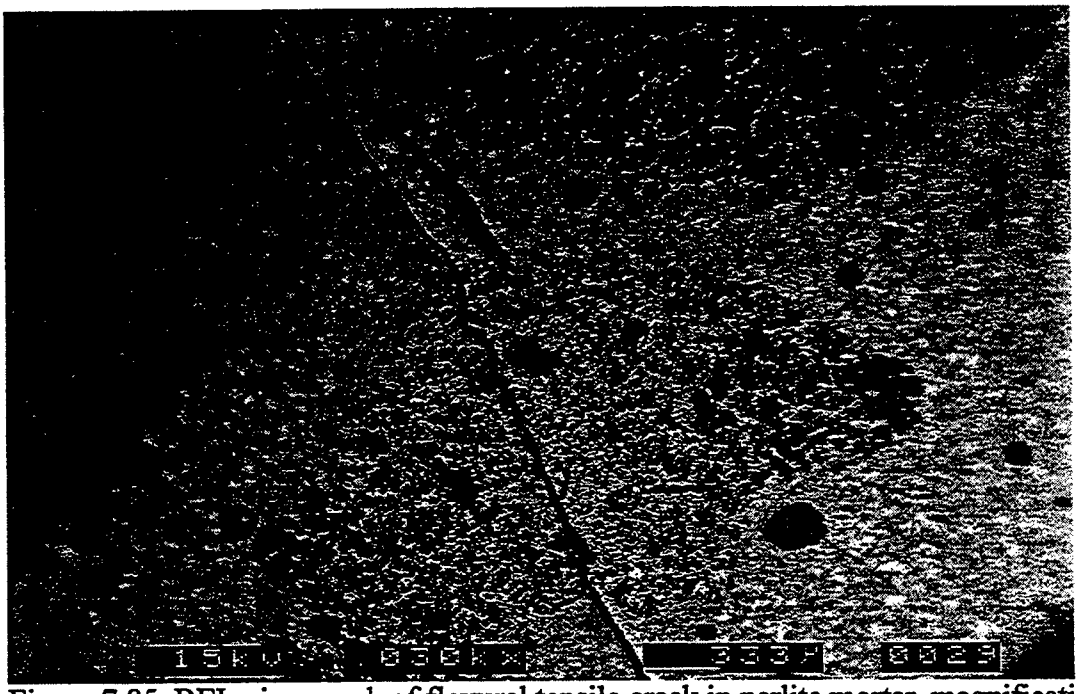

Figure 7.85 BEI micrograph of flexural tensile crack in perlite mortar, magnification 30×, mixture proportion 37_52_00, aggregate size #4~#8.

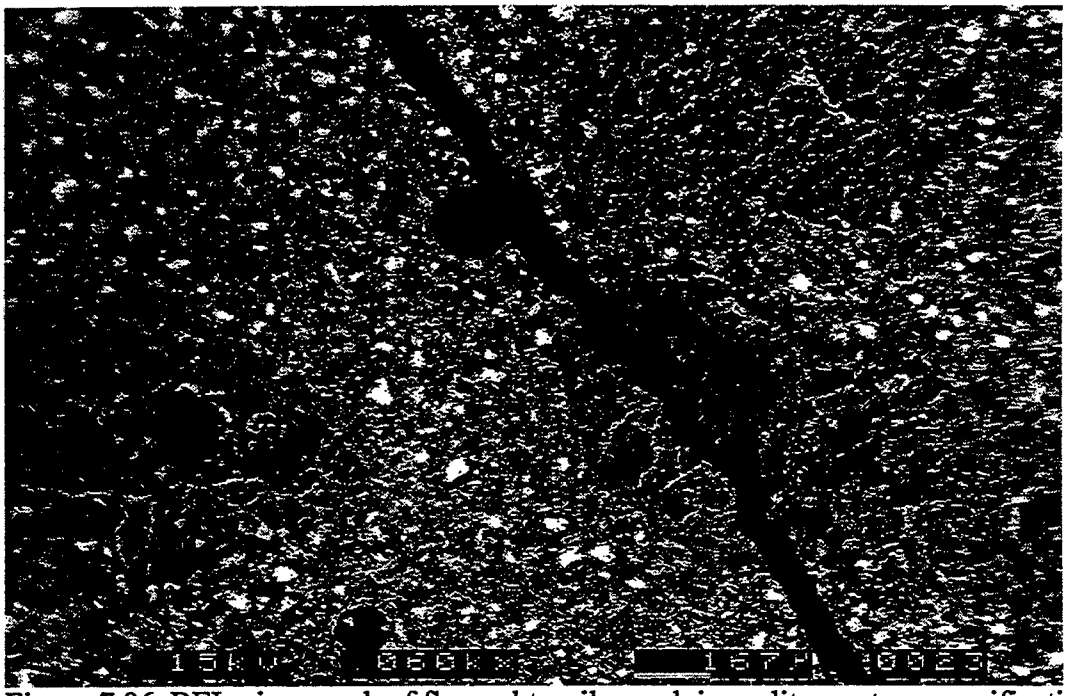

Figure 7.86 BEI micrograph of flexural tensile crack in perlite mortar, magnification 60×, mixture proportion 37_52_00, aggregate size #16~#30.

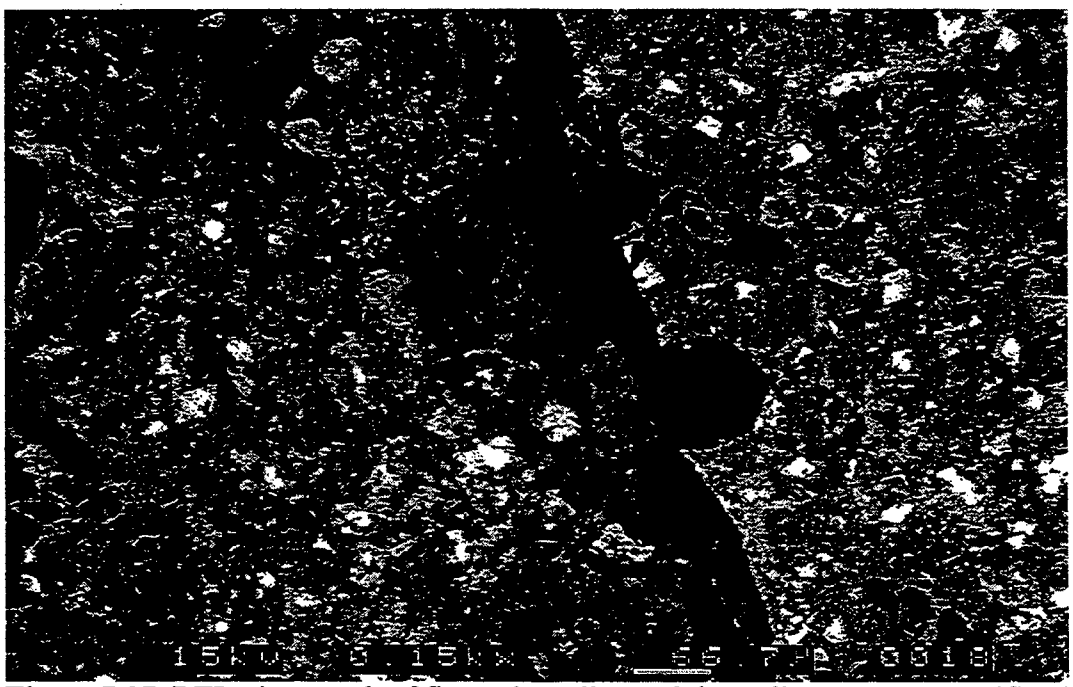

Figure 7.87 BEI micrograph of flexural tensile crack in perlite mortar, magnification 150×, mixture proportion 37_52_00, aggregate size #50~#100.

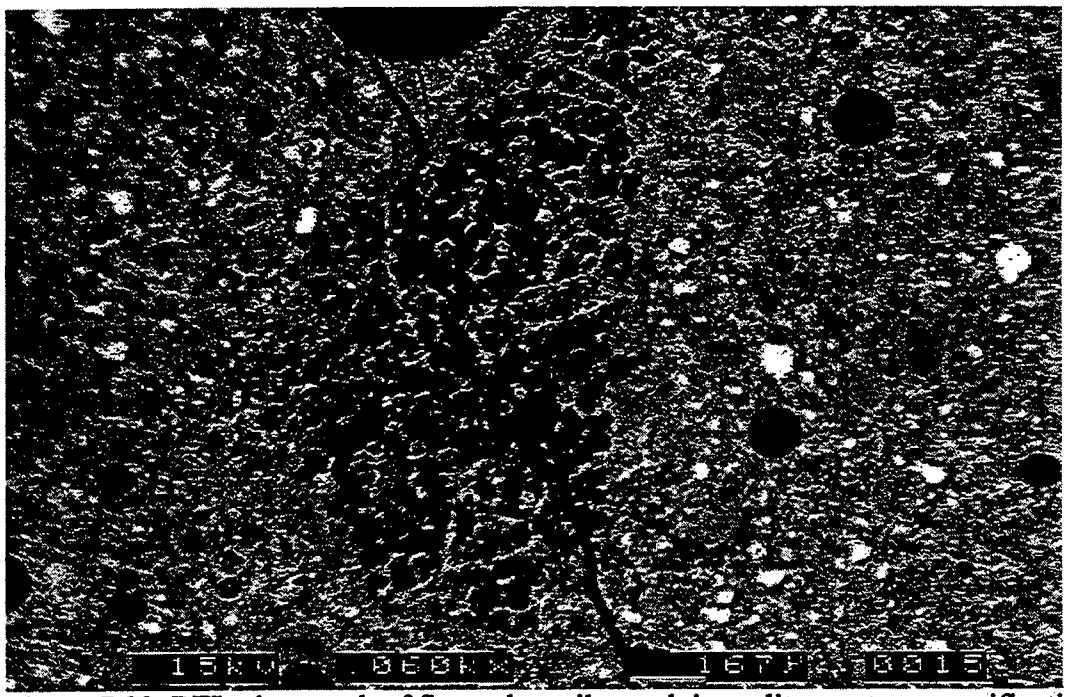

Figure 7.88 BEI micrograph of flexural tensile crack in perlite mortar, magnification 60×, mixture proportion 37_52_10, aggregate size #4~#8.

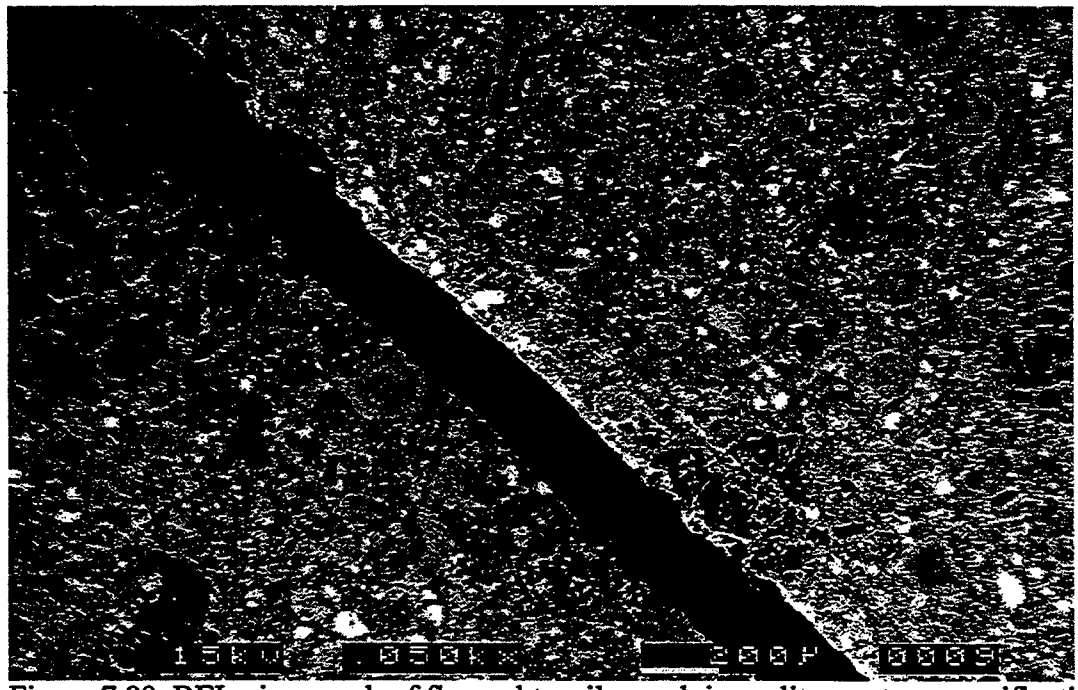

Figure 7.89 BEI micrograph of flexural tensile crack in perlite mortar, magnification 50×, mixture proportion 37_52_10, aggregate size #16~#30.

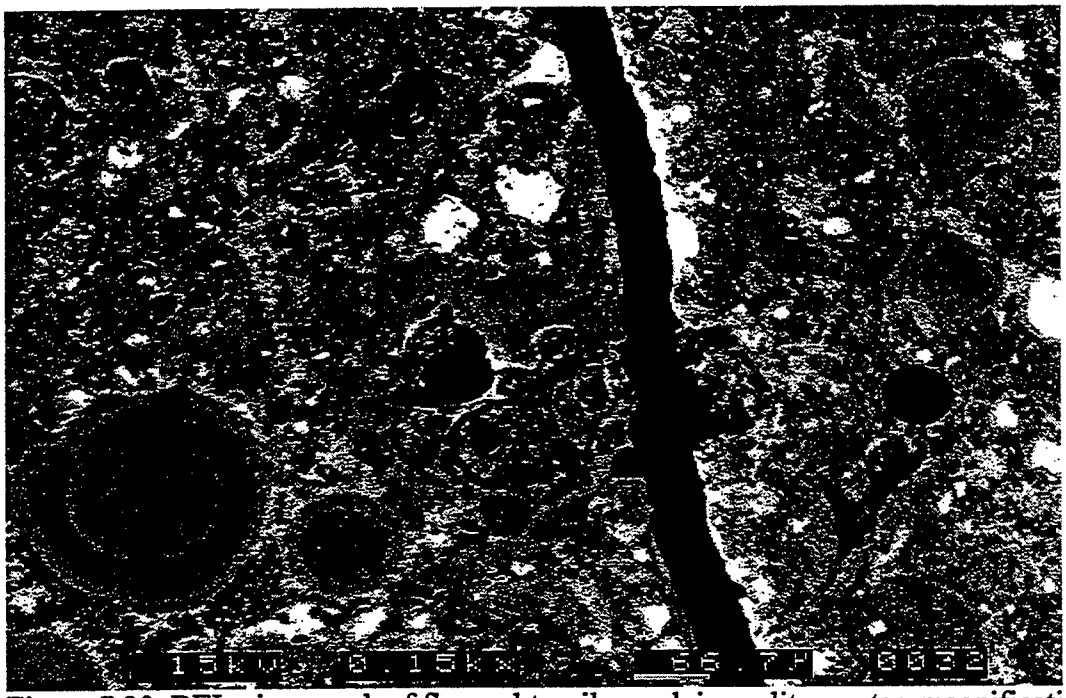

Figure 7.90 BEI micrograph of flexural tensile crack in perlite mortar, magnification 150×, mixture proportion 37_52_10, aggregate size #50~#100.

of aggregate particle included, which may be due to the perlite aggregate particle being much weaker than bulk paste or the transition zone.

7.6 Logarithmic Decrement of Damping of the Transition Zone

Figure 7.91 presents the relationship between logarithmic decrement damping in flexural mode and a SA for 28 days old dolomite mortars having mixture proportions of 40_35_00, 40_42_00, 40_50_00, 40_35_07, 40_42_07, and 40_50_07 respectively. Figure 7.92 presents the relationship between logarithmic decrement of damping in longitudinal mode and a SA for the same mortars as shown in Figure 7.91. Figure 7.93 presents the relationship between the logarithmic decrement of damping in torsional mode and the SA for the same mortars used in Figure 7.91. The data show that the logarithmic decrement of damping of mortars in flexural, longitudinal, and torsional mode becomes stable after seven days and with values ranging from 0.04 to 0.06. These results are consistent with the experimental results reported previously by Swamy and Rigby [1971]. Their experiments used concrete and mortar of a different W/C, and tested wet and dry specimens at different ages. In this study, the damping in all three modes seemed to be quite independent of the changes in SA for dolomite mortars. This may indicate that in dolomite mortars the logarithmic decrement of damping of the transition zone in flexural, longitudinal, or torsional modes is not very different from that of bulk paste, and that it is also independent of the changes in W/C and Va.

Figure 7.94 presents the relationship between the logarithmic decrement of damping in flexural mode and the SA for dolomite mortars at 28 days, having mixture proportions of 25_42_00, 40_42_00, 55_42_00, 25_42_07, 40_42_07, and 55_42_07 respectively. Figure 7.95 presents the relationship between the logarithmic decrement of damping in longitudinal mode and the SA for the same mortars as used in Figure 7.94. Figure 7.96 presents the relationship between the logarithmic decrement of damping in torsional mode and SA for the same mortars used in Figure 7.94. It is observed that when 7% of portland cement weight is substituted by silica fume, it may not have an obvious effect on the damping property of transition zones. This conclusion is based on the comparison of the data of logarithmic decrement of damping between the mortar groups

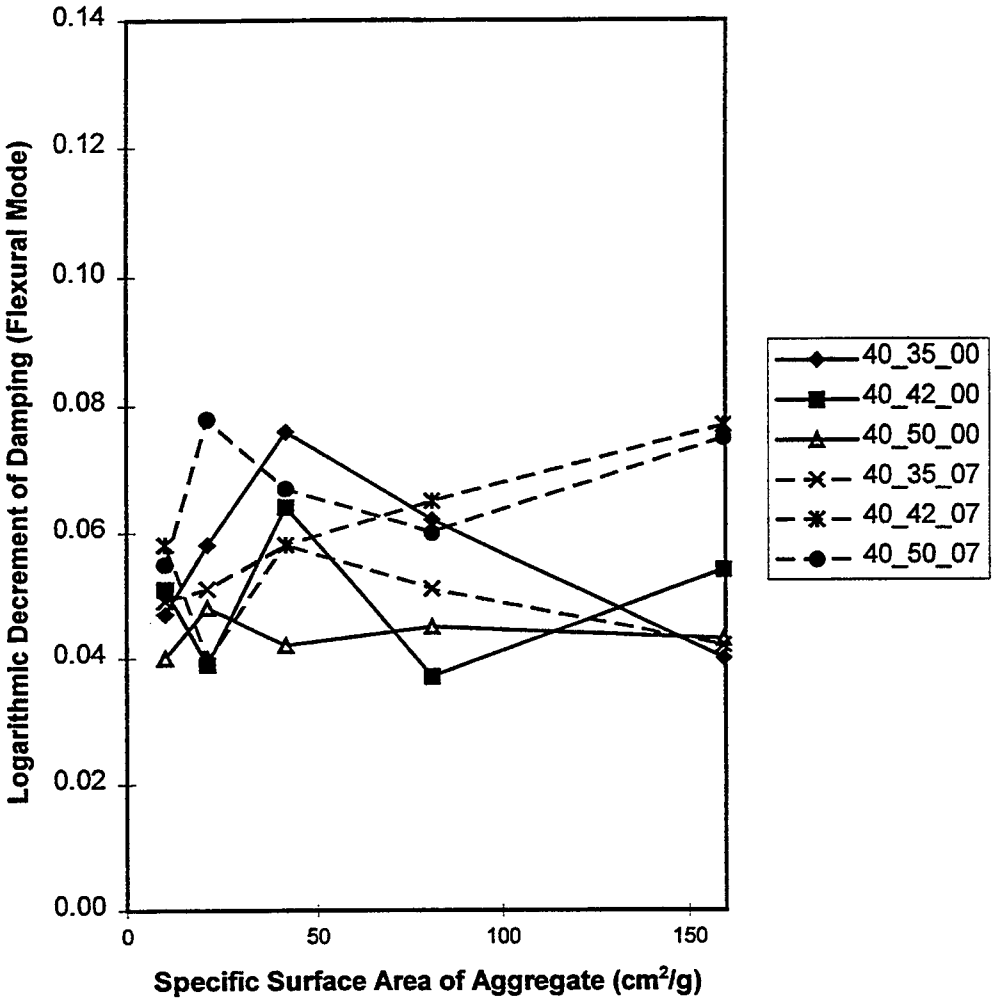

Figure 7.91 Logarithmic Decrement of Damping in Flexural Mode vs. SA for dolomite mortars at 28 days, and having mixture proportions of 40_35_00, 40_42_00, 40_50_00, 40_35_07, 40_42_07, and 40_50_07 respectively.

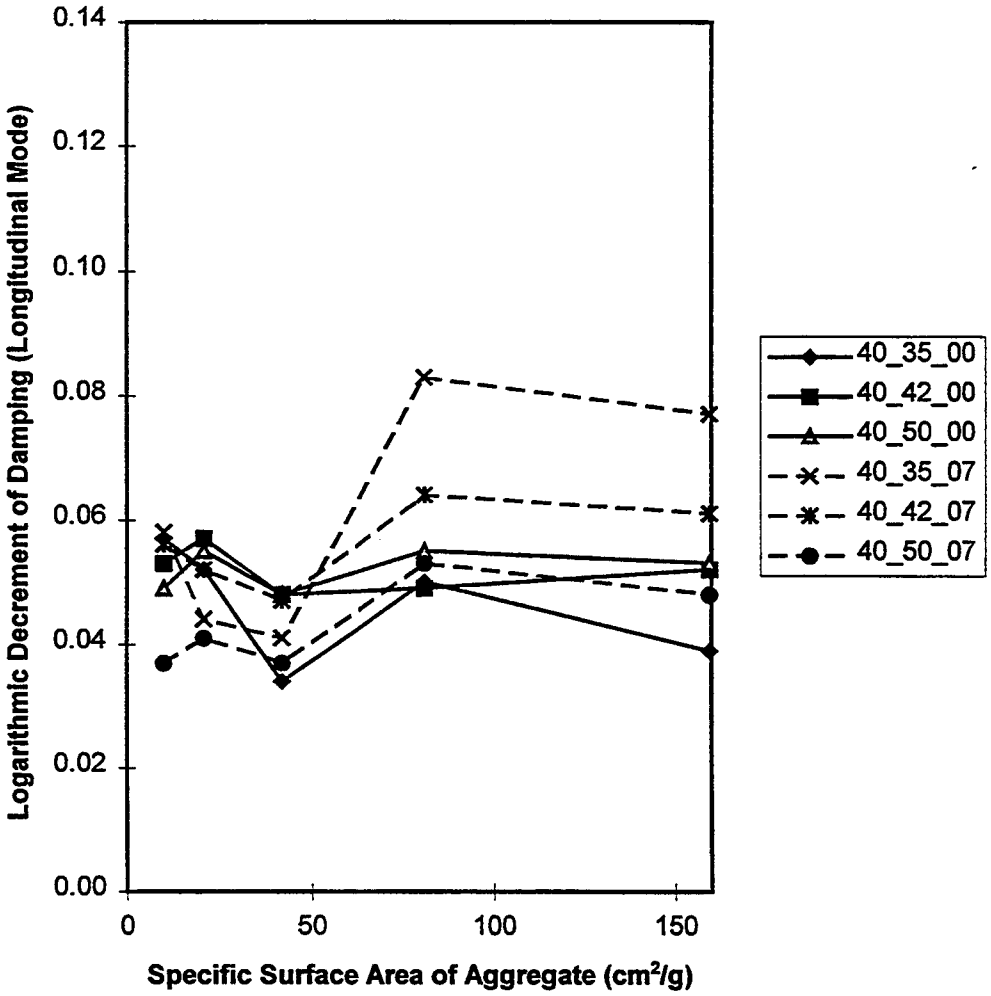

Figure 7.92 Logarithmic Decrement of Damping in Longitudinal Mode vs. SA for dolomite mortars at 28 days, and having mixture proportions of 40_35_00, 40_42_00, 40_50_00, 40_35_07, 40_42_07, and 40_50_07 respectively.

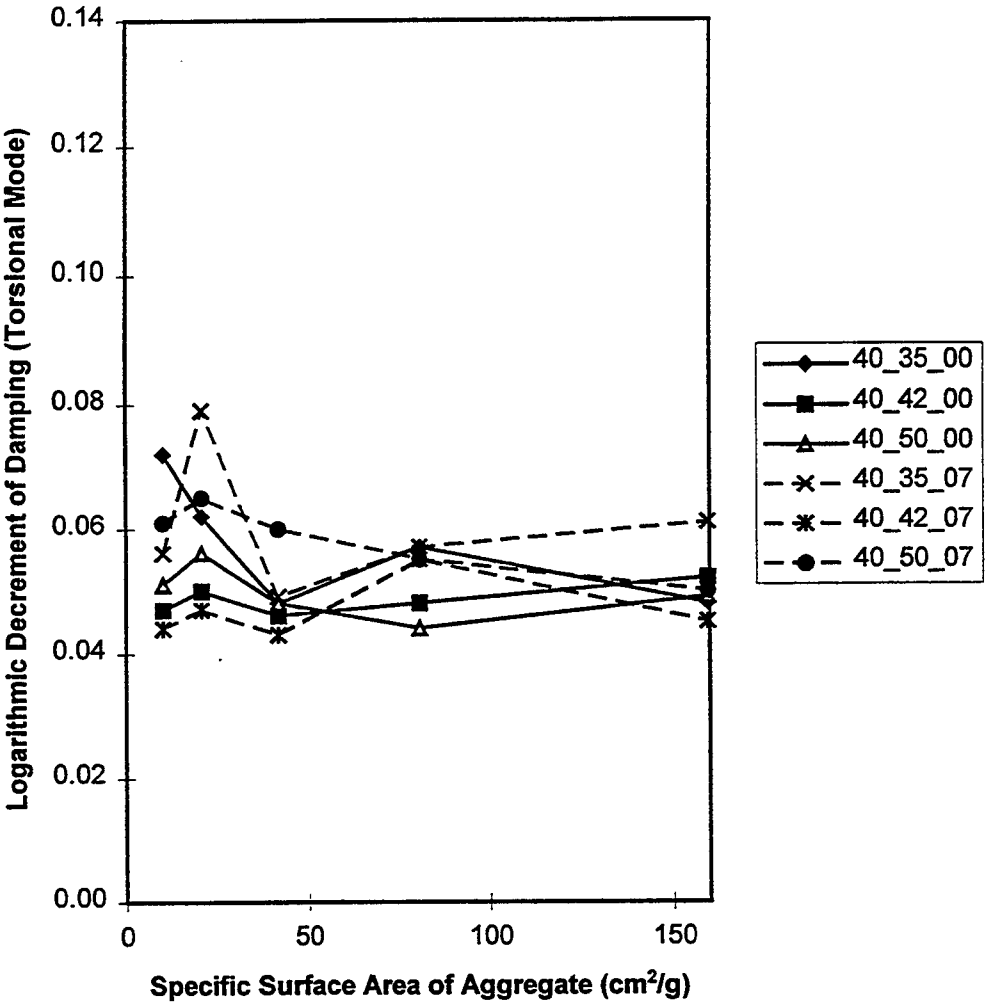

Figure 7.93 Logarithmic Decrement of Damping in Torsional Mode vs. SA for dolomite mortars at 28 days, and having mixture proportions of 40_35_00, 40_42_00, 40_50_00, 40_35_07, 40_42_07, and 40_50_07 respectively.

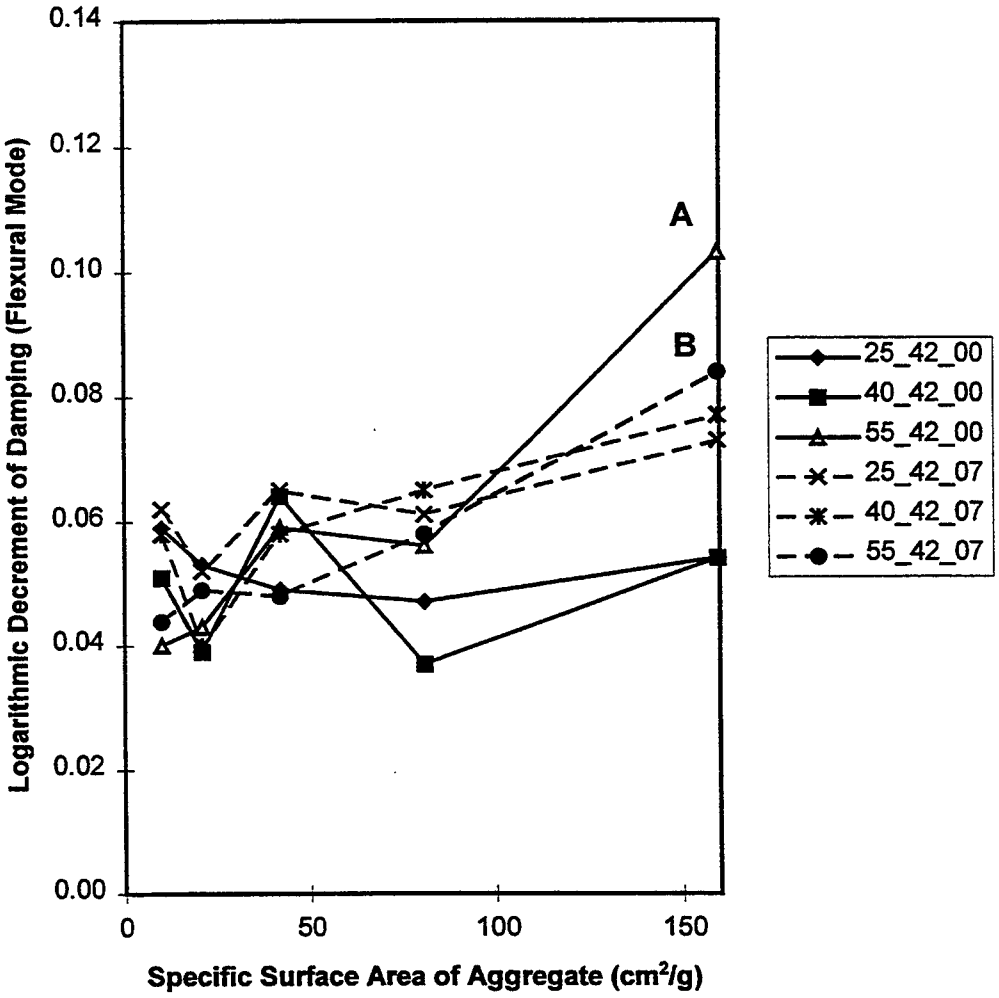

Figure 7.94 Logarithmic Decrement of Damping in Flexural Mode vs. SA for dolomite mortars at 28 days, and having mixture proportions of 25_42_00, 40_42_00, 55_42_00, 25_42_07, 40_42_07, and 55_42_07 respectively.

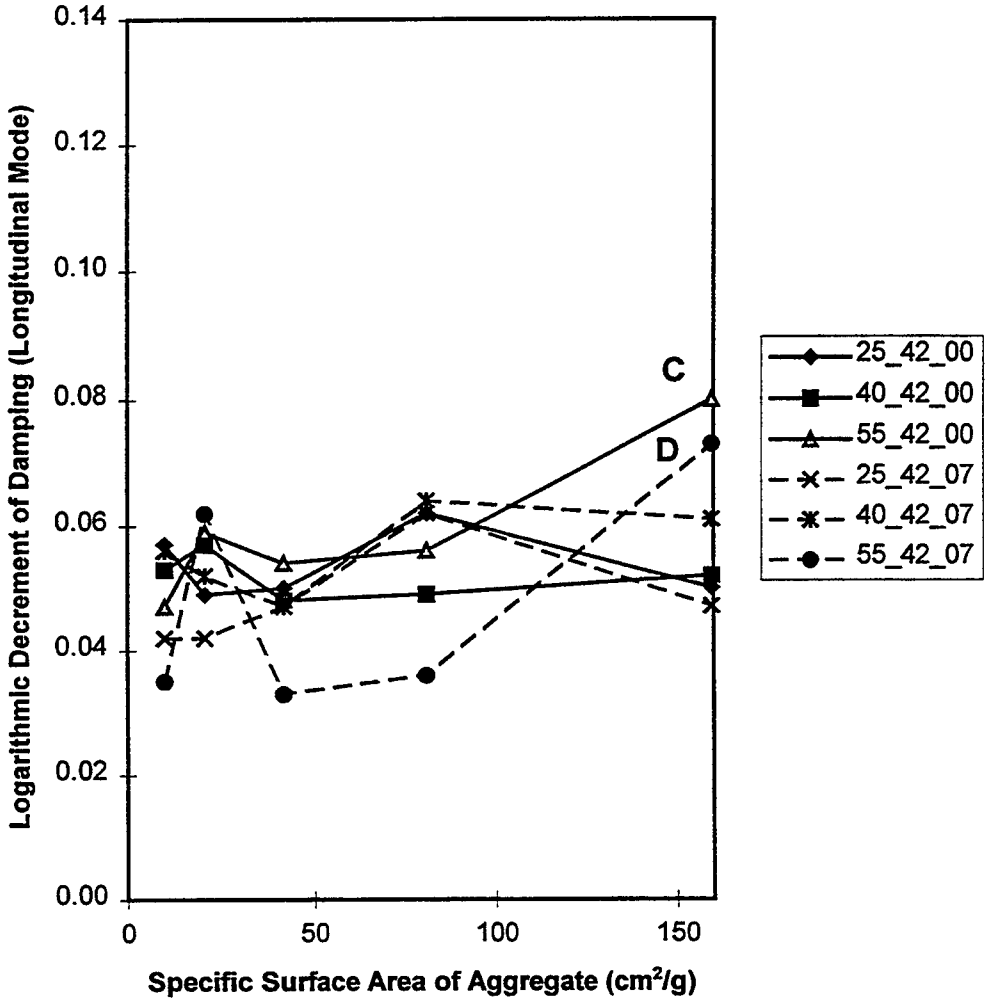

Figure 7.95 Logarithmic Decrement of Damping in Longitudinal Mode vs. SA for dolomite mortars at 28 days, and having mixture proportions of 25_42_00, 40_42_00, 55_42_00, 25_42_07, 40_42_07, and 55_42_07 respectively.

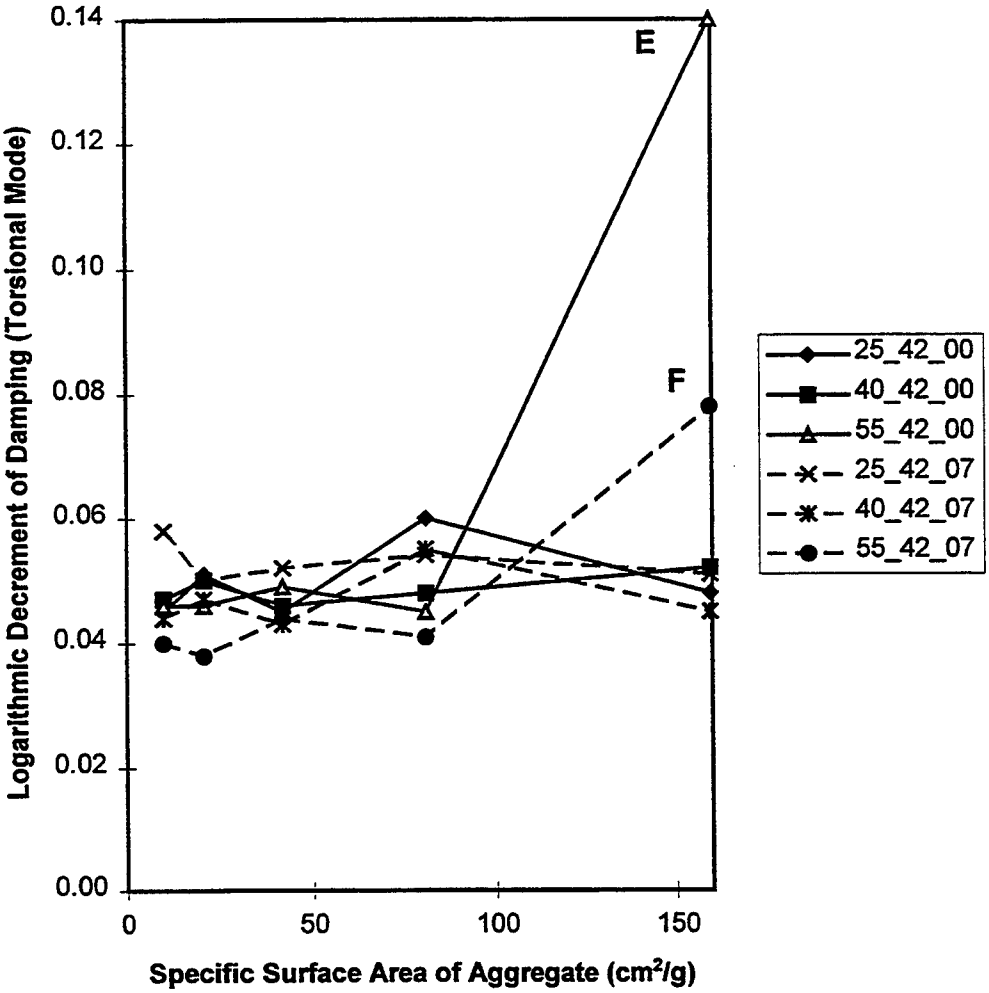

Figure 7.96 Logarithmic Decrement of Damping in Torsional Mode vs. SA for dolomite mortars at 28 days, and having mixture proportions of 25_42_00, 40_42_00, 55_42_00, 25_42_07, 40_42_07, and 55_42_07 respectively.

in each pair such, as 40_35_00 and 40_35_07, 40_42_00 and 40_42_07, 40_50_00 and 40_50_07, 25_42_00 and 25_42_07, and 55_42_00 and 55_42_07 in Figures 7.91~7.96.

In summary, owing to the fact that the logarithmic decrement of damping is inert to the variations of all of the factors, such as W/C, Va, silica fume content, concrete/mortar, and wet/dry, it may indicate that the logarithmic decrement of damping for aggregate, bulk paste, and the transition zone in flexural, longitudinal, and torsional modes remains in the range between 0.04 and 0.06 for concrete and mortar older than seven days, with and without silica fume.

However, there is an exception. For mortar made of a harsh mixture, the logarithmic decrement of damping in flexural, longitudinal, and torsional modes is high when a high gross porosity is measured in the mortar. This is concluded by observing the six points marked by A, B, C, D, E, and F in Figures 7.94~7.96. The data of these six points are determined from testing the mortars having mixture proportions of 55_42_00 and 55_42_07. As discussed in Chapter 6.4, these two groups of mixtures have mixing and compaction problems. This may suggest an explanation for the high values of logarithmic decrement of damping obtained.

CHAPTER 8

SUMMARY, FINDING, AND CONCLUSIONS

It appears that after Ishai [1961] reported that compaction problems may occur in the mortar if Va equals or exceeds 0.52, no further research in this direction has been conducted. The present study addressed the issue of mixing and compaction problems that occur in mortar and suggests that the controlling factor for the mixing and compaction problems is water quantity, not the Va. Consequently, based on the thickness of the virtual water film surrounding aggregate particles, a criterion has been established for predicting whether the mixing and compaction problems could occur in mortar. This is a new field to be explored and only minimal work has been done so far. However, this is an important area to explore because of a recent tendency to use a lower W/C for concrete in order to gain higher strength.

In accordance with the mixture proportioning, the water film criterion developed in this study may be used to predict whether or not mixing and compaction problems will occur in mortar. Moreover, an optimal water content for a mixture to gain its highest possible strength may be attainable from this criterion. It also may help in sifting out abnormal experimental data, i.e., the data that is influenced by the mixing and compaction problems, rather than the effect of transition zones, which is important in this study because it avoids the potential mistake in analyzing the experimental data.

Since Hashin-Shtrikman [1963] published their theory of bounds, almost all of the further studies have applied their bounds based on two phases. No work based on three phases was found by the author, which may be due to the mathematical complexity of applying three or more phases to Hashin-Shtrikman bounds. This study tried to adopt

three-phase Hashin-Shtrikman bounds and applied the experimental data of this study to test and verify the validation of three-phase Hashin-Shtrikman bounds for mortar.

A modification to the theoretical three-phase Hashin-Shtrikman bounds attempts to correlate Hashin-Shtrikman bounds to an experimental result, namely, the relationship between dynamic modulus of elasticity and SA in the mortar. This relationship was originally introduced by Cohen et al. [1994] in their researches on the dynamic modulus of elasticity of transition zones. The results of this theoretical study seem reasonable and were helpful in interpreting the experimental data of dynamic moduli in this study.

The volume of voids detected by MIP increases with the increasing volume of transition zones. This may be due to the fact that many agglomerated pores exist and surround aggregate particles, which seems to be observed by SEM. However, this phenomenon does not happen uniformly in mortar. One of the conclusions of this study suggests that the information supplied by MIP may not truly reflect the real quantity of voids in the mortar, which may be due to the aggregate particles probably playing a role in interrupting the path of intruding mercury.. However, this inference needs to be confirmed with more advanced apparatus and experimental techniques as discussed in Chapter 7.2.1.

The dynamic moduli of transition zones may be close to those of bulk paste, as found in dolomite mortar and perlite mortar. However, in quartzite mortar, the dynamic moduli of transition zones may be less than those of bulk paste. Silica fume may reduce the dynamic moduli of bulk paste and may have the same effect on transition zones in dolomite mortar. In quartzite mortar, silica fume may more effectively modify the transition zones so that they have dynamic moduli similar to bulk paste. For perlite mortar, silica fume seems to have no (or minor) effect on the dynamic moduli of both bulk paste and the transition zones. This may be due to the fact that the transition zone of perlite mortar is not obvious.

In this study, excluding calcium hydroxide detected in the transition zone, the chemical composition of the EDS result found no difference between bulk paste and the transition zones in any one of dolomite, quartzite, or perlite mortar.

W/C and Va do not alter the trend in dynamic moduli with a varying SA for dolomite and perlite mortars. This may indicate that W/C has the same effect on bulk paste and the transition zone, and that Va does not influence either bulk paste or the transition zone.

Percolation may have an important influence on the durability property of cementitious material. However, it does not show any apparent influence on dolomite mortar and perlite mortar in dynamic moduli, tensile strength, and compressive strength. The transition zones in dolomite mortar may be as strong as the bulk paste. This inference is based on the experimental results discussed in Chapter 7.5. With percolation of transition zones in mortar and despite the stress concentration that occurred in transition zones, the overall tensile strength of mortar associated with the intergranular tensile crack is not reduced.

The variables of logarithmic decrement of damping of transition zones in flexural, longitudinal, and torsional modes are quite inert to the variation of W/C, Va, and silica fume content. All of the measured variables of logarithmic decrement of damping for the mature mortar specimens are in a range of 0.04 to 0.06. This may also indicate that the values of logarithmic decrement of damping of transition zones in flexural, longitudinal, and torsional modes are similar to those of other constituents, all being in the range of 0.04 to 0.06.

As a whole, the mechanical properties of transition zones do not appear to be very different from those of bulk paste except in the quartzite mortar, which may be due to the specimens used for studying being quite young, less than two months old, and that they are cured and protected well. Thus, they do not have a durability problem. The durability problem of cementitious material usually starts from the deterioration of transition zones, especially the dissolution of calcium hydroxide in transition zones. Therefore, for old and deteriorated cementitious material, the difference in mechanical properties between transition zones and bulk paste may be more significant.

CHAPTER 9

RECOMMENDATIONS

It is useful to establish a more advanced criterion for detecting mixing and compaction problems because such a criterion may potentially be used to optimize mixture proportion. For high-strength concrete, some mixture proportions are proposed by using low W/C and adding silica fume and superplasticizer. Thus, a further investigation may include studying the influence on the criterion by varying the quantity of W/C, silica fume content, and superplasticizer.. A form of the advanced criterion may be primarily proposed as

$$M_{H_2O} = \frac{1}{f_3(SP)}[f_1(SA) + f_2(\frac{W}{C+SF})] \tag{9.1}$$

where M_{H_2O} is the optimal water content in per unit volume of mixture,

f_1, f_2, and f_3 are three functions,

SA is the specific surface area of aggregate by volume,

W/(C+SF) is the mass ratio of water to cement and silica fume, and

SP is the quantity of superplasticizer based on *(C+SF)*.

The concept behind Equation (9.1) may be explained as follows. By holding water on the surface, aggregate particles are competing with cement grains and silica fume particles for water. Thus, three functions are considered on the right hand side of Equation (9.1). One is $f_1(SA)$, which is related to the water held on aggregate surface; another is $f_2(W/(C+SF))$, which is related to the water for hydration of binders; and the last one is $f_3(SP)$. Because superplasticizer may have influence on the two functions $f_1(SA)$ and $f_2(W/(C+SF))$, function $f_3(SP)$ is therefore outside the brackets. If the water

added to mixture is reduced, the W/C of the paste is decreased. Thus, the moduli, strengths, and density of the mixture will increase. However, if the water is reduced below a certain level, the mixing and compaction problems begin to surface, as discussed in Chapter 5. These problems will lower the moduli, strengths, and density of the mixture. Therefore, by varying the water content, these two opposite effects will compete within the mixture. This indicates that in the theory an optimal water content can be found for a mixture to gain its highest moduli, strengths, and density, thus, leading to an optimal design for mixture proportion.

The proposed 3-D Hashin-Shtrikman bounds must be tested on more three-phase composite material in order to increase its credibility for application.

The transition zone in dolomite mortar may have higher elastic moduli than that in quartzite mortar. Therefore, if higher stiffness and rigidity are needed, dolomite aggregate may be the better choice than quartzite aggregate for the mixtures. However, other factors such as strength, durability, and stress concentration may also need to be considered. In particular, the intensity of stress concentration may be dependent on the shape of aggregate particles and the relative stiffness and rigidity between the aggregate and the transition zones. The transition zone in perlite mortar is not obvious, which may be due to perlite aggregate's inability to absorb large quantities of water. This mechanism may offer a way to study how to reduce or even eliminate the quantity of transition zones. However, the stress concentration phenomenon can only be decreased by raising the stiffness and rigidity of transition zones to the same level as those of the aggregate.

The results of this study indicate that the mechanical properties of transition zones in a young dolomite mortar may be similar to those of bulk paste. However, in old or deteriorated cementitious material, the mechanical properties of transition zones might be different from those of bulk paste. Thus, the direction of further investigation may be the study of old or deteriorated concrete or mortar. The role and significance of transition zones and the underlying mechanisms in the overall mechanical behavior of old concrete or mortar could then be further understood.

In this study, the tensile and compressive strengths of transition zones were experimentally studied by intentionally designing a percolation mechanism in the specimen and comparing the test result with the one without a percolation mechanism. The information supplied by this technique is quite limited because the result can only be qualitatively described in terms of whether or not the transition zone is stronger than bulk paste. Perhaps, with the aid of theoretical models, a study on the strengths of transition zones can be more detailed and clear.

BIBLIOGRAPHY

BIBLIOGRAPHY

1. Alexander M.G., and Milne T.I., *Influence of Cement Blend and Aggregate Type on Stress-Strain behavior and Elastic Modulus of Concrete*, ACI Materials Journal, Vol. 92, No. 3, pp. 227-235, May-June, 1995.

2. Babu K.G., and Prakash P.V.S., *Efficiency of Silica Fume in Concrete*, Cement and Concrete Research, Vol. 25, No. 6, pp. 1273-1283, 1995.

3. Bache H.H., and Nepper-Christensen P., *Observations on Strength and Fracture in Lightweight and Ordinary Concrete, The Structure of Concrete and its Behaviour under Load*, Proceedings of International Conference, London, Sep., 1965.

4. Barnes B.D., Diamond S., and Dolch W.L., *The Contact Zone Between Portland Cement Paste and Glass Aggregate Surfaces*, Cement and Concrete Research, Vol. 8, pp. 233-244, 1978(1).

5. Barnes B.D., Diamond S., and Dolch W.L., *Hollow Shell Hydration of Cement Particles in Bulk Cement Paste*, Cement and Concrete Research, Vol. 8, pp. 263-272, 1978(2).

6. Barnes B.D., Diamond S., and Dolch W.L., *Micromorphology of the Interfacial Zone Around Aggregates in Portland Cement Mortar*, Journal of the American Ceramic Society, Vol. 62, No.1-2, pp. 21-24, 1979.

7. Bentur A., and Cohen M.D., *Effect of Condensed Silica Fume on the Microstructure of the Interfacial Zone in Portland Cement Mortars*, Journal of the American Ceramic Society, Vol. 70, No. 10, pp. 738-743, 1987.

8. Bentur A., Goldman A., and Cohen M.D., *The Contribution of the Transition Zone to the Strength of High Quality Silica Fume Concrete*, Materials Research Society, Symposium, Proceedings. Vol. 114, pp. 97-103, 1988.

9. Bentz D.P. and Garboczi E.J., *Percolation of Phases in a Three-Dimensional Cement Paste Microstructural Model*, Cement and Concrete Research, Vol. 21, pp. 325-344, 1991.

10. Bourdette B., Ringot E., and Ollivier J.P., *Modelling of the Transition Zone Porosity*, Cement and Concrete Research, Vol. 25, No. 4, pp. 741-751, 1995.

11. Charles-Gibergues A., Grandet J., and Ollivier J.P., *Contact Zone Between Cement Paste and Aggregate*, in Bond in Concrete, Ed. by Bartos P., Applied Science Publishers, p. 24, 1982.

12. Chen W.-F. and Zhao X.-H. *Influence of Interface layer on Mechanical Behavior of Concrete*, Report CE-STR-95-14, Purdue University, 1995.

12. Cohen L.J., and Ishai O., *The Elastic Properties of Three-Phase Composites*, Journal of Composite materials, Vol. 1, pp. 390-403, 1967.

13. Cohen M.D., Goldman A., and Chen W.-F., *The Role of Silica Fume in Mortar: Transition Zone versus Bulk Paste Modification*, Cement and Concrete Research, Vol. 24, pp. 95-98, 1994.

14. Cohen M.D., Lee T.-F., and Goldman A., *A Method for Estimating the Dynamic Moduli of Cement Paste-Aggregate Interfacial Zones in Mortar*, Materials Research Society, Symposium., Proceedings. Vol. 370, pp. 407-412, 1995.

15. Counto U.J., *The Effect of the Elastic Modulus of the Aggregate on the Elastic Modulus, Creep and Creep Recovery of Concrete*, Magazine of Concrete Research, Vol. 16, No. 48, pp. 129-138, Sep., 1964.

16. Garboczi E.J., Schwartz L.M., and Bentz D.P., *Modeling the Influence of the Interfacial Zone on the DC Electrical Conductivity of Mortar*, Advanced Cement Based Materials, Vol. 2, pp. 169-181, 1995.

17. Grandet J. and Ollivier J.P., *ETUDE DE LA FORMATION DU MONOCARBOALUMINATE DE CALCIUM HYDRATE AU CONTACT DUN GRANULAT CALCAIRE DANS UNE PATE DE CIMENT PORTLAND*, Cement and Concrete Research, Vol. 10, pp. 759-770, 1980. (in French)

18. Hadley D.W., *The Nature of the Paste-Aggregate Interface*, Ph.D. Dissertation, Purdue University, August 1972.

19. Hansen T.C., *Influence of Aggregate and Voids on Modulus of Elasticity of Concrete, Cement Mortar, and Cement Paste*, ACI Journal, Vol. 62, No. 2, pp. 193-215, Feb., 1965.

20. Hashin Z., *Thermoelastic Properties of Particulate Composites with Imperfect Interface*, Journal of the Mechanics and Physics of Solids, Vol. 39, No. 6, pp. 745-762, 1991.

21. Hashin Z., *Extremum Principles for Elastic Heterogeneous Media with Imperfect Interfaces and Their Application to Bounding of Effective Moduli*, Journal of the Mechanics and Physics of Solids, Vol. 40, No. 4, pp. 767-781, 1992.

22. Hashin Z., and Shtrikman S., *A Variational Approach to the Theory of the Elastic Behaviour of multiphase Materials*, Journal of the Mechanics and Physics of Solids, Vol. 11, pp. 127-140, 1963.

23. Hirsch T.J., *Modulus of Elasticity of Concrete Affected by Elastic Moduli of Cement Paste Matrix and Aggregate*, ACI Journal, Proceedings, Vol. 59, pp. 427-451, 1962.

24. Ishai O., *Influence of Sand Concentration on Deformations of Mortar Beams Under Low Stresses*, ACI Journal, pp. 611-622, Nov. 1961.

25. Karihaloo B.L., Carpinteri A., and Elices M., *Fracture Mechanics of Cement Mortar and Plain Concrete*, Advanced Cement Based Materials, Vol. 1, No. 2, pp. 92-105, Dec. 1993.

26. Katz A., and Bentur A., *Mechanical Properties and Pore Structure of Carbon Fiber reinforced cementitious Composites*, Cement and Concrete Research, Vol. 24, No. 2, pp. 214-220, 1994.

27. Kayyali O.A., *Mercury Intrusion Porosimetry of Concrete Aggregate*, Matériaux et Constructions, Vol. 18, N°106, pp. 259-262, 1985.

28. Kayyali O.A., *Porosity of Concrete in Relation to the Nature of the Paste-Aggregate Interface*, Materials and Structures, Vol. 20, pp. 19-26, 1987.

29. Khokhrin N.K., *The Durability of Lightweight Concrete Structural Members*, Kuibyshev, U.S.S.R. 1973.

30. Langton C.A., and Roy D.M., *Morphology and Microstructure of Cement Paste/Rock Interfacial Regions*, Seventh International Congress on the Chemistry of Cement, Paris, Vol. 3, VII, pp. 127-132, 1980.

31. Lindholm U.S., *Experimental Mechanics: New Challenges in Micromechanics*, Mechanics of Materials, Vol. 10, pp. 31-42, 1990.

32. Loudon A.G., *The Computation of Permeability from Simple Soil Test*, Geotechnique, Vol. III, pp. 165-183, 1952.

33. Lutz M.P., and Monteiro P.J.M., *Effect of the Transition Zone on the Bulk Modulus of Concrete*, MRS Symp., Proc. Vol. 370, pp. 413-418, 1995.

34. Lydon F.D., and Iacovou M., *Some Factors Affecting the Dynamic Modulus of Elasticity of High Strength Concrete*, Cement and Concrete Research, Vol. 25, No. 6, pp. 1246-1256, 1995.

35. Malhotra V.M., and Sivasundaram V., *Resonant Frequency Methods*, CRC Handbook on Nondestructive Testing of Concrete, edited by V. M. Malholtra and N. J. Carino, Chapter 6, CRC Press, 1991.

36. Maso J.C., *The Bond Between Aggregates and Hydrated Cement Paste*, Proceedings of the Seventh International Congress on the Chemistry of Cements, Editions Septima Vol. 1, VII-1/3-1/15, , Paris, 1980.

37. Mehta P.K., and Monteiro P.J.M., *Effect of Aggregate, Cement and Mineral Admixtures on the Microstructure of the Transition Zone*, Material Research Society, Symposium, Proceeding, Vol. 114, pp. 65-75, 1988.

38. Mehta P.K., and Monteiro P.J.M., *Concrete - Structure, Properties, and Materials*, 2nd ed., Prentice Hall, New Jersey, p. 18, 1993.

39. Monteiro P.J.M., and Andrade W.P., *Analysis of the Rock-Cement paste Bond Using Probabilistic Treatment of Brittle Strength*, Cement and Concrete Research, Vol. 17, pp. 919-926, 1987.

40. Monteiro P.J.M., Maso J.C., and Ollivier J.P., *The Aggregate Mortar Interface*, Cement and Concrete Research, Vol. 15, pp. 953-958, 1985.

41. Monteiro P.J.M., and Mehta P.K., *Ettringite Formation on the Aggregate-Cement Paste Interface*, Cement and Concrete Research, Vol. 15, pp. 378-380, 1985.

42. Monteiro P.J.M., and Mehta P.K., *Interaction Between Carbonate Rock and Cement Paste*, Cement and Concrete Research, Vol. 16, pp. 127-134, 1986 (1).

43. Monteiro P.J.M., and Mehta P.K., *Improvement of the Aggregate-Cement Paste Transition Zone by Grain Refinement of Hydration Products*, Proceedings of the eighth International Congress on the Chemistry of Cement, Rio Brasilia, Vol. 3, pp. 433-437, 1986 (2).

44. Mori T., and Tanaka K., *Average Stress in Matrix and Average Elastic Energy of Materials with Misfitting Inclusions*, Acta Metallurgica, Vol. 21, pp. 571-574, 1973.

45. Naik T.R., and Malhotra V.M., *The Ultrasonic Pulse Velocity Method*, CRC Handbook on Nondestructive Testing of Concrete, edited by V. M. Malholtra and N. J. Carino, Chapter 7, CRC Press, 1991.

46. Neville A.M., Properties of Concrete, 3rd ed., Longman Scientific & Technical, p. 564, 1993.

47. Olek J., Cohen M.D., and Lobo C., *Determination of Surface Area of Portland Cement and Silica Fume by Mercury Intrusion Porosimetry*, ACI Material Journal, pp. 473-478, Sep.-Oct. 1990.

48. Ollivier J. P., Maso J. C., and Bourdette B., *Interfacial Transition Zone in Concrete*, Review Article, Advanced Cement Based Materials, Vol. 2, pp. 30-38, 1995.

49. Ping X., and Beaudoin J.J, *Effects of Transition Zone Microstructure on Bond Strength of Aggregate-Portland Cement Paste Interfaces*, Cement and Concrete Research, Vol. 22, pp. 23-26, 1992.

50. Ping X., Beaudoin J.J., and Brousseau R., *Effect of Aggregate Size on Transition Zone Properties at the Portland Cement Paste Interface*, Cement and Concrete Research, Vol. 21, pp. 999-1005, 1991.

51. Popovic S., and Erdey M., *Estimation of the Modulus of Elasticity of Concrete-like Composite Materials*, Matériaux et Constructions, Materials and Structures, Research and Testing (RILEM, Paris), Vol. 3, N° 16, pp. 253-260, 1970.

52. Reuss A., *Berechnung der Fliessgrenze von Mischkristallen auf Grund der Plastizitatsbedingung für Einkristalle*, Zeitschrift für angewandte Mathematik und Mechanik, Vol. 2, pp. 49-58, 1929.

53. Scrivener K.L., Crumbie A.K., and Pratt P.L., *A Study of the Interfacial Region Between cement Paste and Aggregate in Concrete*, Materials Research Society, Symposium, Proceeding, Vol. 114, pp. 87-88, 1988.

54. Scrivener K.L., and Gartner E.M., *Microstructural Gradients in Cement Paste Around Aggregate Particles*, Materials Research Society, Symposium, Proceedings, Vol. 114, pp. 77-85, 1988.

55. Scrivener K.L. and Nemati K.M., *The Percolation of Pore Space in the Cement Paste/Aggregate Interfacial Zone of Concrete*, Cement and Concrete Research, Vol. 26, No. 1, pp. 35-40, 1996.

56. Simeonov P.I., and Ahmad S.H., *Interface Transition Zone and the Elastic Modulus of Cement-Based Composites*, Materials Research Society, Symposium, Proceeding, Vol. 370, pp. 397-406, 1995.

57. Spinner S., and Tefft W.E., *A Method for Determining Mechanical Resonance Frequencies and for Calculating Elastic Moduli from These Frequencies*, Proceedings of ASTM, Vol. 61, pp. 1221-1238, 1961.

58. Struble L., Skalny J., and Mindess S., *A Review of the Cement-Aggregate Bond*, Cement and Concrete Research, Vol. 10, pp. 277-286, 1980.

59. Swamy N., and Rigby G., *Dynamic Properties of Hardened Paste, Mortar, and Concrete*, Matériaux et Constructions, Vol. 4, N° 19, pp. 13-40, 1971.

60. Tamimi A.K., *The Effects of a New Mixing Technique on the Properties of the Cement Paste-Aggregate Interface*, Cement and Concrete Research, Vol. 24, No. 7, pp. 1299-1304, 1994.

61. Vervuurt A., and Van Mier J.G.M., *Optical Microscopy and Digital Image Analysis of Bond-Cracks in Cement Based Materials*, Materials Research Society, Symposium, Proceedings, Vol. 370, pp. 337-345, 1995.

62. Voigt W., Lehrbuch der Kristallphysik, Teubner, Leipzig, pp. 962, 1928.

63. Wakeley L.D., and Roy D.M., *A Method for Testing the Permeability Between Grout and Rock*, Cement and Concrete Research, Vol. 12, pp. 533-534, 1982.

64. Wasserman R., and Bentur A., *Interfacial Interactions in Lightweight Aggregate Concretes and their Influence on the Concrete Strength*, Cement and Concrete Composites, Vol. 18, pp. 67-76, 1996.

65. Winslow D.N., Cohen M.D., Bentz D.P., Snyder K.A., and Garboczi E.J., *Percolation of Interfacial Zone Pores in Cement Mortar and Concrete*, Cement and Concrete Research, Vol. 24, No. 1, pp. 25-37, 1994.

66. Winslow D.N. and Liu D., *The Pore Structure of Paste in Concrete*, Cement and Concrete Research, Vol. 20, No. 2, pp. 227-235, 1990.

67. Yamaguchi E., and Chen W.-F., *'Post-Failure Behavior of Concrete materials in Compression'*, Engineering Fracture mechanics, Vol. 37, No. 5, pp. 1011-1023, 1990.

68. Yamaguchi E., and Chen W.-F., *'Microcrack Propagation Study of Concrete Under Compression'*, Journal of Engineering Mechanics, Vol. 117, No. 3, pp. 653-673, March 1991.

69. Yuan C.Z. and Odler I., *The Interfacial Zone Between Marble and Tricalcium Silicate Paste*, Cement and Concrete Research, Vol. 17, pp. 784-792, 1987.

70. Zampini D., Jennings H.M., and Shah S.P., *The Interfacial Transition Zone and Its Influence on the Fracture Behavior of Concrete*, Material Research Society, Symposium, Proceeding, Vol. 370, pp. 357-366, 1995.

71. Zhao X.-H. and Chen W.-F., *Stress Analysis of a Sand Particle with Interface in Cement Paste Under Uniaxial Loading*, Report CE-STR-94-23, Purdue University, Sep. 1994.

72. Zimbelmann R., *A Contribution to the Problem of Cement-Aggregate Bond*, Cement and Concrete Research, Vol. 15, pp. 801-808, 1985.

APPENDICES

APPENDIX A

The Proof of Positive Values of Variables; R, S, P, Q, V, W, T, and U in Equations (6.23) ~ (6.30), if $K_3 > K_2 > K_1$ and $G_3 > G_2 > G_1$.

1. R

$= v_1(K_3 - K_1)(3K_3 + 4G_3)^2 + (1 - v_1 - v_3)(K_3 - K_2)(3K_3 + 4G_3)^2 - 3(1 - v_3)(K_3 - K_1)(K_3 - K_2)(3K_3 + 4G_3)$

$= (3K_3 + 4G_3)[v_1(K_3 - K_1)(3K_2 + 4G_3) + v_2(K_3 - K_2)(3K_1 + 4G_3)]$

> 0 if $K_3 > K_1$ and $K_3 > K_2$.

2. S

$= (3K_3 + 4G_3)^2 - 3(1 - v_1)(K_3 - K_1)(3K_3 + 4G_3) - 3(v_1 + v_3)(K_3 - K_2)(3K_3 + 4G_3) + 9v_3(K_3 - K_1)(K_3 - K_2)$

$= (3K_1 + 4G_3)(3K_2 + 4G_3) + 3v_2(K_3 - K_2)(3K_1 + 4G_3) + 3v_1(K_3 - K_1)(3K_2 + 4G_3)$

> 0 if $K_3 > K_1$ and $K_3 > K_2$.

3. P

$= v_3(K_3 - K_1)(3K_1 + 4G_1)^2 + (1 - v_1 - v_3)(K_2 - K_1)(3K_1 + 4G_1)^2 + 3(1 - v_1)(K_3 - K_1)(K_2 - K_1)(3K_1 + 4G_1)$

> 0 if $K_3 > K_1$ and $K_2 > K_1$.

4. Q

$= (3K_1 + 4G_1)^2 + 3(1 - v_3)(K_3 - K_1)(3K_1 + 4G_1) + 3(v_1 + v_3)(K_2 - K_1)(3K_1 + 4G_1) + 9v_1(K_3 - K_1)(K_2 - K_1)$

> 0 if $K_3 > K_1$ and $K_2 > K_1$.

5. V

$= 25v_1G_3^2(G_3 - G_1)(3K_3 + 4G_3)^2 + 25(1 - v_1 - v_3)G_3^2(G_3 - G_2)(3K_3 + 4G_3)^2 - 30(1 - v_3)G_3(G_3 - G_1)(G_3 - G_2)(3K_3 + 4G_3)(K_3 + 2G_3)$

$= 5G_3(3K_3 + 4G_3)\{5v_1G_3(3K_3 + 4G_3)(G_2 - G_1) + (1 - v_3)(G_3 - G_2)[G_3(9K_3 + 8G_3) + 6G_1(K_3 + 2G_3)]\}$

> 0 if $G_3 > G_2$ and $G_2 > G_1$.

6. W

$= 25G_3^2(3K_3 + 4G_3)^2 - 30(1 - v_1)G_3(G_3 - G_1)(3K_3 + 4G_3)(K_3 + 2G_3) - 30(v_1 + v_3)G_3(G_3 - G_2)$
$(3K_3 + 4G_3)(K_3 + 2G_3) + 36v_3(G_3 - G_1)(G_3 - G_2)(K_3 + 2G_3)^2$
$= [G_3(9K_3 + 8G_3) + 6G_1(K_3 + 2G_3)] \times [G_3(9K_3 + 8G_3) + 6G_2(K_3 + 2G_3)] + 6v_1(G_3 - G_1)(K_3 + 2G_3)$
$[G_3(9K_3 + 8G_3) + 6G_2(K_3 + 2G_3)] + 6v_2(G_3 - G_2)(K_3 + 2G_3)[G_3(9K_3 + 8G_3) + 6G_1(K_3 + 2G_3)]$
> 0 if $G_3 > G_2$ and $G_3 > G_1$.

7. T

$= 25v_3G_1^2(G_3 - G_1)(3K_1 + 4G_1)^2 + 25(1 - v_1 - v_3)G_1^2(G_2 - G_1)(3K_1 + 4G_1)^2 + 30(1 - v_1)G_1(G_2 - G_1)$
$(G_3 - G_1)(3K_1 + 4G_1)(K_1 + 2G_1)$
> 0 if $G_3 > G_1$ and $G_2 > G_1$.

8. U

$= 25G_1^2(3K_1 + 4G_1)^2 + 30(v_1 + v_3)G_1(G_2 - G_1)(3K_1 + 4G_1)(K_1 + 2G_1) + 30(1 - v_3)G_1(G_3 - G_1)$
$(3K_1 + 4G_1)(K_1 + 2G_1) + 36v_1(G_2 - G_1)(G_3 - G_1)(K_1 + 2G_1)^2$
> 0 if $G_3 > G_1$ and $G_2 > G_1$.

APPENDIX B

The Proof of Negative Values of dK_{UC}/dv_1 in Equation (6.43), dK_{LC}/dv_1 in Equation (6.46), dG_{UC}/dv_1 in Equation (6.49), and dG_{LC}/dv_1 in Equation (6.52), if $K_3 > K_2 > K_1$ and $G_3 > G_2 > G_1$.

1. dK_{UC}/dv_1

$$= \frac{1}{S}\left(-\frac{dR}{dv_1} + \frac{R}{S}\frac{dS}{dv_1}\right) = \frac{1}{S}M$$

Assume $M = -\frac{dR}{dv_1} + \frac{R}{S}\frac{dS}{dv_1} < 0$

then $R\frac{dS}{dv_1} < S\frac{dR}{dv_1}$ since $S > 0$ if $K_3 > K_1$ and $K_3 > K_2$

$\therefore$

$$[v_1(K_3 - K_1)(3K_3 + 4G_3)^2 + (1 - v_1 - v_3)(K_3 - K_2)(3K_3 + 4G_3)^2 - 3(1 - v_3)(K_3 - K_1)(K_3 - K_2)(3K_3 + 4G_3)] \times 3(K_2 - K_1)(3K_3 + 4G_3) < [(3K_3 + 4G_3)^2 - 3(1 - v_1)(K_3 - K_1)(3K_3 + 4G_3) - 3(v_1 + v_3)(K_3 - K_2)(3K_3 + 4G_3) + 9v_3(K_3 - K_1)(K_3 - K_2)] \times (K_2 - K_1)(3K_3 + 4G_3)^2$$

$\therefore$ $(3K_1 + 4G_3)(3K_2 + 4G_3) > 0$ is sustained. So, $M < 0$.

Therefore, it is true that $dK_{UC}/dv_1 < 0$ if $K_3 > K_1$ and $K_3 > K_2$.

2. dK_{LC}/dv_1

$$= \frac{1}{Q}\left(\frac{dP}{dv_1} - \frac{P}{Q}\frac{dQ}{dv_1}\right)$$

$$\frac{dP}{dv_1} = (K_1 - K_2)(3K_1 + 4G_1)(3K_3 + 4G_1) < 0 \text{ if } K_2 > K_1$$

$$\frac{dQ}{dv_1} = 3(K_2 - K_1)(3K_3 + 4G_1) > 0 \text{ if } K_2 > K_1$$

Since $P > 0$ and $Q > 0$ if $K_3 > K_1$ and $K_2 > K_1$, it is true that $dK_{LC}/dv_1 < 0$ if $K_3 > K_1$ and $K_2 > K_1$.

3. dG_{UC}/dv_1

$$= \frac{1}{W}\left(-\frac{dV}{dv_1} + \frac{V}{W}\frac{dW}{dv_1}\right) = \frac{1}{W}N$$

Assume $N = -\frac{dV}{dv_1} + \frac{V}{W}\frac{dW}{dv_1} < 0$

then $V\frac{dW}{dv_1} < W\frac{dV}{dv_1}$ since $W > 0$ if $G_3 > G_2$ and $G_3 > G_1$

$\therefore$

$$[25v_1G_3^2(G_3 - G_1)(3K_3 + 4G_3)^2 + 25(1 - v_1 - v_3)G_3^2(G_3 - G_2)(3K_3 + 4G_3)^2 - 30(1 - v_3)G_3(G_3 - G_1)$$
$$(G_3 - G_2)(3K_3 + 4G_3)(K_3 + 2G_3)] \times 30G_3(G_2 - G_1)(3K_3 + 4G_3)(K_3 + 2G_3) < [25G_3^2(3K_3 + 4G_3)^2 -$$
$$30(1 - v_1)G_3(G_3 - G_1)(3K_3 + 4G_3)(K_3 + 2G_3) - 30(v_1 + v_3)G_3(G_3 - G_2)(3K_3 + 4G_3)(K_3 + 2G_3) +$$
$$36v_3(G_3 - G_1)(G_3 - G_2)(K_3 + 2G_3)^2)] \times 25G_3^2(G_2 - G_1)(3K_3 + 4G_3)^2$$

$\therefore$ $[G_3(9K_3 + 8G_3) + 6G_1(K_3 + 2G_3)] \times [G_3(9K_3 + 8G_3) + 6G_2(K_3 + 2G_3)] > 0$ is sustained. So, $N < 0$.

Therefore, it is true that $dG_{UC}/dv_1 < 0$ if $G_3 > G_2$ and $G_3 > G_1$.

4. dG_{LC}/dv_1

$$= \frac{1}{U}\left(\frac{dT}{dv_1} - \frac{T}{U}\frac{dU}{dv_1}\right)$$

$$\frac{dT}{dv_1} = 5G_1(G_1 - G_2)(3K_1 + 4G_1)[6G_3(K_1 + 2G_1) + G_1(9K_1 + 8G_1)] < 0 \quad \text{if } G_2 > G_1$$

$$\frac{dU}{dv_1} = 6(G_2 - G_1)(K_1 + 2G_1)[6G_3(K_1 + 2G_1) + G_1(9K_1 + 8G_1)] > 0 \quad \text{if } G_2 > G_1$$

Since $T > 0$ and $U > 0$ if $G_3 > G_1$ and $G_2 > G_1$, it is true that $dG_{LC}/dv_1 < 0$ if $G_3 > G_1$ and $G_2 > G_1$.